DYNAMIC INTERRELATIONSHIP BETWEEN TECHNOLOGY AND ARCHITECTURE IN TALL BUILDINGS

by

Kyoung-Sun Moon

B.S. in Architecture, Seoul National University, Seoul, Korea, February 1992
M.Arch., University of Illinois at Urbana-Champaign, May 2000
M.S.C.E.E., University of Illinois at Urbana-Champaign, May 2000

Submitted to the Department of Architecture
in Partial Fulfillment of the Requirement for the Degree of

Doctor of Philosophy in Architecture: Building Technology

at the

Massachusetts Institute of Technology

June 2005

Signature of Author .....
Department of Architecture
April 22, 2005

Certified by .....
John E. Fernandez
Associate Professor of Architecture
Thesis Supervisor

Certified by .....
Jerome J. Connor
Professor of Civil and Environmental Engineering
Thesis Supervisor

Accepted by .....
Adèle Naudé Santos
Chair, Committee on Graduate Students
Acting Head, Department of Architecture
Dean, School of Architecture and Planning

DYNAMIC INTERRELATIONSHIP BETWEEN TECHNOLOGY AND ARCHITECTURE IN TALL BUILDINGS

by

Kyoung-Sun Moon

Submitted to the Department of Architecture
in Partial Fulfillment of the Requirement for the Degree of

Doctor of Philosophy in Architecture: Building Technology

at the

Massachusetts Institute of Technology

June 2005

Thesis Committee:

John E. Fernandez
Associate Professor of Architecture
Department of Architecture
Massachusetts Institute of Technology

Jerome J. Connor
Professor of Civil and Environmental Engineering
Department of Civil & Environmental Engineering
Massachusetts Institute of Technology

Michael K. Kim
Professor of Architecture
Department of Architecture
University of Illinois at Urbana-Champaign

Dynamic Interrelationship between Technology and Architecture in Tall Buildings

by

Kyoung-Sun Moon

Submitted to the Department of Architecture on April 22, 2005
in Partial Fulfillment of the Requirement
for the Degree of Doctor of Philosophy in Architecture: Building Technology

Abstract

The interrelationship between the technology and architecture of tall buildings is investigated from the emergence of tall buildings in the late 19th century to the present. Through the historical research, a filtering concept is developed – *original technology* and *remedial technology* – through which one can clearly understand the interrelationship between the technological evolution and architectural esthetic and further stylistic transition of tall buildings. More desirable visions for the future can be constructed based on this concept.

Contemporary design practice of tall buildings is reviewed, and design guidelines are provided for new design trends. Investigated in depth are the behavioral characteristics and design methodology for diagrid structures, which emerge as a new direction in the design of tall buildings with their powerful structural rationale and symbolic architectural expression. Moreover, new technologies for tall building structures and facades are developed for performance enhancement through design integration, and their architectural potentials are explored. Special emphasis is placed on the research on the structural dynamic motion control using double skin facades / distributed tuned mass dampers.

Design integration among architecture-related disciplines is emphasized throughout the research process as a means to more effectively overcome or at least minimize contemporary technological limitations and to create architecture of higher quality. While each study makes its own contribution theoretically and in a particular design situation, from a wider viewpoint, the contribution of this thesis is to create more constructive relationships of architecture-related disciplines to produce better architecture through synergistic effects.

Thesis Supervisor: John E. Fernandez
Title: Associate Professor of Architecture

Thesis Supervisor: Jerome J. Connor
Title: Professor of Civil and Environmental Engineering

Acknowledgements

I am very grateful to Professor John E. Fernandez for his guidance and encouragement throughout my research work. He has always been open-minded and encouraged me to explore potentials and to pursue my interests. His enthusiasm as a teacher is inspiring, and his wise suggestions have always been very helpful. This work would not have been possible without his ceaseless support.

I also would like to express my deepest gratitude to Professor Jerome J. Connor for his invaluable guidance and support. His capacity for clear scientific thinking led this work to become a valuable intellectual contribution that will hopefully help the practice of tall building design go in a more integrative and efficient direction. Working with him has been one of the greatest experiences of my life at MIT.

Special thanks go to Professor Michael K. Kim for his continual support, confidence, and dedication to my education since my time in the Master's program at the University of Illinois at Urbana-Champaign. He has taught me not only the fundamentals but also the strategic problem solving that is critical to their application. I am very fortunate to have him as a committee member for this work.

I am grateful to Building Technology Group friends who have added immeasurably to my experience through their insights, generosity, and enthusiasm.

I cannot thank my father enough for believing in me, for so generously supporting me, and encouraging me to focus on this work.

My utmost gratitude and love go to my wife, Se-Gyoung, whose quiet support is incomparable, whose love and understanding gave me the strength to complete this work, and to whom this thesis is dedicated.

Table of Contents

APPENDICES

Table of Figures

8.18: Dynamic Response of the 60-Story Structure without TMD: Modal Displacement Profile – Real Part – for the Primary Structure; Modal Damping Ratio without Feedback; Profile of the Maximum Nodal Relative Displacement – Primary Structure; and Profile of the Maximum Nodal Total Acceleration/g – Primary Structure

8.19: Dynamic Response of the 60-Story Structure with a TMD tuned to the 1st Mode when Forcing Period = 1st Mode Frequency of the Structure: Modal Displacement Profile – Real Part – for the Primary Structure; Modal Damping Ratio without Feedback; Profile of the Maximum Nodal Relative Displacement – Primary Structure; Profile of the Maximum Nodal Total Acceleration/g – Primary Structure, and Time History of the Nodal and Damper Displacement

8.20: Dynamic Response of the 60-Story Structure with a TMD tuned to the 1st Mode when Forcing Period = 2nd Mode Frequency of the Structure: Profile of the Maximum Nodal Relative Displacement – Primary Structure; Profile of the Maximum Nodal Total Acceleration/g – Primary Structure; and Time History of the Nodal and Damper Displacement

8.21: Dynamic Response of the 60-Story Structure with a TMD tuned to the 2nd Mode when Forcing Period = 2nd Mode Frequency of the Structure: Modal Displacement Profile – Real Part – for the Primary Structure; Modal Damping Ratio without Feedback; Profile of the Maximum Nodal Relative Displacement – Primary Structure; Profile of the Maximum Nodal Total Acceleration/g – Primary Structure; and Time History of the Nodal and Damper Displacement

8.22: Vertically Distributed TMD Design Strategy for a 60-Story Building

8.23: Dynamic Response of the 60-Story Structure with Vertically Distributed TMDs tuned to the 1st and 2nd Modes when Forcing Period = 1st Mode Frequency of the Structure: Modal Damping Ratio without Feedback; Profile of the Maximum Nodal Relative Displacement – Primary Structure; Profile of the Maximum Nodal Total Acceleration/g – Primary Structure; Time History of the Nodal and Damper Displacement; and Profile of the Maximum Inter-nodal Displacement – Tuned Mass Dampers

8.24: Dynamic Response of the 60-Story Structure with Vertically Distributed TMDs tuned to the 1st and 2nd Modes when Forcing Period = 2nd Mode Frequency of the Structure: Modal Damping Ratio without Feedback; Profile of the Maximum Nodal Relative Displacement – Primary Structure; Profile of the Maximum Nodal Total Acceleration/g – Primary Structure; Time History of the Nodal and Damper Displacement; and Profile of the Maximum Inter-nodal Displacement – Tuned Mass Dampers

8.25: Various TMD Distribution Strategies

8.26: Enlarged View of 4 Different TMD Location Schemes

8.27: DSF Construction Unit

8.28: Future Research

List of Tables

INTRODUCTION

Tall building development involves various complex factors such as economics, architectural style, technology, municipal regulations, and politics. Among these, economics has been the primary governing factor since the emergence of the skyscrapers in the late 19th century. However, without supporting technologies, this new building type itself would not have been possible. A structural revolution – the steel skeletal structure – and consequent glass curtainwall system, which occurred in Chicago, has led to the present status of the skyscraper. In addition, the inherent monumentality of skyscrapers resulting from their scale makes their architectural expression very significant in any urban context. Based on these technological and architectural viewpoints, the objectives of this thesis are twofold.

In Part I of this thesis, the interrelationship between the technological evolution and architectural style of tall buildings is investigated from the emergence of tall buildings in the late 19th century to the present. Various technologies have been involved in tall building development. Among them, structural systems and façade systems are mainly investigated in this research. They are considered to be the most important technologies in terms of their conspicuous function/performance, which allows the existence of tall buildings, and their major impact on building esthetics and, in turn, architectural style. Here, the concept of *original technology* – revolutionary technology that redefines the artifact in terms of both function/performance and esthetics – and *remedial technology* – evolutionary technology that refines original technology mostly in the domain of function/performance – is developed, and its incorporation with the architectural style of tall buildings is investigated.

There has been notable evolution of technology since the emergence of tall buildings. However, many technological limitations still exist. Indeed, this is inevitable due to the conflicting dual characteristics of any modern technology. The promising reliability of modern technology enabled architecture to transform from traditional to modern architecture. However, the other side of this promise has been the ephemeral nature of technology. This is because the expected rate of technological evolution exceeds the actual rate of the evolution to meet this expectation. In addition, the incremental rate of technology-related human requirements of modern society exceeds the actual rate of the evolution to meet these requirements, making the status of technology ever imperfect. This ephemeral character and the promise of technology have been in a certain conflict in modern architecture. In tall buildings, which generally require the most advanced contemporary technologies due to their very tallness and scale, this conflict can be observed in terms of the limits of technology.

The prevailing strategy to overcome, or at least minimize, the technological limitations of tall buildings, especially with regard to structures and facades, is developing remedial technology through a design integration approach, which corresponds to the coevolution process in nature, recognizing the symbiotic relationship of the two systems. Based on this notion, Part II of this thesis studies today's practice of tall building design first, and

then investigates the potential solutions for contemporary technological limitations through design integration and their architectural implications.

The direction of evolution of tall building structural systems has been towards more efficient systems. As a result, today's tall buildings are in general much lighter than the earlier ones, and consequently motion-induced human discomfort problem is now a serious design issue. Basically two structural properties govern this problem: stiffness primarily for static loads and damping for dynamic loads. Today's most popular tall building structural systems are various tubular structures, core supported outrigger systems with super columns, and more recently diagrid structures. The main characteristic of these structural systems is that they have their major lateral load resisting systems at the perimeter of the building in order to maximize structural depth. Considering their structural efficiency and architectural significance as a newly emerging esthetics of tall buildings at the time of this research, special emphasis is given here to investigating diagrid structures mainly with regard to static lateral loads. Since diagrids are located at the perimeter of the building and generally there are only slanted structural members without any conventional vertical columns, their architectural implications are significant, especially with respect to façade system design. From this perspective, the architectural potentials of diagrid structures are also investigated.

With regard to dynamic loads, new technologies are investigated through design integration between the structural and façade systems of tall buildings. Special focus is given to double skin façade (DSF) systems considering their increasing significance in today's architecture from the viewpoint of both esthetic expression – augmented perceptual transparency – and function – one of the most advanced environmental mediators between the exterior and interior. Studied is the effective structural use of the gap DSF systems provide in order to dissipate dynamic wind loads. The strategy of low stiffness DSF connector design is investigated first, followed by a study on distributing multiple tuned mass dampers within DSF cavities. Considering its practicality, much more focus is given to the latter scheme. Since the system is different from any other conventional system, its comparative advantages and disadvantages are investigated first from the viewpoint of the structural behavior of a building that adopts this system, and then its architectural implications from the viewpoint of its contribution to both esthetics and functions.

The impact of technology is significant in tall buildings due to their very tallness. Consequently technology tends to govern the design of tall buildings more than that of other building types. This trend may conflict with architectural aspects of tall buildings. Good design involves resolving this possible conflict. It depends on the capability of architects and engineers to transform any present challenges into the potentiality of enhanced design integration. This thesis is devoted to demonstrating this potential through collaborative works between architects and engineers.

PART I:

TECHNOLOGY AND ARCHITECTURAL STYLE OF TALL BUILDINGS

CHAPTER 1: TECHNOLOGY AND STYLE IN ARCHITECTURE

Technology has very often been considered in terms of its relation to science and its ability to apply critical scientific discoveries. However, the relationship between technology and art has been investigated less intensely. Nevertheless, as Bruno (1995) has noted, the nature of technology is quite similar to that of art in the sense that both create something for humans unlike science, which pursues truth of nature for its own sake. Architecture is one of the disciplines that encompass both technology and art. In architecture, especially in modern architecture, its functional and performance attributes as well as its esthetics aspects are produced through the functionalities and limitations of technology. The very products of modern technology – from form-making structures to surface-defining enclosures – are assembled to create architecture. Physical components of architecture are nothing but cold steel members, massive concrete, aluminum panels, various kinds of glass panes, etc. However, once these modern-technology-produced elements are assembled together in a certain way through the process of design and construction, they are no longer mere technological elements. They transform into the components of both the functional and the esthetical. From this viewpoint, technology and esthetics of modern architecture are inseparable.

Considering more intrinsic attributes of technology and observing any building as a whole as an artifact produced by technology, the esthetic aspect of it is superfluous. However, this superfluous aspect of technology is one of the essential attributes of architecture. Modern architecture has been transformed based on the evolution of modern technology. Sublimating technology into the art of architecture has been the major task of architects throughout the history of modern architecture. It is also true that there has been some skepticism with regard to the compatibility between modern technology and architecture. In his influential book *Theory and Design in the First Machine Age*, Banham wrote that "what we have hitherto understood as architecture and what we are beginning to understand of technology are incompatible disciplines." And more recently, Leatherbarrow and Mostafavi (2002) argued that "production and representation are in conflict" in modern architecture. However, the history of architecture demonstrates strong interaction between technology and architecture and even shows that new technology has led to a new architectural style in certain circumstances, a typical case of which can be observed in the transitional process from Romanesque to Gothic architecture.

Viollet-le-Duc wrote that "everything is function of structure" in Gothic architecture. However, as Grodecki (1985) pointed out, "Gothic space is not merely an enclosed volume to be geometrically defined. It is function of light; it is transfigured by light. Purely formal, spatial, and structural analyses all appear to be inadequate tools in the search for a precise delineation of this architectural style." Gothic architecture's dematerialization for opening up the walls through structural innovation was primarily to introduce more light – "symbol of the grace of God" – into the building for religious purposes. In addition, its pursuing unprecedented height through the structural invention was for religious reasons. Thus, the fundamental driving force of the emergence of Gothic architecture was not structural but absolutely religious, and this religious purpose

was accomplished physically through new technology. In general, technology as a means to accomplish a certain function/performance is its fundamental attribute, and its esthetic contribution is peripheral or superfluous. However, when technology is considered in disciplines that encompass art, its esthetic expression is no longer superfluous. In fact, in a case when a technological leap is conspicuous, such as in the emergence of Gothic architecture, technology defines the esthetics of the artifacts created by it. Function/performance-driven technology acts as an esthetic driver as well, transforming the essential nature of architecture of a certain age and eventually originating a new style.

Observing the history of technology, an epochal leap of technology rarely occurs. In general, development of technology is not revolutionary but evolutionary. Mostly in very rare revolutionary cases, new technology changes the nature of artifacts in terms of both function/performance and esthetics. This phenomenon is in a sense natural because an epoch-making technological leap means that there have been no precedents. In a case when new technology creates an artifact of new configuration using new material to hold new function/performance, if the artifact is in a discipline that encompasses art, new esthetic expression is sought continuously and finally generalized into a new style. In that case, this new technology may be called *original technology* in the sense that it modifies the essential nature of an artifact by not only generating an unprecedented function/performance but also originating a new style in terms of esthetics. Original technology redefines an artifact in terms of both function/performance and esthetics.

Any originality in technology is experimental because it has not been proven to perform as intended, and since a revolutionary technological leap occurs very rarely, its capability superficially perceived is in general much greater than its actual capability. Also, the intrinsic nature of any technology is ephemeral and ever-evolving towards efficiency and better performance. Thus, original technology is followed by refinements based on the results of its performance. However, this new set of refining technology following the original one does not change the nature of artifacts but evolves from the original one and remedies its unforeseen problematic aspects to make it perform as intended or even better. In this sense, this evolutionary technology following the revolutionary original one may be called *remedial technology* and it is mostly in the function/performance domain.[1]

Modern architecture is the product of modern technology incorporated with new architectural style. Compared with the massiveness of traditional architecture, the lightness of modern architecture was accomplished through technological revolution. The promising reliability of modern technology enabled architecture to finally move

[1] Some technologies in the remedial era have been driven not by function but by esthetics. This is because in this era technologies are already in the domain of both function/performance and esthetics through the process of the redefinition of artifacts in both ways by original technology. In tall buildings, esthetic-driven technologies are sometimes found mostly in their façade systems due to the intrinsic nature of the systems. Included in typical cases are structural silicones, point fixings, etc. These technologies are driven by architects' esthetic aspirations to greatly minimize supporters of façade glasses – traditionally metal mullions – visible from outside and achieve smoother and uninterrupted glass surfaces. In structures, esthetic-driven technologies are much harder to find. Thus, in general, esthetic-driven technologies are much rarer than function/performance-driven technologies due to the fundamental nature of any technologies.

away from traditional to modern. However, the other side of this promise was the imperfection of experimental original technology and intrinsic ephemeral nature of any technology. In addition, the power of technology superficially perceived by architects in the early modern period was much stronger than the actual capability of technology. Modern architecture was born in this physical and mental gap. This circumstance led to the next step of technology that smoothly fills and connects this gap in order to augment the integration between technology and architecture originally produced by technological revolution. This is remedial technology, distinguished from millennia-breaking original technology. Modernism, as Steele (1997) noted, despite repeated declarations to the contrary, is far from dead and may now be entering its culminating phase through remedial technology.

CHAPTER 2: TECHNOLOGY AND ARCHITECTURAL STYLE OF TALL BUILDINGS

Various technologies have been involved in the design and construction of modern buildings. Also, since the emergence of modern architecture many stylistic transitions have occurred. Some have been global, and others have been regional. Some have lasted longer, and others lasted a shorter time. Technological evolutions and technology itself are fundamentally in the domain of function/performance as a means for a certain end. However, this chapter hypothesizes that some technologies have had major impacts on the esthetics of architecture as well due to the intrinsic nature of architecture, which must satisfy not only functional but also esthetic requirements. Consequently, some other technologies have had only minor impacts, and the rest of the technologies have had no impact at all on the esthetics of architecture.

Tall buildings are, in a sense, the accumulation of the most advanced modern architectural technologies due to their extreme height. Because of their enormous scale, which comes again from their height, the impacts of their architectural esthetic expressions are also significant in any context where they soar. Considering this special significance of the technologies and esthetics in tall buildings, the second hypothesis in this chapter is that the interactions between these two issues have been more conspicuous in tall buildings than in any other building type. Based on both hypotheses, the purpose of this chapter is to investigate the interrelationship between the technological evolution and architectural esthetics – further architectural styles – of tall buildings from their emergence in the late 19th century to the present. Among the various technologies involved, structural systems and façade systems are mainly investigated in this thesis. They are considered to be the most important technologies in tall buildings in terms of not only their fundamental function/performance, which allows for the very existence of tall buildings, but also their major influence on architectural esthetics and, in turn, style.

Finding symbiotic interrelationships between technology and esthetics is fraught with misleading and sometimes erroneous linkages. Tracing both chronologically, technologies follow evolutionary paths with fluctuating rates; and styles, in a sense, follow cyclic paths with varying periods. From a wider viewpoint, this chapter investigates the way of their marriages and divorces following their historical paths up to the present and the reasons for the paths. From a narrower viewpoint, this chapter studies specifically which technologies are in the domain of both function/performance and esthetics, which other technologies are in the domain of only function/performance, and what the specific characteristics of these technologies of different natures are. In this way, through the filter of historical facts, current situations regarding these relationships can be clearly illuminated. Further, based on that, more desirable visions for the future may be constructed.

The investigation of the relationships is conducted through the case studies of tall buildings, many of which are still standing and some demolished for various reasons, mostly economical ones. The choices of buildings studied are based on the significance of applied technologies and that of esthetic expression. Thus, considering the nature of the field of architecture, the buildings chosen for esthetic reasons are all renowned ones

recognizable by anyone interested in architecture. However, some buildings chosen for technical reasons may not be renowned and thus may not be known except to those who have special interest in the evolution of architectural technology. In fact, many chosen buildings are renowned for both their esthetics and applied technologies, demonstrating the strong interaction between them, as is hypothesized in this chapter.

2.1. Early Skyscrapers in the Late 19th Century: Economy Governs, Technology Supports Them, and a New Style Burgeons in Chicago.

Generally, the Home Insurance Building (completed in 1885) by William LeBaron Jenny in Chicago is considered as the first skyscraper (Figure 2.1 and Figure 2.2: Demolition of Home Insurance Building showing metal skeletons). This is based on the consideration of its tallness, spatial configuration related to function, and the applied technologies of the building. These factors opened a great potential for a new building type, and ultimately generated one. The combination of these criteria is of critical importance. If only the tallness of a building, which mainly contains the spaces people can occupy, is considered, some Gothic cathedrals can place the height of the Home Insurance Building underneath the vaulted ceilings of their naves.[2] However, while a modern skyscraper has layers of horizontal planes within its height for maximum occupancy, underneath the ceiling of a Gothic cathedral is only a very high single story space.

Figure 2.1: Home Insurance Building

Figure 2.2: Demolition Scene of Home Insurance Building

The importance of applied technologies in early skyscrapers exists in their potential. For instance, the height of some tall office buildings, such as the Montauk Building in Chicago or the Western Union Building and the Tribune Building in New York (constructed earlier than the Home Insurance Building) are comparable to, or even much greater than, that of the Home Insurance Building.[3] Yet, they achieved their heights by employing

[2] For example, the ceiling heights of the Amiens Cathedral and the Beauvais Cathedral are 138 feet and 158 feet respectively.

[3] The heights of the Western Union Building and Tribune Tower were 230 feet and 260 feet respectively. The heights of these multi-story office buildings were possible due to the invention of the automated vertical transportation system – elevators – which is one of the most important technologies for the emergence of tall buildings. However, the discussion on elevators is limited here because it is less relevant to the theme of this thesis. The first passenger elevator, designed by Elisha Otis, was installed in the 5-story Haughwout Building in 1857. For office buildings, the first use of elevators was in the Equitable Building in New York in 1870.

the traditional load-bearing masonry structures, which required the wall thicknesses of several feet on their ground levels.[4] Thus, these earlier tall office buildings did not have the potential to grow further because of the technological limitations of their structural system. In these technological contexts in both New York and Chicago – the only two skyscraper cities in the world at that time – the invention of the iron/steel skeletal structure for the Home Insurance Building was a remarkable breakthrough toward the development of new building type.

In fact, the invention of the iron/steel skeletal structure was driven not by the structural aspiration to build buildings higher but rather by its economic purpose to introduce as much natural daylight as possible into the interior office spaces to attract higher rents. This very well explains the fundamental nature of technology as a means to an end in the function/performance domain. Before the invention of fluorescent lamps in the office buildings, daylight was the main source of light. Incandescent lamps were invented much earlier than fluorescent lamps and available beginning in the late 19th century. However, in order to achieve appropriate indoor lighting environments, the heat gains through incandescent lamps were too intense. Since modern mechanical HVAC systems were not invented yet, these conditions were not easily dealt with by natural ventilation. In traditional masonry construction, very thick and deep masonry piers were necessary, especially in the lower floors of tall buildings.[5] This was a quite undesirable condition because it kept daylight from entering the interior spaces of tall buildings, resulting in lower rental income. Thus, the primary motive behind the invention of the iron/steel skeletal frame for tall buildings was to overcome this limitation of traditional masonry construction. This can be observed from Jenny's writing in 1885:

"As it was important in the Home Insurance Building to obtain a large number of small offices with abundance of light, the piers between the windows were reduced to the minimum, and the following system of construction was adopted. Iron was used as the skeleton of the entire building except the party walls, and every piece of iron was protected from fire by masonry, excepting only some columns so situated as not to be dangerous if left exposed."[6]

With regard to the technological achievement of the Home Insurance Building, architectural historian Carl Condit (1968) was skeptical about the general acceptance of this building as the first skyscraper because there were no provisions for lateral wind

---

[4] For instance, the wall thicknesses of the Tribune Building on the ground floor varied from 3 feet 4 inches to 5 feet 2 inches.

[5] Generally, the thickness of the brick masonry wall at the topmost story of the building was 12 inches with 4 inch increments every story downward to the ground. For example, the wall thickness on the ground of the 16 story Monadnock Building in Chicago is 12 + 4x15 = 72 inches = 6 feet.

[6] In his 1934 Architectural Record article *Neither a Skyscraper nor of Skeleton Construction*, architect Irving Pond was opposed to calling the Home Insurance Building the first skyscraper due to masonry party walls. However, it was inevitable because Chicago's building code at that time did not accept iron/steel skeleton as party walls.

loads in this 10-story building. Actually, there is no generally accepted definition of tall buildings. However it is widely accepted that, from a structural viewpoint, if the tallness of a building significantly influences its structural design and performance, that building is considered a tall building. In fact, the tallness of the Home Insurance Building had little effect on its structural design, resulting in Condit's skepticism. However, the importance of any technological breakthrough should be measured not by how close it is to the fully developed conditions but by its potential for further development. In the case of the steel skeletal structure, the Chicago invention in the late 19th century eventually led to the present status of tall buildings. And there lies its significance. Since the construction of the Home Insurance Building, its iron/steel skeletal structure has become the major prototype for the structural systems of tall buildings.

Following the emergence of iron/steel skeletal frame structure, various lateral load resisting systems were developed. Systems developed in the late 19th century were riveted steel connections, portal bracings, and braced frames. Riveted connections were introduced in Holabird and Roche's Tacoma Building (1889) in Chicago. Portal bracings were employed first in Burnham and Root's Monadnock Building (1891) and Jenny's Manhattan Building (1891) in Chicago. And braced frames were used widely. These series of structural innovations, occurring within the real estate boom in the late 1880s in Chicago, established a solid technological foundation for much taller buildings to come. However, following the financial panic in 1893 due to the excessive development of tall buildings in previous years, the Chicago City Council was forced to limit the height of buildings to 130 feet. This height limitation over the next three decades made the development of tall buildings in Chicago much less active than in New York (Carol Willis, 1995).[7]

With the invention of steel skeletal structures, the curtainwall concept was consequently developed to clad them. The biggest challenge for architects confronted with an unprecedented building type and new technology was how to design the façades of tall buildings, especially in terms of esthetics. What should be clearly noted here is that esthetic expression was not within the initial criteria of the development of new technology. However, due to the nature of architecture, new esthetic expression corresponding to a new building type was sought by architects. Strategies differed in New York and Chicago, and various factors influenced the design of tall buildings in the two skyscraper cities.

New York is a much older city than Chicago, and thus there was a prevalent architectural stylistic trend already established. Naturally, this existing trend was directly applied to early masonry load-bearing tall buildings. Thus, most early tall buildings looked odd because existing styles were developed not for a new building type, tall buildings, but for buildings usually lower than five stories. This oddness came from the awkward vertical grouping of tall buildings. The early skyscraper architects had a hard time finding out how to deal with this unprecedented tallness. Thus, they often located vertical grouping design devices, such as cornices, at every two or three stories, or sometimes irregularly,

[7] The height limitation fluctuated from minimum 130 feet (1893) to maximum 264 feet (1921) over the next three decades before the first Zoning Ordinance of Chicago in 1923.

making the building look as if it had been constructed in stages. Typical examples include the Mills Building, completed in 1883 (Figure 2.3).

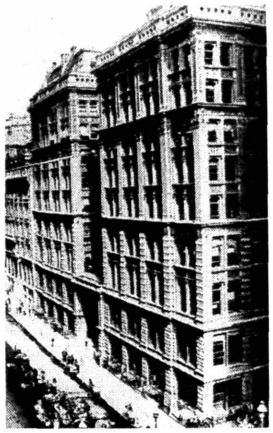

Figure 2.3: Mills Building

From the late 1880s, the awkward vertical grouping approach was replaced by the tripartite system, which was widely accepted by contemporary critics and architects, such as Montgomery Schuyler in New York and Louis Sullivan in Chicago. A typical example is the American Surety Building (Figure 2.4) designed by Bruce Price and completed in 1895.[8] One of the most influential architectural critics at that time, Montgomery Schuyler presented his interpretation of the emerging tripartite style in his 1899 article *The "Sky-Scraper" Up-To-Date.*

"It is true that the skyscraper is in fact a series of equal cells, and that the only suggestions for a triple division that inhere in the conditions are the facts that the ground floor has a different destination from that of the floors above, and suggest a distinctive treatment of the bottom, and the fact that a visible roof or in default of it the necessity for a protective and projecting cornice, compels a distinctive treatment for the top.

....

Most successful of the skyscrapers are those in which the shaft is made nothing of in which necessary openings occur at the necessary places, are justified by their necessity but draw no attention to themselves."

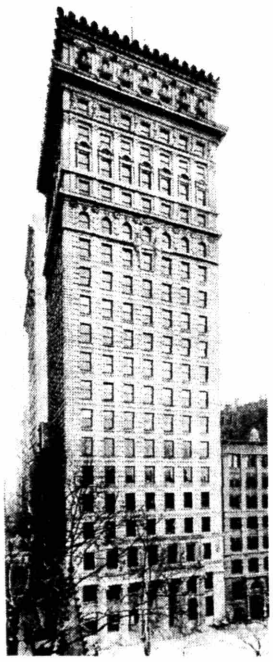

Figure 2.4: American Surety Building

At the very end of the century, this comment about pure functionalism is in exact agreement with Sullivan's dictum, "Form Follows Function,"[9] and also Mies's "Less is More" decades later. He accurately predicted the 20th century architecture. In the same article, he clearly stated the inadequacy of applying masonry to the steel skeleton as its façade material.

---

[8] Even though the tripartite façade design approach prevailed at the end of the 19th century, the previous vertical grouping design was still applied for some buildings such as the Park Row Building completed in 1889, the tallest building at the time of its completion.

[9] Sullivan said that the "lower two (or possibly three) stories of a tall office building had a destination so different from that of the superstructure, that a distinguishing treatment for them was not only required but demanded, and that the uppermost story in turn, being in great part devoted to the circulation system of the building should also be differentiated." Even though he declared "form ever follows function," in reality, his form sometimes followed his esthetic viewpoint. As Hoffman (1998) pointed out, in his early masterpiece, Wainwright Building, the second floor and typical floor plan are exactly identical offices. However, the second floor was not grouped with typical floors to compose the shaft but grouped with the first floor to comprise the base. This design decision came clearly not from functional but from esthetic considerations.

"Almost without exception, the designers of tall buildings ... [designed] buildings of masonry, instead of merely wrapping skeletons of metal in fire-resisting material. .... traditions of masonry have no relevance at all to the new construction."

Here, he was addressing the 19th century schism in architecture, and declared that tall building design should be integrated with new technology.

Nonetheless, beginning from the French Second Empire Style in the Equitable Building, constructed before this structural innovation, most New York skyscrapers in the late 19th century were clad in a historical architectural language, hiding technological innovation behind their façades. Even after the introduction of the iron/steel skeletal structure, every tall building did not entirely employ this new structural system.[10] Quite a few tall buildings at that time adopted a hybrid structure, a skeletal structure for the interior framing and a masonry structure for the façade. This was due to not only the stylistic reason but also the profound distrust of irons/steel's durability against weather. Typical buildings of this design trend include the Havemyer Building (Figure 2.5 and Figure 2.6) designed by George Post and completed in 1893. While constructed five years after the introduction of skeletal structure in New York, this building adopted the hybrid structure described above. As for the composition of its façade, this building employs the tripartite system based on the classical order, with rich ornaments and emphasis on the features of masonry structures. In fact, what led the design of tall buildings to the tripartite system was not, for many architects, function but classical orders.[11] During the technological transition period, inharmonious marriage prevailed between contemporary new technology and traditional style.

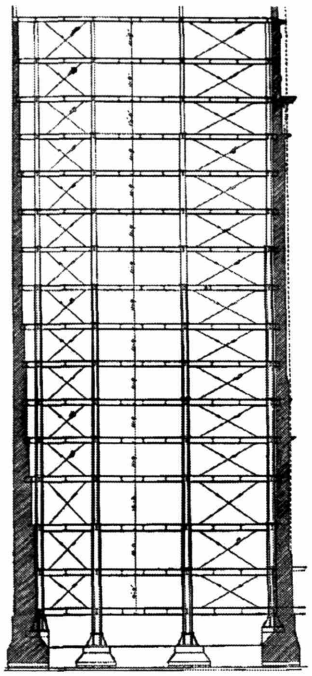

Figure 2.5: Havemyer Building Section

Figure 2.6: Havemyer Building

[10] Iron/steel skeletal construction was introduced in New York in the Tower Building designed by Bradford Gilbert and completed in 1889 – four years after the completion of the Home Insurance Building in Chicago. In this building, structural frames for the first through seventh story were entirely braced iron skeleton (cast iron columns and wrought iron beams).

[11] For instance, John Moser's 1894 article in "American Architect and Building News" reads as follows. "to express, not hide or falsify, our incomparable modern steel construction, ... I found myself getting very close to the Classic."

The fact that Chicago has a much shorter history than New York, and the Great Fire in 1871 burned down almost the entire city, made Chicago's design of tall buildings different from New York designs. There was no existing urban context to follow in Chicago at the early stage of skyscraper development. Naturally this allowed Chicago architects to be free from existing styles. This is one of the most important factors of the so-called "Commercial Style" of the first Chicago School.[12]

The Chicago School's design approach to tall buildings can be observed well from John Root's 1890 remark about modern business buildings.

"...to lavish upon them profusion of delicate ornament is worse than useless... Rather should they by their mass and proportion convey in some large elemental sense an idea of the great, stable, conserving forces of modern civilization."

The idea behind this remark is the same as that of Adolf Loos, the author of *Ornament and Crime* in the early 1900s. The same idea was manifested decades later by Henry-Russell Hitchcock and Philip Johnson to represent the International Style.

Sigfried Gidion described his interpretation of the significance of the Chicago School in his *Space, Time and Architecture:*

"The importance of the school for the history of architecture lies: for the first time in the 19th century the schism between construction and architecture, between the engineer and architect, was healed."

Chicago, like New York, also experienced a stylistic transition period. For instance, the Home Insurance Building used bricks as the material for construction of its curtainwall. Even though each bay of brick façade was supported by shelf angles fixed to the spandrel girders, its tenth story façade had an arched form, which is appropriate not for the new technology introduced but for a traditional masonry structure.[13] As a link between the masonry/skeleton hybrid structure and the true skeletal structure, this design produced a transitional style that was applied to many later tall buildings. For three decades after its completion, the Masonic Temple (Figure 2.7), which had been the tallest skyscraper in Chicago with its height of 302 feet,[14] employed the most advanced contemporary

---

[12] The influence of William LeBaron Jenny, the inventor of iron/steel skeletal frame for tall buildings, can be considered as another very important factor. Jenny was an architect/engineer who had been trained as an engineer in France. Naturally he designed his tall buildings using new technologies and applying the simplest forms without much ornament compared with his New York counterparts at that time. Most important skyscraper architects such as Louis Sullivan, Martin Roche, Holabird, and Daniel Burnham were trained at his firm and it is very probable that Jenny's approach directly or indirectly influenced their later tall building designs.

[13] The Home Insurance Building has an arched façade also at its second level, which is actually masonry structure. (The first and second levels of this building are masonry structure. The upper levels from the third floors are iron/steel skeletal frame structure.)

[14] This was due to height limitation between 1893 and 1923 in Chicago.

structural system – a rigid steel frame with wrought iron diagonal wind bracings. Like the Home Insurance Building, however, this building was also clad in brick, following the curtainwall concept. With its arched facades and pitched roof, it looked like a traditional masonry structure building with its vertically extruded form. From today's viewpoint, architectural style seems to have lagged is observed behind advanced technology. However, at that time, technology was not considered something to be esthetically expressed for some architects.

Figure 2.7: Masonic Temple

Unlike their New York counterparts, however, Chicago architects passed through the transitional period relatively quickly. They developed new esthetic expression corresponding to the structural innovations and curtainwall concepts. They saw the potential of lightness and transparency as a new esthetic direction for a new building type accomplished through the use of new technologies. These new esthetic expressions culminated in the Reliance Building (1894-1895, Figure 2.8) ten years after the introduction of the new technologies. With its unique technique used during the initiation of the construction,[15] this 14-story building employed a riveted steel frame clad in unprecedented white enameled terra cotta. Compared to brick curtainwalls prevalent at that time, shiny hollow terra cotta tiles gave the building its physical and visual lightness. Goldberger (1981) admired this building as the forerunner of the glass skyscraper of the mid-20th century, comparing it with SOM's Lever House, which after the war dramatically broke the preceding skyscraper style. The architectural success of the Reliance Building was accomplished by interpreting new technologies as vehicles for appropriating new style representing an unprecedented building type.

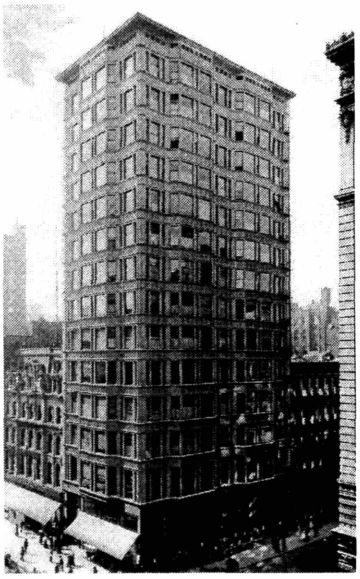

Figure 2.8: Reliance Building

Clearly economy was the fundamental driving force of tall building developments both in Chicago and New York, and technology was the supporting backbone of them. With regard to style, as Huxtable wrote in her 1992 essay, *The Tall Building Artistically Reconsidered*, "design was tied to the business equation, and style was secondary to the primary factors of investment and use." Within the existing architectural context, New York did not promptly develop new esthetic

---

[15] While the upper four stories of the old existing building on the site were held up on screws due to the remaining lease, the construction of the foundation and the first story of the new Reliance Building was performed.

expressions corresponding to new technologies, while Chicago did, in a quite different circumstance. Steel braced frames and curtain walls, with their revolutionary technological impact, created a new architectural esthetic potential.

2.2. Skyscrapers in the Early 20th Century: Return to Schism in the U.S. vs. the Modern Movement in European

As was discussed in the previous section, from around the end of the 19th century Chicago was not as active as New York in developing tall buildings. Despite the fact that Chicago accomplished significant technological development for further growth, capping the height due to the financial panic in 1893 made the development of tall buildings shrink. Thus, from that point, New York became the leading city of tall buildings in terms of both amount of construction and heights.[16]

The symbolic power of skyscrapers being recognized, a notable phenomenon occurred with regard to the development of tall buildings from the turn of the century. A skyscraper height race began, starting from the Park Row Building, which had already reached 30 stories in 1899. This height race culminated with the completion of the 102 story tall Empire State Building in 1931 (Figure 2.9).

Figure 2.9: Tall Building Height Race

Even though the heights of skyscrapers were significantly increased during this period, contrary to intuition, there had not been much conspicuous technological evolution. In terms of structural systems, most tall buildings in the early 20th century employed steel braced frames just as those built during the previous century did. Among them are the renowned Woolworth Building and the Empire State Building completed in 1913 and 1931 respectively. Their enormous heights at that time were accomplished not through notable technological evolution but through excessive use of structural materials. Due to the absence of advanced structural analysis techniques, they were quite over-designed. It can be noticed from the amount of steel used per square foot of floor area (Table 2.1) and

[16] According to Carol Willis (1995), as late as 1923, only 92 buildings of 10 to 22 stories were built in the Loop, while almost 1000 buildings of 11 to 20 stories were built in Manhattan by 1913. "During the boom of the 1920s, New York, with its more active speculative environment, pulled farther ahead of Chicago in the number and height of its towers. The tallest building in the Loop in 1931 was the 45-story, 612 ft Board of Trade; in Manhattan, 16 spires exceeded that height, including the Empire State Building, at 1250 ft."

shear links. However, for the Empire State Building at that time, the eccentricity was introduced not for this advanced structural reason but simply to provide door openings through the walls which contain braces. The Empire State Building's typical column spacing of only about 20 feet is very narrow if measured from today's standard. Thus, interior office spaces are interrupted by many rows of columns, which is quite different from today's typical tall building plan.

Since the structural systems for tall buildings were still skeletal structures, façade systems were constructed following the curtainwall concept without significant technical advances. In fact, the basic concept of skeletal structures and curtainwall façades has not changed since the emergence of tall buildings. However, the "schism between construction and architecture," which began to be healed in Chicago, reappeared and even more strongly governed the architectural style of tall buildings of the early 20th century.

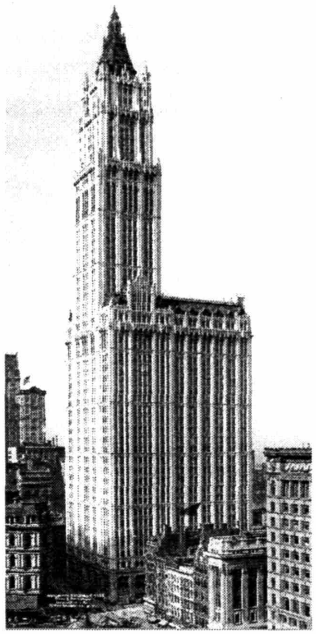

Figure 2.12: Woolworth Building

Instead of exploring new-technology-driven styles, architects at that time relied on easy solutions found from traditional architectural styles. In this kind of environment, the Woolworth Building was built following Gothic architecture (Figure 2.12), the New York Municipal Building following Classical, and the Empire State Building following Art Deco. Construction process of the New York Municipal Building and the Empire State Building (Figure 2.13 & 2.14) clearly reveals the 19th century schism again. Their esthetic destination was clearly oversized old-technology-based traditional architecture.

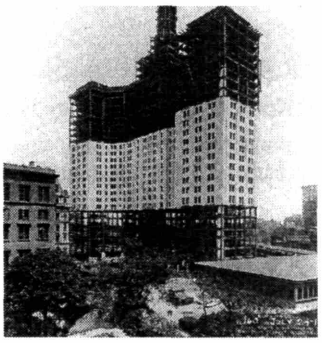

Figure 2.13: Municipal Building

In their *Surface Architecture*, Leatherbarrow and Mostafavi (2002) discuss the problem of modern production in terms of its lacking representation in contemporary architectural practice. This problem is widely observed from the tall buildings of the mid-20th century. Many tall buildings constructed during that period were a large scale re-production achieved by assembling modern-technology-produced building components. Representational quality was lost in a great degree in those buildings. Before entering this period, architects in the early 20th century returned to the traditional architecture for representation ironically with new technologies, after a short pursuit of a new style for a new building type mostly by Chicago architects in the late 19th century.

Figure 2.14: Empire State Building

shear links. However, for the Empire State Building at that time, the eccentricity was introduced not for this advanced structural reason but simply to provide door openings through the walls which contain braces. The Empire State Building's typical column spacing of only about 20 feet is very narrow if measured from today's standard. Thus, interior office spaces are interrupted by many rows of columns, which is quite different from today's typical tall building plan.

Since the structural systems for tall buildings were still skeletal structures, façade systems were constructed following the curtainwall concept without significant technical advances. In fact, the basic concept of skeletal structures and curtainwall façades has not changed since the emergence of tall buildings. However, the "schism between construction and architecture," which began to be healed in Chicago, reappeared and even more strongly governed the architectural style of tall buildings of the early 20th century.

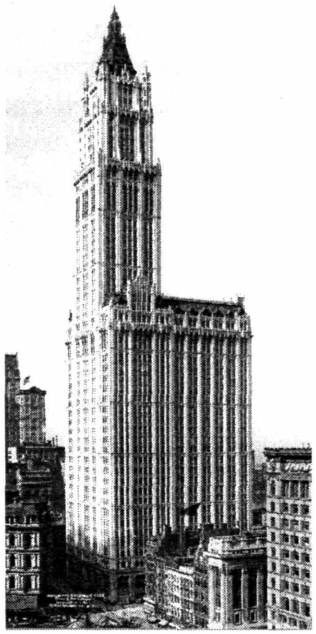

Figure 2.12: Woolworth Building

Instead of exploring new-technology-driven styles, architects at that time relied on easy solutions found from traditional architectural styles. In this kind of environment, the Woolworth Building was built following Gothic architecture (Figure 2.12), the New York Municipal Building following Classical, and the Empire State Building following Art Deco. Construction process of the New York Municipal Building and the Empire State Building (Figure 2.13 & 2.14) clearly reveals the 19th century schism again. Their esthetic destination was clearly oversized old-technology-based traditional architecture.

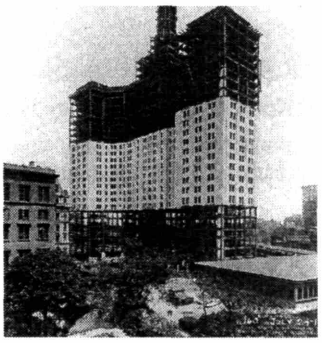

Figure 2.13: Municipal Building

In their *Surface Architecture*, Leatherbarrow and Mostafavi (2002) discuss the problem of modern production in terms of its lacking representation in contemporary architectural practice. This problem is widely observed from the tall buildings of the mid-20th century. Many tall buildings constructed during that period were a large scale re-production achieved by assembling modern-technology-produced building components. Representational quality was lost in a great degree in those buildings. Before entering this period, architects in the early 20th century returned to the traditional architecture for representation ironically with new technologies, after a short pursuit of a new style for a new building type mostly by Chicago architects in the late 19th century.

Figure 2.14: Empire State Building

However, as can be seen from the various international entries for the Chicago Tribune Tower Competition in 1922 (Figure 2.15), the rebirth of the early Chicago spirit and the application of European modern movements in tall buildings were only a matter of time. Even though Hood and Howell's Gothic style entry won the competition, many entries such as ones by Gropius and Hilbersheimer clearly denoted the upcoming International Style skyscrapers.

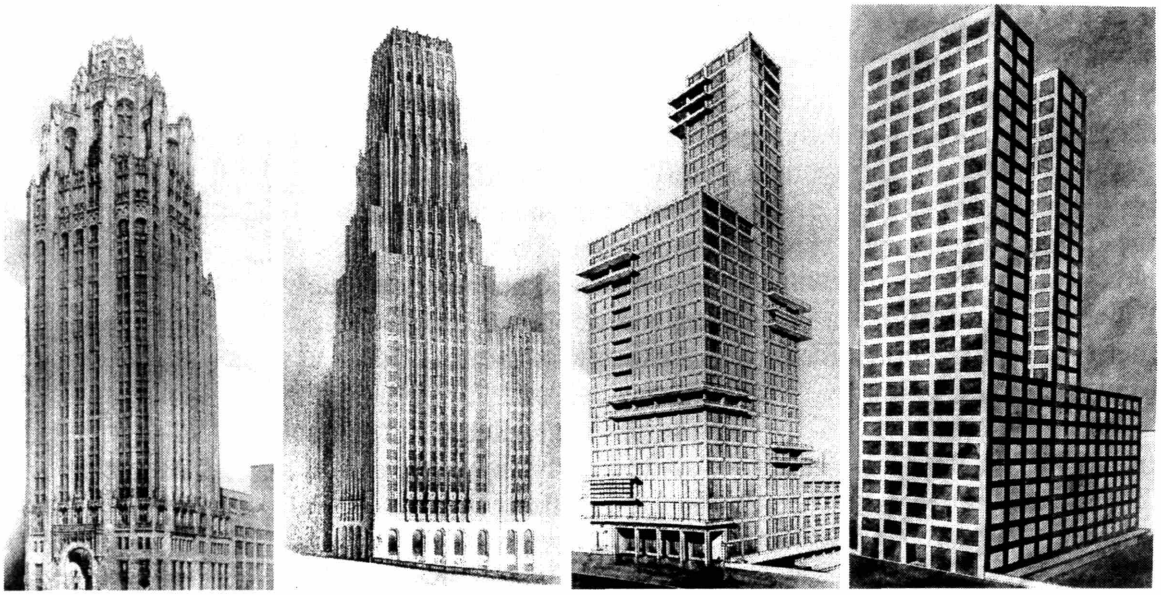

Hood & Howel Saarinen Gropius Hilbersheimer

Figure 2.15: Chicago Tribune Tower Competition Entries

2.3. Skyscrapers of the International Style / Modernism

"Each new style gradually emerged from the earlier one when new methods of construction, new materials, new human tasks and viewpoints demanded a change or reconstitution of existing forms." - Otto Wagner -

In 1828, German architect Heinrich Hubsch posed a serious architectural question, "In What Style Should We Build?" With regard to architectural style, the 19th century was a transitional period. In the absence of a strongly governing architectural style, architects tried to find stylistic solutions from Classical or Medieval ones. Instead of stone – the major material for traditional architecture and civil structures – the new material, iron, had begun to be used in civil structures such as bridges and incidentally in architecture from the late 18th century. However, at the time of Hubsch's publication, the use of iron in architecture was not significant. Some embryo of new style began to grow, but it was not conspicuous until around the turn of the century.

A stylistic breakthrough using iron and glass as building materials can be found from the renowned Crystal Palace constructed during the mid-19th century. The Crystal Palace is, as Nikolaus Pevsner noted, "the mid-nineteenth century touchstone, if one wishes to

discover what belongs wholly to the nineteenth century and what points forward into the twentieth." This was the skeletal structure with glass skin, "architecture as volume" with "regularity" without "applied decorations." It literally fitted the definition of the International Style of the mid-20th century. However, architects and critics did not welcome this new architecture at the time of its construction, and, as a consequence, it did not immediately further grow as a new style. For instance, Pugin called the Crystal Palace a "glass monster."

The most significant use of iron/steel and glass in architecture emerged during the late 19th century in the U.S. The development of a new building type – skyscrapers – necessitated the use of iron – later steel – skeleton and glass skin. The iron/steel skeletal structure for tall buildings was the invention of the Chicago architects as was discussed earlier.[18] In terms of style, early tall buildings in Chicago foresaw the emergence of the International Style decades later.

In his book, Hubsch noted that climate and building material are the two principal formative factors of style. They are fundamental considerations in any architecture, which must be built with proper materials on a particular site of a certain climate. Thus, in describing each building element that is the very component of any specific architectural style, his statement regarding climatic condition is quite elaborate.

"In our northern climate, more care must be taken to protect buildings against rain or snow than in the south. The pitch of the roof, normally covered with slate or perhaps even with tiles, must be steeper than on Greek monuments. Furthermore, the projecting upper surface of cornices or other similar parts must have a distinct slope for the water to run off .... If the surface of a projecting cornice is not sufficiently sloped, this surface itself will suffer from weathering. Decay will soon set in ...."

About a century later, the definition of the International Style by Hitchcock and Johnson was concerned with only esthetic qualities of the style as Barr noted. Comparing the description of the roof by Hubsch with that by Hitchcock and Johnson gives interesting insight.

.... the flat roofs normal with modern methods of construction have an essential aesthetic significance. Roofs with a single slant, however, have occasionally been used with success. For they are less massive and simpler than the gabled roofs usual on the buildings of the past. Flat roofs are so much more useful that slanting or rounded roofs are only exceptionally justified.

Climatic considerations could not be found in their book, *The International Style*. This ignorance of the importance of "uncommon ground" in architecture was based on a too

[18] It is interesting to note that New York had much more potential to initiate tall buildings than Chicago with Bogardus' works of iron frames that contained essential features of skeletal frames and curtainwall concepts. However, ironically as Condit pointed out tall buildings emerged from Chicago where iron works were not as developed as New York.

strong belief in promising modern technology at that time because the International Style was the only style based on new technology for the first time since the Gothic style.

Nonetheless, the meaning of the International Style as the definer of the newly emerging esthetic trend in architecture was significant. The early Chicago spirit, which introduced tall buildings of steel frames and glass curtain walls, and various reductionistic modern movements in Europe eventually grew up as a new style. Lightness and transparency based on new technologies were finally defined as a new style and this style prevailed for decades. After the 1893 World Faire, the trend of returning to the traditional image of architecture was strong in New York and even in Chicago.[19] Thus, it seemed as though the new esthetic search was almost forgotten. However, even in the dominance of strong eclecticism, a new esthetic search survived through the buildings such as Sullivan's Carson Pierie Scott Department Store in Chicago (Figure 2.16) and Polk's Hallidie Building in San Fransisco (Figure 2.17). Moreover, European counterpart was already prevalent with new architecture such as Mies' Glass Tower (Figure 2.18), Gropius' Bauhous and Fagus Factory, etc. In spite of so many reactions to the International Style from around the late 1960s, many trends of today's architecture in plural directions are still not quite off the mainstream ideology of it. This is because the esthetic aspiration of the style was based on and integrated with new technologies of the age.

The mid-twentieth century, after the war, was the era of mass production based on the style defined, and technologies developed earlier. The major driving force of tall building developments was economy. Even the once-prevalent height race did not occur after the war until the construction of the World Trade Center and the Sears Tower, completed in 1973 and 1974, respectively. Most tall buildings of the mid-twentieth century employed basically the same structural systems, steel skeletal frames with diagonal wind bracings, developed in the previous century. As the forms of many tall buildings were pure rectangular boxes, even some structural

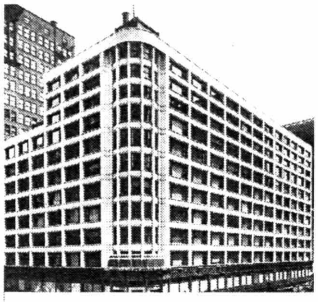

Figure 2.16: Carson Pierie Scott Department Store

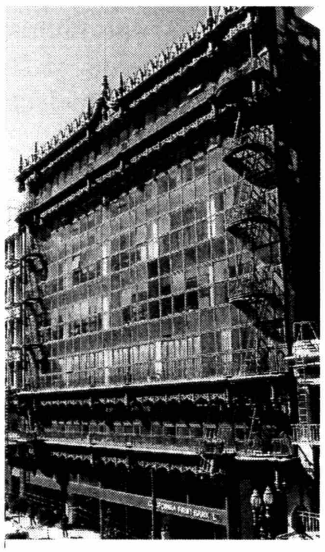

Figure 2.17: Hallidie Building

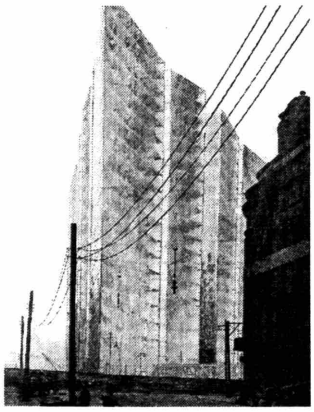

Figure 2.18: Glass Tower

[19] Sullivan commented about the World Faire that "the damage wrought to this country by the Chicago World Faire will last a half a century." And as Gideon noted, his prediction was generally what happened to architecture in the U.S.

adjustments such as transfer girders required to produce setback forms of previous decades were seldom necessary.

Each floor of the early tall buildings was composed of small offices divided by fixed partitions. As the system of business became bigger and as new scientific management systems emerged, the demand for open space increased. In order to create more desirable column-free office spaces more efficiently, a modified structural concept emerged. Even though a very early example of the column-free office space can be found in the Gulf Oil Building (1932) in Pittsburgh [20] (Figure 2.19: Typical Floor Structural Framing Plan), it was from the 1960s that major new structural systems began to be developed for that purpose.

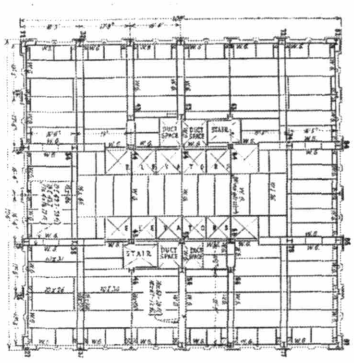

Figure 2.19: Gulf Oil Building

Tubular structures concentrate most lateral load-resisting structural members on the perimeters of buildings in order to achieve cantilevered tube action. As modified versions of the earlier framed structures, this approach generated varied versions of esthetics as well with, its several different configurations. A framed tube system was employed for the World Trade Center in New York (Figure 2.20), a braced tube for the John Hancock Building in Chicago (Figure 2.21), and a bundled tube system for the Sears Tower in Chicago (Figure 2.22). In these types of structures, structural members no longer exist intermittently behind glass curtain walls. They express themselves more actively on facades. In fact, structure itself becomes façade.

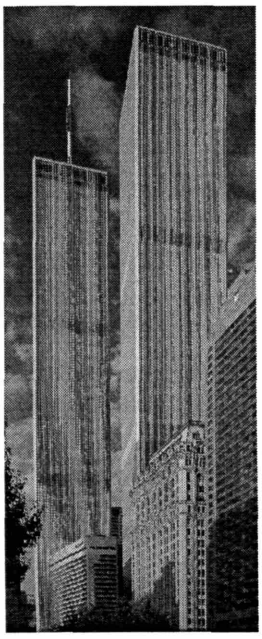

Figure 2.20: World Trade Center

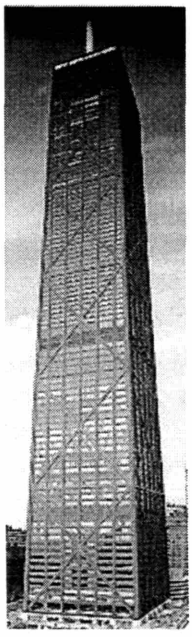

Figure 2.21: John Hancock Center

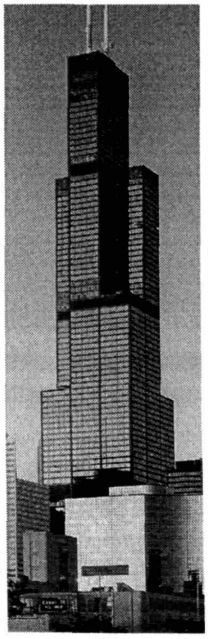

Figure 2.22: Sears Tower

[20] Condit (1961), *American Building Art: The 20th Century,* p. 25

Another concept developed was core-supported outrigger structures. While the nature of tubular structures requires many very closely spaced perimeter columns, this structural system, in most cases, needs only several super-columns connected to the shear walls of the building core by outriggers and some gravity columns on the building perimeter. (Sometimes belt trusses are employed in the system at the locations of outriggers to connect the perimeter columns. In that case, the columns may or may not be super-columns.) A very early example of outrigger structure can be found in the 1960s Place Victoria Office Tower in Montreal designed by Nervi and Moretti (Figure 2.23 and 2.24). However, major application of this type of structural system is on contemporary tall buildings such as the Jin Mao Building in Shanghai and the Taipei 101 in Taipei. Even though the structural systems employed are basically the same, the Place Victoria Office Tower, built during the peak modern period, boasts prismatic modern esthetics, whereas the Jin Mao Building and the Taipei 101, built in the late 20th and very early 21st century, respectively, borrow regional motives for their esthetics.

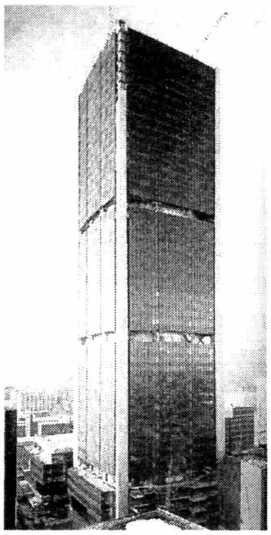

Figure 2.23: Place Victoria Office Tower

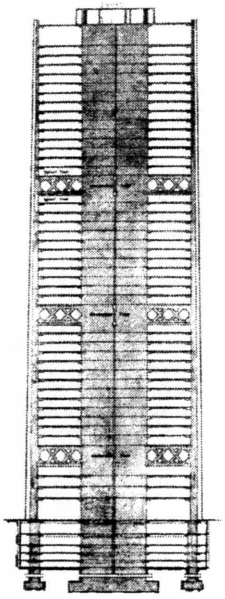

Figure 2.24: Place Victoria Office Section

More recently, diagrid structural systems, with their powerful structural rationale, are emerging as a new esthetic direction in the design of tall buildings. The difference between conventional exterior-braced frame structures and today's diagrid structures is that, for diagrid structures, almost all the conventional vertical columns are eliminated. This is possible because the diagonal members in diagrid structural systems can carry not only lateral forces but also gravity forces due to their triangulated configuration, whereas the diagonals in conventional braced frame structures carry only lateral loads. An early example of the diagrid structure is the IBM building (Figure 5.2) in Pittsburgh built in the early 1960s. With its 13-story height, this building was not given much attention by architects and engineers at that time. Only recently have notable diagrid tall buildings been commissioned. More detailed discussion on diagrid structures is presented in Chapter 6.

There also have been some other structural approaches for tall buildings such as staggered truss system developed by William LeMessurier at MIT in the 1970s and stressed steel skins employed for the One Mellon Bank Center in the 1980s. All of these structural variations, coming from the efforts to find more efficient systems than already-traditional steel braced frames to satisfy varying requirements, are on the general evolutionary track of technology. Primarily, they are driven by function/performance. However, depending on the configuration of each system, some systems such as tubular structures and diagrid structures have major impact on the building esthetics as well. In addition, some tall buildings, such as Hotel de las Artas in Barcelona (Figure 2.25) or

Tokyo Marine Building in Osaka (Figure 2.26), locate their primary lateral load resisting systems even farther out, away from their glass facades, letting them act as primary building identifiers.

Some other important – but not tall building specific – sub-technologies, such as the development of high strength steel and replacement of riveted connections with welded or bolted ones, had significant influence on the evolution of tall building structural systems. However, due to their nature, they did not have much direct impact on the building esthetics.

From the 1950s, not only steel but also reinforced concrete (RC) began to be more frequently used for tall building structures, producing different esthetic expressions from those produced by steel. In fact, the use of reinforced concrete in tall buildings was not new. Already in 1903, the Ingalls Building by Elzner and Anderson in Cincinnati reached 15 stories. However, it was not until the 1950s that reinforced concrete began to be more actively adopted for the structures of tall buildings with the development of RC shear wall structures with flat plates and load-bearing screen walls. Sometimes reinforced concrete was used alone and sometimes it was combined with steel structures.

Tall building envelope systems also went through many variations under the umbrella of Modernism. From Viollet-le-Duc's metaphor of architecture as crystal, through Scheerbart[21] and Taut's Glass Chain and later Rowe and Slutzky's literal and phenomenal transparency, to the present, transparency has been one of the most significant themes of the modern architecture. Following Rowe and Slutzky's distinction, literal transparency has been achieved through the use of glass in architecture.[22] Visual transparency also meant, however, environmental transparency due to the characteristics of glass – especially early uses of glass. Consequently, environmental control relied mostly on mechanical HVAC systems developed by Carrier in

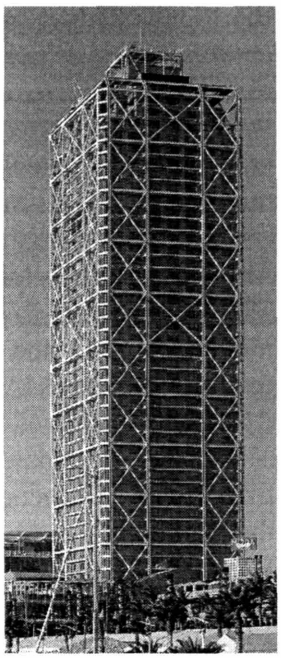

Figure 2.25: Hotel de las Artas

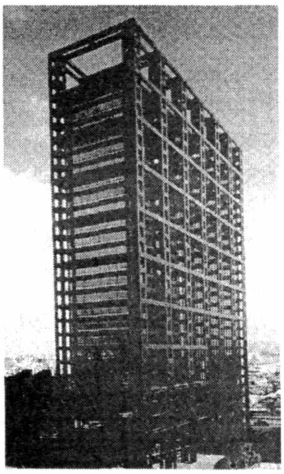

Figure 2.26: Tokyo Marine Building

[21] *"We mostly live in enclosed rooms. These form the environment that gives rise to our culture. In a way our culture is a product of our architecture. In order to raise our culture to a higher level, we are forced, whether we like it or not, to change our architecture. And this will be possible only if we free the rooms in which we live of their enclosed character. This, however, we can only do by introducing a glass architecture, which admits the light of the sun, of the moon, and of the stars into the rooms, not only through a few windows, but through as many walls as feasible..... The new environment we produce in this way has to bring us a new culture."* - Sheerbart -

[22] In fact, by comparing Gropius and Corbusier's works, Rowe and Slutzky evaluated Corbusier's phenomenal transparency as having much superior esthetic value than Gropius' literal transparency, which was achieved by actual transparent glasses.

the 1930s. This apparent architectural conflict between the contemporary esthetic ideology and the more fundamental functional requirement was won by esthetics, and the weakened function of building façades as an environmental mediator was maintained by consuming more energy.

The early tall buildings of the International Style in the 1930s were not so transparent and not so modern yet, including even the tall buildings exhibited during the exhibition at MoMA. The McGraw Hill Building (Figure 2.27) was criticized for its regular setback. Even though setback was mandated by the New York zoning law at that time, from Hitchcock and Johnson's esthetic viewpoint, the setback should be subtle as with the Daily News Building (Figure 2.28). However, the Daily News Building was not an exception from criticism due to its vertical expression instead of horizontality. In fact, despite the fact that these two buildings were included in the exhibition, they are highly ornamental if observed closely, which is directly adverse to the third principle of the style, avoidance of applied decoration.

Figure 2.27: McGraw Hill Building

Frederick Koeper well describes the scale-wise characteristic of the decoration applied to the exterior of modernistic tall buildings.

"Curiously and not altogether appropriately, this style of surface ornament and rich materials, so effective in interior design and objects of luxury, was applied to the outside of giant skyscrapers. The small scale characteristic of Art Deco was hardly suited to the bulk and economic purpose of the skyscraper; yet Art Deco ornament satisfied a certain self-conscious urban taste for modernity, albeit much of it is lost to the distant eye."[23]

Figure 2.28: Daily News Building

Tall buildings employing truly modern style facades began to be built after the war.[24] A notable example is the SOM-

[23] Built in the transitional period, the McGraw Building and Daily News Building stand stylistically somewhere between Modern and Art Deco.

[24] It is worth to noting that PSFS building designed by Howe and Lescaze is an early modern style skyscraper constructed before the war. This building is modern style not only in terms of aesthetics but also the technological features it employed. In terms of structure, overall an ordinary steel skeletal structure is used, but a special feature included is 17 feet deep huge trusses, which span 63 feet and transfer the load from 30 stories above in order to provide a second floor banking hall. The façade is composed of

designed Lever House (Figure 2.29). The original curtainwall of the Lever House constructed a half century ago was composed of stainless steel mullions (supported from inside by carbon steel channels and angles), blue-green wire-glass spandrel, and light green tinted vision glass (Figure 2.30). With its very thin mullions and clear light tinted glass, it has the quality of "literal transparency" and through this transparency the structural columns inside are visible. Architecture as a volume with regularity without applied ornaments was truly achieved by modern technology in the Lever House. New architectural style incorporating new technology thus reflecting the spirit of the age was accomplished in the Lever House and numerous imitation works followed after this building.

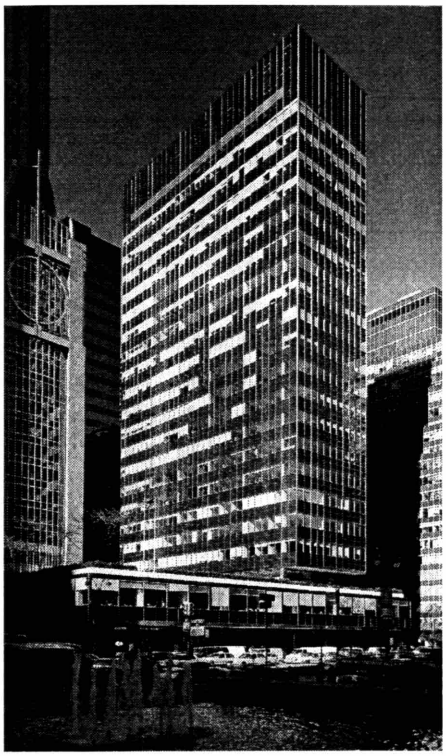

Figure 2.29: Lever House

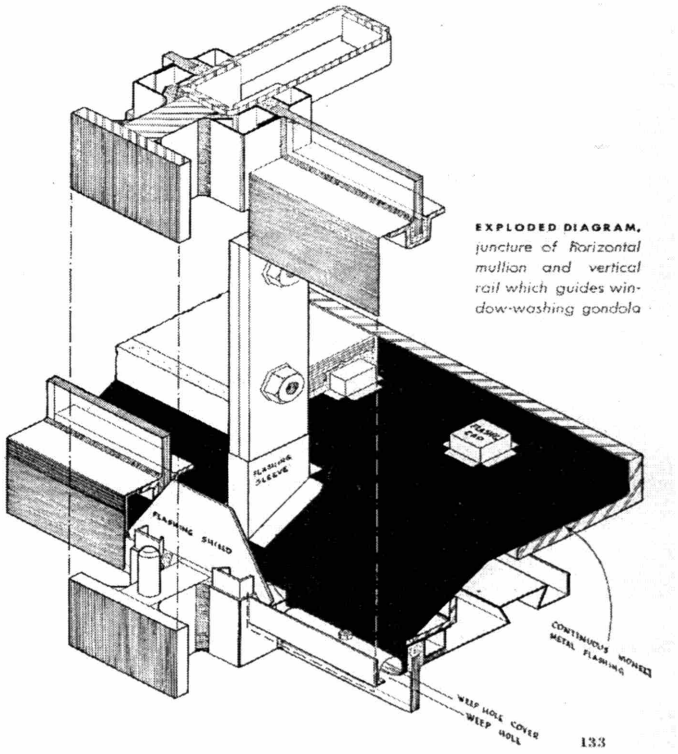

Figure 2.30: Curtain Wall Detail of Lever House

Time did not flow without giving any penalty, however, for using the technology in its infancy. Most original glass curtainwall systems on the façade of the Lever House failed, and as a consequence this building recently went through an entire exterior curtainwall restoration.[25] Due to its significant position in the history of modern architecture, debates

---

horizontal bands of aluminum windows and brick spandrels. Also, PSFS was the second major building equipped with modern mechanical HVAC systems. This more than 70 year old building is still well functioning without major restoration works, especially with regard to façade, which has much to do with the style.

[25] Even though a drainage mechanism was provided in the mullion system, due to the inadequate characteristics of polysulfide as a sealant and also inadequate provision of weep holes, water penetrated through the stainless steel mullion cover, corroding the carbon channels and the ends of wire in the wire-glass spandrels. As the wire expanded due to the corrosion and also because it is inherently less resistant to

on authenticity prevailed at the time of the restoration of the façades of the Lever House and it left a question regarding one extreme branch of metaphors of modern architecture, the metaphor of the machine initially conceived by Viollet-le-Duc. If considered as a machine, any components of a modern building can be replaced whenever their longevity is reached without considering authenticity because they were designed as parts of a machine to make it fully functional. Thus, if a copy of the original part is not available due to the time gap, any compatible part that can make the machine fully functional or possibly even more functional can replace the original part.

The restoration process of the Lever House was, however, different from that of any machine part. To preserve the Lever House built a half century ago, exact imitation was deliberately pursued. Light green tinted single pane vision glass panels, which represent the status of the technology at the time of original construction but do not correspond to the technology and energy-conscious design at the time of restoration, were selected in order to give the building façade exactly the same tone and transparency as the original. Moreover, fake mullions were introduced at the middle of the spandrel panels (Figure 2.32). The original spandrel panels were composed of two panes of blue-green wire-glasses connected by mullions in-between, due to the limitation of size available at the time of original construction (Figure 2.31). However, the blue-green back-painted spandrel glass panels used for restoration works were single panes divided by non-functioning fake mullions at the mid-height in order to imitate the original look.

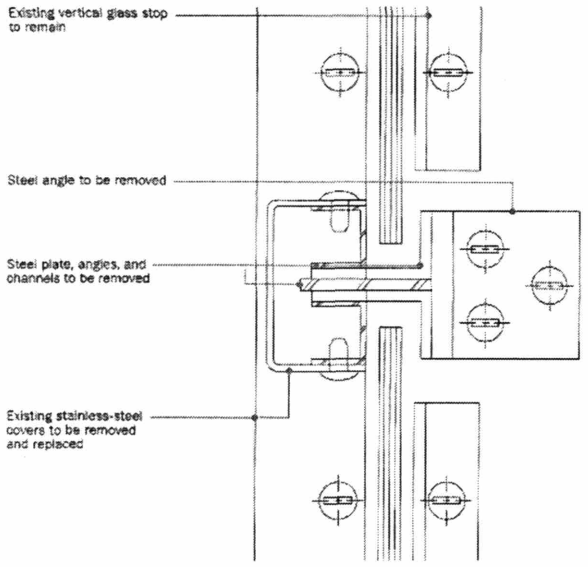

Figure 2.31: Original Spandrel Glass Mullion Detail of Lever House

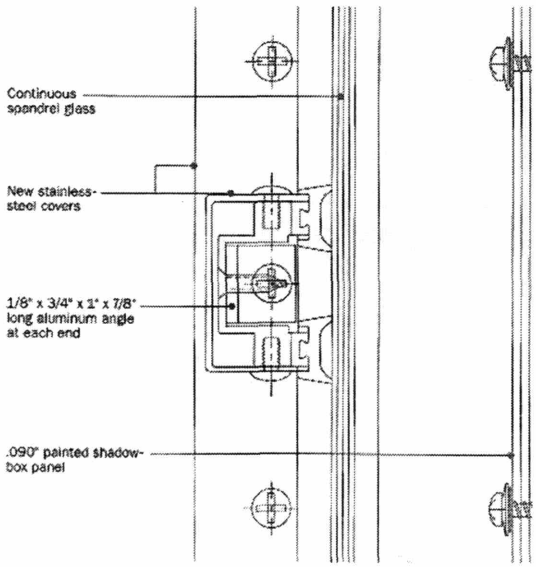

Figure 2.32: New Spandrel Glass Mullion Detail of Lever House

temperature fluctuation, the spandrel panels began to crack, leaving almost no original panels at the time of the restoration. Some vision glass panels also cracked, possibly due to the compression from the hardened polysulfide sealant, thermal movement, and corrosion of carbon steel channels.

Truly technology-based machine architecture is ephemeral. Is modern architecture ephemeral or is the machine metaphor just a metaphor? If modern style curtainwall façades and traditional load-bearing stone façades are compared, in a sense, similar effort is discovered with regard to their complexity, but in a reversed fashion. Inside the elaborately decorated stone façade is just solid stone itself, which also acts as load-bearing structural members that are stacked using relatively simple joints. In contrast, even though modern metal and glass façades are designed to look very simple to observers, their usually hidden connection mechanisms to the primary structures and inside of some mullions, especially horizontal ones, are quite sophisticated.

Modern style was achieved based on new technology that supports, or was believed to support, new design ideology. This new design approach converted the ornamental complication of traditional architecture to the machine-like complication. Here comes the conflict between modern technology and representation, raising another serious question regarding function/performance. Did modern technology work as a supporting backbone of new style? Traditional architecture, which is more representational, is different from modern architecture, which has more technology-oriented machine-like character. The Parthenon still appeals to people's emotion more than two millennia later. Do people expect the same response from the Lever House? Traditional architecture and modern architecture are different breeds. Buildings are designed and built within the limitation of the available technology at the time of their construction. The limitation was much more severe in previous eras. Today, architectural style has become a matter of choice from a broader library based on accumulated available technologies. Modern architecture might be understood as a compromise between ephemeral technology and eternal representation.

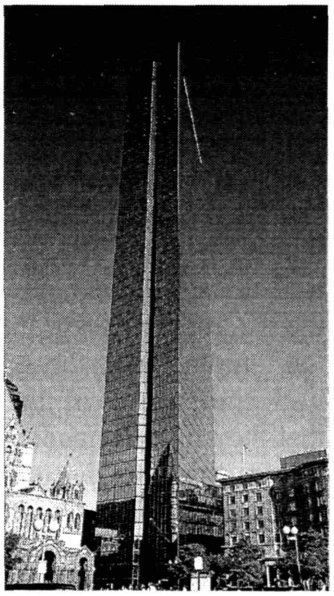

Figure 2.33: John Hancock Building

From around the late 1960s, a new esthetic aspiration different from that of the Lever House began to emerge. Instead of the articulated surfaces through the neo-classical arrangement of Miesian mullions, preference for smoother surfaces prevailed. An initial design strategy to accomplish this smoothness was to minimize the visible portions of mullions from the surface of the facades as in the John Hancock Building in Boston (Figure 2.33). Soon, esthetic-driven new technology – structural silicone – enabled architects to visually eliminate mullions from the exterior as in the Allied Bank in Houston (Figure 2.34). Almost parallel with the preference for smooth surfaces, transparent tinted glasses began to be replaced by mirrored glasses.

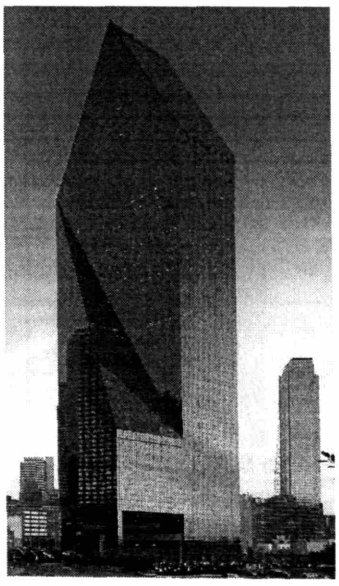

Figure 2.34: Allied Bank

See-through Miesian glass boxes with hierachical articulations of structures and mullions transformed into geometric forms of mirrored glasses that reflect the surroundings in the daytime and expose Miesian articulations at night. Recently, point fixings have been used for glass façade constructions for mullionless surfaces, producing somewhat different esthetics from what structural silicones generate.

More recent environmental design strategy has produced many notable tall buildings that employ various advanced technologies such as double skin facades.[26] They are on the general path of performance-based technological evolution. However, their esthetic impact is not ignorable. Their perceptual visual transparency is much greater than conventional single skin facades. (Thus, not surprisingly in the field of architecture, some architects use this system primarily for esthetic reasons and justify it with its better performance.) This design strategy is in the continuing mainstream of modern architecture today.

2.4. Reactions to International Style

Reactionary movements to modern tall buildings occurred from the early 1980s based on the theoretical background of the late 1960s. The first work of the so-called post-modern tall buildings was the AT&T building (Figure 2.35) in New York by Philip Johnson, one of the proponents of the International Style decades before. Post-modern architects noted that they tried to recover the meaning lost during the Modern period and to continue the culture that was discontinued also during the Modern period. As the means to achieve these goals, they adopted various traditional architectural forms and clothes for their buildings, even though in most cases it is very difficult to find the relevance of these to the context in which they were inserted.

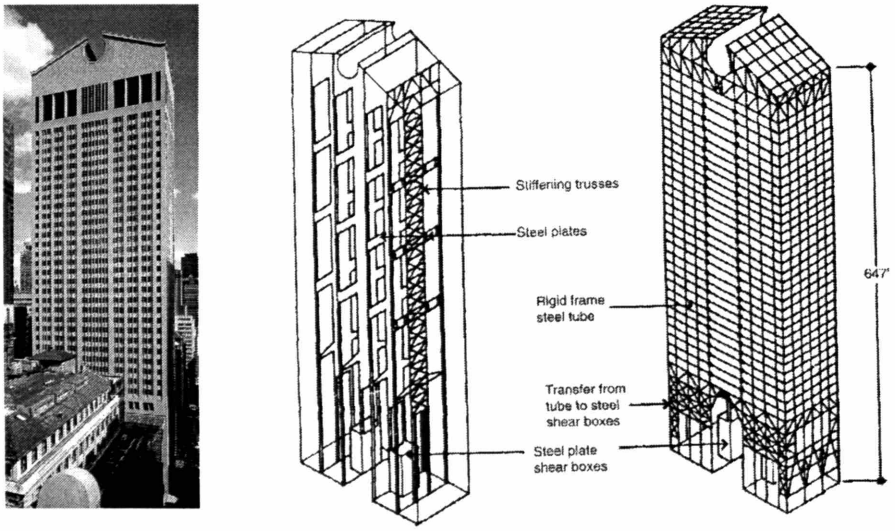

Figure 2.35: AT&T Building

[26] Double skin facades showed up intermittently in the U.S. such as Warren Petroleum Building in Tulsa in 1950s and Occidental Chemical Center in 1980s.

Behind these traditional gestures were apparently modern technologies - steel skeletal structures and curtainwall concept a century old already. Thus, post-modern tall buildings can be interpreted as the products of reaction to the evolutionary pace of modern technology compared with the revolutionary one of the previous century. They camouflage a hundred-year-old technological solution with traditional-looking façades produced and hung by modern technology. Indeed, with the lapse of time accompanying technological advances, architectural styles have accumulated and it has become possible for architects to choose any style from a broader library. However, the choice should be made with zeitgeist. Arbitrary choices may create only an anachronistic architectural environment.

Another type of reaction to the evolutionary pace of technology is ironically exaggerated advocatative expression of technology through the design of building exteriors. In terms of actually applied technology, so-called high-tech architecture still employs general contemporary technology in most cases. However, the architecture of this trend tries to elaborately express it in order to pretend that there has been a significant technological evolution. Even though technological evolution generally accompanies economy of building construction, the architecture of this style is never economic. In fact, it is much more expensive.

Comparison of the statistics of tall building developments between overall and the last ten years denotes that the most active tall building development region has been shifting from North America to Asia over the last decade (Table 2.2 from www.skyscrapers.com). In terms of architectural design, the most significant trend of those tall buildings constructed in various Asian countries is that they use their own regional architectural traditions as main design motives. This trend can be easily seen from notable recent tall buildings such as the Jin Mao Building in Shanghai (Figure 2.36), Petronas Tower in Kuala Lumpur (Figure 2.37), and Landmark Tower in Yokohama (Figure 2. 38).

HIGH-RISE BUILDINGS BY REGION (OVERALL)

	Region	Bldgs	Percent
1	N. America	17,765	51.49%
2	Europe	5,881	17.04%
3	Asia	5,412	15.69%
4	Middle East	2,071	6.00%
5	Oceania	1,637	4.74%
6	S. America	1,352	3.92%
7	Africa	386	1.12%

HIGH-RISE BUILDINGS BY REGION (LAST 10 YEARS)

	Region	Bldgs	Percent
1	Asia	1,797	32.67%
2	N. America	1,711	31.11%
3	Europe	905	16.45%
4	Middle East	488	8.87%
5	Oceania	335	6.09%
6	S. America	213	3.87%
7	Africa	51	0.93%

Table 2.2

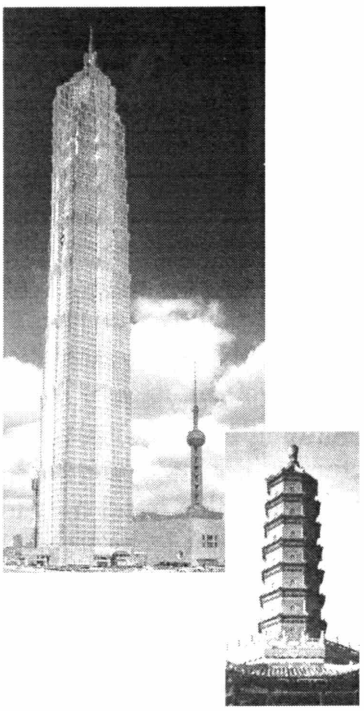

Figure 2.36: Jin Mao Building

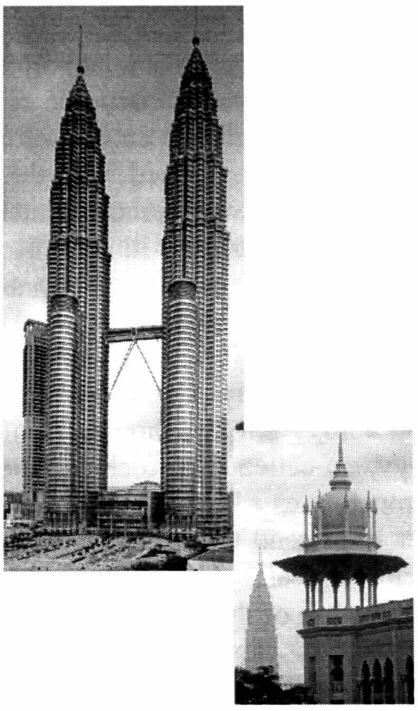

Figure 2.37: Petronas Tower

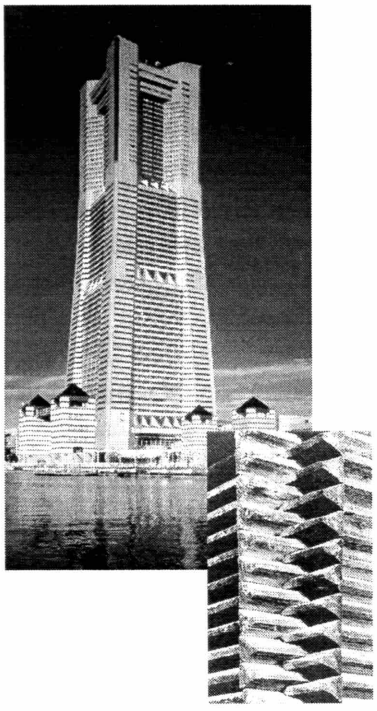

Figure 2.38: Landmark Tower

The history of Regionalism has comes with the history of architecture from Roman Vitruvius to recent Critical Regionalism of Tzonis, Lefaivre and Frampton. Regional architecture was understood very skeptically by many architects of the International Style. This can be well observed from the "What is happening in modern architecture?" conference held in the MoMA in 1948. Many important figures in modern architecture such as Barr, Hitchcock, Gropius, Blake, Mumford debated on International Style and Regionalism without any fruitful results. Below is part of Mumford's presentation. Certainly his remark did not receive any agreement from architects of the International Style at that time.

"Regionalism has to help people come to grips with the actual conditions of life that make them feel at home. Regional insight has to be used to defend us from the international style, the absurdities of present technology and the despotism of the mechanical order."

Contemporary tall buildings in Asian countries may be categorized as romantic regionalism architecture. These buildings pursue only the images of the traditional architecture of their regions, and their designers are in many cases American architects.[27] This is the marriage of the image of a particular region and the technology of the

[27] Jin Mao building was designed by Skidmore Owings and Merrill, Petronas Tower by Cesar Pelli, and Landmark Tower by Stabins Associates.

International Style. Thus, this trend is, at least, more contextual than post-modern architecture in general.

Another reactionary architectural trend has been so-called deconstructivism since the early 1980s. While post-modern architecture mainly reacts to form and surface of the International Style, deconstructivist architecture does not consider rational planning necessary. Even though there have not been any notable tall buildings built in deconstructivism, some proposals were made by Peter Eisenman and Frank Gehry.[28]

[28] Frank Gehry's works were included in Deconstructivist Architecture exhibition held in the MoMA. However, Gehry does not consider himself as a deconstructist architect.

CHAPTER 3: ORIGINAL AND REMEDIAL TECHNOLOGY IN TALL BUILDINGS

3.1. Original Technology in Tall Buildings

The emergence of Gothic architecture clearly demonstrated the strong interaction between technological evolution and esthetic transitions in the history of architecture. A broad and holistic set of functions was impressively achieved through new technology. The flying buttresses and ribbed vaults of this architecture defined a new and unprecedented benchmark for technology acting as a primary esthetic driver. This development in the structural use of stone for very large buildings signaled an architecture that had no direct precedents and eventually came to originate a new architectural style. This thesis returns to this moment of original invention as evidence of the transformative power of technologically-based esthetic development in architecture. Centuries later, a very similar architectural phenomenon occurred in Chicago and New York when skyscrapers emerged as a new building type.

Considered simply as physical constructs, the early tall buildings in the late 19th century were the results of the pursuit of unprecedented height without the sacrifice of abundant interior light. However, these aspirations can also be explained as the means to a particular economic end. Technological evolution of many kinds often serves in this way.[29] In fact, early tall building developments were based on economic equations - increasing rentable area by stacking office spaces vertically and maximizing the rents of these offices by introducing as much natural light as possible. In order to serve this economic driver, new technologies were pursued that improved upon the conventional load-bearing masonry structures with relatively small punched openings. The result was the iron/steel braced frame structure which minimized the structural depth and width of the building perimeters in order to introduce as much natural light as possible through large openings between the load-bearing elements. Consequently, for the same purpose, the openings were filled with transparent glasses, while the iron/steel structures were clad with other solid materials such as brick or terra cotta. However, fundamental change occurred here in terms of construction. Claddings did not carry any loads from buildings except their own weights. Due to this characteristic of the new cladding systems, they were called "curtain walls" from the time of their emergence in the late 19th century.

Architects at that time then had to confront the startling novelty of this system and formulate esthetic positions that were both respectful of current notions of design while acknowledging the opportunity for innovation. As was discussed earlier, when technology is considered in disciplines that are actively engaged in the interests of art, such as architecture, its esthetic expression is no longer superfluous. Thus, as has happened during shifts in primary building technologies in the past, the architects of Chicago and New York tried to capture the esthetic potentials of the new technology. Lightness and transparency produced by the new technologies of steel skeletal structural

[29] George Basalla (1988) acknowledges that "necessity is the mother of invention." However, he also argues that "necessity is an erroneous explanation of diversity which acknowledges the vast number of different kinds of artifacts or made things available for a long time."

and glass curtainwall systems clearly anticipated new stylistic implications, just as ribbed vaults and flying buttresses had generated Gothic architecture centuries ago. As Turner (1986) pointed out, "a time lag exists between the introduction of new technology and its large scale application to major building projects and a further chronological gap appears between the technological advance and stylistic incorporation of it." However, observing the evolution of tall buildings, the time gaps between these events were very short. In fact, in Chicago, the invention of iron/steel skeletal structures, the application of it to major building projects, and its stylistic incorporation occurred almost simultaneously in the late 19th century, generating the first Chicago School's "Commercial Style."[30]

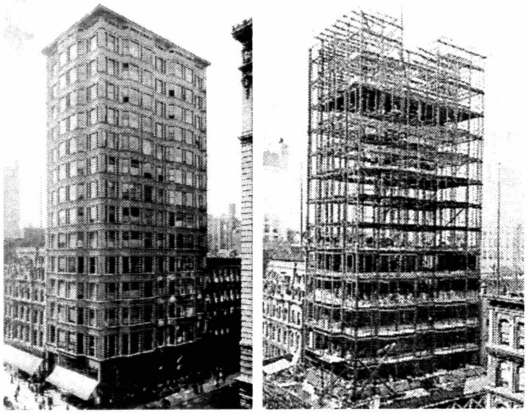

Figure 3.1: Embryo of International Style

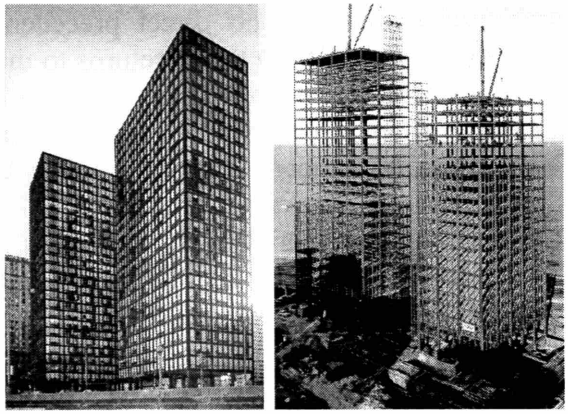

Figure 3.2: International Style

Beginning in the early 1930s and growing strongly after the war, the International Style became the new culmination of technology and architecture. Arising from the stylistic embryo of steel framing and glass curtainwalls introduced in Chicago, the International Style was born (Figure 3.1 and Figure 3.2). The new technology of lightness and transparency fully incorporated the new esthetics, which so consciously expressed the ideology of current technology in terms of its functional goals and performance attributes. In this sense, the new technology of modern steel framing and curtainwall assemblies produced a new building type for the new function of the modern office space. This generated a new esthetic expression, and ultimately originated a new architectural style. For this reason the new technologies of braced steel skeletal structures and glass

[30] This stylistic transition, which began at the turn of the century, was interrupted for about three decades. During the early twentieth century, while European architects were going toward a new reductionistic movement, American counterparts involved in tall building design indulged in eclectic styles, especially Art Deco, from the 1920s to the early 1930s. This phenomenon might be understood as an effort of architects to recover the representational characteristics of architecture lost due to the new technology. Thus, they tried to return to the traditional architecture for representation ironically with new technologies. However, as was discussed in Section 2.2 of this thesis, application of modern movements in tall buildings was only a matter of time. For example, even though Hood and Howell's Gothic style entry won the Chicago Tribune Tower competition in 1922, many entries, such as one by Gropius and Hilbersheimer, clearly denoted upcoming International Style skyscrapers.

curtainwalls may be called "original technology." The 1950s and 1960s were the era of production based on this original technology, without notable technological evolution. As the technologies of these buildings developed and the interest in the esthetics of the International Style grew, the tall buildings of that period were becoming literally "international". Miesian tall buildings could be found not only in Chicago and New York but also in major cities all over the world. The technology was understood and applied internationally and the esthetic interests that supported and resulted from these new assemblies were also adopted globally.

3.2. Remedial Technology for Tall Building Structural Systems

Some notable technological evolution began to occur in the structures of tall buildings from around the late 1960s. For example, tubular structures, which locate primary lateral load-resisting systems at the perimeter of tall buildings, made the structural systems for tall buildings much more efficient and economical. However, despite the economy achieved, the tubular structure is still a varied version of the skeletal frame structure. Thus, even though the tall buildings that employ the tubular concept as their structural systems are quite expressive due to the configuration of the system, it did not shift the intrinsic nature of tall buildings in terms of function and esthetics.

In fact, as a result of increasingly economical structural solutions using less material arranged more efficiently, a new structural motion problem was created. Tall buildings were now safe but not stiff enough for human comfort, a problem not anticipated during the earlier days of structural innovation for these kinds of buildings. For example, the Empire State Building, completed in 1931, could have been designed more efficiently, using less material, if engineered today. The lack of structural analysis tools meant that those involved in its design were understandably conservative in the amount of material necessary for a safe structure. However, this building did not produce any motion-induced human discomfort problem despite its unprecedented enormous height. It was structurally over-designed by today's standards and thus stiff enough not to cause that problem. In contrast, even though 1960s and 1970s' tall buildings, which adopted much lighter structural systems, achieved higher efficiency, they caused serious motion-induced human discomfort problems. This comparison demonstrates the imperfect character of the introduction of original technologies and the necessity for ameliorating steps in subsequent development.

And yet, it is clear that the evolution of structural systems for tall buildings in the direction of lightness, and therefore greater efficiency, is an inevitable and irreversible process. Thus, new technology that emerges to overcome, or at least to reduce, the problems caused by this inevitable evolutionary process in tall buildings is absolutely necessary. Included in this category of new technology are auxiliary damping devices such as the tuned mass dampers installed in the John Hancock Building in Boston (Figure 3.3) and the Citicorp Building in New York, or the viscoelastic dampers of the World Trade Center in New York (Figure 3.4). These new refining technologies, intended to address the issue of excessive motion in towers, do not change the nature of tall buildings

but remedy unforeseen problematic aspects that compromise an acceptable level of performance. In this sense, this evolutionary technology following the revolutionary original one may be called 'remedial technology,' primarily found in the domain of performance.

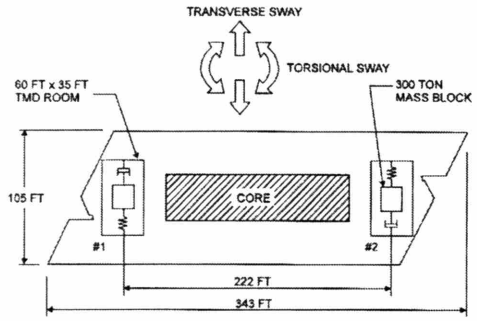

Figure 3.3: Tuned Mass Dampers
Installed in the John Hancock Building

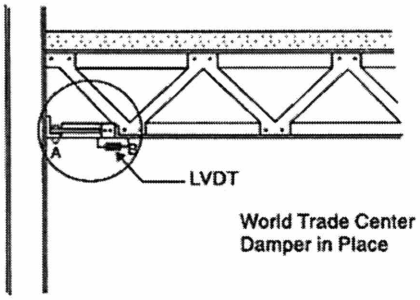

Figure 3.4: Visco-elastic Damper
Installed in the World Trade Center

3.3. Remedial Technology for Tall Building Facade System

Not only structural systems but also façade systems for tall buildings have been going through remedial processes following the breakthrough original technology. Pursuance of transparency in modern architecture dates back to Viollet-le-Duc's Crystal Metaphor in his *Discourses* and culminated in the 1950s and 1960s' modern tall buildings.[31] Even though transparency introduced an abundance of light into building interior spaces, it failed to be an effective environmental mediator between the interior and the exterior.[32]

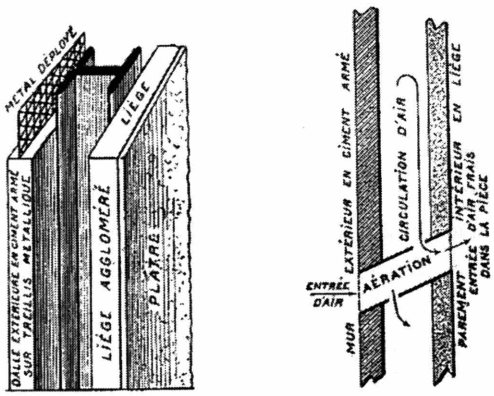

Figure 3.5: Maison Isotherme

---

[31] There were some opposing trends with regard to transparency intervening between the emergence of tall buildings in the late 19th century and the culmination of them in the mid 20th century after World War II. For instance, renowned Art Deco skyscraper architect Ralf Walker's concept of architectural space was opposed to that of transparent volumes. He notes that "to merely build a shed with one or two walls of glass does not create space...it merely interrupts it." While American eclectic architects in the early 20th century were going in a direction somewhat opposed to transparency, their European counterparts pursued it more rigorously. Notable examples among them are Glass Chain's pursuit for transparency through glass in architecture, Mies' glass skyscraper projects during the 1920s, Gropius' Bauhaus design in Dessau, etc.

[32] In fact, fluorescent lamps introduced commercially in April 1938 and displayed publicly in 1939 at the New York World's Fair and the Golden Gate Exposition in San Francisco made the role of natural light much less important than earlier days. According to Murdoch, from 1952, fluorescent lamps passed incandescent lamps as the major source of general lighting in the United States.

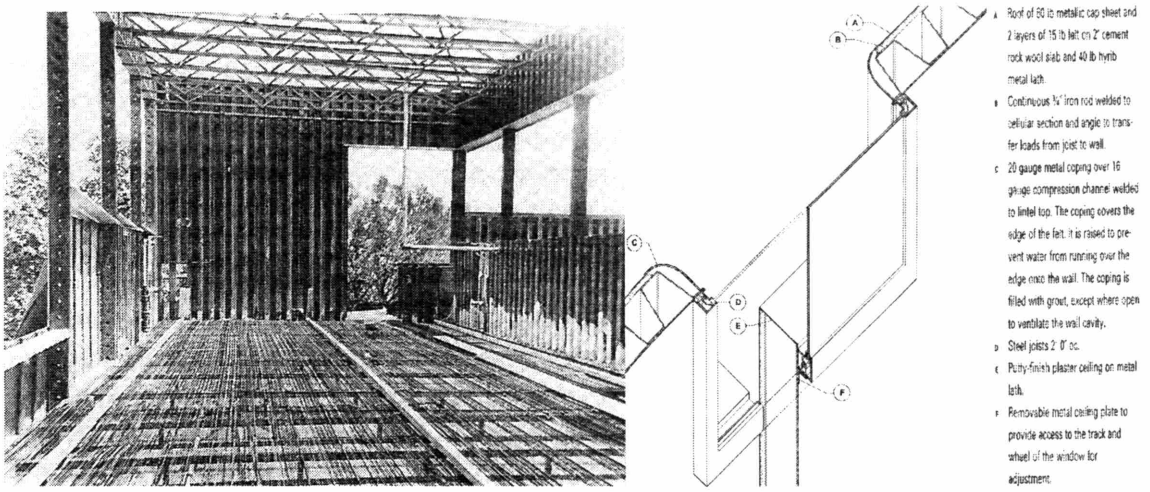

Figure 3.5: Metal Decking Used for Exterior Walls for Ventilation in Beard House

In fact, maintaining the role of the transparent glass façade as an environmental mediator was not neglected at the beginning of the modern movement, especially in Europe. The year 1903 already saw the very early example of glass double skin façade in the Steiff Factory building in Germany. In addition, Paul Scheerbart, while declaring glass as the only proper material for new architecture that can raise our culture to a higher level, proposed the double glass wall as an essential condition for glass architecture, recognizing the inadequacy of the single pane glass wall as an environmental mediator and the role of air as a very effective insulation medium.[33] Also, Le Corbusier's *mur neutralisant* concept, inspired by Maison Isotherme by Raoul Decourt (Figure 3.5), employed a double layer exterior wall, within which conditioned air circulated. In the U.S., even though not a glass wall in particular, Neutra's Beard House in 1935 used metal decking for its exterior wall in order to achieve façade ventilation to provide a more comfortable interior environment (Figure 3.6).

From the early 1950s, the double layer glass, Thermopane, was commercially available. Also, in Germany in 1962, the thermal break was introduced for curtainwall mullion systems. However, it was not until the early 1970s' OPEC oil embargo that energy consumption by buildings was more seriously considered than ever. Recognizing the problem of single pane transparent glass façades, numerous remedial technologies, including reflective glass, insulating glasses, low-E coatings, double skin facades, etc., have been developed. Among them, double skin facades might be considered as the most advanced technology from the viewpoint of performance. Double skin facades being remedial technology, most tall buildings employing glass double skin facades as an exterior envelope system stylistically fall within the category of Modernism in this esthetically plural age. Perceptually, double skin facades produce even more transparent expression.

---

[33] "*As air is one of the worst conductors of heat, the double glass wall is an essential condition for all glass architecture. The walls can be one meter apart - or even farther...*" - Sheerbart -

Today, tall buildings with glass double skin facades can be easily found in Europe. As was discussed earlier, the environmental consideration of workplaces was somehow lost in early days, especially after the Hawthorne Effect in 1924. And ineffective modern glass façade was managed by consumption of more energy. However, consideration of work place environments for better productivity began to be reconsidered by architects and environmental psychologists from the 1960s. Since then, while Europe has been continuously pursuing this goal toward its limit, the interest of the American counterparts has not been as strong as that of Europe. This explains the more advanced status of façade technology in Europe. In the U.S. no notable tall buildings have employed double skin facades. It can be understood in the way that Europe has been much more sensitive to environmental design and also has a much longer history of double skin facades than the U.S. Earlier double skin facades can be found in the U.S. in the Warren Petroleum Building, built in 1958, and the Occidental Chemical Center, completed in1980. Much more recent U.S. examples of double skin facades include the Manulife Building in Boston (Figure 3.7) and the Genzyme Building in Cambridge (Figure 3.8), both completed in the very early 21st century. Considering the increased interest in energy-efficient architecture, it is expected that major tall buildings adopting double skin facades will emerge in the U.S. soon.

Figure 3.7: Manulife Building

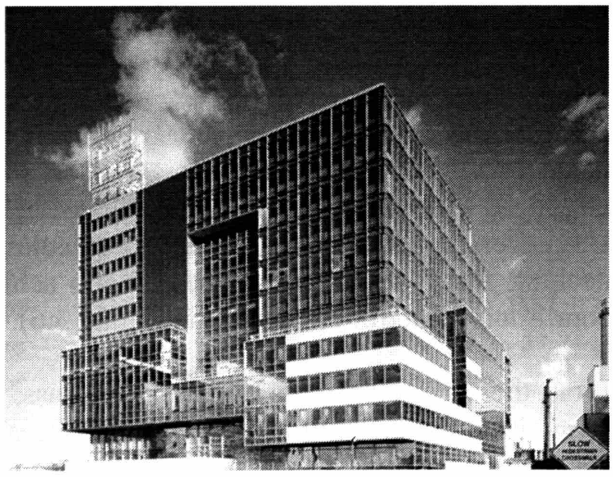

Figure 3.8: Genzyme Building

3.4. Conclusion

Modern architecture means discontinuation of millennia-long traditional architecture. Based on new material/technology, new architecture was created. Classical orders and heavy masonry walls with punched openings were replaced by steel columns/beams and transparent glass curtainwalls. Traditionally hand-crafted architectural elements were replaced by mass-produced ones in factories. The machine metaphor originally introduced by Viollet-le-Duc and reemphasized by Le Corbusier was not just a metaphor any longer. Architecture became a machine itself, and accordingly new esthetic

expression was sought and generalized as a new style. This phenomenon prevailed in the field of architectural practice including tall building developments for decades.

Compared with revolutionary original technology, which introduced a new breed of architecture, remedial technologies follow a typical evolutionary process. In terms of tall buildings, this phenomenon can be well observed by comparing a 1930's study on the most economic height of a tall building in Manhattan with the number of stories of the 200 tallest skyscrapers built up to the present. While engineering height means the height structurally feasible on a given site, the most economic height is the one that would produce the maximum percentage of net return. As Carol Willis noted in her *Form Follows Finance*, at some point in the construction of every skyscraper, the law of diminishing returns sets in, and rents for the additional stories do not cover costs. As buildings go higher, additional cost for most building systems, such as structural systems, becomes greater than proportional. On the contrary, as buildings grow upward, the rentable space is expanded less than proportional due to the encroachment on rentable area by the structural and vertical transportation systems. This sets the most economic height at a certain level. According to Clark and Kingston's study in 1930 among several different height schemes, 63 stories was the most economical choice for a

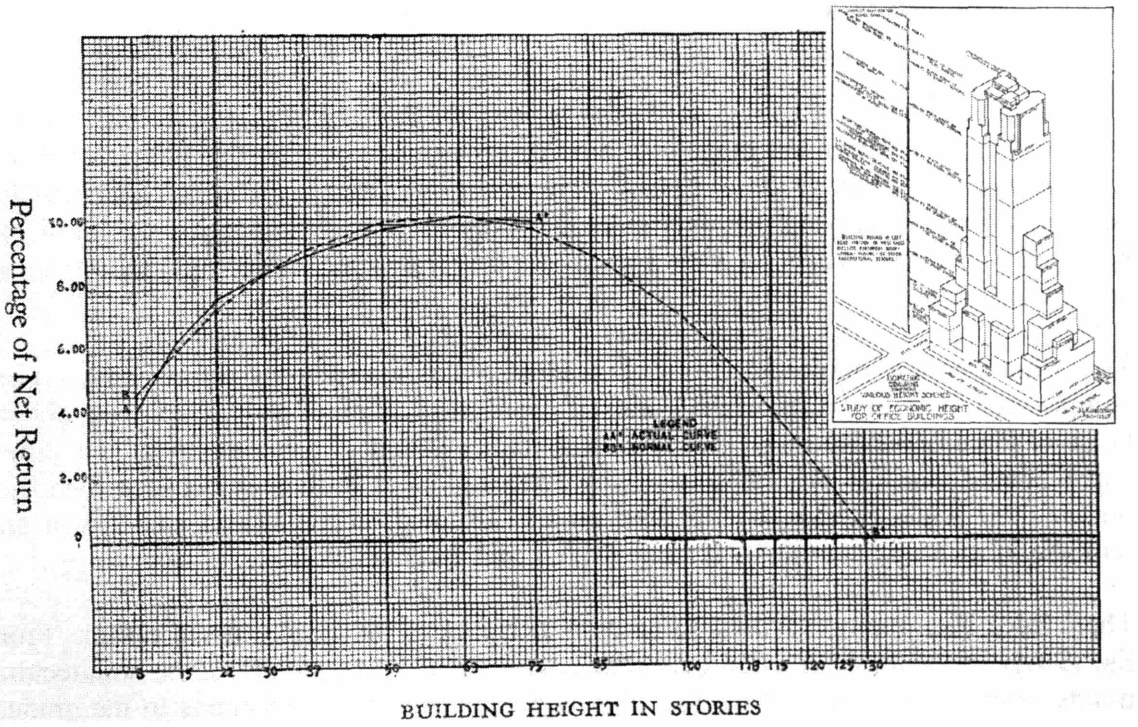

Figure 3.9: Economic Manhattan Building Height Study by Clark and Kingston in 1930

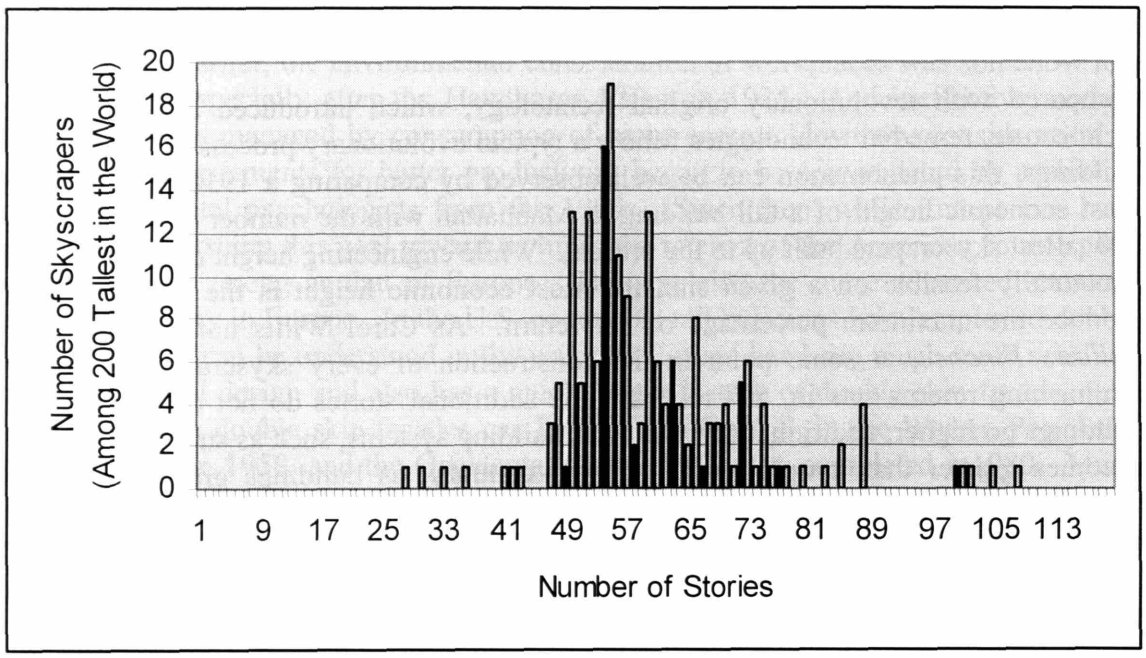

Figure 3.10: Story Heights of 200 Tallest Buildings in the World

Manhattan skyscraper (Figure 3.9). Today, among the 200 tallest buildings in the world, 76% of them are within the range of 50 to 70 stories, showing that this range is still the most economic height (Figure 3.10).[34] There has not been significant change in the economic height, implying that over more than seventy years technological evolution has been very gradual, which is very typical for any remedial technology following an epochal original one.

This phenomenon may look ironical because today's technologies are much more complicated than the crude original one. (If the sophistication of technology were able to be measured quantitatively, today's technology might be more than ten times sophisticated than the original one.) However, the major difference between them lies not in their sophistication but in their nature. Original technology is idea-driven and remedial ones today are mostly science-driven, and that matters.

There have been many reactions to modern architecture, as was discussed earlier. From the viewpoint of the interaction between technology and architecture, some architectural trends, such as post-modernism and high tech architecture, are reactions to the gradual phase of technological evolution after the breakthrough original technology.

[34] Land value is also an important factor in deciding a tall building's economic height. However, even considering the importance of land value (e.g. Manhattan vs. the average big city of the world), there is no better explanation for the lack of significant change of economic building height than the gradual evolution process of technology after the breakthrough.

Today's architecture, including tall buildings, can be understood only through recognition of the dominance of cultural pluralism. However, it is also useful to recognize that today's pluralism in architecture can be substantially understood as the result of an intellectual and cultural "branching out" from the notion of a modern architecture based on modern technology. In fact, viewed in this way, modern architecture may now be entering its culminating phase through necessary accretion of remedial technologies. Reactions to this phase may be understood as premature pursuance of new architecture even when the typical follow-up evolutionary phase of technology after the initial revolutionary one has not yet been finished. This viewpoint well explains many recent "-isms" of short longevity. Another revolutionary technology might put an end to today's pluralism and lead to a new breed of architecture. And that new breed of architecture will be again followed by refining remedial technologies for its culmination, just as is happening with today's architecture.

CHAPTER 4:
TECHNOLOGICAL LIMITATIONS OF TALL BUILDINGS AND FUTURE DIRECTION

As has been discussed so far, there has been notable evolution of technology since the emergence of tall buildings in the late 19th century. However, many technological limitations still exist. Indeed this is inevitable because of not only the experimental imperfect nature of original technology but also the conflicting perceptual dual characteristics of any modern technology. The promising reliability of modern technology enabled architecture to finally move away from traditional architecture toward a more modern approach. However, the other side of this promise has been the ephemeral nature of technology. This is because the expected rate of technological evolution based on the promising attributes exceeds the actual rate of the evolution to meet this expectation. Also, the incremental rate of technology-related human requirements of modern society exceeds the actual rate of the evolution to meet these requirements, making the status of technology ever imperfect.

The ephemeral nature and the promise of technology are in conflict in modern architecture. In tall buildings, which generally require the most advanced and varied contemporary technologies due to their very tallness and scale, this conflict is dominantly observed as their technological limitations. The most critical technological limitations of tall buildings can be found in their structures, facades, and vertical transportations. The following sections primarily discuss the first two systems in more detail. The discussion of vertical transportation systems is limited in this thesis, not because it is less important but because it is less relevant to the theme of this research.

4.1 Technological Limitations of Structures in Tall Buildings

The direction of the evolution of tall building structural systems, based on new structural concepts with newly adopted materials and construction methods, has been towards augmented efficiency. Variously configured tubular structures and core-supported outrigger structures demonstrate this fact well. Consequently, tall building structural systems have become much lighter than earlier ones. This direction of the structural evolution toward lightness has caused serious structural motion problems – primarily wind-induced lateral motion problems. The control of this structural motion should be considered with regard to static loads as well as dynamic loads. Against the static portion of wind loads, stiffer structures produce less lateral displacement. With regard to the dynamic portion of wind loads, the response of not only windward direction but also across-wind direction should be considered. Generally, in tall buildings, the lateral vibration of vortex-shedding-induced across-wind direction is much greater than that of windward direction. Regarding both directions, structures with more damping reduce the magnitude of vibration and cease the vibration more quickly. With regard to the vibration of vortex-shedding-induced across-wind direction, a stiffer structure reduces the probability of lock-in condition because as a structure's fundamental frequency increases, wind velocity that causes the lock-in condition also increases (Figure 4.1).

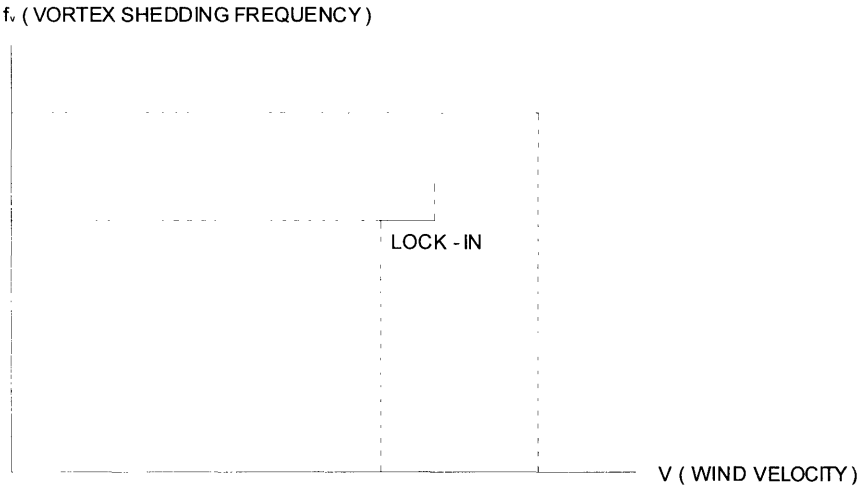

Figure 4.1: Vortex-Shedding-Induced Lock-In Condition

Since the natural direction of structural evolution towards lightness will not be reversed, more stiffness and more damping should be achieved with a minimum amount of material. Recently, diagrid structures have been emerging as a new structural trend, providing stiffness very efficiently in tall buildings. Considering its structural efficiency and architectural significance as a newly emerging esthetics of tall buildings at the time of this research, Chapter 6 of this thesis is devoted to the investigation of the structural performances and architectural potentials of diagrid structures. Chapter 7 and Chapter 8 investigate the strategy of increasing damping through design integration between the structural system and the façade system. Both studies are approached not only as appropriate structural design strategies to minimize the technological limitations – structural-motion-related problems – but also as potential architectural esthetic drivers in tall buildings.

From the viewpoint of structural material's property, as Connor (2003) noted "the lag in material stiffness versus material strength has led to a problem with satisfying the serviceability requirements on the various motion parameters and indeed for very high strength materials it is possible for the serviceability requirements to be dominant." For instance, today structural steels are available from 24 to 100 ksi (170 to 690 MPa). However, its modulus of elasticity remains nearly the same without regard to the change of its strength (Figure 4.2). The change of production process or heat treatment gives impact on the strength but not on the modulus of elasticity of steel. There has been some increase in the modulus of elasticity of concrete (Figure 4.3). However, this increase is relatively small compared with the increase of strength. Also, steel, as the tall-building-originating material from the 19th century, is the more dominant structural material than concrete in tall buildings.

Another structural limitation is highly related to spatial requirements of tall buildings. Each floor of early tall buildings was composed of small offices divided by fixed partitions. As business operation has expanded and as new scientific management systems have emerged, the demand for open space has increased. Also, with the

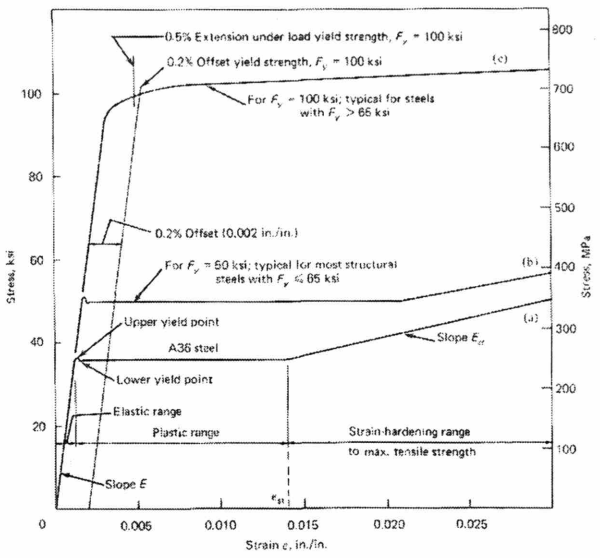

Figure 4.2: Stress vs. Strain for Steel

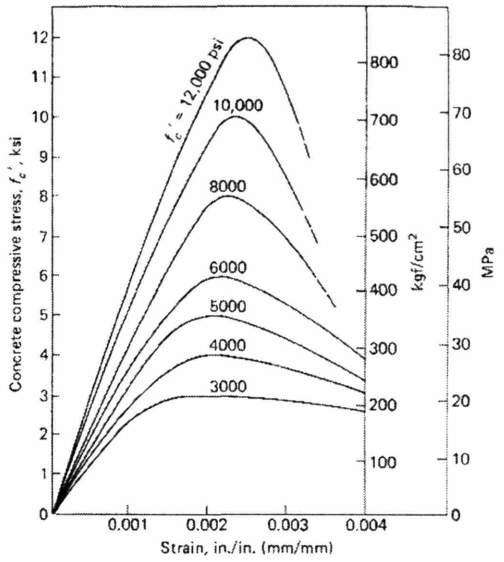

Figure 4.3: Stress vs. Strain for Concrete

development of fluorescent lamps and mechanical HVAC systems during the late 1930s, the substantial increase of office depth – typically measured from the inner face of exterior facade to the outer face of interior core walls – has become possible because the dependence on exterior windows for natural lighting and ventilation has been reduced. Thus, column-free open office spaces have become much more desirable than the earlier fixed-partitioned ones. Even though today's information flow through computer networks makes column-free open plans less necessary, they are still preferable.[35] This preference for column-free open space requires long structural spans, requiring deep beams or trusses, which increase story heights and consequently building heights. In addition, higher demand for HVAC and information system requires deep ceiling space and/or sometimes raised floors. For instance, while the story height of the Empire State Building, whose typical span is about 20 feet, is 11 feet 6 inches, that of the Sears Tower, whose typical span is 75 feet, is 12 feet 10.5 inches. This phenomenon related to spatial requirement makes today's skyscraper structures much taller and thus more flexible compared with the old ones if the same total number of stories are built.

4.2 Technological Limitations of Facades in Tall Buildings

The exterior wall system is normally supported by the primary structural system of tall buildings. As Korista (1989) noted that "the behavior at the interface between the relatively weak, generally non-ductile, individually determinant exterior wall system elements with the higher strength, more ductile, highly redundant structural frame elements is of critical importance …," the differential deformation compatibility between

[35] For a more in-depth discussion on the evolution of space planning in tall office buildings, see Abalos & Herreros, "Tower and Office – From Modernist Theory to Contemporary Practice," Chapter 5, pp. 177 – 215.

the primary structure and façade system is one of the very challenging technical issues of tall building developments, especially in terms of long-term serviceability.[36] Since the emergence of skeletal structure and the curtainwall concept, leading the current status of modern architecture from the viewpoint of technology – thus, even though this new design and construction strategy must be appreciated overall – numerous facade failures have occurred, especially in tall buildings, due to the incompatible deformation performances between their primary structures and façades. These are caused by the relatively large various loads tall buildings should carry due to their tallness.[37]

Another critical consideration with regard to the exterior walls of tall buildings is their fundamental function/performance. The exterior walls act not only as façades, which govern the esthetics of buildings to a great degree, but also as an environmental mediator between the exterior and interior. Often, there have been conflicts between these very subjective and relatively objective requirements. In many cases, especially before early 1970s OPEC oil embargo, the performance requirements of façades as an environmental mediator have been sacrificed, resulting in more energy consumption. However, today's profound shifts in design approaches toward sustainable architecture take energy-saving issues more seriously than ever, leading to the technological challenge to produce more effective and efficient façade systems. Considering this, Chapters 7 and 8 of this thesis are devoted to investigating the potential of double skin facades, not only as an effective environmental mediator but also as a possible structural damping mechanism. Through design integration between primary structures and double skin façades, also pursued are architectural esthetic potentials.

4.3 Design Integration Approach

Modern architecture was technologically approached by using new materials and separating the role of structures and that of non-structural vertical plane architectural components from the traditional load-bearing walls that acted as both. Among the walls freed from their structural roles, facades are of conspicuous importance as building identifiers[38], significant definers of building esthetics, and environmental mediators. Indeed, this separation initiated the history of tall buildings. The meaning of the relative independence of the two systems is more important in tall buildings than in any other building type. Low-rise buildings are still buildable and built with traditional methods of construction in many cases without changing the qualities intended too much. However, it is not feasible to build even medium-rise buildings with traditional load-bearing walls

---

[36] Michael Kim specifies the four fundamental criteria of successful building design; function/performance, esthetics, constructability, and long-term serviceability.

[37] For more detailed discussion on this, see Korista, "Exterior Façade System – Building Structure System, Load-Deformation Behavioral Inter-Relationship," presented in the 1989 Fall Symposium on "Exterior Claddings on High Rise Buildings" in Chicago.

[38] Leatherbarrow, *Uncommon Ground,* p. 72.

because they must occupy too much space at their lower levels to provide sufficient lateral stability. Thus, in tall buildings, adopting the modern concept of design and construction – frame structures and curtainwalls – is not an option but a necessity.[39]

The separation of roles regarding structural and facade systems, however, did not accompany physical separation. In fact, these two distinct systems have always been together with physical contacts for their mutual benefit. Because of this symbiotic relationship between them, it is useful to observe the co-related development of these two systems through the various aspects of the theory of coevolution. However, one must always be careful about applying the theories of one discipline into another due to their similarity. Coevolution is not a human affair, but rather describes what happens in nature with regard to living creatures' function/performance. The judgment of the esthetics of the possible physical changes resulting from coevolution is not within the realm of the human. In contrast, the technological co-development of structures and facades of tall buildings is a process done not by nature but by humans – architects/engineers. In addition, since this co-development is not within the domain of nature but within that of artifacts that encompass art, not only its functional aspect but also its esthetic expression are of critical importance. Thus, the theory of coevolution about the living creatures in the nature can be adopted for a clearer understanding, adjusted in order to be more discipline-specific, and finally transformed into that of design integration regarding architecture in human society.

The separation in conjunction with new materials was the threshold idea of new technology – original technology – and in turn new architecture. Since then, a substantial portion of the primary structural system and the entire façade system have been juxtaposed and connected together at the perimeter of a building. Two systems once-fully-integrated with serious limitations have been relatively separated with minimum connections necessary to contribute to each other to overcome the limitations. Facades have been supported by the components of the primary structures at building perimeters, and in many cases primary structures have been protected from ever-changing harsh outdoor environments by facades. Based on these fundamental mutual contributions, these two systems have (or at least should have) coevolved in order to more effectively minimize the contemporary technological limitations and also towards each other's – in turn a whole building's – better performance. As nature determines the direction of coevolution, architects/engineers control the direction of co-development of the two independent but very closely related systems. In both nature and architecture, one common goal is in the function/performance domain. However, in architecture – a discipline which is actively engaged in the interests of both technology and art – both the functional effectiveness/efficiency and the successful esthetic expression of integrally-designed systems have equal importance.

---

[39] This explains well the traditional theory of the technological invention based on necessity and utility in terms of tall building construction. In terms of tall building development, as George Basalla (1988) noted "necessity is a relative term." "A necessity for one people, generation, or social class may have no utilitarian value or may be a superficial luxury for another people, generation, or social class. A skyscraper is not a structure to protect people from the vagaries of the weather. Necessity is not something imposed by nature upon humanity but is a conceptual category created by cultural choice."

In tall buildings, the meaning of the design integration between their structural system and facades system is of special importance. The location of building perimeters has more structural significance in tall buildings than in any other building type due to their very tallness, which means greater vulnerability to lateral forces, especially wind loads. Also, the role of façade systems in terms of function and esthetics is more significant in tall buildings. In most cases, tall office buildings are stacks of many very similar floors, which have relatively simple space organization – generally open spaces between the inner face of the exterior façade and the outer face of the interior cores with movable partition walls. Thus, the role of facades as an environmental mediator as well as a fundamental building esthetic definer is conspicuous in tall buildings. Due to this special importance of the structural system and façade system at the perimeter of tall buildings and their inevitable physical connections, design integration, which corresponds to the coevolution process in nature, is the approach to be pursued to minimize technological limitations and, in turn, to lead to refined better performance and esthetics.

Due to the special importance in many ways of perimeters in tall buildings, it is expected that many building components are congested at this location. For instance, from the viewpoint of structural behavior, it is quite desirable to concentrate as much lateral load-resisting systems as possible on the perimeter of tall buildings where building facades always are. This may not be architecturally desirable as well, and may even limit architectural potentials at the building perimeter. However, observed from a slightly different angle, this could mean more possibility of design integration because more maneuverable components are concentrated at the same location. It depends on the capability of architects/engineers to transform inevitably-looking factual limitations to potentiality of augmented design integration.

PART II:
TECHNOLOGY IN TALL BUILDINGS AND THEIR ARCHITECTURAL IMPLICATIONS

CHAPTER 5: CONTEMPORARY TALL BUILDING DESIGN PRACTICE

5.1. Technology and Architecture in Contemporary Tall Building Design Practice

Contemporary design practice of tall buildings in many cases is going in the direction of minimizing the technological limitations discussed in the previous chapter. In some cases, technological strategies, induced primarily by function/performance requirement, is fully incorporated with architectural esthetic expression. In other cases, technological strategies serve only for the intended function/performance, and esthetic directions are sought from other sources. This chapter investigates various contemporary tall building design practices through the filter of these issues. Emphasis is given to investigating the interrelationship between the technologies related to structural performance and their esthetic expression.

As buildings become taller, the impact of lateral forces becomes much greater. Lateral forces carried by buildings are typically wind loads and earthquake loads. Tall buildings, which have fundamental periods of several seconds, are in general much more vulnerable to wind loads than seismic loads because a typical period of seismic loads is in the neighborhood of about a second, whereas that of gust and vortex-shedding can be very similar to the fundamental period of tall buildings, resulting in resonance condition.

Various design strategies are employed to reduce the effect of wind loads applied to tall buildings. They can be divided into two categories, passive systems and active systems. Passive systems have fixed properties, and, in order to be performed as intended, they do not require energy, while active systems do need energy source to modify the system properties against ever-changing loads. Thus, active systems are in general much more effective than passive systems. However, due to their economy, passive systems are more commonly used than active systems.

5.1.1. Tall Building Designs with Passive Systems

The first strategy of the passive system category is to increase the lateral stiffness of the structure, which is also the most traditional approach. In order to obtain the necessary lateral stiffness, introduced first were braced frames followed by tubular structures, core-supported outrigger structures, and more recently diagrid structures. In the early braced frames, the braces – the main lateral stiffness provider – are generally constrained within the interior cores, and serve only for structural performance. Consequently, no esthetic expressions are sought from those interior-core-embedded bracings. In the outrigger structures, a lateral load-resisting system is extended from the conventional core to the building perimeter columns through the outriggers that connect them. This basic configuration often requires perimeter super columns and/or belt trusses at the outrigger levels, and these elements of the outrigger system are sometimes incorporated into building esthetics.

Tubular and diagrid structures locate their major lateral load-resisting components at the building perimeters where building facades are. This performance-induced juxtaposition

naturally leads to integrative design approach between the structural system and façade system. As a consequence, in tall buildings that employ these types of structural systems, technological components and architectural esthetic components of building facades are inseparable – eventually the same. These circumstances require very intimate cooperation between architects and engineers.

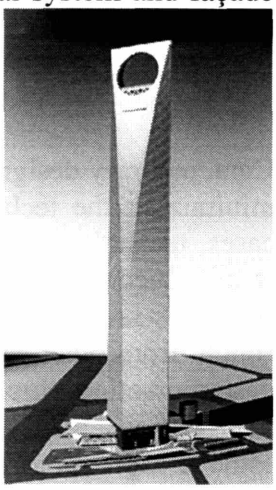

Figure 5.1: World Financial Center

It is not possible to be a master builder today in this culturally and intellectually plural and technologically flooded era. However, what is possible and desirable is to understand fundamental principles of architecture-related disciplines. Understanding the technology, science, and mathematics behind the behavior of building systems is the responsibility of the contemporary architects who want to create high quality architecture. Likewise, understanding fundamental architectural design principles is the responsibility of the engineers who want to achieve high quality engineering products that are incorporated into architecture. This mutual understanding can eventually become the potentiality of enhanced design integration. In this professional context, diagrid structures are investigated in depth as a vehicle to examine this potentiality in Chapter 6.

The second strategy of the passive system category is to improve aerodynamic properties of tall buildings to reduce wind forces carried by them. This can be achieved by various treatments of building masses and forms. Examples employed in contemporary tall building designs are chamfered or rounded corners, streamlined forms, tapered forms, openings through a building, and notches. The Shanghai World Financial Center project by KPF employs a 51-meter diameter through-building round opening at the top of the building combined with a tapered form. The 7 South Dearborn project by SOM has a very slender tower with notches and rounded corners. Due to the nature of the strategy which manipulates building masses and forms, this approach is always incorporated with architectural esthetics[40].

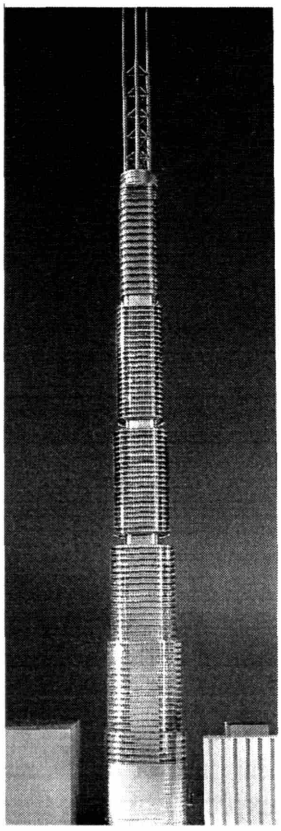

Figure 5.2: 7 South Dearborn

[40] As their primary structural system, the Shanghai World Financial Center employs a tubular structure, and the 7 South Dearborn employs a core-supported outrigger structure below the first notch from the ground. However, in these buildings, these primary structural systems were not explicitly utilized as esthetic drivers of the buildings.

Another interesting approach, which may in a sense be included in the second category, is twisted forms. Twisted forms employed for today's tall buildings can be understood as a reaction to boxed forms of modern architecture. This contemporary architectural phenomenon is not new in architecture. It is comparable to twisted forms of Mannerism architecture at the end of Renaissance architecture. For example, in Cortile della Cavallerizza at Palazzo Ducale in Mantua, Giulio Romano designed twisted columns (Figure 5.2). This twisted form can be found again in today's tall building designs such as the Turning Torso, apartment and office tower, in Malmo, Sweden (Figure 5.3) and the Freedom Tower in the New World Trade Center in New York (Figure 5.4) designed by Santiago Calatrava and SOM respectively. In fact, twisted forms are found not only in contemporary architecture but also in other small scale designs such as vase, perfume container, beverage bottles (Figure 5.5).

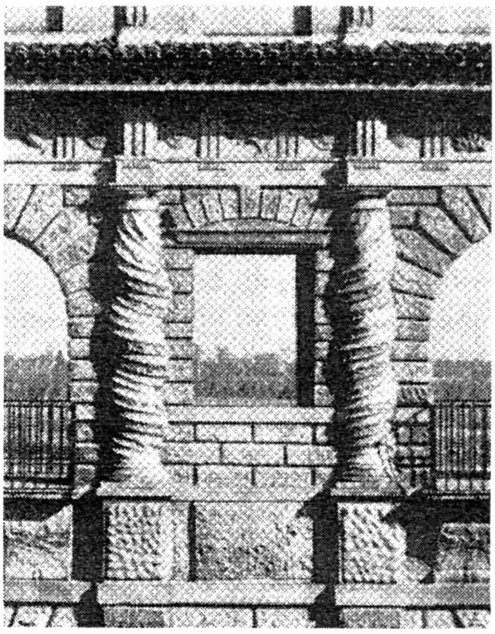

Figure 5.2: Cortile della Cavallerizza, Palazzo Ducale, Mantua

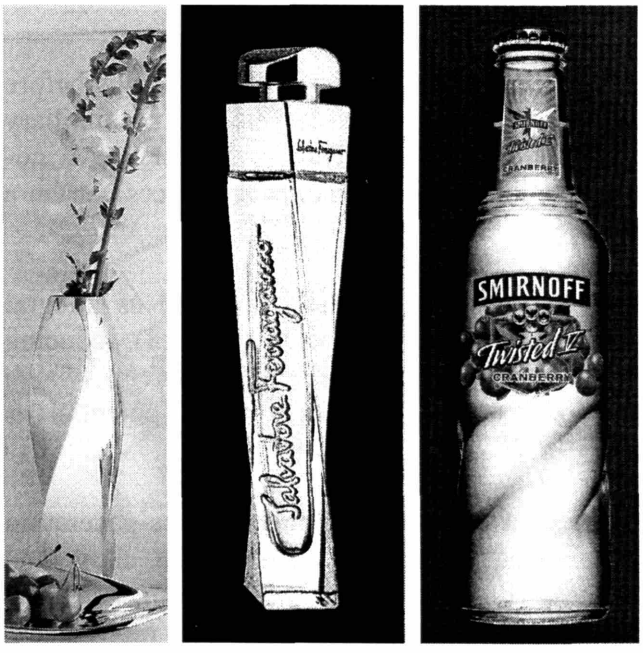

Figure 5.5: Small scale twisted form designs

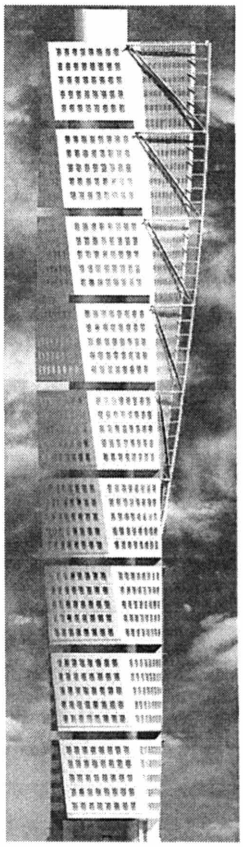

Figure 5.3: Turning Torso

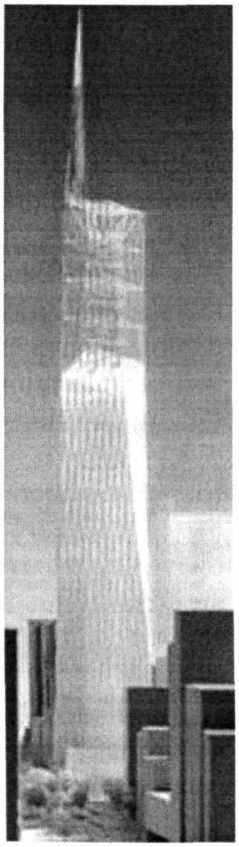

Figure 5.4: Freedom Tower

In general, twisted forms are more effective in reducing vortex-shedding-induced dynamic response of tall buildings by disturbing vortex shedding, which in many cases causes the maximum wind-induced dynamic response. In terms of static response, twisted forms are not beneficial. If solid sections are considered, the moment of inertia of a square plan is the same without regard to its twisted angle (Figure 5.6 and 5.7). Thus, the displacements due to bending are the same as well. However, if the building type frames are considered, the lateral stiffness of the twisted forms is not great as straight forms.

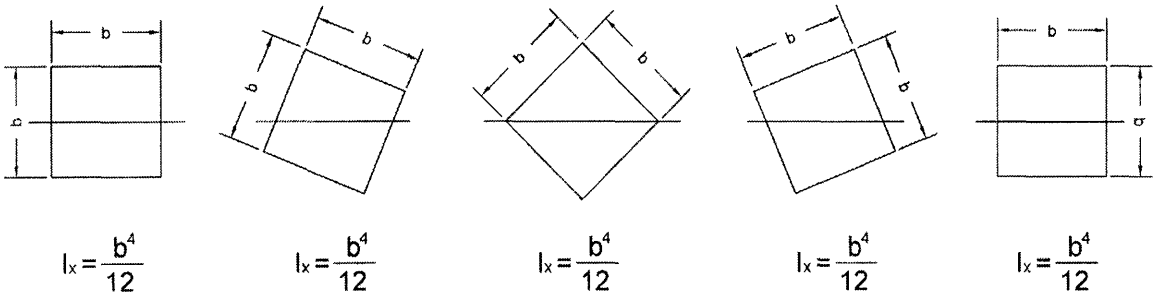

Figure 5.7: Moment of inertia depending on twisted angle

The third strategy of the passive system category is to use auxiliary damping devices. This strategy can be further divided into two categories: 1) Installing energy-dissipating-damping-material-based damping systems such as viscous dampers and visco-elastic dampers, and 2) Installing auxiliary mass systems to generate counteracting inertia forces such as tuned mass dampers and tuned sloshing dampers.

It is very difficult to estimate inherent structural damping ratios of tall buildings before their constructions are completed. However, damping added by employing auxiliary damping devices can be relatively accurately estimated. Thus, when severe wind-induced vibration problems are expected, installing auxiliary damping devices can be a reliable solution.

Energy-dissipating-material-based damping systems are generally installed as integral parts of primary structural systems (i.e. part of a bracing member, Figure 5.8), reducing the structural dynamic response of tall buildings. Thus, these damping systems, which are mainly in the functional performance domain, do not have much potential as architectural esthetic drivers.

A tuned mass damper (TMD) is composed of a counteracting-inertia-force-generating huge mass accompanying relatively complicated mechanical devices that allow and support the intended performance of the mass (Figure 5.8). A TMD system, generally located near the top of the building for its best performance, is installed in a room that is usually not accessible to public. Due to these characteristics of TMDs, they are also in most cases only in the functional performance domain. However, the pendulum type TMD installed in the Taipei 101 is used as an ornamental element in the building interior.

Tuned sloshing dampers use waving water mass as a counteracting inertia force generator. Thus, this system is usually designed using the existing water source in tall buildings, such as a pool or water tank located at the top of a building. Sloshing frequencies are tuned by adjusting the dimensions of the water container and the depth of water.

Another strategy of the passive system category is to increase building mass to reduce acceleration, which is, in general, the measure of motion-induced human discomfort. However, this strategy is not feasible due to its practical limitation of increasing building mass only for the acceleration control. In addition, in case of earthquake, added mass increases seismic loads.

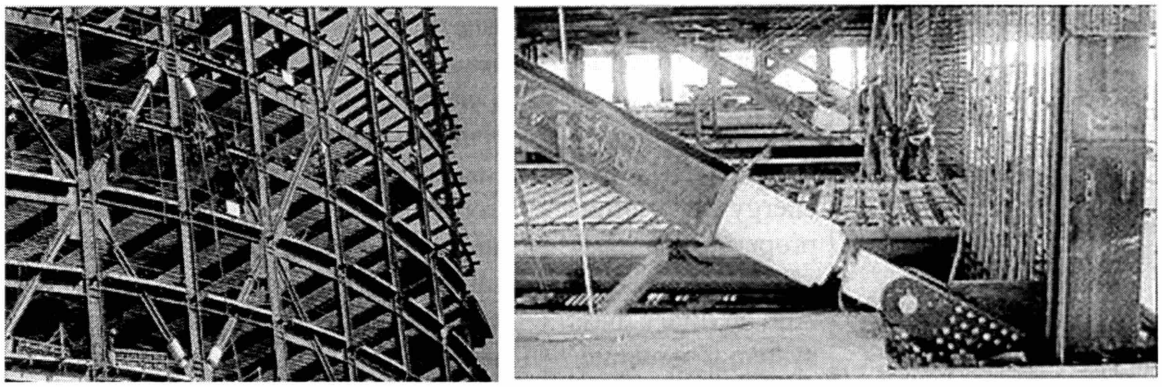

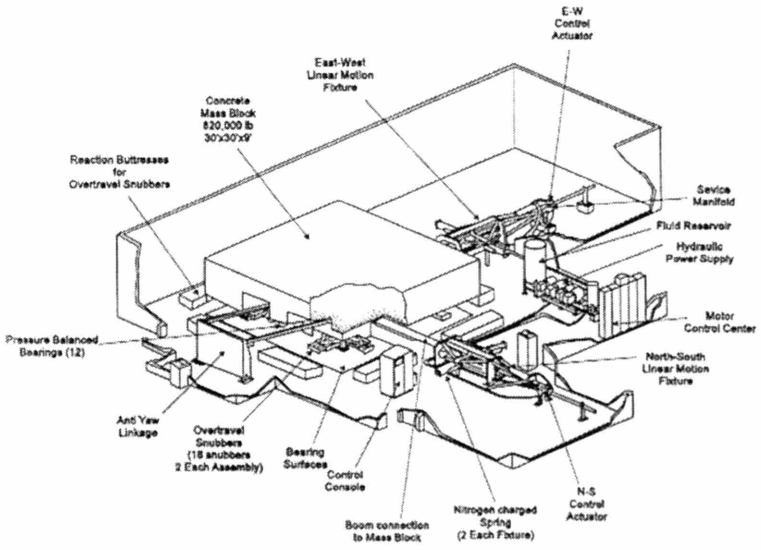

Figure 5.8: TMD installed in Citicorp Building, New York

:mbers in Torre Mayor, Mexico City

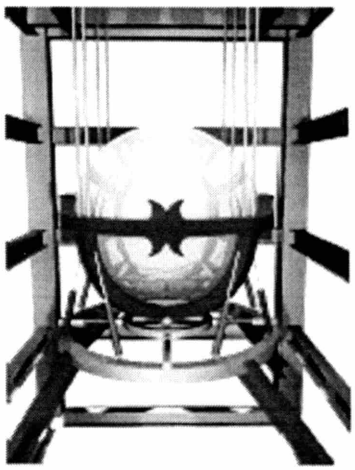

Figure 5.9: Pendulum Type TMD installed in Taipei 101

Type	Means	Method	Application	Considerations
Passive	Primary Structure Design	Increase stiffness to reduce lateral displacement and probability of vortex-shedding-induced lock-in condition	Braced Frames, Tubular Structures, Core-Supported Outrigger Structures, Diagrid Structures	
		Increase building mass to reduce acceleration	Increase Building Material	Not practical to increase mass, Amplifies seismic loads
	Aerodynamic Design	Improve aerodynamic properties to reduce wind force	Chamfered Corners, Streamlined Form, Tapering, Openings, Notches	Reduces occupiable building areas
	Auxiliary Damping Device	Add materials with energy-dissipating properties	Viscous Damper, Visco-Elastic Damper, Hysteretic Damper	
		Add auxiliary mass system to generate counteracting inertia force	Tuned Mass Damper, Tuned Liquid Damper, Impact Damper	Occupies valuable building space near the top of a building
Active		Generate control force using inertia effects to minimize response	Active Mass Damper	More expensive than passive control system
		Generate aerodynamic control force to reduce wind force	Aerodynamic Appendage	More expensive than passive control system
		Change stiffness to avoid resonance condition	Active Variable Stiffness System	More expensive than passive control system

Table 5.1: Strategies to reduce wind-induced response of tall buildings

5.1.2. Tall Building Designs with Active Systems

Connor (2003) defines the active structural control system as "one that has the ability to determine the present state of the structure, decide on a set of actions that will change this state to a more desirable one, and carry out these actions in a controlled manner and in a short period time." While some passive systems, such as tuned mass dampers or sloshing

dampers, are effective only for a narrow range of loading conditions, active systems can perform effectively over a much wider range and they are a more advanced form of functional performance-driven technologies in architecture, and in most cases they remain in the performance domain. Examples are active mass dampers, active variable stiffness systems, etc. The systems discussed so far are summarized in Table 5.1.

CHAPTER 6: DIAGRID STRUCTURES IN TALL BUILDING: CHARACTERISTICS AND METHODOLOGY FOR PRELIMINARY DESIGN

Diagrid structural systems are emerging as structurally efficient as well as architecturally pleasing structural systems for tall buildings. This chapter investigates structural behavior and a preliminary design methodology for diagrid structural systems. The optimal range of angles for diagrid members is studied for representative tall buildings ranging from 20 to 60 stories. A simple methodology for determining preliminary member sizes of diagrid structures is presented. The optimal angle study and the simple member sizing methodology will be useful at the early stage of diagrid structural design for both engineers and architects interested in utilizing this structural system. Also discussed are the architectural, constructability, and urban contextual issues of diagrid structures. Based on this research, it is expected that structural and architectural decisions at the early stage of design can be made in a more integrative way and efficiently.

6.1. History and General Characteristics of Diagrid Structure

The early designs of tall buildings in the late 19th century recognized the effectiveness of diagonal bracing members in resisting lateral forces. Most of the structural systems deployed for early tall buildings were steel frames with diagonal bracings of various configurations such as X, K, eccentric, etc. However, while the structural importance of diagonals was well recognized, the esthetic potential of them was not explicitly appreciated. Thus, diagonals were generally embedded within the building cores which were usually located in the interior of the building.

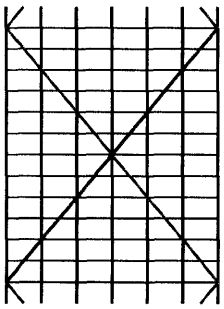

Braced Tube

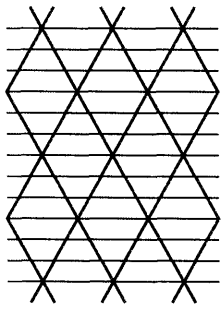

Diagrid

Figure 6.1: Braced Tube vs. Diagrid Structure

A major departure from this design approach occurred when braced tubular structures were introduced in the late 1960s. For the 100-story tall John Hancock Building in Chicago, the diagonals were located along the entire exterior perimeter surfaces of the building in order to maximize their structural effectiveness and capitalize on the aesthetic innovation. This strategy is much more effective than confining diagonals to narrower building cores. Despite the clear symbiosis between structural action and esthetic intent of the Hancock Tower, this overall design approach has not emerged as the sole aesthetic preference of architects. However, recently the use of perimeter diagonals – thus the term "diagrid" – for structural effectiveness and esthetics has generated renewed interest from architectural and structural designers of tall buildings (Figure 6.1).

The difference between conventional exterior-braced frame structures and current diagrid structures is that, for diagrid structures, almost all the conventional vertical columns are

eliminated. This is possible because the diagonal members in diagrid structural systems can carry gravity loads as well as lateral forces due to their triangulated configuration, whereas the diagonals in conventional braced frame structures carry only lateral loads. Compared with conventional framed tubular structures without diagonals, diagrid structures are much more effective in minimizing shear deformation because they carry shear by axial action of the diagonal members, while conventional tubular structures carry shear by the bending of the vertical columns.

Another prevalent structural system for today's tall buildings is outrigger structures with either reinforced concrete cores or steel braced cores. Properly designed, an outrigger structure is effective in reducing the moment and drift of the building below outriggers. However, the system does not provide shear rigidity, whereas the diagrid structure provides both bending and shear rigidity. Thus, tall buildings that employ outrigger systems require cores having significant shear rigidity. Diagrid structures do not need high shear rigidity cores because shear can be carried by the diagrids located on the perimeter.

The lateral stiffness of diagrid structures is desirable not only for static loads but also for dynamic loads that generate responses in both the windward and across-wind directions. In most cases, the lateral motion in the across-wind direction due to vortex shedding is much greater than the motion in the windward direction. Stiffer structures have a lower probability of the vortex frequency locking on a modal frequency (i.e. a lock-in condition) because as a structure's fundamental frequency increases, the wind velocity required to cause a lock-in condition also increases. Thus, due to their greater lateral stiffness, diagrid structures are less prone to a lock-in condition.

An early example of the diagrid structure is the IBM building (Figure 6.2) in Pittsburgh built in the early 1960s. With its 13-story building height, this building was not given much attention by architects and engineers. In the early 1980s Humana Headquarters competition, a diagrid structure was proposed by Sir Norman Foster (Figure 6.3). However, the winning entry at that time was a historicist building of the post-modern style designed by Michael Graves. Only recently have notable diagrid tall buildings been commissioned. Examples are the Swiss Re Building

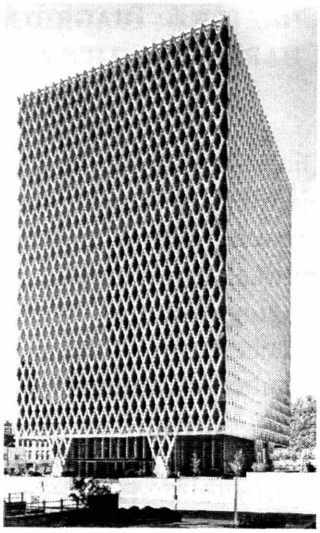

Figure 6.2: IBM Building, Pittsburgh

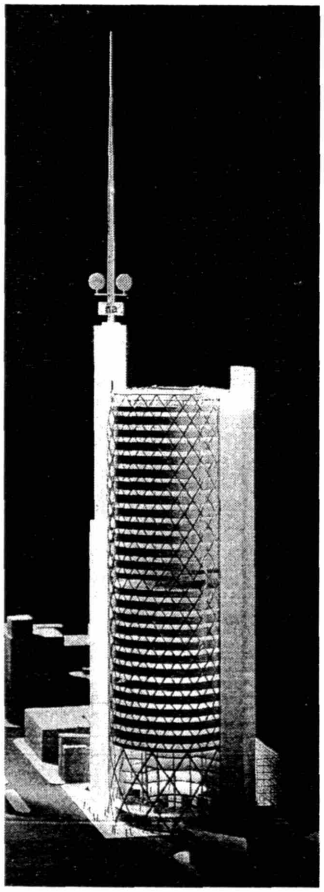

Figure 6.3: Humana Headquarters Competition Entry by Sir Norman Foster

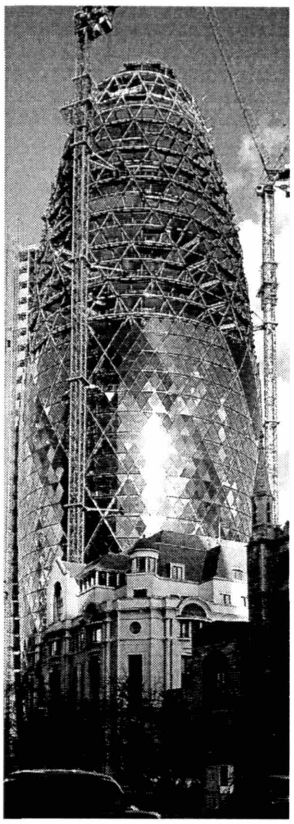

Figure 6.4: Swiss Re Building, London

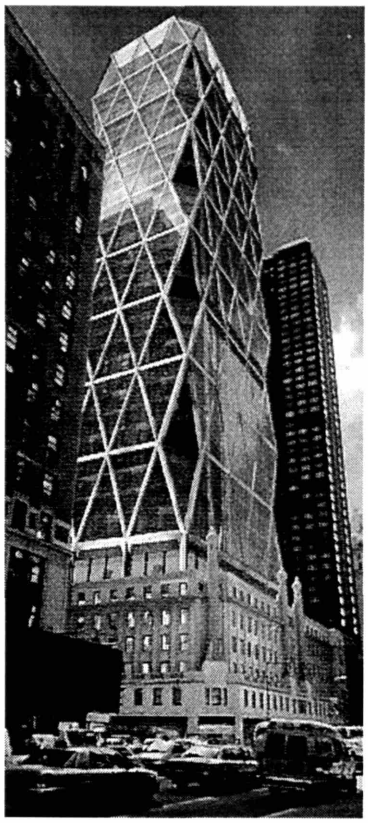

Figure 6.5: Hearst Headquarters (Under Construction), New York

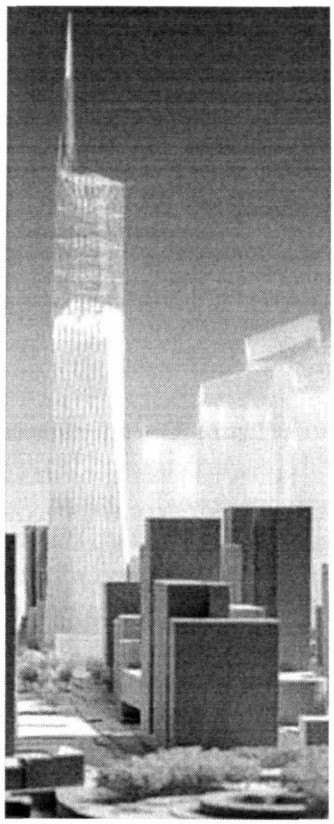

Figure 6.6: Freedom Tower, New World Trade Center (Under Design), New York

(completed, Figure 6.4) in London, the Hearst Headquarters (under construction, Figure 6.5) in New York, both by Sir Norman Foster, and the new World Trade Center (under design, Figure 6.6) in New York by SOM.

The geometry of a diagrid structure is generally customized in order to satisfy building-specific requirements. The purpose of this chapter is to provide preliminary design guidelines for a typical range of diagrid structures. Firstly, the structurally optimal range of angles of diagonal members is investigated for typical 60-, 42- and 20-story buildings, using a conventional iterative design approach. Then, a simple methodology for determining preliminary diagrid member sizes is introduced and applied to the previous set of buildings. Lastly, the design parameters generated with this procedure are verified and compared with the previous set. The proposed methodology was found to produce good estimates of the design variables with minimal effort.

6.2. Optimal Angles of Diagrids for 60-Story Structures

6.2.1. Optimal angle of Diagonal members for Maximum Shear Rigidity

Considering only shear rigidity, the optimal angle for diagonal members can be estimated using the simple braced frame model shown in Figure 6.7. The key assumption is that the

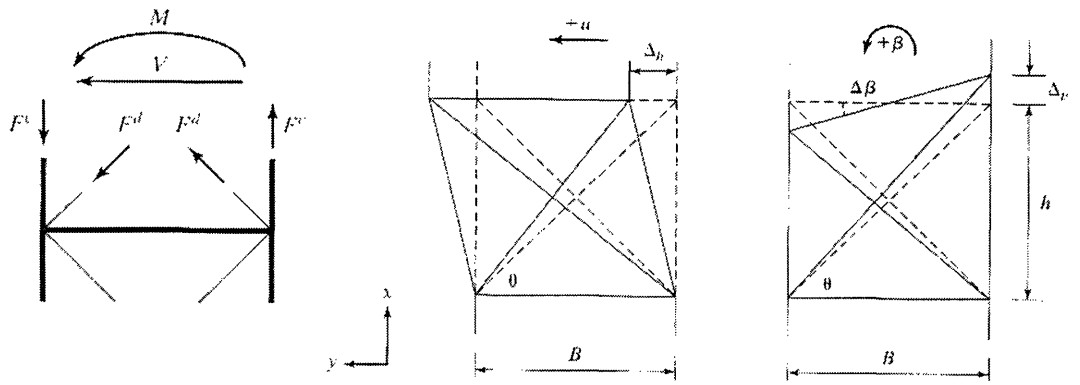

Figure 6.7: Brace Frame Model

members carry only axial forces. The cross section shear force is related to the diagonal member forces by

$$V = 2F_d \cos\theta . \tag{6.1}$$

Assuming linear elastic behavior, the member forces are also related to the diagonal extensional strain, ε_d, by

$$F_d = A_d\sigma_d = A_d E_d \varepsilon_d . \tag{6.2}$$

The extensional strain due to the relative lateral motion between adjacent nodes is a function of Δ_h and θ:

$$\varepsilon_d = \frac{e_d}{L_d} = \frac{\Delta_h \cos\theta}{\frac{h}{\sin\theta}} = \frac{\Delta_h \cos\theta \sin\theta}{h} \tag{6.3}$$

Neglecting the extensional strain in the diagonal due to rotation, $\Delta\beta$, and approximating transverse shearing strain, γ, as

$$\gamma \approx \frac{\Delta_h}{h} \tag{6.4}$$

we obtain the following approximation for the total extensional strain:

$$\varepsilon_d \approx \gamma \cos\theta \sin\theta \approx \frac{\gamma \sin 2\theta}{2} . \tag{6.5}$$

Combining the above equations results in the following expression for this shear force,

$$V = (A_d E_d \sin 2\theta \cos \theta)\gamma . \tag{6.6}$$

By definition, the transverse shear rigidity relates the shear force and shear strain,

$$V = D_T \gamma . \tag{6.7}$$

It follows that

$$D_T = A_d E_d \sin 2\theta \cos \theta . \tag{6.8}$$

The plot of $\sin 2\theta \cos \theta$ is shown in Figure 6.8, indicating that the optimal angle for maximum shear rigidity of the system is about 35 degrees. In typical braced frames, the bending moment is carried by the axial forces in the vertical columns. However, for diagrid structures that do not have vertical columns, bending is carried by the axial forces in the diagonals. Since the optimal angle of the columns for maximum bending rigidity is 90 degrees and that of the diagonals for maximum shear rigidity is about 35 degrees, it is expected that the optimal angle of the diagonal members of diagrid structures will fall between these angles. Short buildings of low aspect ratio (height/width) behave like shear beams, and tall buildings of high aspect ratio tend to behave like bending beams. Thus, it is expected that as the building height increases, the optimal angle also increases. In order to verify these assumptions and also to find the actual range of optimal angles, a set of 60-story buildings having various diagrid angles are designed and analyzed using SAP2000. The study is repeated for 42- and 20-story buildings. Details are presented in the following sections.

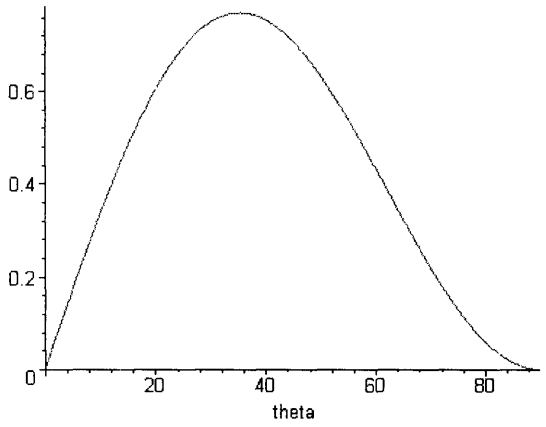

Figure 6.8: $\sin 2\theta \cos \theta$

6.2.2. Design Studies: 60-Story Structures

Figure 6.9 shows 3D and 2D plan views of a typical candidate building. Geometric parameters for the buildings are listed in Table 6.1. Core bracings are configured to generate different fundamental periods in the x and y directions, while diagrids are configured symmetrically in both directions.

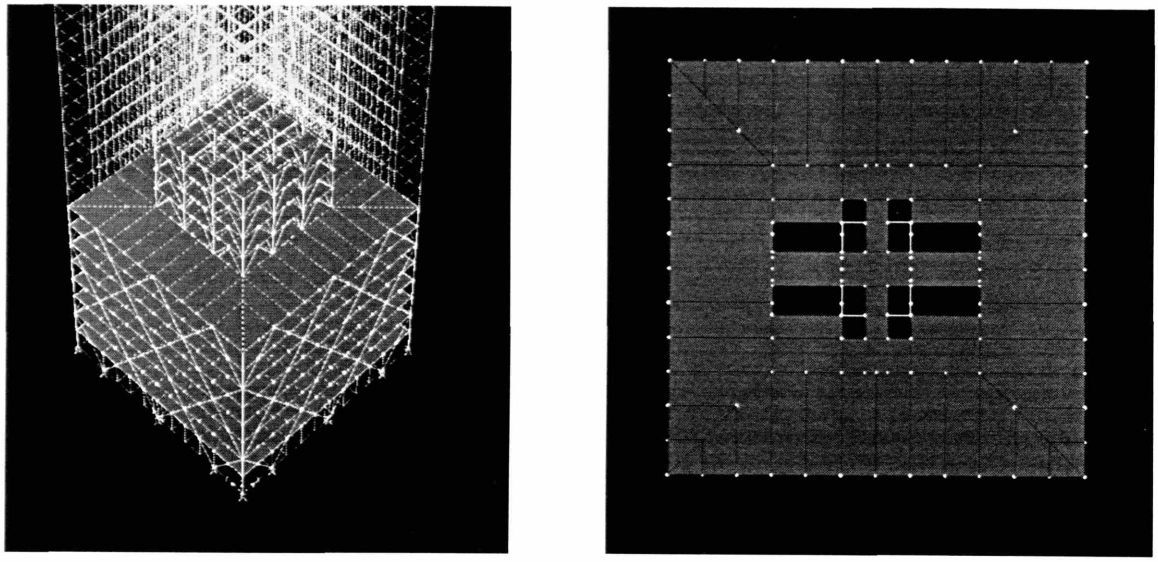

Figure 6.9: 3D and 2D Plan View of the Diagrid Structure Model

Description	Value
Height	240 m
Width	36 m (square plan)
Ext. Wall to Core Wall Distance	9 m typical
Core Area	25 % of floor area
Story Height	4 m typical
Beam Span	9 m typical
Beam Spacing	3 m typical
Floor Slab	12 cm Concrete (w/ WWF) on Metal Decking
Floor Live Load	50 psf

Table 6.1: Geometric Parameters for the 60-Story Diagrid Structure

For the diagrid members, custom-made grade 50 steel pipes of varying diameters from 33 inches to 15 inches are used. Their thickness varies from 3 inches for the 33-inch diameter pipes to 1.5 inches for the 15-inch diameter pipes. Box shape grade 50 steel built-up sections of varying dimensions are used for the core columns. Grade 36 W16 sections are selected for the beams, and W18 sections for the core bracings.

The document SEI/ASCE 7-02 (Minimum Design Loads for Buildings and Other Structures) is used to establish the wind load. The buildings are assumed to be in Boston and within category III, which implies that there is a substantial hazard to human life in the event of failure. Based on the code, the basic wind speed is 110 mph. Lastly, one percent damping is assumed for the calculation of the gust effect factor.

Two different diagrid structural schemes are examined. Scheme 1 includes four vertical corner columns; scheme 2 has no vertical corner columns. The same set of 7 different diagrid angles (Figure 6.10) is considered for both schemes, resulting in 14 different building structures. Scheme 2 requires slightly larger members and uses about 10% more steel than scheme 1. For instance, for scheme 2, the diagrid members at the ground level are 33-inch diameter pipes, while only 27-inch diameter pipes are required for scheme 1.

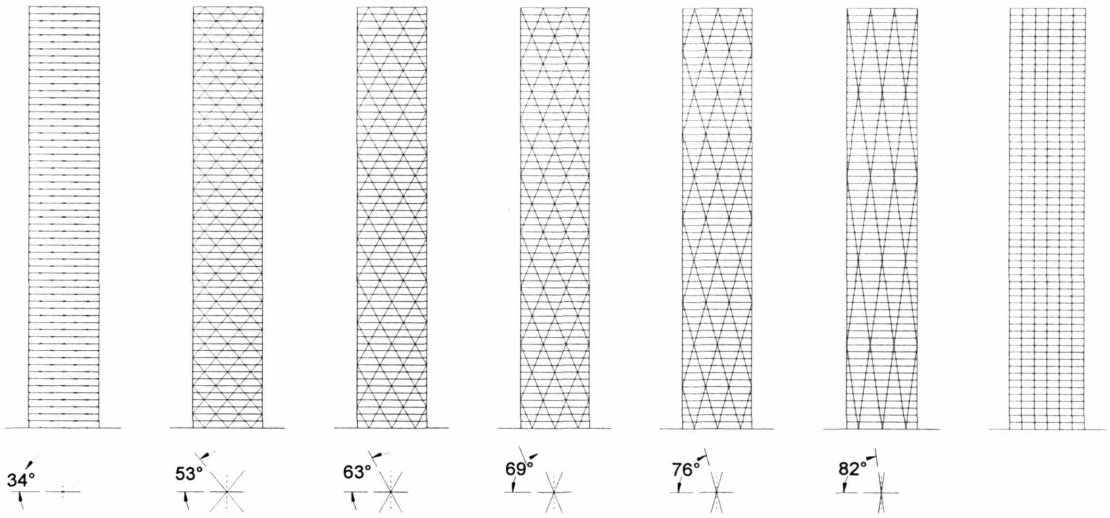

Figure 6.10: 60-Story Structures with Various Diagonal Angles

Member sizes were generated for the building with a diagrid angle of 63 degrees by iterating on the sizes until the deflection constraint for the top floor,

$$u(H) \leq \frac{H}{500} = 0.48m$$

was satisfied. This design process is based on the assumption that motion constraints rather than strength constraints control the design of tall buildings. The design was checked for strength using the LRFD code and found to be acceptable. A value of 63 degrees was taken since our preliminary study indicated that it was close to optimal. These member sizes were also used as initial estimates for the other 6 diagrid systems corresponding to different diagrid angles. Calculations indicated that the lateral stiffness is not too sensitive to angle in the region of 63 degrees. Thus, the member sizes were slightly increased so that the structures with angles of 53, 69 and 76 degrees also satisfied the maximum displacement requirement. Strength checks were also made on these structures. Figure 6.11 contains a plot of the lateral displacements for the scheme 1 structures. The results indicate that angles between 53 and degrees and 76 degrees are reasonable choices.

Diagrid Angle (degree)	Mode 1 Period (sec.)	Horiz. Displ. @ Top (m)	Vert. Displ. @ Top (m)
34	4.53	0.63	0.17
53	3.84	0.47	0.09
63	3.66	0.42	0.07
69	3.71	0.43	0.06
76	4.10	0.50	0.06
82	5.45	0.87	0.05
90	7.95	1.88	0.05

Table 6.2: Scheme 1 (60-Story Diagrid Structures with Corner Columns)

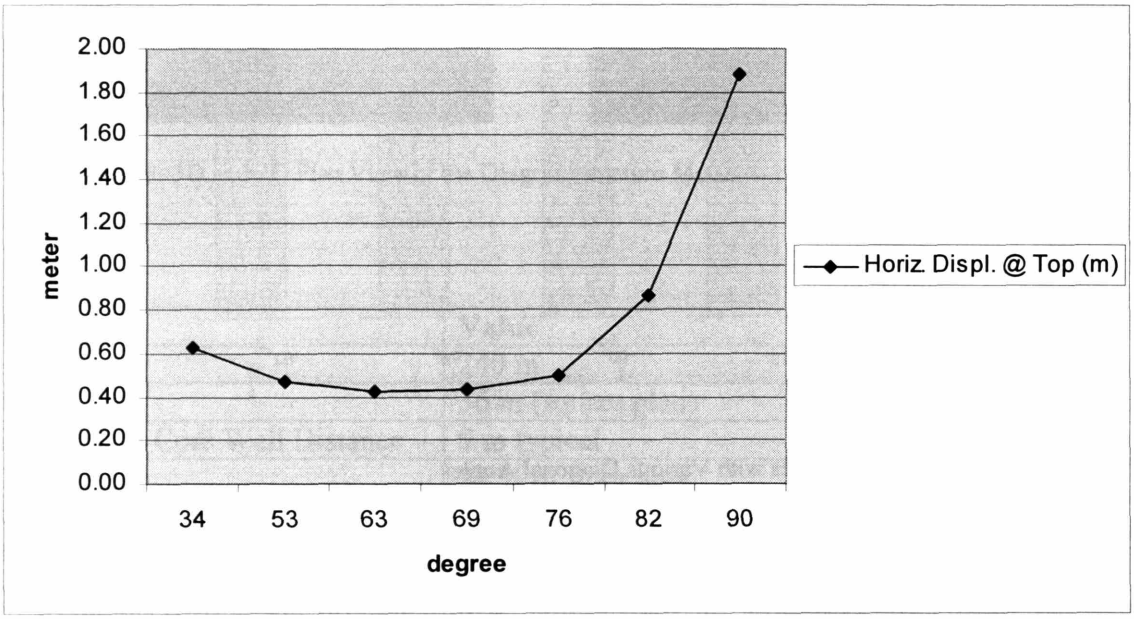

Figure 6.11: Scheme 1 (60-Story Diagrid Structures with Corner Columns)

A similar process was used to select member sizes for the scheme 2 structures. Member sizes were generated to satisfy the maximum displacement requirement for the structures with angles of 63, 69 and 76 degrees in this case. Displacement results for the scheme 2 structures are plotted in Figure 6.12. Since all the vertical columns that provided some of the bending rigidity have been removed, the diagrids need now to provide not only all the shear rigidity but also all the bending rigidity. Thus, the angle range is shifted upward, and centered on about 70 degrees.

Results are summarized in Table 6.2 and 6.3. Comparing Table 6.2 and 6.3, one observes that for diagrid structures with small angles, the vertical displacement is higher than for conventional structures with vertical columns. However, this problem is not so significant.

Diagrid Angle (degree)	Mode 1 Period (sec.)	Horiz. Displ. @ Top (m)	Vert. Displ. @ Top (m)
34	7.44	1.67	0.40
53	4.55	0.66	0.12
63	3.86	0.47	0.08
69	3.73	0.44	0.06
76	3.96	0.48	0.05
82	5.18	0.79	0.05
90	8.21	2.00	0.05

Table 6.3: Scheme 2 (60-Story Diagrid Structures without Corner Columns)

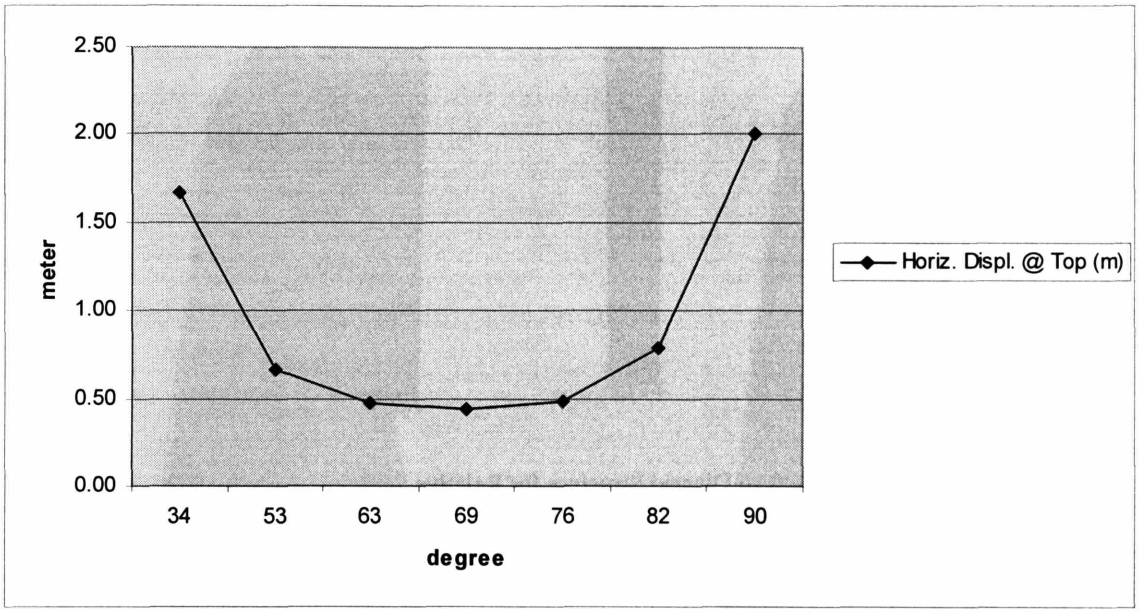

Figure 6.12: Scheme 2 (60-Story Diagrid Structures without Corner Columns)

6.2.3. Stiffness Distribution between Diagrid and Braced Core

In order to estimate the respective contributions of the perimeter diagrids and the braced core to the lateral stiffness, each scheme 2 structure is divided into two separate structures, a braced core and a diagrid (Figure 6.13). Then, each structure is loaded with the same wind forces applied previously, and the displacement at the top of each structure is measured.

As can be seen from the relative stiffness plot (Figure 6.14), the relative stiffness of the diagrids with optimal angles is about five times that of the braced core. The braced core generally has much greater relative stiffness in conventional structures. It follows that in a diagrids/core structure, diagrids provide most of the lateral stiffness, and bracings in the core might not be necessary. In that case, the core can be designed to carry only gravity loads without any bracings. Based on these results, core bracings are eliminated and

lateral stiffness is provided only by the diagrids for the 42 and 20 story structures presented later in this chapter.

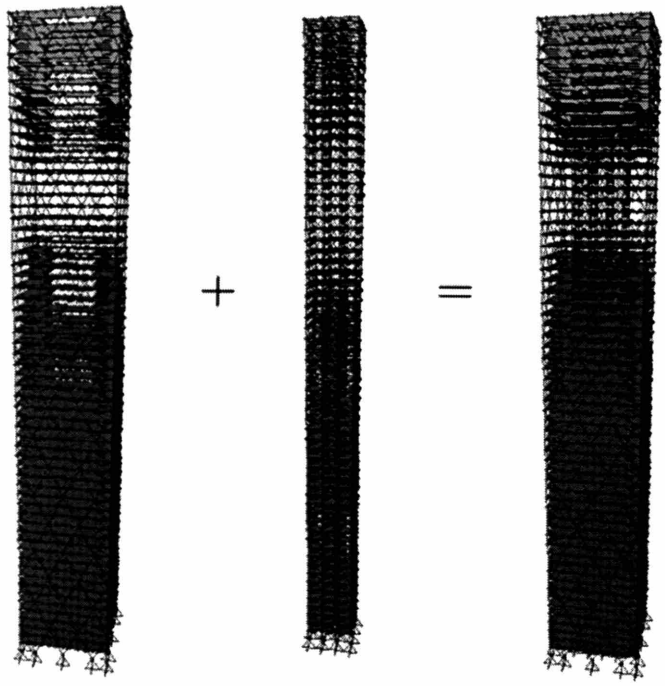

Figure 6.13: Anatomical Models of Diagrid Structure for Relative Stiffness Assessment

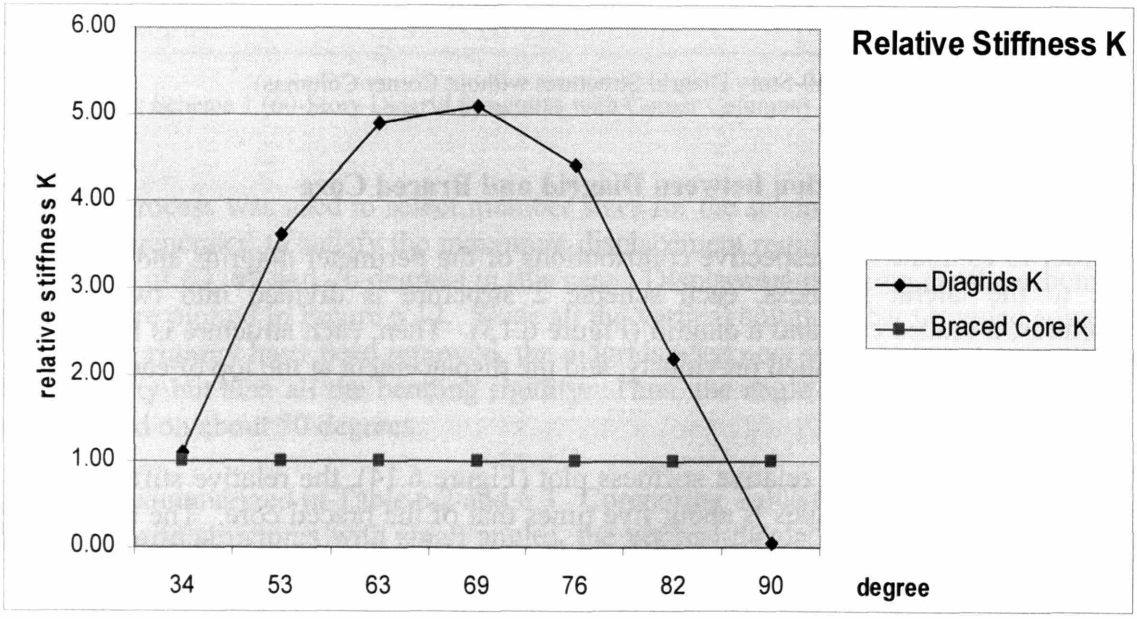

Figure 6.14: Relative Stiffness of Diagrids and Braced Core

6.2.4. Architectural Consideration of Scheme 1 and Scheme 2

Slightly different behavioral characteristics were observed between the scheme 1 (diagrid structure with corner columns) and scheme 2 (diagrid structure without corner columns). Both schemes can create very effective structures for tall buildings. However, observed from architectural viewpoints, scheme 2 has more attractive aspects. Scheme 2 creates valuable columnless corner spaces, which will provide better views as well as higher rents. Also, it is expected that scheme 2 will be preferred by architects. Thus, for the 42- and 20-story structures, only scheme 2 is considered.

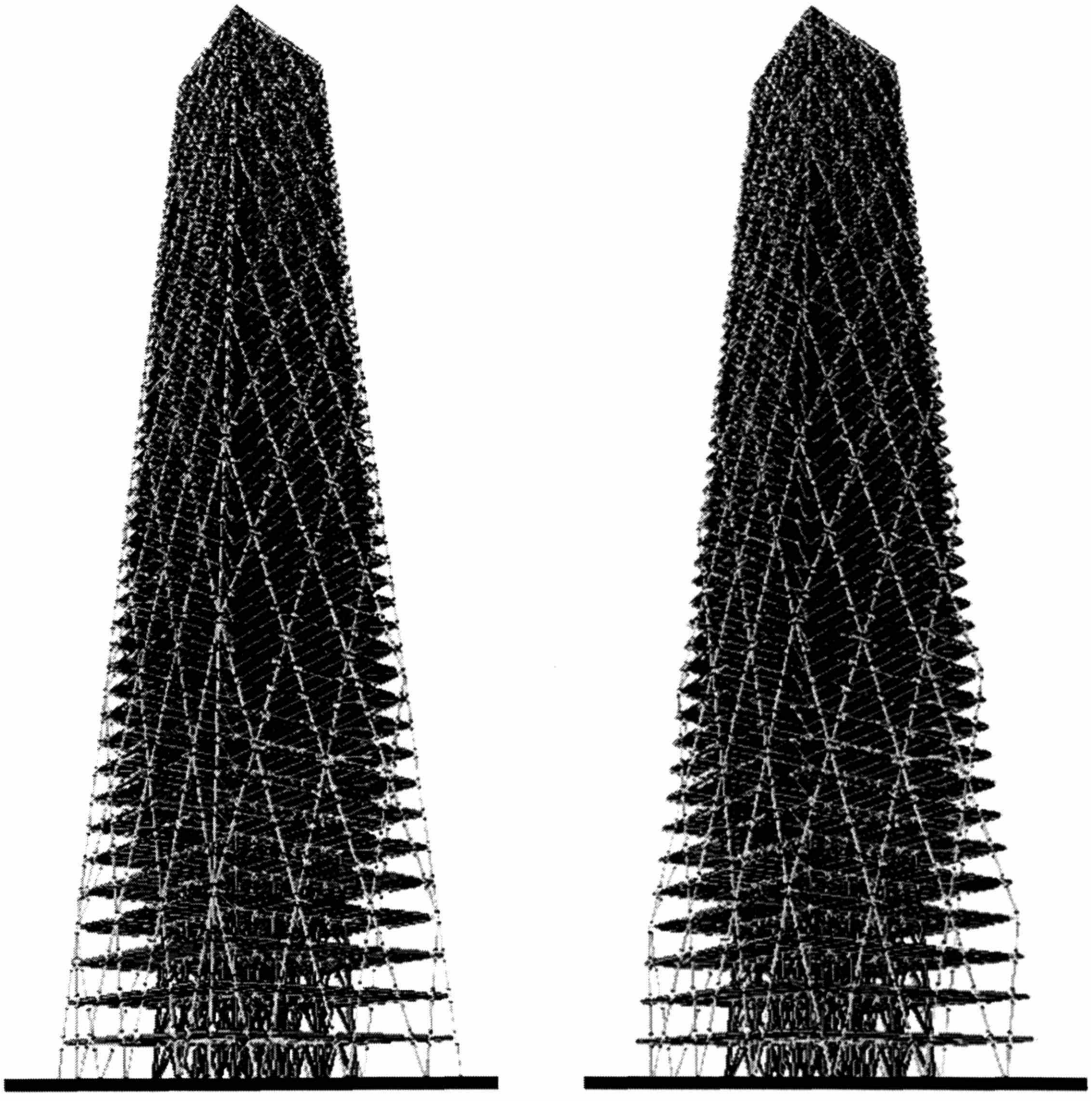

Figure 6.15: Scheme 1 (With Corner Columns) and Scheme 2 (Without Corner Columns) Models

6.3. Optimal Angles of Diagrids for 42 and 20 Story Structures

The process described earlier for the set of 60-story diagrid structures was also used to investigate the sensitivity of the lateral stiffness with diagonal angle for 42- and 20-story structures with no corner columns or core bracings. The maximum deflection requirement at the top is still taken as H/500. The member sizes were selected such that the structures with angles of 53, 63, and 69 degrees satisfied the displacement criteria. The variation of lateral displacement with angle is plotted in Figure 6.16 and 6.17. Note that the optimal angle decreases with decreasing story height since shear deformation becomes more dominant.

The stresses in the diagrid members of every structural configuration that satisfies the lateral displacement requirement were checked with the LRFD code. All the 60- and 42-story buildings satisfied the code. However, all the 20-story structures failed the code check. Therefore, we conclude that when the displacement constraint of H/500 is imposed, the design of 42- to 60-story diagrid structures having an aspect ratio, H/B, ranging from about 5 to 7 is governed by lateral stiffness, and the design of 20-story diagrid structures having an aspect ratio of about 2, is governed by strength. Thus, in what follows, we consider only 60- and 42-story structures.

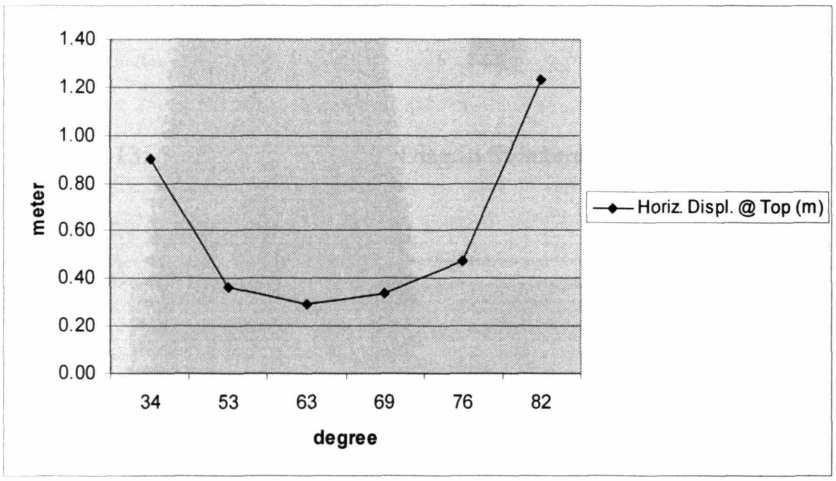

Figure 6.16: Lateral Displacement at the Top of the 42-Story Diagrid Structures

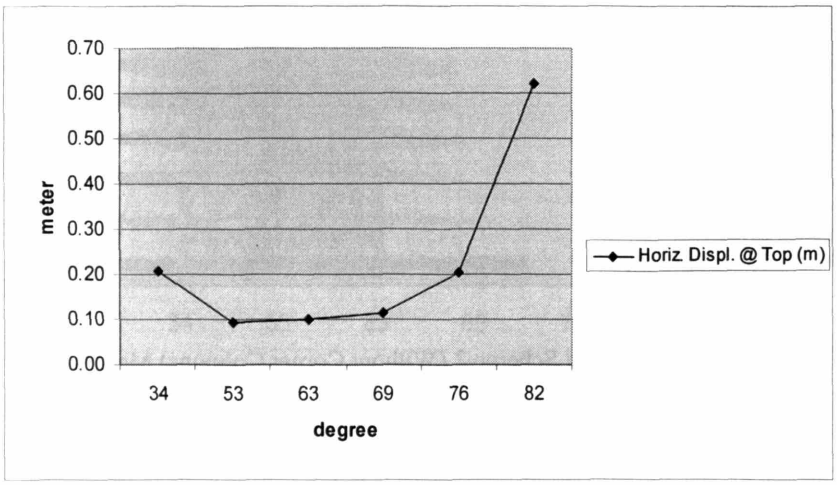

Figure 6.17: Lateral Displacement at the Top of the 20-Story Diagrid Structures

6.4. Methodology of Preliminary Design of Diagrid Structures

In this section, a simple methodology for the preliminary design of diagrid structures is introduced. As was discussed earlier, typical braced cores contribute only 15 to 20% of the total lateral rigidity in properly designed diagrid tall buildings. For this reason and because we can more accurately estimate the lateral rigidity provided by diagrids, all the required lateral stiffness is allocated to the diagrids.

The procedure begins by specifying the contributions to the total lateral displacement of the structure due to bending and shear deformation. This allocation is based on an assessment of the intrinsic attributes of diagrid structures and the behavioral characteristics of tall buildings related to their height to width ratio, and leads to the required values of shear and bending deformation. Simple equations, which convert these required deformation values into cross sectional areas for the diagrid members, are derived.

This design methodology is applied to several diagrid structures of various heights and aspect ratios. Based on these studies, empirical guidelines for assessing the relative contribution of bending and shear deformations to the total lateral displacement of diagrid tall structures are derived. With this formula, the process is essentially automated.

6.4.1. Shear Stiffness and Bending Stiffness of Diagrid Structure

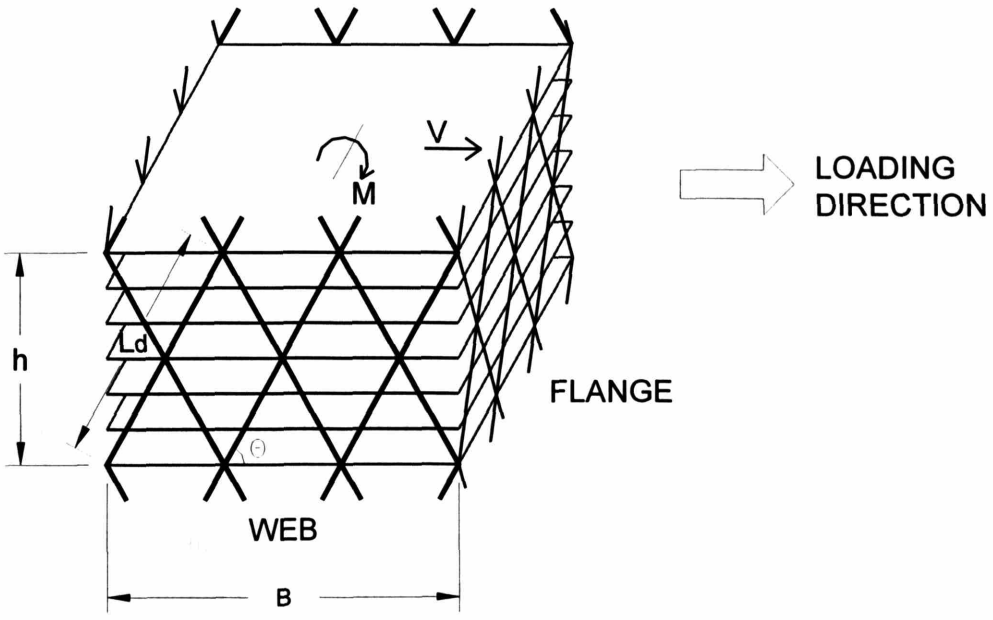

Figure 6.18: 6-Story Diagrid Structure Module

The building is considered as a beam, subdivided longitudinally into modules according to the repetitive diagrid pattern. Each module is defined by a single level of diagrids that extend over n stories. Figure 6.18 illustrates the case of a 6-story module. Depending upon the direction of loading, the faces act as either web or flange elements. The diagonal members are assumed to be pins-ended, and therefore to resist the transverse shear and moment through only axial action. With this idealization, the design problem reduces to determining the cross-sectional area of typical web and flange members for each module. These quantities are established with a stiffness based approach (Connor, 2003).

The shear force, V, and bending moment, M, are expressed in terms of the relative displacement and rotation measures, Δu and $\Delta\beta$, for the module as

$$V = K_T \Delta u \tag{6.9}$$

$$M = K_B \Delta\beta . \tag{6.10}$$

The motion measures are related to the transverse shear and bending deformation measures by

$$\Delta u = \gamma \cdot h \tag{6.11}$$

$$\Delta\beta = \chi \cdot h \tag{6.12}$$

where h is the height of the module, and χ is curvature. Following the process described in Section 6.2.1, the module stiffness measures are given by

$$K_T = 2N_w \left(\frac{A_{d,w} E}{L_d} \cos^2 \theta \right) \tag{6.13}$$

$$K_B = N_f \left(\frac{B^2 A_{d,w} E}{2L_d} \right) \sin^2 \theta \tag{6.14}$$

where N_w is the number of diagonals extending over the full height in one web plane, and N_f is a similar count for one flange plane.

Given V and M, one specifies the desired transverse shear and bending deformations, γ^* and χ^*, and determines the required stiffness using Equations 6.9 and 6.10:

$$K_T = \frac{V}{\gamma^* h} \tag{6.15}$$

$$K_B = \frac{M}{\chi^* h} \tag{6.16}$$

Lastly, substituting for the stiffness terms, one obtains expressions for the typical areas in the web and flange:

$$A_{d,w} = \frac{VL_d}{2N_w E_d h\gamma \cos^2\theta} \tag{6.17}$$

$$A_{d,f} = \frac{2ML_d}{N_f B^2 E_d \chi h \sin^2\theta} \tag{6.18}$$

Since the diagonal members are assumed to be constant in a plane, one needs to consider loading in both directions in order to establish an upper board value for the areas.

6.4.2. Specifying the Shear and Bending Deformation Measures

Optimal design from a motion perspective corresponds to a state of uniform shear and bending deformation under the design loading. Uniform deformation states are possible only for statically determinate structures. Assuming the diagrid structure is modeled as a cantilever beam, the deflection at the top is given by

$$u(H) = \gamma^* H + \frac{\chi^* H^2}{2} \tag{6.19}$$

where $\gamma^* H$ is the contribution from shear deformation and $\chi^* H^2/2$ is the contribution from bending. In order to specify the relative contribution of shear versus bending deformation, we introduce a dimensionless factor s, which is equal to the ratio of the displacement at the top of the structure due to bending and the displacement due to shear:

$$s = \left(\frac{\chi^* H^2}{2}\right) / \left(\gamma^* H\right) = \frac{H\chi^*}{2\gamma^*} \tag{6.20}$$

The maximum allowable displacement is usually expressed as a fraction of the total building height.

$$u(H) = \frac{H}{\alpha}. \tag{6.21}$$

Noting Equation 6.19 and 6.20, Equation 6.21 expands to

$$u(H) = (1+s)\gamma h = \frac{H}{\alpha} \quad . \tag{6.22}$$

Then,

$$\gamma^* = \frac{1}{(1+s)\alpha} \quad . \tag{6.23}$$

Also, χ^* is determined using Equation 6.20.

$$\chi^* = \frac{2\gamma^* s}{H} = \frac{2s}{H(1+s)\alpha} \tag{6.24}$$

Typical values for α are in the neighborhood of 500. It remains to establish a value for s. We introduce a dimensionless factor, f, which is defined as the ratio of the strain in a web diagonal due to shearing action to the strain in a flange diagonal due to bending action. Both strains are produced by lateral loading.

$$f = \frac{\varepsilon_{d,web}}{\varepsilon_{d,flange}} \tag{6.25}$$

The strains, $\varepsilon_{d,web}$ and $\varepsilon_{d,flange}$, can be expressed as

$$\varepsilon_{d,web} = \frac{\Delta u \cos\theta}{L_d} = \frac{\Delta u \cos\theta \sin\theta}{h} = \gamma \cos\theta \sin\theta \tag{6.26}$$

$$\varepsilon_{d,flange} = \frac{B\Delta\beta \sin\theta}{2L_d} = \frac{B\Delta\beta \sin^2\theta}{2h} = \frac{B}{2}\chi \sin^2\theta \,, \tag{6.27}$$

and the equation for f expands to

$$f = \frac{\varepsilon_{d,web}}{\varepsilon_{d,flange}} = \frac{2\gamma \cos\theta \sin\theta}{B\chi \sin^2\theta} = \frac{2\gamma}{B\chi \tan\theta} \,. \tag{6.28}$$

Combining Equation 6.28 and Equation 6.24 leads to an equation for s in terms of f, the diagonal angle, and the aspect ratio.

$$s = \frac{H\chi}{2\gamma} = \frac{H(2\gamma / Bf \tan\theta)}{2\gamma} = \frac{H}{Bf \tan\theta} \tag{6.29}$$

When a truss beam model is used to represent a tall building, the chords correspond to the columns of the building. These elements are required to carry both gravity and lateral loading, whereas the diagonals carry only lateral loading. Since the column force required by the gravity loading may be of the same order as the force generated by the lateral loading, the allowable incremental deformation in the column due to lateral loading must be less than the corresponding incremental deformation in the diagonal. Thus, f for braced frame type tall buildings must be greater than 1. Typical values range from 3 for elastic behavior to 6 for inelastic behavior. However, in diagrid structures, the diagonals in both the web and flange planes are strained equally by the gravity loading. The diagonals at the interface between the web and flange are subjected to both shearing and bending deformation. Therefore, f for diagrid tall buildings is generally less than 1. Studies indicate that for optimally configured diagrid tall buildings having an aspect ratio (H/B) greater than about 5, f ranges from about 0.5 to 1. As the aspect ratio increases, the building tends to act more like a bending beam, and f decreases. Figure 6.19 illustrates in a qualitative sense the trends for f and s as a function of aspect ratio.

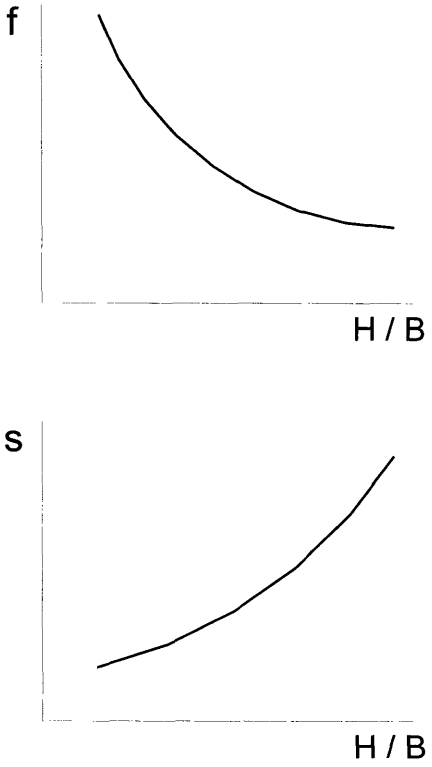

Figure 6.19: f vs. s

6.4.3. Design Studies

The methodology is applied to 60-story and 42-story diagrid structures with an angle of 63 degrees. The first step is to divide the structure into appropriate structural modules. For the 60-story building, every 6-story segment is used as a structural module in this example. For each structural module, shear forces and bending moments are calculated using the code loadings described in Section 6.2.3. The 60-story building has an aspect ratio of about 7, and 'f' was taken equal to 0.5. The corresponding value for s is about 6. Deformation measures were based on a maximum lateral displacement of H/500 = 0.48 meters. Member sizes for the modules were computed using the following equations customized for the 6-story module shown in Figure 6.18.

$$A_{d,w} = \frac{VL_d}{2N_w E_d h\gamma \cos^2\theta} = \frac{VL_d}{12E_d h\gamma \cos^2\theta} \tag{6.30}$$

$$A_{d,f} = \frac{2ML_d}{N_f B^2 E_d \chi h \sin^2\theta} \approx \frac{2ML_d}{(6+2)B^2 E_d \chi h \sin^2\theta} \tag{6.31}$$

An estimate of the contribution of the diagonals on each web to the bending rigidity is made by adding one extra diagonal on each flange, resulting in $N_f \approx 6+2$. Profiles of the required areas for the typical diagonals in the web and flange planes are plotted in Figure 6.20. Since the wind can blow in either direction, the role of a plane can be either a flange or a web. The building considered here has a square plan and the preliminary design value for the module is taken as the larger of the two values (bold face in Table 6.4)

Story	V(KN)	M(KN-M)	Ad(bndg)	Ad(Shear)
55th - 60th	2,650	7,950	0.0008	**0.0207**
49th - 54th	5,300	71,550	0.0069	**0.0414**
43rd - 48th	7,950	198,750	0.0191	**0.0621**
37th - 42nd	10,442	389,076	0.0374	**0.0816**
31st - 36th	12,845	639,417	0.0615	**0.1004**
25th - 30th	15,248	947,697	0.0911	**0.1191**
19th - 24th	17,384	1,312,848	0.1262	**0.1358**
13th - 18th	18,986	1,728,462	**0.1662**	0.1483
7th - 12th	20,588	2,184,126	**0.2100**	0.1608
1st - 6th	22,190	2,788,776	**0.2681**	0.1734

Table 6.4: Preliminary Member Sizing for the 60-Story Diagrid Structure

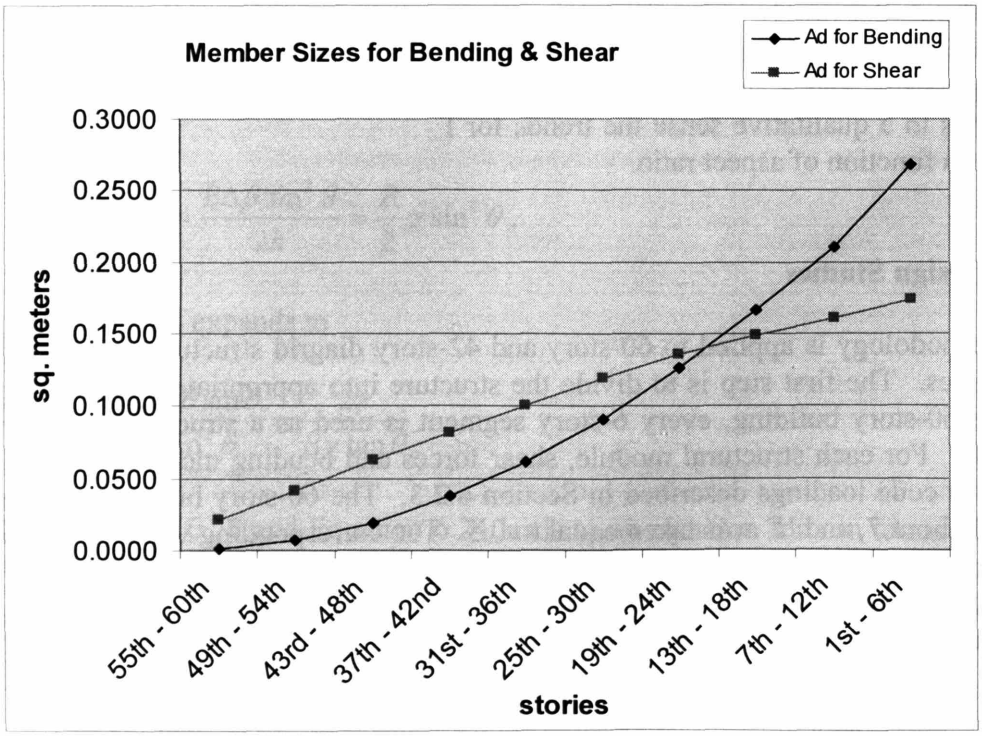

Figure 6.20: Preliminary Member Sizing for the 60-Story Diagrid Structure

A similar study is carried out for a 42-story structure with an aspect ratio of 5 and angle of 63 degrees. The parameters for this case are f = 1 and s = 2. Diagonal areas predicted by Equations 6.30 and 6.31 are plotted in Figure 6.21, and the suggested design values are listed in Table 6.5 (bold face).

Story	V(KN)	M(KN-M)	Ad(bndg)	Ad(Shear)
37th - 42nd	2,492	7,476	0.0006	**0.0083**
31st - 36th	4,895	67,017	0.0058	**0.0164**
25th - 30th	7,298	184,497	0.0160	**0.0244**
19th - 24th	9,434	358,848	0.0311	**0.0316**
13th - 18th	11,036	583,662	**0.0505**	0.0370
7th - 12th	12,638	848,526	**0.0734**	0.0423
1st - 6th	14,240	1,262,376	**0.1092**	0.0477

Table 6.5: Preliminary Member Sizing for the 42-Story Diagrid Structure

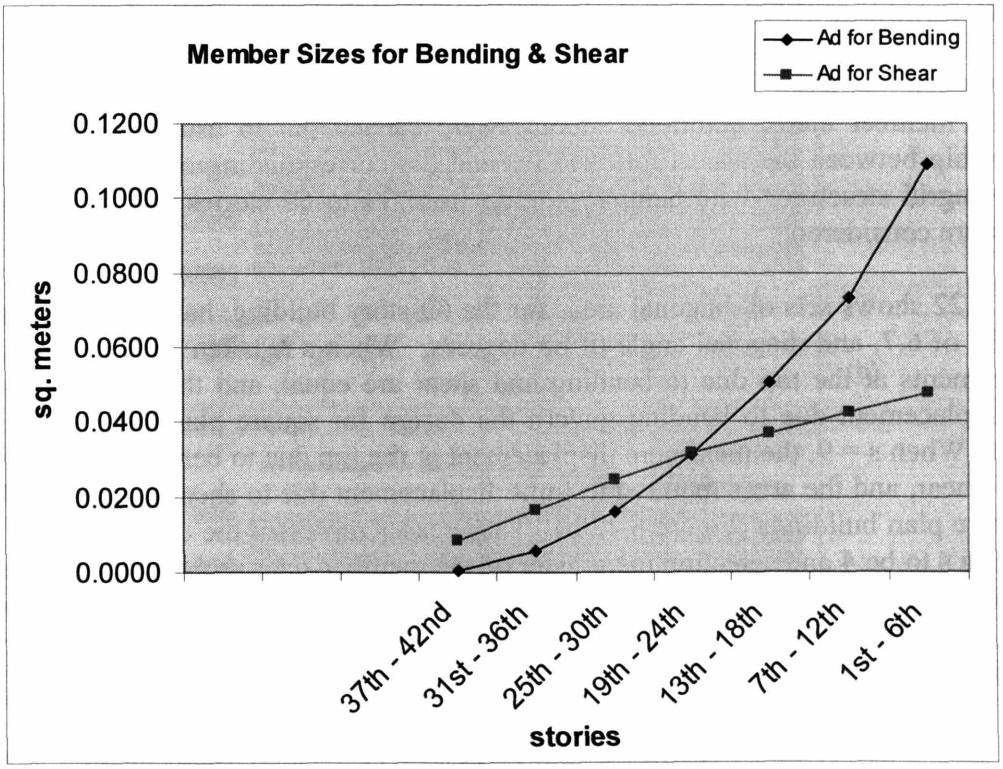

Figure 6.21: Preliminary Member Sizing for the 42-Story Diagrid Structure

The structures having these "preliminary" design areas were analyzed with SAP2000 to assess the accuracy of the preliminary sizing methodology. Table 6.6 compares the results for the displacement at the top of the structure and the required steel tonnage with the conventional approach. There is reasonably close agreement. Considering that no iteration is required, we conclude that the methodology is useful for member sizing at the preliminary design stage.

Structure	H	B	f	s	u_{max} (Target)	Method	u_{max}	Steel Tonnage
42 story	168 m	36 m	1.0	2	0.34 m	Proposed Method	0.30m	1,620t
						Conventional Method	0.29m	1,850t
60 story	240 m	36 m	0.5	6	0.48 m	Proposed Method	0.43m	6,080t
						Conventional Method	0.47m	5,440t

Table 6.6: Comparison between Proposed and Conventional Method

6.4.4. Determining Optimal Value of s for Diagrid Tall Buildings

Even though an assumption-based choice of s values resulted in reasonably good diagonal member areas, additional studies were carried out to establish an empirical relationship between the aspect ratio (H/W) and the corresponding optimal s value. A set of diagrid structures with heights ranging from 33 to 69 stories and various aspect ratios were considered.

Figure 6.22 shows sets of diagonal areas for the 60-story building, having an aspect ratio of (H/B) of 6.7, and diagonal angle of 63 degrees. When s is taken as 1, the maximum displacements at the top due to bending and shear are equal, and the areas required to limit displacement due to bending govern the design for square plan buildings (Figure 6.22 a). When s = 9, the maximum displacement at the top due to bending is 9 times that due to shear, and the areas required to limit displacement due to shear govern the design for square plan buildings (Figure 6.22 b). These cases represent the extreme limits for s. Choosing s to be 4 and selecting the greater of the member sizes required for the bending and shear criteria, leads to the most economical design (Figure 6.22 c). In this case, the bending deformation requirement governs for the lower half of the building, and shear deformation requirement for the upper half.

Table 6.7 contains a comparison of the targeted maximum displacement and the displacements computed with SAP2000. The results show that all the designs are conservative, and the designs corresponding to s values of 3, 4 and 5 appear to be closer to optimal. A closer estimate can be obtained by comparing the steel tonnage required for each design. These results are plotted in Figure 6.23, and indicate that values of s between 3 and 5 are equally optimal.

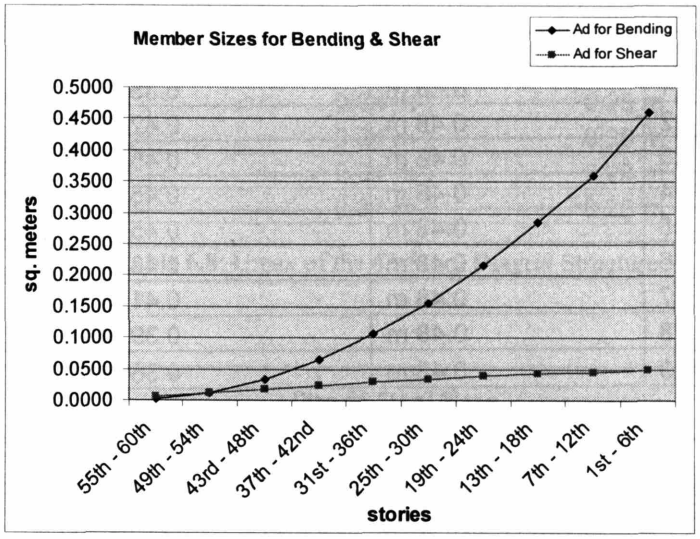

(a)

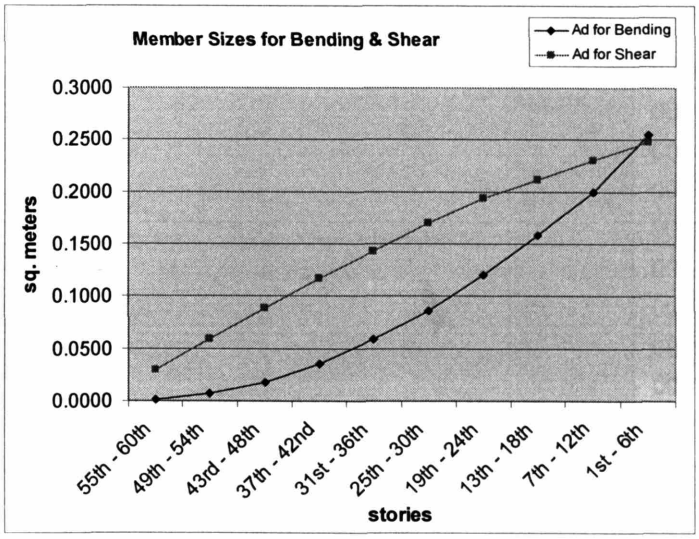

(b)

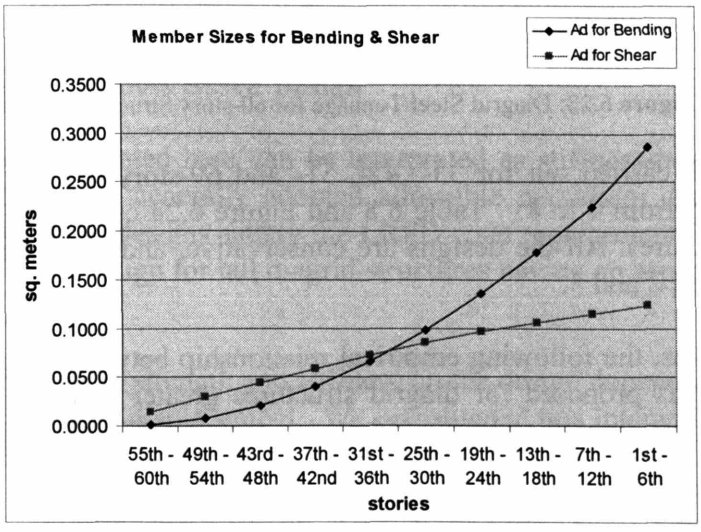

(c)

Figure 6.22: Preliminary Member Sizing for the 60-Story Diagrid Structure with Various s

s	u_{max} (target)	u_{max} (SAP2000)
1	0.48 m	0.35 m
2	0.48 m	0.42 m
3	0.48 m	0.45 m
4	0.48 m	0.45 m
5	0.48 m	0.45 m
6	0.48 m	0.43 m
7	0.48 m	0.41 m
8	0.48 m	0.39 m
9	0.48 m	0.36 m

Table 6.7: Umax of the 60-Story Diagrid Structure

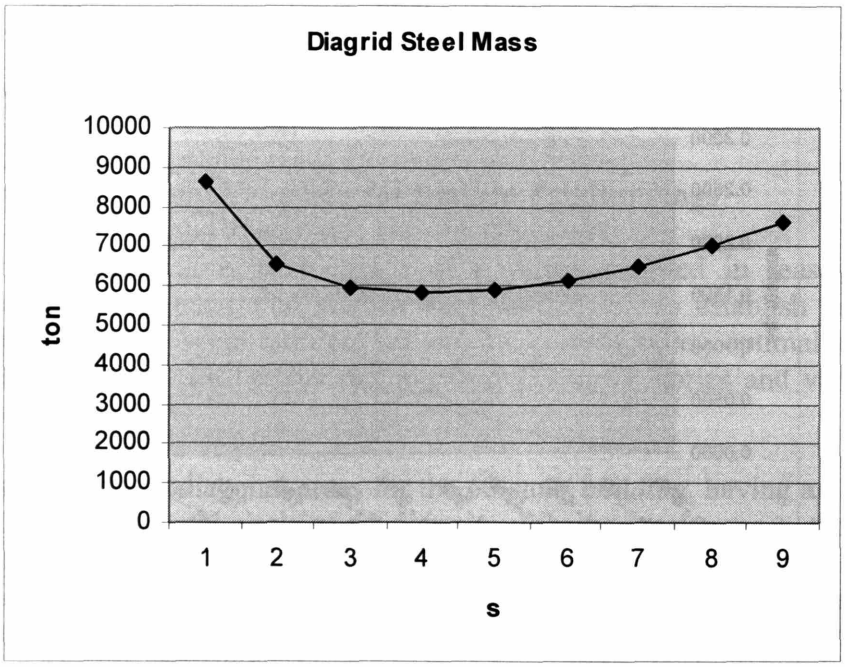

Figure 6.23: Diagrid Steel Tonnage for 60-story Structure

Similar studies were carried out for 33-, 42-, 51- and 69-story diagrid structures with aspect ratios ranging from 4 to 8. Table 6.8 and Figure 6.24 contain the results for the set of 42-story structures. All the designs are conservative, and the optimal range for s appears to be between 2 and 3.

Based on these studies, the following empirical relationship between the optimal s value and the aspect ratio is proposed for diagrid structures greater than 40 stories with an aspect ratio greater than about 5 and a diagrid angle between 60 and 70 degrees.

$$s = \left(\frac{H}{B} - 3\right), \quad \frac{H}{B} \geq 5 \tag{6.32}$$

s	u_{max} (target)	u_{max} (SAP2000)
1	0.34 m	0.25 m
2	0.34 m	0.30 m
3	0.34 m	0.28 m
4	0.34 m	0.26 m

Table 6.8: Umax of the 42-Story Diagrid Structure

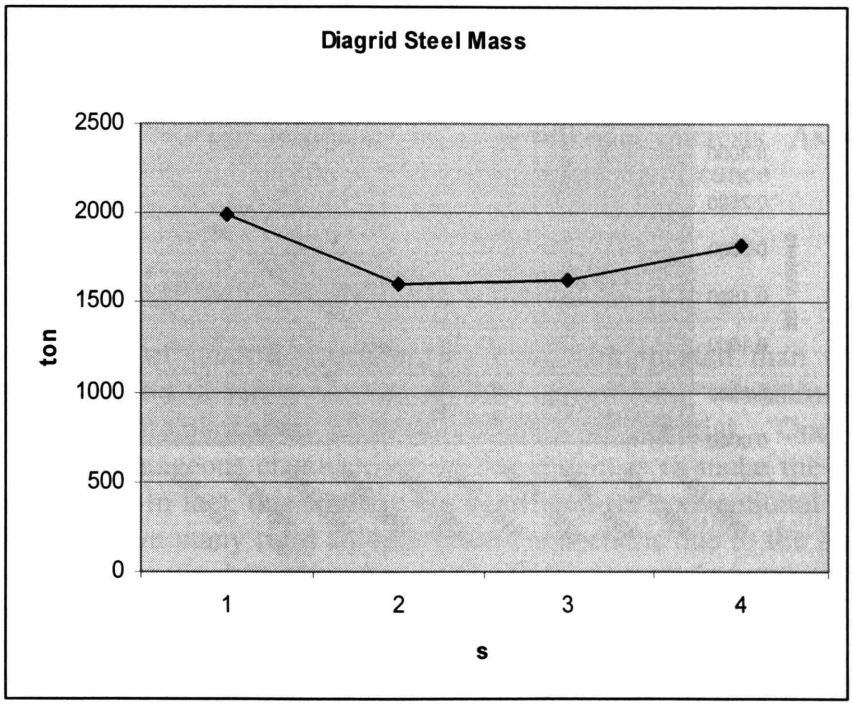

Figure 6.24: Diagrid Steel Tonnage for 42-story Structure

6.4.5. Strength vs. Stiffness Based Design

The methodology presented here can be interpreted as stiffness-based design. Designs were generated using a generally adopted allowable maximum displacement criterion, $u \leq H/500$. All these designs satisfy the LRFD code requirement, verifying that lateral stiffness controls the design for tall diagrid structures having an aspect ratio (H/B) greater than about 5.

The relative influence of strength and stiffness on the design depends on the magnitude of the allowable maximum displacement. We investigated this interaction by carrying out a series of design studies on a 60-story tall diagrid structure with s = 4 and gradually increasing the allowable displacement (H/450, H/400, H/350, H/300, H/250). Figure 6.25 shows the member sizes for 60 story diagrid structures based on two different maximum displacement criteria, H/500 (0.48 m) and H/250 (0.96 m). It was found that,

for H/250, some of the diagrid members failed the code requirements. The most severe failure occurred on the leeward face of the structure.

The same study was repeated for the 42-story diagrid structure with s = 2. Figure 6.26 shows the member sizes for 42-story diagrid structures based on two different maximum displacement criteria, H/500 (0.34 m) and H/400 (0.42 m). It was found that, for H/400, some of the diagrid members fail the code requirements. Again, the most severe failure occurred on the leeward face of the structure.

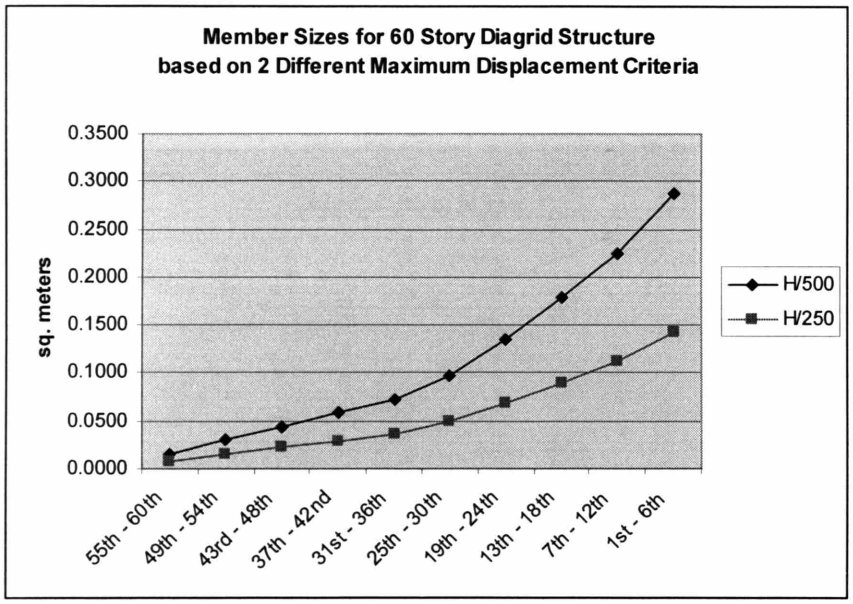

Figure 6.25

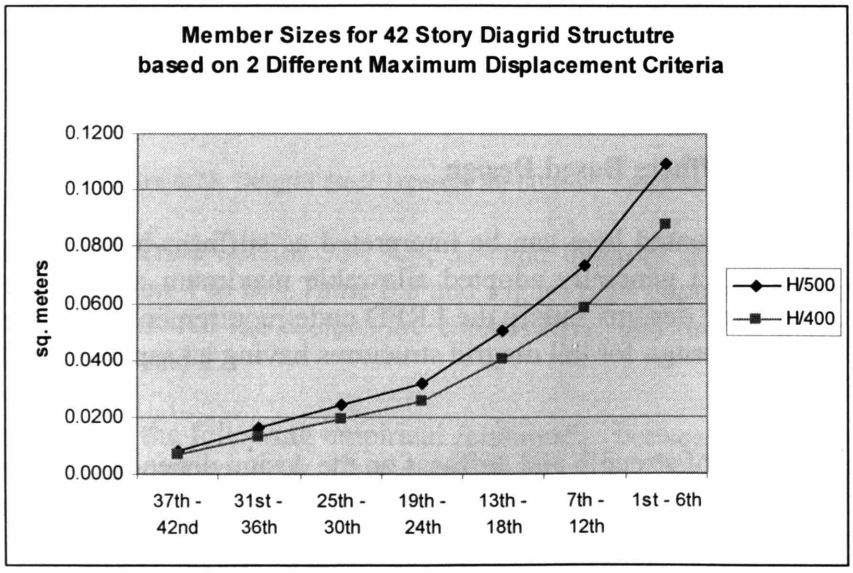

Figure 6.26

6.5. Diagrids in Urban Contexts

The inherent monumentality of skyscrapers resulting from their scale makes their architectural expression very significant in any urban context. Thus, constructing any tall building requires careful studies on esthetic adequacy of the new structure within the existing urban context. Tall buildings, like other building types, are composed of various building components. Modern architecture has always been primarily composed of pure verticals and horizontals. This is generally true of the components of the exterior surfaces of tall buildings.

In contemporary urban contexts, diagrid tall structures are strikingly dissimilar to their tall neighbors. While many contemporary esthetic decisions are substantially guided by subjective visual judgments, the use of diagrid structures stands as an innovation that requires a partnership between technical and compositional interests. As such, these structures are set apart in both their iconic and technological significance

6.6. Constructability of Diagrid

In general, the joints of diagrid structures are more complicated than conventional orthogonal structures and therefore tend to be more expensive. Constructability is a serious concern, and prefabrication of nodal elements is essential. One strategy to overcome this disadvantageous characteristic of the system is to make the complicated joints shop-fabricated. In fact, this strategy has been used for conventional steel tubular structures, which involve many rigid column-beam connections due to the large number of perimeter columns required in general to make the system work as intended. Due to the triangular configuration of the diagrid structural system, rigid connections are not necessary. Pin connections at the complicated joints for diagrids work well. If considerately designed using prefabrication strategy, constructability will not be such a limiting factor of the diagrid structures.

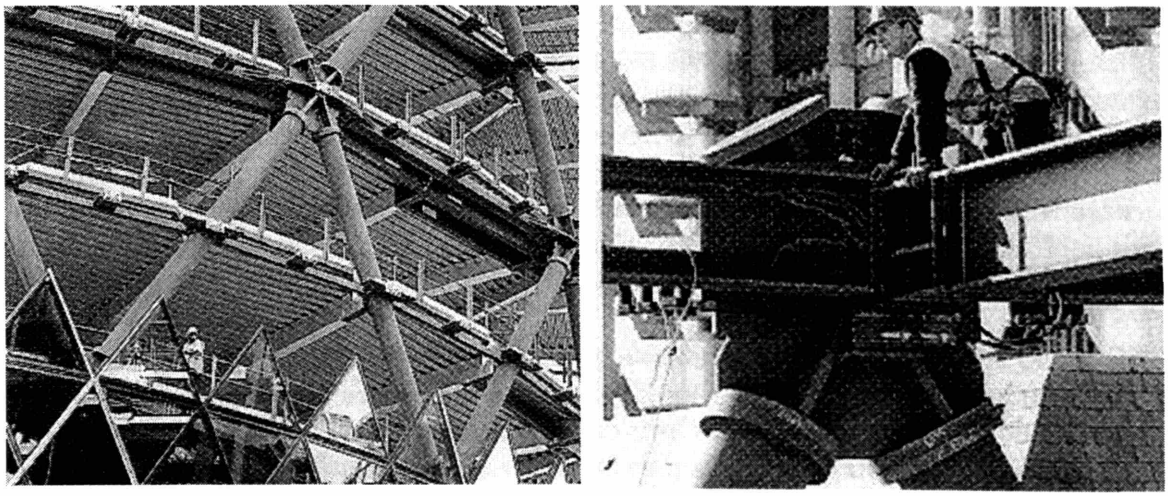

Figure 6.27: Diagrid Construction in Swiss Re Building

6.7. Conclusion

The influence of the diagonal angle on the behavior of diagrid type structures was studied. The schemes presented earlier in this chapter are several design alternatives for both architects and engineers. Subjective contemporary esthetic choices from those design alternatives having various diagrid configurations may or may not coincide with optimal structural performance. Thus, design decisions should be made based on the recognition of this fact.

For 60-story diagrid structures having aspect ratio of about 7, the optimal range of diagrid angles is from about 65 degrees to 75 degrees. For 42-story buildings having aspect ratio of about 5, the range is lower by around 10 degrees because the importance of bending to the total lateral displacement is reduced as the building height decreases.

A stiffness-based methodology for determining preliminary sizes for the diagonals was introduced and applied to a representative set of steel buildings. Results for displacement and required steel tonnage demonstrate the practical usefulness of the proposed preliminary design method. Compared with a conventional strength-based iterative methodology, a stiffness-based methodology is more efficient for today's relatively light and flexible structures such as tall buildings, the design of which is in many cases governed by motion rather than strength.

The importance of interactions between architects and engineers based on mutual understanding is emphasized through this thesis to produce better architecture. Based on this recognition, emphasis was placed on developing relatively simple methodology that is easy to follow. This methodology will be accessible not only for engineers but also for architects so that they can communicate better toward more integrative design.

It is expected that the optimal angle study results, the simple member sizing methodology, and other topics discussed, such as architectural, constructability and urban contextual issues, will be very useful to both architects and engineers for preliminary design of diagrid structure. Based on these studies, structural and architectural decisions at the early stage of design can be made in a more integrative and efficient way.

CHAPTER 7:
STRUCTURAL DYNAMIC MOTION CONTROL USING DOUBLE SKIN FACADES: LOW STIFFNESS DSF CONNECTORS AS DAMPING MECHANISM

Double skin facades were introduced, earlier in this thesis, as a remedial technology that remedies the problematic aspect of single skin facades as an environmental mediator. Double skin facades create new space between the inner and outer skins. This depth not only contributes to enhanced environmental control but also creates augmented perceptual transparency as well. Since the emergence of this space is relatively new, its functional and esthetic potential is not well defined yet. Thus, more possibilities of this new additional space, introduced by new technology, are explored in this and the next chapter.

7.1. Introduction to the System

Tall buildings, which emerged in the late 19th century in the U.S, were a so-called "American Building Type," meaning that the most important modern tall buildings were built in the U.S. Today, however, they are a worldwide architectural phenomenon. Many tall buildings are built especially in Asian countries, such as China, Korea, Japan, and Malaysia. There has been some skepticism regarding constructing tall buildings since September 11, 2001. Nonetheless, due to their significant economic benefits in dense urban land use, tall buildings are and will be built continuously all around the world.

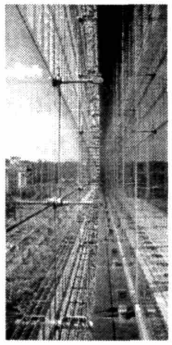

Figure 7.1: DSF

Various façade systems, such as glass/metal curtainwalls, precast concrete panels, and stressed steel skins, are used to clad tall buildings. Generally, most façade systems are composed of several layers. In conventional cases, there are no substantial gaps between the façade layers. The double skin façade (DSF) system (Figure 7.1), which has a substantial cavity between the façade layers, has been obtaining increased interest especially in Europe mainly due to its energy efficiency by enhanced performance as an environmental mediator. Through the cavity, for example, hot air can be effectively removed in summertime, and also natural ventilation can be introduced even at tall buildings' higher levels because there are additional exterior skins that act as wind buffers. These functions of the DSF system reduce energy usage in building operation, resulting in economic benefits in the long run, even though their initial construction cost is higher than conventional single skin façades.

While many studies have been done regarding environmental/energy aspects of the DSF system, no research has been done on the structural capability of the system. In tall buildings – especially at their upper portion – excessive movement/acceleration can cause serious human discomfort. This chapter investigates tall building dynamic motion control by introducing energy dissipating mechanisms within the DSF cavities. Furthermore, their architectural implications are discussed.

Two schemes are studied. The first one introduces low stiffness connectors in the DSF system (Figure 7.2). The concept is designing the connectors between the DSF outer skin and the building's primary structure to be relatively soft so that the transmissibility of the dynamic portion of wind load can be reduced through them. As a result, the DSF outer skin moves back and forth substantially, but the vibration of the primary structure, which is enclosed by the inner skin and contains occupants within it, is reduced significantly. Dynamic motion control for tall buildings is achieved through this mechanism. However, one challenge in this scheme is how to minimize the outer skin's vibration, which may involve serious constructional, visual and psychological concerns, without sacrificing effectiveness of the system.

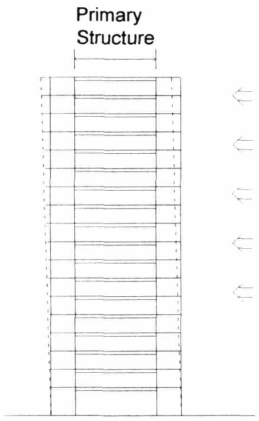

Figure 7.2: Low Stiffness Connector Concept

The second scheme is investigated to overcome the challenges confronted during the study of the first scheme. In this scheme, the DSF outer skin is fixed as in conventional DSF systems. While the DSF outer skin mass itself, attached to soft connectors, is used as a counteracting inertia force generator in the first scheme, additional small masses are inserted into the DSF cavity in this scheme in order to act as distributed tuned mass dampers (TMDs), which effectively control tall building vibration under dynamic loads such as wind (Figure 7.3). Even though the problems of the first scheme are eliminated, the disadvantage of this scheme is that this design requires additional mass, which was not necessary in the first scheme. However, compared with a conventional TMD system, which is usually located near the top of the building, this scheme has the significant benefit of saving valuable occupiable space.

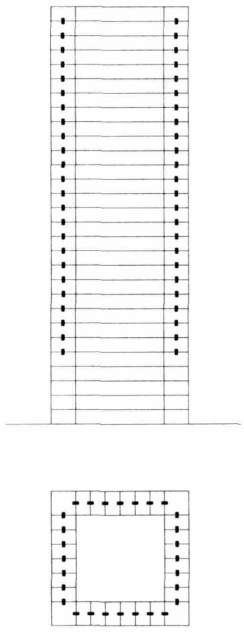

Figure 7.3: Distributed TMD Concept

There are several other benefits of distributing TMDs through the DSF cavity. Since all the TMD masses are located at the extreme perimeter of the building, the torsional resistance exerted by the TMDs is maximized if they are designed to move in the direction parallel to the building façade planes. In addition, by distributing TMDs vertically, not only the first mode, which has its maximum displacement at the top, but also other modes, which may not have their maximum displacement at the top, can be effectively controlled, if necessary. In terms of constructability, TMDs can be more easily installed by making them very small. In fact, vertically distributed small TMDs may be constructed as a part of the prefabricated DSF construction unit. Another advantage of the second scheme is its greater applicability. Vertically distributed multiple small tuned mass dampers do not need to be located within tall building DSF cavities. When a tall building does not employ DSF as its enclosure system, distributed mass dampers can be placed anywhere in the building such as underneath floor slabs possibly integrated with a core and/or girders.

Both the first and second schemes are investigated in more detail through the rest of this thesis. For the low stiffness DSF connector scheme, the system is analyzed using a simplified two degrees of freedom (2DOF) system model. Its effectiveness and limitations are discussed based on the results of the analyses of this system. For the vertically distributed TMD scheme, system analysis theories are introduced, and a 60-story building is simulated using a 60DOF model with vertically distributed TMD system. The result is compared with a conventional TMD scheme, and the advantages and disadvantages of the proposed system are discussed in greater detail.

7.2. Low Stiffness DSF Connectors Subjected to Periodic Loading

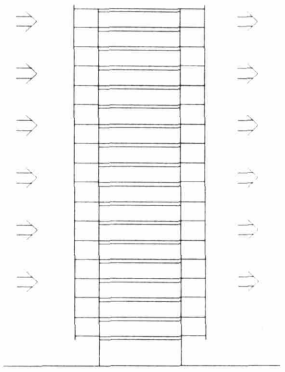

DSF Structure
w/ Isolation / Damping Mechanism

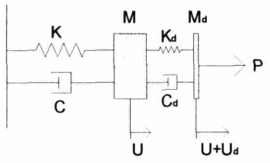

Figure 7.4: 2DOF Model

M: Mass
K: Stiffness
C: Viscous Damping Parameter
P: Applied Loading
U: Displacement
ω: Natural Frequency of Structure
ωd: Natural Frequency of DSF Outer Skin
Ω: Forcing Frequency
ρ: Forcing Frequency to Natural Frequency Ratio (Ω/ϖ)
f: DSF Outer Skin Frequency to Primary Structure Frequency Ratio (ϖd / ϖ)
ξ: Primary Structure Damping Ratio
ξd: Façade Connector Damping Ratio

This section investigates the strategy of designing the connectors between the DSF outer skin and building primary structure to be relatively soft so that the transmissibility of the dynamic portion of wind load can be reduced through them. In order to clearly understand the behavioral characteristics of the system, a 2DOF system is studied. The system is composed of the primary mass, which corresponds to the primary building structure including the inner skin of the DSF system, and the secondary mass, which corresponds to the outer skin of the DSF system. The two masses are connected by the low-stiffness spring (Kd) and damper (Cd) components. Sinusoidal load, which represents simplified dynamic wind load, is applied to the secondary mass in order to obtain a clear solution.

7.2.1. Dynamic Response of the System

Below are the governing equations of the system shown in Figure 7.4.

$$m\ddot{u} + c\dot{u} + ku = c_d\dot{u}_d + k_d u_d \tag{7.1}$$

$$m_d(\ddot{u}_d + \ddot{u}) + c_d\dot{u}_d + k_d u_d = p \tag{7.2}$$

It is convenient to work with the solution expressed in terms of complex quantities. The force is expressed as

$$p = \hat{p}e^{i\Omega t} \tag{7.3}$$

where $\hat{p}$ is a real quantity. The response is taken as

$$u = \bar{u}e^{i\Omega t} \tag{7.4}$$

$$u_d = \bar{u}_d e^{i\Omega t} \tag{7.5}$$

where the response amplitudes, $\bar{u}$ and $\bar{u}_d$, are considered to be complex quantities. Then the corresponding solution is given by either the real or imaginary parts of u and u_d. Substituting Equations 7.3, 7.4 and 7.5 in the set of governing Equations 7.1 and 7.2 results in

$$-\Omega^2 m\bar{u} + i\Omega c\bar{u} + k\bar{u} = i\Omega c_d\bar{u}_d + k_d\bar{u}_d \tag{7.6}$$

$$-\Omega^2 m_d(\bar{u}_d + \bar{u}) + i\Omega c_d\bar{u}_d + k_d\bar{u}_d = \hat{p}\,. \tag{7.7}$$

Considering the following notations,

$$\omega^2 = k/m \tag{7.8}$$

$$c = 2\xi\omega m \tag{7.9}$$

$$\omega_d^{\,2} = k_d/m_d \tag{7.10}$$

$$c_d = 2\xi_d\omega_d m_d \tag{7.11}$$

defining $\bar{m}$ as the mass ratio,

$$\bar{m} = m_d/m, \tag{7.12}$$

defining 'f' as the DSF outer skin frequency to primary structure frequency ratio,

$$f = \omega_d/\omega, \tag{7.13}$$

and defining 'ρ' as the forcing frequency to primary structure frequency ratio,

$$\rho = \Omega/\omega, \tag{7.14}$$

the governing Equations 7.6 and 7.7 become

$$\left(-\rho^2 + 2i\rho\xi + 1\right)\bar{u} - \left(2i\rho\xi_d fm + f^2 m\right)\bar{u}_d = 0 \tag{7.15}$$

$$-\rho^2 m\bar{u} - \left(\rho^2 m - 2i\rho\xi_d fm - f^2 m\right)\bar{u}_d = \hat{p}/k\,. \tag{7.16}$$

Then, the solutions due to a harmonic excitation can be expressed as

$$\bar{u} = \frac{\hat{p}}{k} H e^{i\delta_1} \tag{7.17}$$

$$\bar{u}_d = \frac{\hat{p}}{k} H_d e^{i\delta_2}\,. \tag{7.18}$$

Here, H is the dynamic amplification factor of the primary structure, and Hd is that of the DSF outer skin. Figure 7.5 contains the plots of H and Hd with various DSF connector damping ratios. The DSF outer skin mass is assumed to be 1% of the primary structure mass. Soft connectors between the primary structure and the DSF outer skin are employed to reduce the transmissibility between them. Frequency ratio f (DSF outer skin frequency / primary structure frequency) is 0.5, and the primary structure damping ratio is 5% in this study. With this 5% structural damping ratio, the maximum H value of the primary structure without the DSF energy dissipating mechanism is about 10.

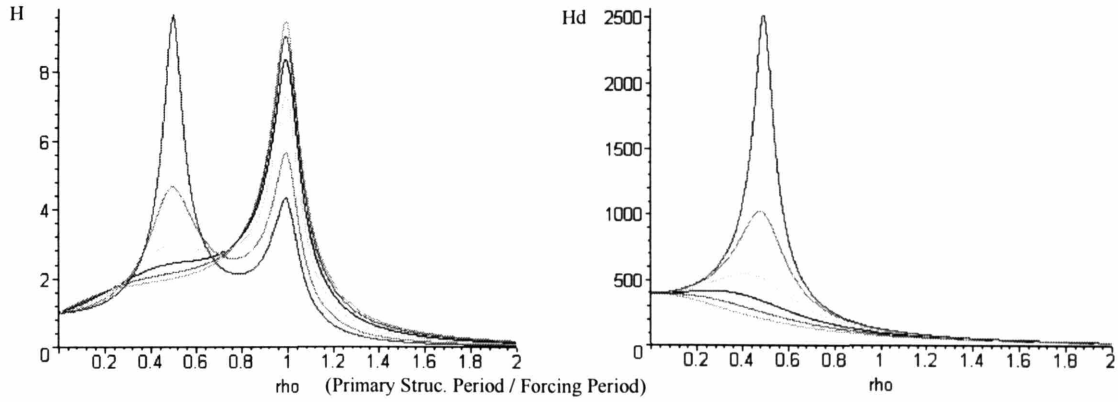

DYNAMIC AMPLIFICATION FACTOR
FOR PRIMARY STRUCTURE (H)

H plot , U= (P/K) H
Mass Ratio (Md/M) = 0.01
Structure Damping Ratio = 0.05
Façade Damping Ratio = 0.08, 0.2, 0.4, 0.6, 0.8, 1.0
f (Primary Struc. Period /Façade Period) = 0.5

DYNAMIC AMPLIFICATION FACTOR
FOR DSF OUTER SKIN (Hd)

Hd plot , U= (P/K) Hd
M.R. (Md/M) = 0.01
S.D.R = 0.05
F.D.R. = 0.08, 0.2, 0.4, 0.6, 0.8, 1.0
f = 0.5

Figure 7.5

As can be seen from Figure 7.5, when the façade connector damping ratio is 0.2, the maximum H value is reduced about 50%, compared with the case when there is no DSF energy dissipating system. As the façade connector damping ratio increases above 0.2, H

value increases, eventually reaching about 10, at ρ (forcing frequency / natural frequency of the primary structure) = 1 and when the critical damping ratio is used for DSF connectors. As the façade damping ratio is lowered below 0.2, H value also increases at $\rho = 0.5$. When the façade connector damping ratio is 0.08, H reaches about 10, and when the façade connector damping ratio is 0, the primary structure resonates at $\rho = 0.5$. With regard to the vibration of the DSF outer skin, higher façade damping ratio is always better to reduce H_d.

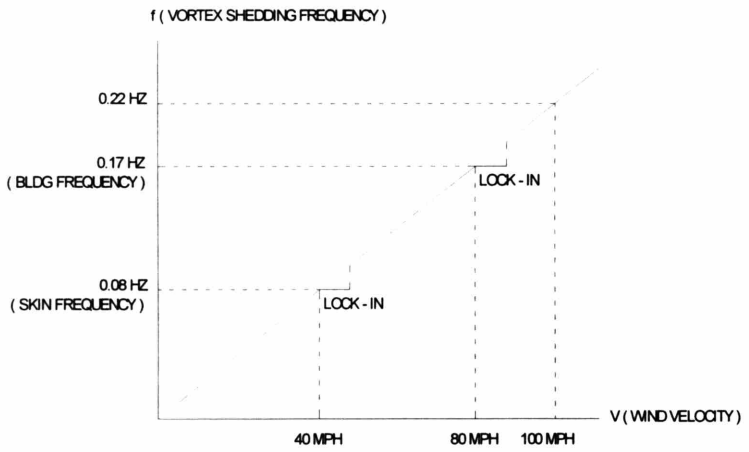

Figure 7.6: Primary Structure and Façade Lock-In Condition

In general, the vortex-shedding-induced lock-in phenomenon produces the most severe vibration problem. When 20% façade connector damping ratio is considered to minimize the motion of the primary structure, at ρ = 0.5, the façade lock-in condition will occur, even in moderate wind speed since the natural frequency of the façade connector is half of the building frequency. Under this condition, as can be seen from H_d plot in Figure 7.5, dynamic amplification factor of the façade, H_d, becomes very large.

For example, for a 40m x 40m square plan tall building, when wind velocity varies from 20mph to 100mph, the vortex shedding frequency f_v varies from 0.04 to 0.22, following the approximate Equation 7.19 and assuming the Strouhal Number as 0.2.

$$f_v = VS/D \tag{7.19}$$

V: Wind Velocity
S: Strouhal Number (Reynolds Number & Building Geometry dependant)
D: Across-Wind Dimension of the Building Plan

Considering the approximate natural period of tall buildings (about 60 stories) to be approximately 6 seconds, this frequency as well as the low stiffness DSF connector frequency is within the possible vortex shedding frequency, resulting in lock-in conditions. The primary structure lock-in condition will occur around 80 mph wind speed, and façade lock-in condition around 40 mph wind speed when f = 0.5 (Figure 7.6). During the primary structure lock-in condition, the dynamic response of the primary structure will be reduced due to the low stiffness DSF connectors. However, during the façade lock-in condition, the DSF outer skin will vibrate severely. In fact, in this case, the DSF outer skin acts as a force amplifier for the primary structure.

7.3. Conclusion

The purpose of this study was to investigate if DSF systems can be designed to control the dynamic structural motion of tall buildings. In terms of architectural perspective, this study was an experimental study on oscillating façades (DSF outer skins) that produce ever-changing building form depending on ever-changing building exterior environments (primarily wind loads), while the motion of the building interior space (inside DSF inner skins) is extremely controlled due to the motions of facades (DSF outer skins). In addition, this study was an exploration of the potential of new space – DSF cavity space – created by new technology.

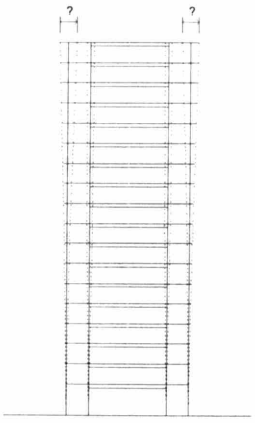

Figure 7.7: Design Limitations of Low Stiffness Connectors

The motion can be reduced when the DSF façade connectors are designed to have relatively low stiffness. However, as can be concluded from the discussion so far, there is a serious practical limitation. The DSF outer skin moves too much (i.e., on the order of several meters). Excessive movements of DSF outer skin can be adjusted by increasing connector damping ratio. However, it increases the primary structure dynamic amplification factor as well, resulting in very low effectiveness of the system. Both primary structure and DSF outer skin dynamic response can be reduced by increasing DSF outer skin mass. However, certainly there is a practical limitation in doing that also. In order to overcome the excessive DSF outer skin motion problem, the vertically distributed multiple TMD concept is introduced in the next chapter.

CHAPTER 8:
STRUCTURAL DYNAMIC MOTION CONTROL USING DOUBLE SKIN FACADES: VERTICALLY DISTRIBUTED TMDS WITHIN THE DSF CAVITIES

8.1. Introduction to the System

Tuned mass dampers are generally used to reduce wind-load-induced dynamic response of tall buildings. TMDs are usually located near the top of tall buildings because they work most effectively when they are located where maximum lateral displacement occurs. However, as a result, very valuable top floor space is sacrificed merely as TMD room.

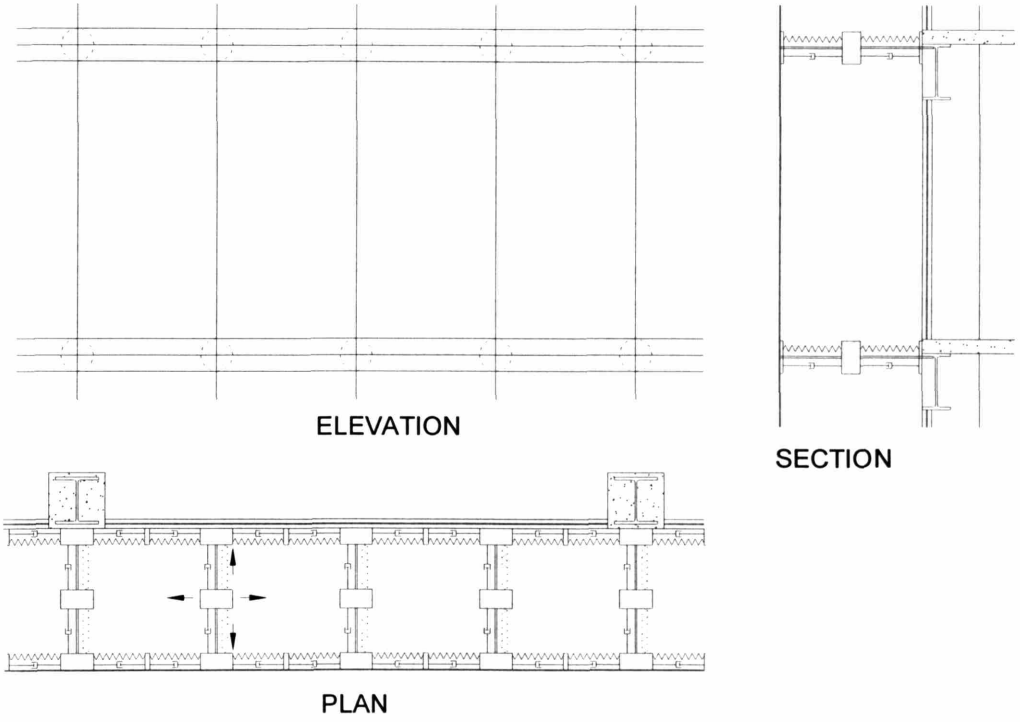

Figure 8.1: Conceptual Sketch of Vertically Distributed TMDs within DSF Cavities

As mentioned in Chapter 7, there are several benefits of distributing TMDs through the DSF cavity. First of all, by doing this, no occupiable building area is used as a room for conventional huge TMDs. Second, since all TMD masses are located at the extreme perimeter of the building, torsional resistance exerted by TMDs is maximized if they are designed to move in the direction parallel to the building façade planes. Third, by distributing TMDs vertically not only the first mode, which has its maximum displacement at the top, but also other modes, which may not have their maximum displacement at the top, can be effectively controlled if necessary. In addition, TMDs can be more easily installed by making them small. Figure 8.1 shows the conceptual sketch of distributed multiple small TMDs within the DSF cavity.

8.2. Vertically Distributed Tuned Mass Damper Theory

In order to design a TMD, a tall building primary structure is usually approximated as a single degree of freedom system, and the SDOF/TMD system is optimized. Den Hartog's (1956) optimal stiffness and damping of the TMD result in the lowest peak value of the dynamic structural response. These optimal parameters depend on the primary structure's natural frequency – which is a function of stiffness, mass, and damping – and mass ratio (TMD mass / primary structure mass).

Connor (2003) presented an approximate solution of a multi-degree-of-freedom (MDOF)/TMD system by reducing the problem to an equivalent SDOF/TMD system. This approach is employed for the approximate solution of the MDOF/Vertically Distributed Multiple TMD system.

Also discussed is the exact solution of the system. The exact solution does not reduce the MDOF primary structure to an equivalent SDOF system. Displacement of each node of the exact solution is obtained by superposing all modal contributions, while that of the approximate solution is obtained by considering only one dominant mode (usually the first mode).

Following is more detailed discussion on both the approximate solution and exact solution. The 2DOF/2TMD system is investigated first. Each method gives very similar results with regard to the fundamental mode dynamic response.

8.2.1. Approximate Solution for 2DOF / 2TMD System

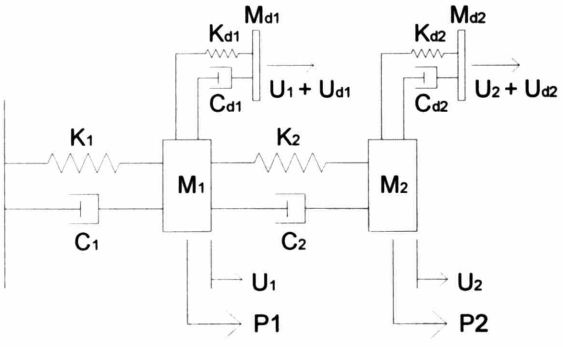

English/Greek Symbols

M: Mass
K: Stiffness
C: Viscous Damping Parameter
P: Applied Loading
U: Displacement
ϖ: Natural Frequency of Structure
Ω: Forcing Frequency
ρ: Forcing Frequency to Natural Frequency Ratio (Ω/ϖ)
f: TMD Frequency to Primary Structure Frequency Ratio ($\varpi d / \varpi$)
ξ: Damping Ratio
ϕ: Mode Shape Vector

Figure 8.2: 2DOF/2TMD System Model

A 2DOF system with TMDs attached to both primary masses 1 and 2 is considered to represent vertically distributed TMDs in a tall building. The governing equations for the system shown in Figure 8.2 are

$$m_1\ddot{u}_1 + c_1\dot{u}_1 + k_1u_1 - c_2(\dot{u}_2 - \dot{u}_1) - k_2(u_2 - u_1) = p_1 + k_{d1}u_{d1} + c_{d1}\dot{u}_{d1} \tag{8.1}$$

$$m_2\ddot{u}_2 + c_2(\dot{u}_2 - \dot{u}_1) + k_2(u_2 - u_1) = p_2 + k_{d2}u_{d2} + c_{d2}\dot{u}_{d2} \tag{8.2}$$

$$m_{d1}\ddot{u}_{d1} + c_{d1}\dot{u}_{d1} + k_{d1}u_{d1} = -m_{d1}\ddot{u}_1 \tag{8.3}$$

$$m_{d2}\ddot{u}_{d2} + c_{d2}\dot{u}_{d2} + k_{d2}u_{d2} = -m_{d2}\ddot{u}_2 . \tag{8.4}$$

Equations 8.1 and 8.2 are combined to reduce the problem to an equivalent SDOF system for the approximate solution. The approach followed here is based on transforming the original matrix equation to scalar modal equations. Introducing matrix notation, Equations 8.1 and 8.2 are written as

$$\begin{bmatrix} m_1 & \\ & m_2 \end{bmatrix}\begin{Bmatrix} \ddot{u}_1 \\ \ddot{u}_2 \end{Bmatrix} + \begin{bmatrix} c_1 + c_2 & -c_2 \\ -c_2 & c_2 \end{bmatrix}\begin{Bmatrix} \dot{u}_1 \\ \dot{u}_2 \end{Bmatrix} + \begin{bmatrix} k_1 + k_2 & -k_2 \\ -k_2 & k_2 \end{bmatrix}\begin{Bmatrix} u_1 \\ u_2 \end{Bmatrix} = \begin{Bmatrix} p_1 \\ p_2 \end{Bmatrix} + \begin{Bmatrix} k_{d1}u_{d1} + c_{d1}\dot{u}_{d1} \\ k_{d2}u_{d2} + c_{d2}\dot{u}_{d2} \end{Bmatrix} \tag{8.5}$$

$$M\ddot{U} + C\dot{U} + KU = \begin{Bmatrix} p_1 \\ p_2 \end{Bmatrix} + \begin{Bmatrix} k_{d1}u_{d1} + c_{d1}\dot{u}_{d1} \\ k_{d2}u_{d2} + c_{d2}\dot{u}_{d2} \end{Bmatrix}. \tag{8.6}$$

Displacement matrix U is substituted in terms of the modal vectors and coordinates.

$$U = \phi_1 q_1 + \phi_2 q_2 = \begin{Bmatrix} \phi_{11} \\ \phi_{12} \end{Bmatrix} q_1 + \begin{Bmatrix} \phi_{21} \\ \phi_{22} \end{Bmatrix} q_2 \tag{8.7}$$

Defining modal mass, stiffness and damping terms,

$$\tilde{m}_i = \phi_i^T M \phi_i \tag{8.8}$$

$$\tilde{k}_i = \phi_i^T K \phi_i = \omega_i^2 m_i \tag{8.9}$$

$$\tilde{c}_i = \phi_i^T C \phi_i \tag{8.10}$$

and assuming damping is proportional to stiffness,

$$C = \alpha K \tag{8.11}$$

a set of uncoupled equations for q_1 and q_2 are obtained.

$$\tilde{m}_1\ddot{q}_1 + \tilde{c}_1\dot{q}_1 + \tilde{k}_1 q_1 = \phi_{11}(p_1 + k_{d1}u_{d1} + c_{d1}\dot{u}_{d1}) + \phi_{12}(p_2 + k_{d2}u_{d2} + c_{d2}\dot{u}_{d2}) \tag{8.12}$$

$$\tilde{m}_2\ddot{q}_2 + \tilde{c}_2\dot{q}_2 + \tilde{k}_2 q_2 = \phi_{21}(p_1 + k_{d1}u_{d1} + c_{d1}\dot{u}_{d1}) + \phi_{22}(p_2 + k_{d2}u_{d2} + c_{d2}\dot{u}_{d2}) \tag{8.13}$$

The displacement at the top of the building is obtained by superposing the modal contributions.

$$u_2 = \phi_{12} q_1 + \phi_{22} q_2 \tag{8.14}$$

However, in general, the first modal response is dominant in tall buildings subjected to wind loads. When the external forcing frequency is close to the fundamental frequency of the primary structure, ω_1, the first mode response will dominate, and it is reasonable to assume

$$u_2 \approx \phi_{12} q_1 . \tag{8.15}$$

Solving for q_1,

$$q_1 \approx \frac{u_2}{\phi_{12}} \tag{8.16}$$

and substituting in Equation 8.12 generate the following equation:

$$\frac{\tilde{m}_1}{(\phi_{12})^2}\ddot{u}_2 + \frac{\tilde{c}_1}{(\phi_{12})^2}\dot{u}_2 + \frac{\tilde{k}_1}{(\phi_{12})^2}u_2 = \frac{\phi_{11}p_1 + \phi_{12}p_2}{\phi_{12}} + \frac{\phi_{11}}{\phi_{12}}(k_{d1}u_{d1} + c_{d1}\dot{u}_{d1}) + (k_{d2}u_{d2} + c_{d2}\dot{u}_{d2}) . \tag{8.17}$$

Defining equivalent SDOF parameters,

$$\tilde{m}_{1e} = \frac{\tilde{m}_1}{(\phi_{12})^2} \tag{8.18}$$

$$\tilde{c}_{1e} = \frac{\tilde{c}_1}{(\phi_{12})^2} \tag{8.19}$$

$$\tilde{k}_{1e} = \frac{\tilde{k}_1}{(\phi_{12})^2} \tag{8.20}$$

$$\tilde{p}_{1e} = \frac{\phi_{11}p_1 + \phi_{12}p_2}{\phi_{12}} \tag{8.21}$$

Equation 8.17 becomes

$$\tilde{m}_{1e}\ddot{u}_2 + \tilde{c}_{1e}\dot{u}_2 + \tilde{k}_{1e}u_2 = \tilde{p}_{1e} + \frac{\phi_{11}}{\phi_{12}}(k_{d1}u_{d1} + c_{d1}\dot{u}_{d1}) + (k_{d2}u_{d2} + c_{d2}\dot{u}_{d2}) . \tag{8.22}$$

Taking $u_2 \equiv u$, $\tilde{m}_{1e} \equiv m$, $\tilde{c}_{1e} \equiv c$, $\tilde{k}_{1e} \equiv k$, $\phi_{11}/\phi_{12} = \alpha$, Equation 8.22 becomes

$$m\ddot{u} + c\dot{u} + ku = p + \alpha(k_{d1}u_{d1} + c_{d1}\dot{u}_{d1}) + (k_{d2}u_{d2} + c_{d2}\dot{u}_{d2}). \tag{8.23}$$

And Equations 8.3 and 8.4 can be rewritten

$$m_{d1}\ddot{u}_{d1} + c_{d1}\dot{u}_{d1} + k_{d1}u_{d1} = -\alpha m_{d1}\ddot{u} \tag{8.24}$$

$$m_{d2}\ddot{u}_{d2} + c_{d2}\dot{u}_{d2} + k_{d2}u_{d2} = -m_{d2}\ddot{u}\ . \tag{8.25}$$

It is convenient to work with the solution expressed in terms of complex quantities. The force is expressed as

$$p = \hat{p}e^{i\Omega t} \tag{8.26}$$

where $\hat{p}$ is a real quantity. The response is taken as

$$u = \overline{u}e^{i\Omega t} \tag{8.27}$$

$$u_d = \overline{u}_d e^{i\Omega t} \tag{8.28}$$

where the response amplitudes, $\overline{u}$ and $\overline{u}_d$, are considered to be complex quantities. Then the corresponding solution is given by either the real or imaginary parts of u and u_d. Substituting Equations 8.26, 8.27 and 8.28 in the set of governing Equations 8.23, 8.24, and 8.25 results in

$$-\Omega^2 m\overline{u} + i\Omega c\overline{u} + k\overline{u} = \hat{p} + \alpha(k_{d1}\overline{u}_{d1} + i\Omega c_{d1}\overline{u}_{d1}) + (k_{d2}\overline{u}_{d2} + i\Omega c_{d2}\overline{u}_{d2}) \tag{8.29}$$

$$-\Omega^2 m_{d1}\overline{u}_{d1} + ic_{d1}\overline{u}_{d1} + k_{d1}\overline{u}_{d1} = \alpha\Omega^2 m_{d1}\overline{u} \tag{8.30}$$

$$-\Omega^2 m_{d2}\overline{u}_{d2} + ic_{d2}\overline{u}_{d2} + k_{d2}\overline{u}_{d2} = \Omega^2 m_{d2}\overline{u}\ . \tag{8.31}$$

Considering the following notations

$$\omega^2 = k/m \tag{8.32}$$

$$c = 2\xi\omega m \tag{8.33}$$

$$\omega_d^{\ 2} = k_d/m_d \tag{8.34}$$

$$c_d = 2\xi_d\omega_d m_d \tag{8.35}$$

and defining $\overline{m}$ as the TMD to primary structure mass ratio,

$$\overline{m}_1 = {}^{m_{d1}}\!/_{m}, \quad \overline{m}_2 = {}^{m_{d2}}\!/_{m} \tag{8.36}$$

and defining f as the TMD to primary structure frequency ratio,

$$f_1 = {}^{\omega_{d1}}\!/_{\omega}, \quad f_2 = {}^{\omega_{d2}}\!/_{\omega} \tag{8.37}$$

the governing Equations 8.29, 8.30 and 8.31 become

$$-\alpha(i2\xi_{d1}f_1\overline{m}_1\rho + f_1^2\overline{m}_1)\overline{u}_{d1} - (i2\xi_{d2}f_2\overline{m}_2\rho + f_2^2\overline{m}_2)\overline{u}_{d2} + (-\rho^2 + i2\xi\rho + 1)\overline{u} = {}^{\hat{p}}\!/_{k} \tag{8.38}$$

$$(\overline{m}_1\rho^2 + i2\xi_{d1}f_1\overline{m}_1\rho + f_1^2\overline{m}_1)\overline{u}_{d1} - \alpha\overline{m}_1\rho^2\overline{u} = 0 \tag{8.39}$$

$$(\overline{m}_2\rho^2 + i2\xi_{d2}f_2\overline{m}_2\rho + f_2^2\overline{m}_2)\overline{u}_{d2} - \overline{m}_2\rho^2\overline{u} = 0. \tag{8.40}$$

The solutions due to periodic excitation can be expressed as

$$\overline{u} = \frac{\hat{p}}{k}He^{i\delta_1} \tag{8.41}$$

$$\overline{u}_{d1} = \frac{\hat{p}}{k}H_{d1}e^{i\delta_2} \tag{8.42}$$

$$\overline{u}_{d2} = \frac{\hat{p}}{k}H_{d2}e^{i\delta_3}. \tag{8.43}$$

Figure 8.3 contains the plots of H, H_{d1}, and H_{d2}, when the mass ratio $\overline{m}_1$ and $\overline{m}_2$ are 1.5%, and TMDs are tuned by iteration for optimal performance. 0.5% primary structure damping ratio was used for this plot.

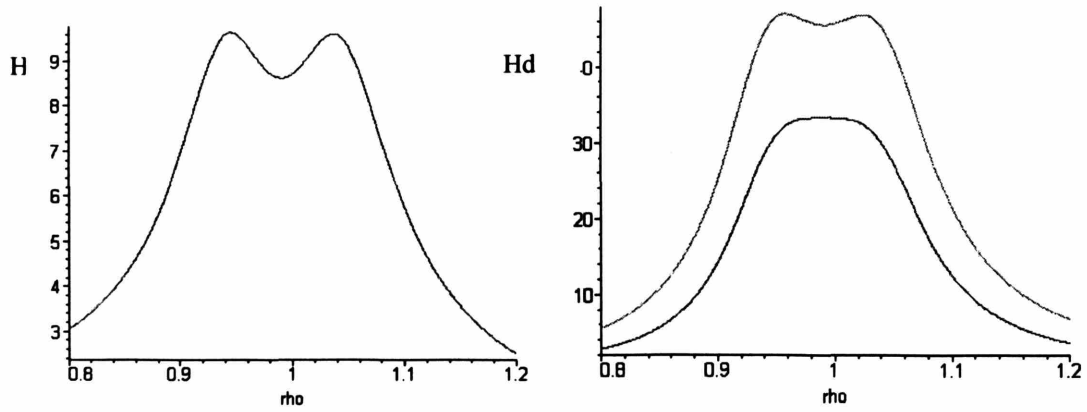

As can be seen from Figure 8.3, the H plot shows only two peaks, even though the original 2DOF/2TMD system was converted to a 3DOF system. In fact, if TMD damping ratio $\xi_d = 0$, we can observe one more peak between the two peaks. However, this peak in-between is very sensitive to TMD damping ratio ξ_d. Thus, introducing even very little damping for TMDs eliminates this peak. This phenomenon is generally observed in vertically distributed TMD systems. In a NDOF+NTMD system, if the NDOF primary structure is reduced to a single degree of freedom system, the H plot for this system has N+1 peaks if $\xi_d = 0$. However, once damping is applied to TMDs for tuning, the H plot has only two peaks, and its overall shape becomes similar to that shown in Figure 8.3.

8.2.2. Exact Solution for 2DOF/2TMD System

In the previous section the approximate solution was introduced in order to simplify the analysis of the vertically distributed TMD scheme. In this section the exact solution is studied: 1) to verify the accuracy of the approximate solution, and 2) to investigate the contribution of the second mode.

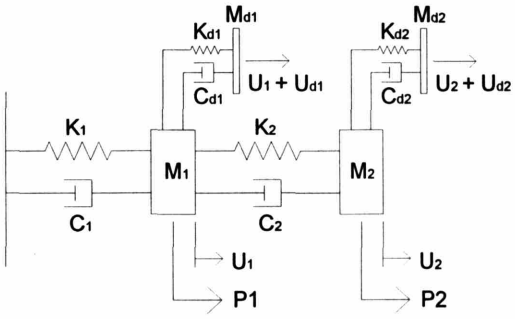

English/Greek Symbols

M: Mass
K: Stiffness
C: Viscous Damping Parameter
P: Applied Loading
U: Displacement
ϖ: Natural Frequency of Structure
Ω: Forcing Frequency
ρ: Forcing Frequency to Natural Frequency Ratio (Ω/ϖ)
f: TMD Frequency to Primary Structure Frequency Ratio (ϖd / ϖ)
ξ: Damping Ratio
ϕ: Mode Shape Vector

For this purpose, our beginning point is Equations 8.12 and 8.13, which are rewritten here, from the previous section:

$$\tilde{m}_1\ddot{q}_1 + \tilde{c}_1\dot{q}_1 + \tilde{k}_1 q_1 = \phi_{11}(p_1 + k_{d1}u_{d1} + c_{d1}\dot{u}_{d1}) + \phi_{12}(p_2 + k_{d2}u_{d2} + c_{d2}\dot{u}_{d2}) \tag{8.12}$$

$$\tilde{m}_2\ddot{q}_2 + \tilde{c}_2\dot{q}_2 + \tilde{k}_2 q_2 = \phi_{21}(p_1 + k_{d1}u_{d1} + c_{d1}\dot{u}_{d1}) + \phi_{22}(p_2 + k_{d2}u_{d2} + c_{d2}\dot{u}_{d2}) \tag{8.13}$$

In the approximate solution, we neglected the second mode, and in turn, Equation 8.13. In the exact solution, it is included. Through the very similar process presented in the previous section, Equation 8.12 can be rewritten

$$(-m_1\Omega^2 + ic_1\Omega + k_1)\bar{q}_1 = \hat{p}_1 + \frac{\phi_{11}}{\phi_{12}}(ic_{d1}\Omega + k_{d1})\bar{u}_{d1} + (ic_{d2}\Omega + k_{d2})\bar{u}_{d2}. \tag{8.44}$$

and Equation 8.44 can be rewritten again

$$(-\rho_1^2 + i2\xi_1\rho_1 + 1)\overline{q}_1 - \frac{\phi_{11}}{\phi_{12}}(i2\xi_{d1}f_1\overline{m}_1\rho_1 + f_1^2\overline{m}_1)\overline{u}_{d1} - (i2\xi_{d2}f_2\overline{m}_2\rho_1 + f_2^2\overline{m}_2)\overline{u}_{d2} = \frac{\hat{p}_1}{k_1}. \quad (8.45)$$

In the same way, Equation 8.13 can be rewritten

$$(-m_2\Omega^2 + ic_2\Omega + k_2)\overline{q}_2 = \hat{p}_2 + (ic_{d1}\Omega + k_{d1})\overline{u}_{d1} + \frac{\phi_{22}}{\phi_{21}}(ic_{d2}\Omega + k_{d2})\overline{u}_{d2} \quad (8.46)$$

and Equation 8.46 can be rewritten again

$$(-\rho_1^2 + i2\xi_2\left(\frac{\omega_2}{\omega_1}\right)\rho_1 + \left(\frac{\omega_2}{\omega_1}\right)^2)\overline{q}_2 - (i2\xi_{d1}f_1\overline{m}_1\rho_1 + f_1^2\overline{m}_1)\overline{u}_{d1} - \frac{\phi_{22}}{\phi_{21}}(i2\xi_{d2}f_2\overline{m}_2\rho_1 + f_2^2\overline{m}_2)\overline{u}_{d2} = \frac{\hat{p}_2}{k_1} \quad (8.47)$$

If $p_1 = p_2$,

$$(-\rho_1^2 + i2\xi_2\left(\frac{\omega_2}{\omega_1}\right)\rho_1 + \left(\frac{\omega_2}{\omega_1}\right)^2)\overline{q}_2 - (i2\xi_{d1}f_1\overline{m}_1\rho_1 + f_1^2\overline{m}_1)\overline{u}_{d1} - \frac{\phi_{22}}{\phi_{21}}(i2\xi_{d2}f_2\overline{m}_2\rho_1 + f_2^2\overline{m}_2)\overline{u}_{d2} = \frac{\hat{p}_1}{3k_1} \quad (8.48)$$

Equation 8.3 can be rewritten by incorporating Equation 8.7

$$m_{d1}\ddot{u}_{d1} + c_{d1}\dot{u}_{d1} + k_{d1}u_{d1} = -m_{d1}(\phi_{11}\ddot{q}_1 + \phi_{21}\ddot{q}_2). \quad (8.49)$$

Equation 8.49 can be further rewritten by working with the solution expressed in terms of complex quantities and using the notations and definitions presented by Equations from 8.32 to 8.37

$$(-\overline{m}_1\rho_1^2 + i2\xi_{d1}f_1\overline{m}_1\rho_1 + f_1^2\overline{m}_1)\overline{u}_{d1} - \overline{m}_1(\phi_{11}\rho_1^2\overline{q}_1 + \phi_{21}\rho_1^2\overline{q}_2) = 0. \quad (8.50)$$

In the same way, Equation 8.4 can also be rewritten by incorporating Equation 8.7

$$m_{d2}\ddot{u}_{d2} + c_{d2}\dot{u}_{d2} + k_{d2}u_{d2} = -m_{d2}(\phi_{12}\ddot{q}_1 + \phi_{22}\ddot{q}_2) \quad (8.51)$$

and Equation 8.51 can also be further rewritten

$$(-\overline{m}_2\rho_1^2 + i2\xi_{d2}f_2\overline{m}_2\rho_1 + f_2^2\overline{m}_2)\overline{u}_{d2} - \overline{m}_2(\phi_{12}\rho_1^2\overline{q}_1 + \phi_{22}\rho_1^2\overline{q}_2) = 0. \quad (8.52)$$

If the stiffness of the primary structure is configured to produce the first mode shape of a linear profile, the solution of the displacement of node 2 due to a periodic excitation can be expressed as

$$u_2 = \phi_{12} q_1 + \phi_{22} q_2 = q_1 - 0.5 q_2 = \left(\frac{p}{k} H_{q1} - 0.5 \frac{p}{k} H_{q2} \right) e^{i\delta} = \frac{p}{k} H e^{i\delta} . \tag{8.53}$$

Here, H is the dynamic amplification factor.

Thus, $H = H_{q1} - 0.5 H_{q2} .$ (8.54)

The plot of H_1 (Dynamic Amplification Factor of Node 1 with regard to Displacement) and H_2 (Dynamic Amplification Factor of Node 2 with regard to Displacement) for the specific configuration used in the example for the approximate solution in the previous section is shown in Figure 8.4. As can be seen from the figure, the maximum H value of node 2 regarding the first mode excitation is almost the same as that obtained from the approximate solution presented in the previous section, demonstrating the accuracy of the approximate solution.

As illustrated in Figure 8.4, both TMDs were tuned to the first mode. Thus, the second mode response was not controlled. In terms of displacement, this was still acceptable for both node 1 and node 2. However, with regard to acceleration, this resulted in the maximum acceleration occurring in the second mode resonance condition. The acceleration at node 1 in the second mode resonance condition was greater than that at node 2 in the first mode resonance condition (Figure 8.5). This phenomenon occurs when the primary structure damping ratio is very small, such as 0.5% in this example. In this case, the second mode excitation control may be necessary.

In order to control the second mode acceleration problem, another distributed TMD configuration is studied and the results are illustrated in Figure 8.6 and 8.7. Now the TMD installed in node 2 is tuned to the first mode, while the TMD installed in node 1 is tuned to the second mode. As can be seen from Figure 8.7, now the acceleration in the second mode is less than that in the first mode.

Acceleration is often expressed as a function of the gravitational acceleration, g. Generally, when acceleration exceeds 0.02g, people begin to feel discomfort. In active TMD systems such as the ones in the John Hancock Tower in Boston or Citicorp Center in New York, whenever the horizontal acceleration exceeds 0.003g for two consecutive cycles, the system is automatically activated. The following relationship exists between H (Dynamic amplification factor regarding displacement) and H_A (Dynamic amplification factor regarding acceleration).

$$H_A = \rho^2 H \tag{8.55}$$

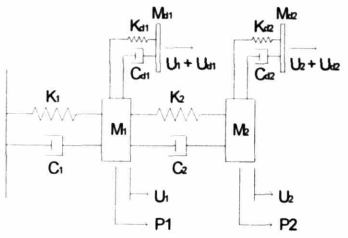

First & Second Mode Resonance Zone
Dynamic Amplification Factor
- TMDs are Tuned to the First Mode
- Optimized for Entire 2DOF/2TMD System by Iteration for Displacement

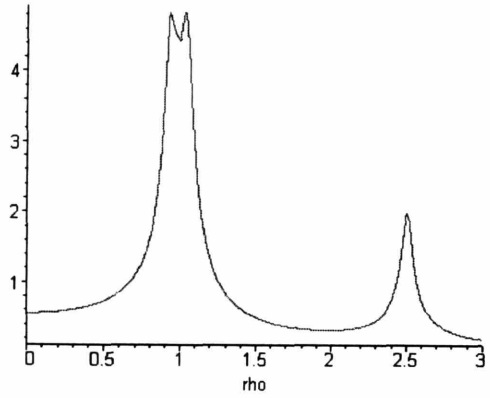

H_1 plot , $U_1 = (P/K)\, H_1$
$\phi 11 = 0.5$, $\phi 12 = 1.0$
$\phi 21 = 1.0$, $\phi 22 = -0.5$
$\omega 1 = 1$
$\omega 2 = 2.5$
Mass Ratio M1 = 0.015
Mass Ratio M2 = 0.015
Struc. Damping Ratio $\xi_1 = 0.005$, $\xi_2 = 0.0132$
f1 = 0.985, f2 = 980
TMD Damping Ratio $\xi_{d1} = 0.065$, $\xi_{d2} = 0.095$

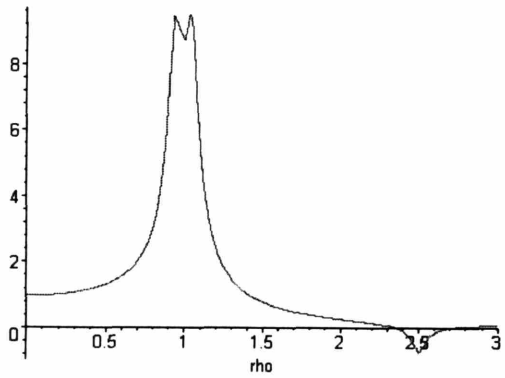

H_2 plot , $U_2 = (P/K)\, H_2$
$\phi 11 = 0.5$, $\phi 12 = 1.0$
$\phi 21 = 1.0$, $\phi 22 = -0.5$
$\omega 1 = 1$
$\omega 2 = 2.5$
Mass Ratio M1 = 0.015
Mass Ratio M2 = 0.015
Struc. Damping Ratio $\xi_1 = 0.005$, $\xi_2 = 0.0132$
f1 = 0.985, f2 = 980
TMD Damping Ratio $\xi_{d1} = 0.065$, $\xi_{d2} = 0.095$

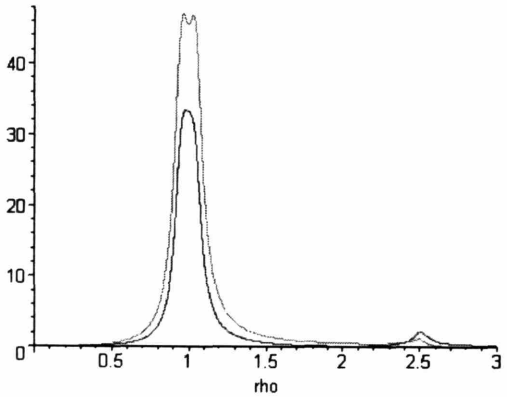

H_{d1}, H_{d2} plot , $U_{d1} = (P/K)\, H_{d1}$, $U_{d2} = (P/K)\, H_{d2}$
$\phi 11 = 0.5$, $\phi 12 = 1.0$
$\phi 21 = 1.0$, $\phi 22 = -0.5$
$\omega 1 = 1$
$\omega 2 = 2.5$
Mass Ratio M1 = 0.015
Mass Ratio M2 = 0.015
Struc. Damping Ratio $\xi_1 = 0.005$, $\xi_2 = 0.0132$
f1 = 0.985, f2 = 980
TMD Damping Ratio $\xi_{d1} = 0.065$, $\xi_{d2} = 0.095$

Figure 8.4

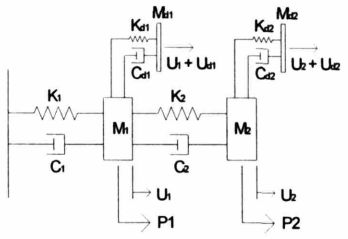

First & Second Mode Resonance Zone
Acceleration Dynamic Amplification Factor
- TMDs are Tuned to the First Mode
- Optimized for Entire 2DOF/2TMD System
by Iteration for Displacement

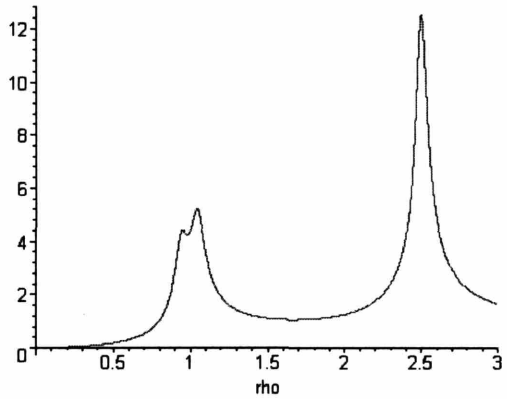

H_{A1} plot , $A_1 = (P/M)\, H_{A1}$
$\phi 11 = 0.5$, $\phi 12 = 1.0$
$\phi 21 = 1.0$, $\phi 22 = -0.5$
$\omega 1 = 1$
$\omega 2 = 2.5$
Mass Ratio M1 = 0.015
Mass Ratio M2 = 0.015
Struc. Damping Ratio $\xi_1 = 0.005$, $\xi_2 = 0.0132$
f1 = 0.985, f2 = 980
TMD Damping Ratio $\xi_{d1} = 0.065$, $\xi_{d2} = 0.095$

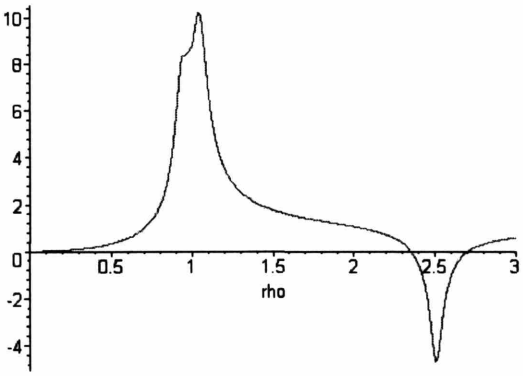

H_{A2} plot , $A_1 = (P/M)\, H_{A2}$
$\phi 11 = 0.5$, $\phi 12 = 1.0$
$\phi 21 = 1.0$, $\phi 22 = -0.5$
$\omega 1 = 1$
$\omega 2 = 2.5$
Mass Ratio M1 = 0.015
Mass Ratio M2 = 0.015
Struc. Damping Ratio $\xi_1 = 0.005$, $\xi_2 = 0.0132$
f1 = 0.985, f2 = 980
TMD Damping Ratio $\xi_{d1} = 0.065$, $\xi_{d2} = 0.095$

Figure 8.5

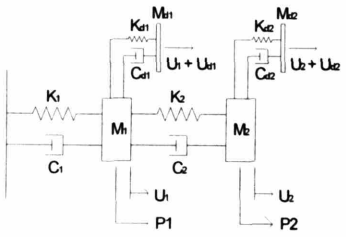

First & Second Mode Resonance Zone
Dynamic Amplification Factor
- TMD1 is Tuned to the 2nd Mode
- TMD2 is Tuned to the 1st Mode
- Optimized for Entire 2DOF/2TMD System by Trial & Error for Displacement

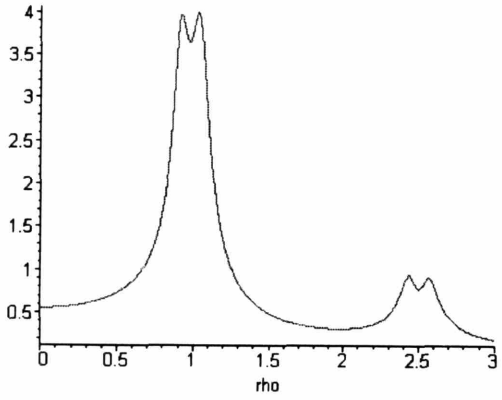

H_1 plot , $U_1 = (P/K)\, H_1$
$\phi 11 = 0.5$, $\phi 12 = 1.0$
$\phi 21 = 1.0$, $\phi 22 = -0.5$
$\omega 1 = 1$
$\omega 2 = 2.5$
Mass Ratio M1 = 0.003
Mass Ratio M2 = 0.030
Struc. Damping Ratio $\xi_1 = 0.005$, $\xi_2 = 0.0132$
f1 = 2.50, f2 = 0.97
TMD Damping Ratio $\xi_{d1} = 0.03$, $\xi_{d2} = 0.11$

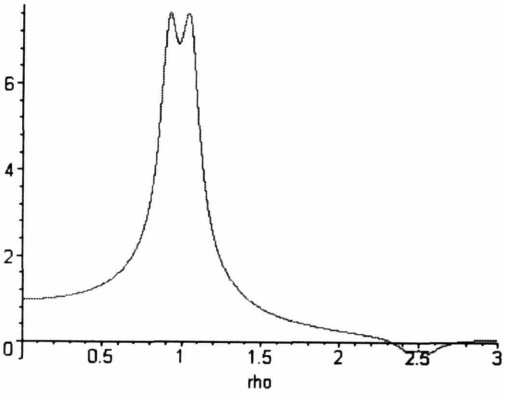

H_2 plot , $U_2 = (P/K)\, H_2$
$\phi 11 = 0.5$, $\phi 12 = 1.0$
$\phi 21 = 1.0$, $\phi 22 = -0.5$
$\omega 1 = 1$
$\omega 2 = 2.5$
Mass Ratio M1 = 0.003
Mass Ratio M2 = 0.030
Struc. Damping Ratio $\xi_1 = 0.005$, $\xi_2 = 0.0132$
f1 = 2.50, f2 = 0.97
TMD Damping Ratio $\xi_{d1} = 0.03$, $\xi_{d2} = 0.11$

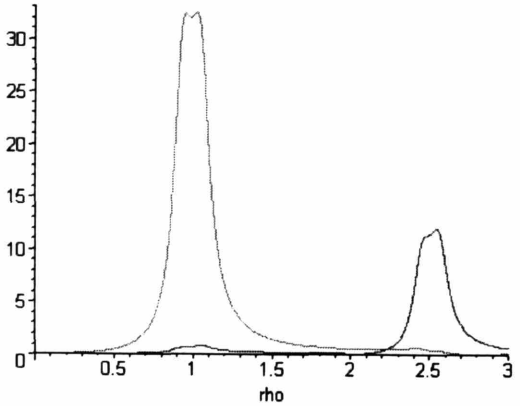

H_{d1}, H_{d2} plot , $U_{d1} = (P/K)\, H_{d1}$, $U_{d2} = (P/K)\, H_{d2}$
$\phi 11 = 0.5$, $\phi 12 = 1.0$
$\phi 21 = 1.0$, $\phi 22 = -0.5$
$\omega 1 = 1$
$\omega 2 = 2.5$
Mass Ratio M1 = 0.003
Mass Ratio M2 = 0.030
Struc. Damping Ratio $\xi_1 = 0.005$, $\xi_2 = 0.0132$
f1 = 2.50, f2 = 0.97
TMD Damping Ratio $\xi_{d1} = 0.03$, $\xi_{d2} = 0.11$

Figure 8.6

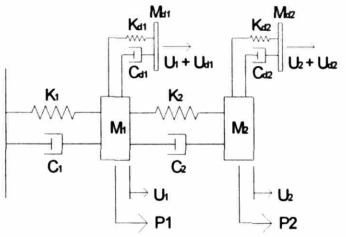

First & Second Mode Resonance Zone
Acceleration Dynamic Amplification Factor
- TMD1 is Tuned to the 2nd Mode
- TMD2 is Tuned to the 1st Mode
- Optimized for Entire 2DOF/2TMD System by Iteration for Displacement

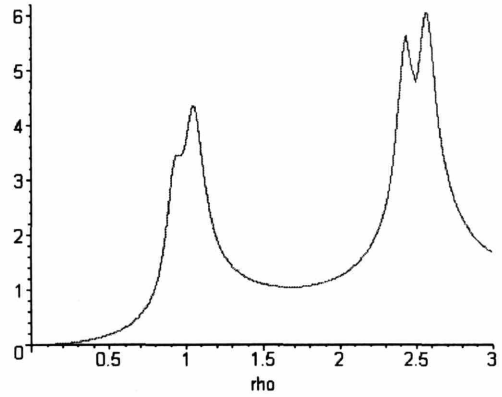

H_{A1} plot , A_1= (P/M) H_{A1}
$\phi 11 = 0.5$, $\phi 12 = 1.0$
$\phi 21 = 1.0$, $\phi 22 = -0.5$
$\omega 1 = 1$
$\omega 2 = 2.5$
Mass Ratio M1 = 0.003
Mass Ratio M2 = 0.030
Struc. Damping Ratio $\xi_1 = 0.005$, $\xi_2 = 0.0132$
f1 = 2.50, f2 = 0.97
TMD Damping Ratio $\xi_{d1} = 0.03$, $\xi_{d2} = 0.11$

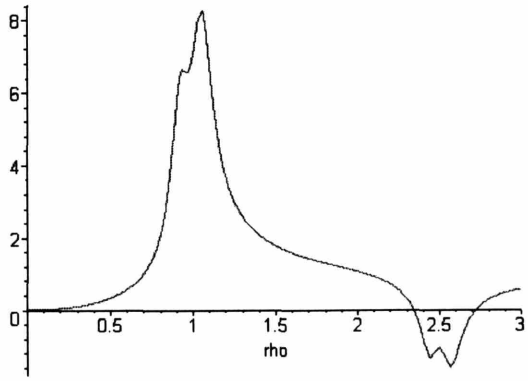

H_{A2} plot , A_1= (P/M) H_{A2}
$\phi 11 = 0.5$, $\phi 12 = 1.0$
$\phi 21 = 1.0$, $\phi 22 = -0.5$
$\omega 1 = 1$
$\omega 2 = 2.5$
Mass Ratio M1 = 0.003
Mass Ratio M2 = 0.030
Struc. Damping Ratio $\xi_1 = 0.005$, $\xi_2 = 0.0132$
f1 = 2.50, f2 = 0.97
TMD Damping Ratio $\xi_{d1} = 0.03$, $\xi_{d2} = 0.11$

Figure 8.7

8.2.3. Approximate Solution for Vertically Distributed TMDs in Tall Buildings

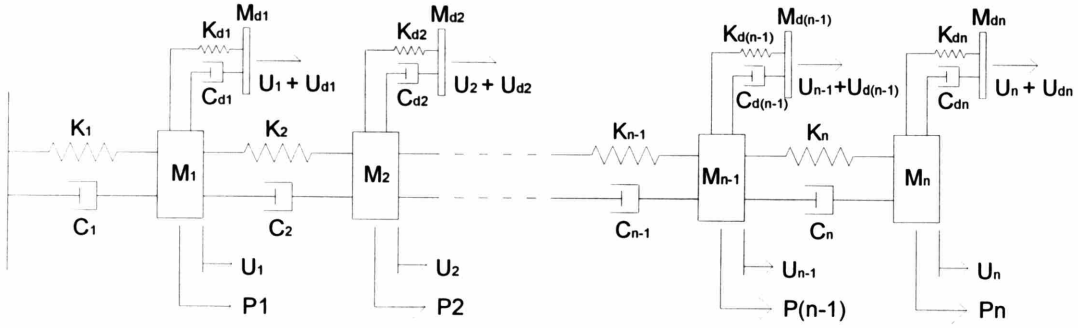

Figure 8.8: NDOF/NTMD System Model

The vertically distributed TMD system equations can be set up approximately by reducing the MDOF system primary structure to a SDOF system, considering the importance of the first mode response. By solving the equations following the process presented earlier, H (Dynamic Amplification Factor of Primary Structure) and Hd (Dynamic Amplification Factor of TMD Mass) plots can be obtained. In addition, using the relationship between H (Dynamic amplification factor regarding displacement) and HA (Dynamic amplification factor regarding acceleration), the HA plot can be produced.

$$m\ddot{u}+c\dot{u}+ku=p+\frac{\phi_{11}}{\phi_{1n}}(k_{d1}u_{d1}+c_{d1}\dot{u}_{d1})+.....+\frac{\phi_{1(n-1)}}{\phi_{1n}}(k_{d(n-1)}u_{d(n-1)}+c_{d(n-1)}\dot{u}_{d(n-1)})+(k_{dn}u_{dn}+c_{dn}\dot{u}_{dn}) \tag{8.56}$$

$$m_{d1}\ddot{u}_{d1}+c_{d1}\dot{u}_{d1}+k_{d1}u_{d1}=-\frac{\phi_{11}}{\phi_{1n}}m_{d1}\ddot{u} \tag{8.57}$$

$$m_{d2}\ddot{u}_{d2}+c_{d2}\dot{u}_{d2}+k_{d2}u_{d2}=-\frac{\phi_{12}}{\phi_{1n}}m_{d2}\ddot{u} \tag{8.58}$$

.....

$$m_{d(n-1)}\ddot{u}_{d(n-1)}+c_{d(n-1)}\dot{u}_{d(n-1)}+k_{d(n-1)}u_{d(n-1)}=-\frac{\phi_{1(n-1)}}{\phi_{1n}}m_{d(n-1)}\ddot{u} \tag{8.59}$$

$$m_{dn}\ddot{u}_{dn}+c_{dn}\dot{u}_{dn}+k_{dn}u_{dn}=-m_{dn}\ddot{u} \tag{8.60}$$

TMDs located on the floors close to the ground are not as effective as the ones located at the higher floors with regard to the first mode. The model shown in Figure 8.8 can be modified and the equations shown above can be adjusted accordingly. The 6DOF/4TMD system study shown in the next section demonstrates this strategy.

8.2.4. 6DOF System with vertically distributed TMD's

The 6DOF/4TMD system (Figure 8.9) is analyzed, using the approximate solution presented in the previous section. The purpose of this study is to investigate: 1) the effectiveness of the TMD depending on its vertical location and 2) a tuning strategy for a vertically distributed TMD system.

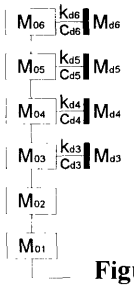

Figure 8.9: 6DOF/4TMD

The 6DOF primary structure is reduced to a SDOF system. Governing equations are shown below.

$$m\ddot{u}+c\dot{u}+ku=p+\frac{\phi_{13}}{\phi_{16}}(k_{d3}u_{d3}+c_{d3}\dot{u}_{d3})+\frac{\phi_{14}}{\phi_{16}}(k_{d4}u_{d4}+c_{d4}\dot{u}_{d4})+\frac{\phi_{15}}{\phi_{16}}(k_{d5}u_{d5}+c_{d5}\dot{u}_{d5})+(k_{d6}u_{d6}+c_{d6}\dot{u}_{d6}) \tag{8.61}$$

$$m_{d3}\ddot{u}_{d3}+c_{d3}\dot{u}_{d3}+k_{d3}u_{d3}=-\frac{\phi_{13}}{\phi_{16}}m_{d3}\ddot{u} \tag{8.62}$$

$$m_{d4}\ddot{u}_{d4}+c_{d4}\dot{u}_{d4}+k_{d4}u_{d4}=-\frac{\phi_{14}}{\phi_{16}}m_{d4}\ddot{u} \tag{8.63}$$

$$m_{d5}\ddot{u}_{d5}+c_{d5}\dot{u}_{d5}+k_{d5}u_{d5}=-\frac{\phi_{15}}{\phi_{16}}m_{d5}\ddot{u} \tag{8.64}$$

$$m_{d6}\ddot{u}_{d6}+c_{d6}\dot{u}_{d6}+k_{d6}u_{d6}=-m_{d6}\ddot{u} \tag{8.65}$$

Through the process presented in Section 8.2.1, the solution due to periodic excitation can be expressed as

$$\bar{u}=\frac{\hat{p}}{k}He^{i\delta}\ . \tag{8.66}$$

Here, $\bar{u}$ is the displacement at node 6 of the 6DOF system, and H is the dynamic amplification factor.

The study is performed in four steps. First, only one TMD, the mass ratio of which is 0.01 ($m_d/\frac{\tilde{m}_1}{(\phi_{16})^2}$), is installed at node 6, 5, 4 and 3, and tuned for optimal performance (Figure 8.10). Second, the four TMDs are installed simultaneously, employing the same tuning parameters used in the first step (Figure 8.11 a). Third, the four TMDs are installed simultaneously, and tuned optimally for this new 6DOF/4TMD system (Figure 8.11 b). Fourth, at node 6, a single TMD, which is equivalent to the four TMD's at nodes 6, 5, 4, and 3, is installed, and tuned, and its response is compared with that of the previous system with four TMDs (Figure 8.12).

a) TMD at Node 6

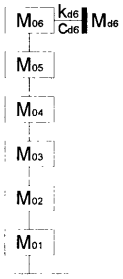

$\xi = 0.005$
$\xi_{d6} = 0.065$
f6 = 0.989
m6 =0.01

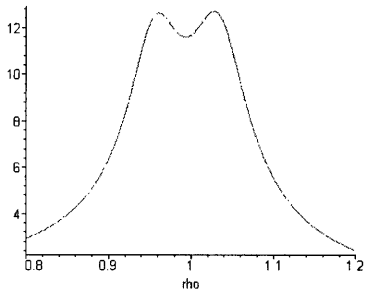

b) TMD at Node 5

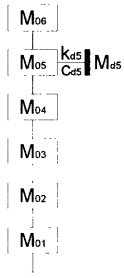

$\xi = 0.005$
$\xi_{d5} = 0.055$
f5 = 0.992
m5 =0.01

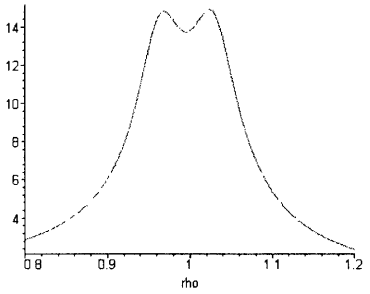

c) TMD at Node 4

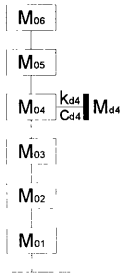

$\xi = 0.005$
$\xi_{d4} = 0.045$
f4 = 0.995
m4 =0.01

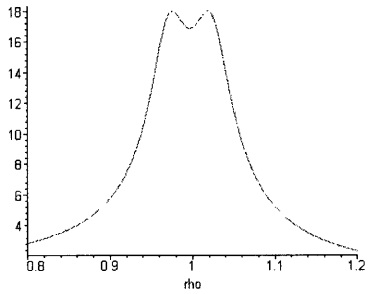

d) TMD at Node 3

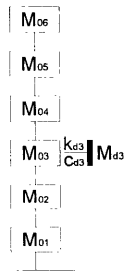

$\xi = 0.005$
$\xi_{d3} = 0.035$
f3 = 0.997
m3 =0.01

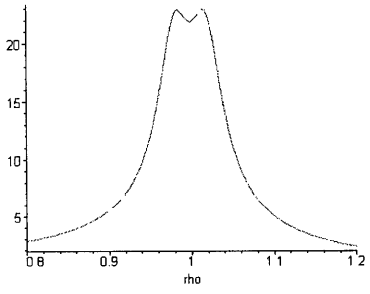

Figure 8.10: Dynamic Amplification Factor in 6DOF/TMD System

a) TMD at Nodes 3, 4, 5 and 6 / tuned individually / $\xi = 0.005$

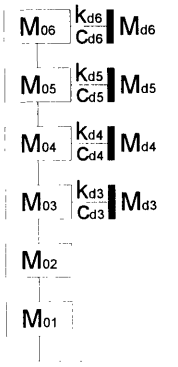

$\xi_{d6} = 0.065$
$\xi_{d5} = 0.055$
$\xi_{d4} = 0.045$
$\xi_{d3} = 0.035$
f6 = 0.989
f5 = 0.992
f4 = 0.995
f3 = 0.997
m6 = 0.01
m5 = 0.01
m4 = 0.01
m3 = 0.01

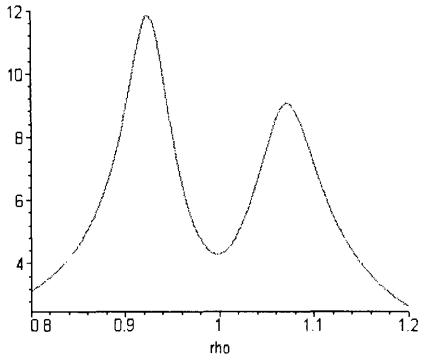

b) TMD at Nodes 3, 4, 5 and 6 / tuned simultaneously / $\xi = 0.005$

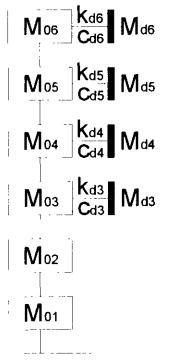

$\xi_{d6} = 0.11$
$\xi_{d5} = 0.10$
$\xi_{d4} = 0.09$
$\xi_{d3} = 0.08$
f6 = 0.961
f5 = 0.978
f4 = 0.985
f3 = 0.990
m6 = 0.01
m5 = 0.01
m4 = 0.01
m3 = 0.01

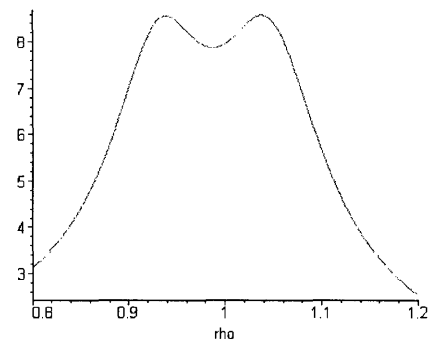

Figure 8.11: Dynamic Amplification Factor in 6DOF/4TMD System

TMD at Node 6/ 40 % TMD Mass Reduction / $\xi = 0.005$

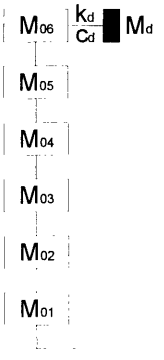

$\xi_{d6} = 0.11$
$\xi_{d5} = 0.10$
$\xi_{d4} = 0.09$
$\xi_{d3} = 0.08$
f6 = 0.961
f5 = 0.978
f4 = 0.985
f3 = 0.990
m6 = 0.024

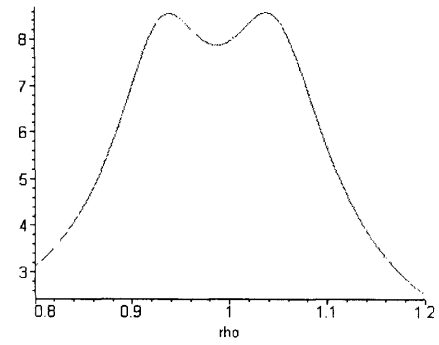

Figure 8.12: Dynamic Amplification Factor in 6DOF/TMD System

As can be seen from Figure 8.10, if a single TMD is installed at different nodes, the one at the top of node 6 is most effective in reducing the first mode dynamic response of the system with stiffness calibrated to produce the first mode shape of a linear profile. As its location is lowered, its equivalent mass ratio and, therefore, its effectiveness decreases. Also, even though the TMD mass of each case in Figure 8.10 is the same, its optimal tuning parameters are different depending on its vertical location.

Figure 8.11 (a) shows the plot of the dynamic amplification factor of the system that combines all the four cases shown in Figure 8.10. As can be seen from the figure, merely combining the four optimally tuned cases as they are does not produce optimal behavior in the combined new system. The system is further tuned for optimal behavior and the result is shown in Figure 8.11 (b). As can be noticed by comparing Figures 8.11 (a) and (b), there are substantial differences in tuning parameters.

Expanding the discussion that generated Equation 8.18 for a 2DOF primary structure, the first mode equivalent generalized mass of the 6DOF primary structure that has a TMD at its n^{th} node is

$$\widetilde{m}_{ie} = \left[\frac{1}{\Phi_{1n}^2}\right]\widetilde{m}_1 = \left[\frac{1}{\Phi_{1n}^2}\right]\Phi_i^T M \Phi_i \quad (n = 1, 2, \ldots, 6)\,. \tag{8.67}$$

The mass ratio is defined in terms of the TMD mass and the equivalent mass of the primary structure:

$$\overline{m} = \frac{m_d}{\widetilde{m}_{1e}} \tag{8.68}$$

For the first mode, Φ_{1n} is 1 for node 6, and it gradually reduces as node number decreases toward the ground. Thus, if the same TMD mass m_d is distributed for every node, the mass ratio $\overline{m}$ gradually decreases as node number decreases because $\widetilde{m}_{1e}$ increases.

For the 6DOF system, the first mode shape of which is a linear profile, if a single TMD is installed at node 6, this configuration requires a total of 40% less mass compared with the distributed system shown in Figure 8.11 to achieve the same equivalent damping ratio (Figure 8.12).

$$\text{Total Mass Reduction (\%)} = \left(\frac{4 - \sum_{n=3}^{6}(\Phi_{1n})^2}{4}\right) \times 100\% \approx 40\% \tag{8.67}$$

8.3. Procedure for Preliminary Design of Vertically Distributed TMDs

8.3.1. Fundamental Mode Vibration Control

The primary structure is reduced to a single degree of freedom system, using the procedure discussed earlier. The allowable maximum displacement at the top of the primary structure is established. Then, on the basis of this displacement constraint, the allowable maximum dynamic amplification factor of the primary structure $H_{displ.}$ is determined.

The maximum dynamic amplification factor, $DAF_{displ.}$, of a damped single degree of freedom system without a TMD with regard to displacement subjected to harmonic load is related by ξ by

$$DAF_{displ.} = \frac{1}{2\xi\sqrt{1-\xi^2}}. \tag{8.68}$$

Since ξ is small for building type structures, a reasonable approximation is

$$DAF_{displ.} \approx \frac{1}{2\xi}. \tag{8.69}$$

Expressing the allowable maximum dynamic amplification factor $H_{displ.}$ for the structure with TMDs in a similar form provides a measure of the necessary equivalent damping ratio ξ_e with regard to displacement:

$$\xi_e \approx \frac{1}{2H_{displ.}} \tag{8.70}$$

A similar procedure is repeated for the desired equivalent damping ratio ξ_e with regard to acceleration. The allowable maximum acceleration at the top of the primary structure is established. On the basis of this acceleration constraint, the allowable maximum dynamic amplification factor of the primary structure $H_{accel.}$ is determined. Then, the necessary equivalent damping ratio ξ_e with regard to acceleration can be expressed as

$$\xi_e \approx \frac{1}{2H_{accel.}}. \tag{8.71}$$

In order to satisfy both the displacement and acceleration requirements, the equivalent damping ratios estimated using Equations 8.70 and 8.71 are compared, and a higher value is selected as a design parameter. Once the desired equivalent damping ratio is obtained, the mass ratio (m_d / m) based on a SDOF/TMD system is determined from Figure 8.13.

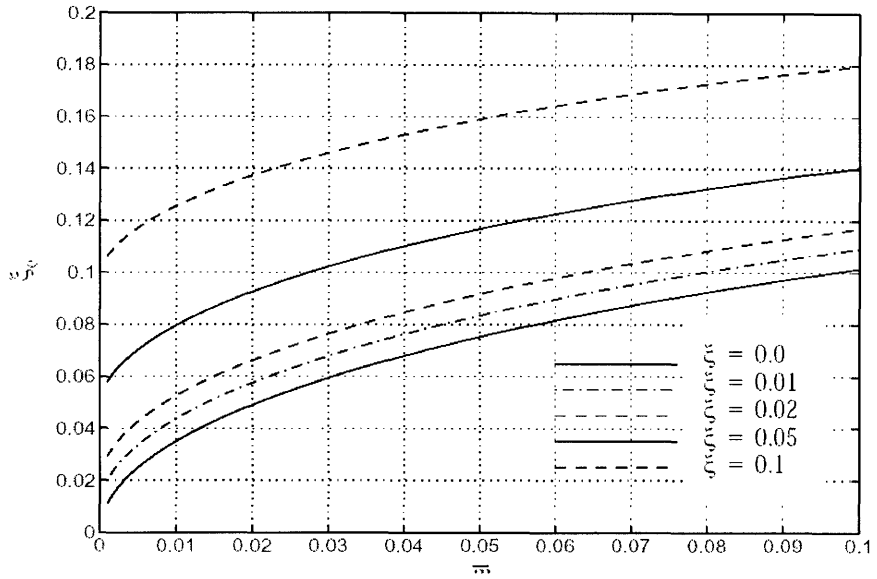

Figure 8.13: Equivalent Damping Ratio for Optimally Tuned TMD

Since we distribute TMDs vertically, not every TMD mass is as effective as the ones at the top. Further expanding Equation 8.67, the i[th] mode equivalent generalized mass of the primary structure that has a TMD at its node n is

$$\widetilde{m}_{ie} = \left[\frac{1}{\Phi_{in}^2}\right]\widetilde{M}_i = \left[\frac{1}{\Phi_{in}^2}\right]\Phi_i^T M \Phi_i \quad (i\text{: mode number, } n\text{: node number}). \tag{8.72}$$

The mass ratio is defined in terms of the TMD mass and the equivalent mass of the primary structure.

$$\overline{m} = \frac{m_d}{\widetilde{m}_{ie}} \tag{8.73}$$

As was discussed in the previous section, if we distribute TMDs vertically, we need more mass overall, compared to the conventional huge single TMD scheme, in order to achieve the same equivalent damping ratio. The additional mass required to compensate for the loss of effectiveness due to vertical distribution can be estimated based on the mode shape and the vertical range of distribution from the top to a certain level for the first mode. If the stiffness of the structure is calibrated to produce the first mode shape of a linear profile and TMD masses are evenly distributed for every node, the total additional mass required is increased as the number of nodes that have TMDs increases. However, the advantage of distributing TMDs over a broader vertical range is that each TMD mass becomes smaller as the range increases to achieve the same equivalent damping. In addition, due to their small sizes, the installation of TMD can be much easier. Thus, the determination of the range of installation is the trade-off process between small individual TMD masses and increased total mass.

For a 60-story building whose first mode shape is a linear profile, for example, if TMDs are evenly distributed for the upper half of the building from the 60th to the 31st level, this configuration requires a total of 67% more mass compared with the conventional system that has a single TMD only at the 60th floor.

$$\text{Total Additional Mass Required (\%)} = \left(\frac{30}{\sum_{n=31}^{60} (\Phi_{1n})^2} - 1 \right) \times 100\% \approx 67\% \tag{8.74}$$

However, compared with the conventional system that has a single TMD at the 60th floor, only 5.6% TMD mass is required for each level by this distribution. Furthermore, in this study, the total required TMD mass for each level represents several dozen small TMDs installed within the DSF system cavity space. If the TMD mass for each level is distributed to 60 TMDs, for example, each TMD mass is less than 0.1% of the conventional huge single TMD located near the top of the building.

Once TMD mass ratio $\overline{m}$ for each level is determined, every TMD at each level can be preliminarily tuned using that mass ratio. The optimal frequency ratio $f_{opt.}$ can be preliminarily estimated using Figure 8.14. Then, preliminary TMD frequency ω_d and stiffness k_d can be computed as follows:

$$\omega_d = f_{opt.}\omega \tag{8.75}$$

$$k_d = m_d \omega_d^2 \tag{8.76}$$

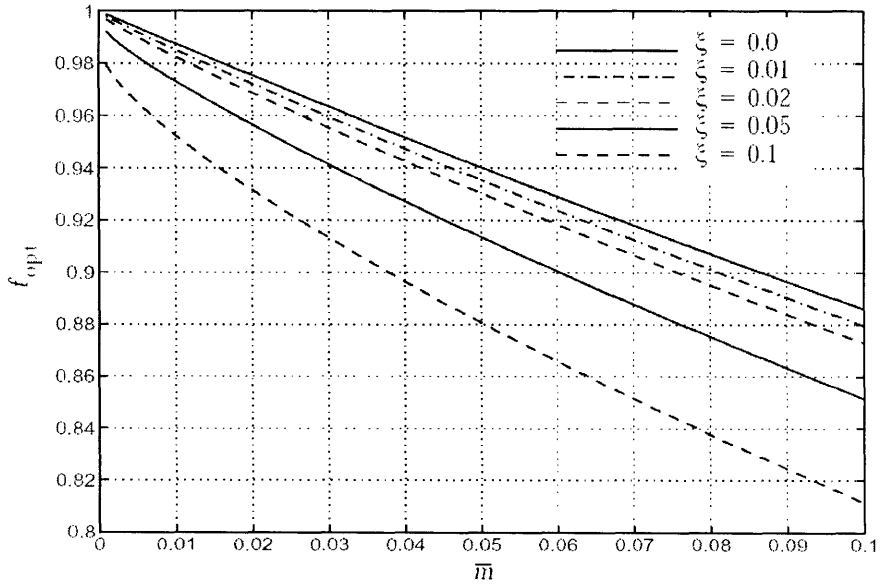

Figure 8.14 : Optimal Tuning Frequency Ratio for TMD

The optimal TMD damping ratio $\xi_d|_{opt.}$ can be preliminarily estimated using Figure 8.15. Then, preliminary TMD damping parameter c_d can be computed as follows:

$$c_d = 2\xi_d|_{opt.}\,\omega_d m_d \tag{8.77}$$

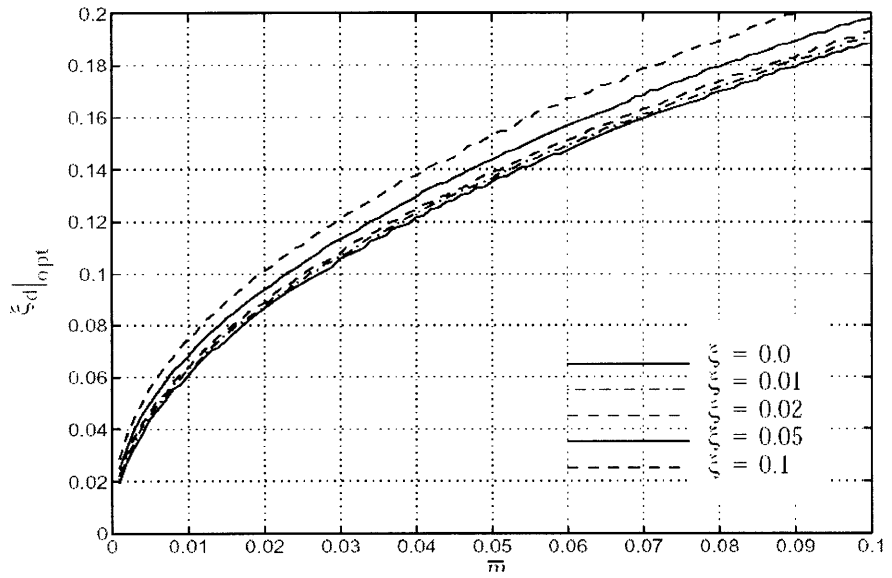

Figure 8.15 : Optimal Damping Ratio for TMD

As was discussed earlier, tuning every TMD for each level based on its mass ratio for each level does not lead to optimal performance of the combined final system. Thus, these processes are used for preliminary tuning only. Iterations are necessary for optimal tuning for the combined new system.

8.3.2. Second and Other Mode Vibration Control

If necessary, second and other higher mode vibration can be controlled using TMDs following the same procedure presented in the previous section. For the first mode, the stiffness can be calibrated to produce a linear profile mode shape. However, for other modes, mode shapes are non-linear. Through eigenvalue analysis, higher mode shapes can be obtained, and the same procedure presented in the previous section can be employed to design the vertically distributed TMDs.

8.4. Design Study: 60-Story Structure

A 60-story structure that has vertically distributed TMDs is studied in this section. In order to establish the analysis program, MotionLab, Matlab is employed. The matrix formulation shown in Equation 7.79 is solved by the program to generate responses of the system.

$$\begin{bmatrix} M & \\ & M_d \end{bmatrix}\begin{Bmatrix} \ddot{U} \\ \ddot{U}_d \end{Bmatrix}+\begin{bmatrix} C+C_d & -C_d \\ -C_d & C_d \end{bmatrix}\begin{Bmatrix} \dot{U} \\ \dot{U}_d \end{Bmatrix}+\begin{bmatrix} K+K_d & -K_d \\ -K_d & K_d \end{bmatrix}\begin{Bmatrix} U \\ U_d \end{Bmatrix}=\begin{Bmatrix} P \\ 0 \end{Bmatrix} \tag{8.78}$$

$$\begin{bmatrix} m_1 & & & & & & \\ & \ddots & & & & & \\ & & m_n & & & & \\ & & & m_{d1} & & & \\ & & & & \ddots & & \\ & & & & & m_{dn} \end{bmatrix}\begin{Bmatrix} \ddot{u}_1 \\ \ddot{u}_2 \\ \vdots \\ \ddot{u}_{n-1} \\ \ddot{u}_n \\ \ddot{u}_{d1} \\ \ddot{u}_{d2} \\ \vdots \\ \ddot{u}_{d(n-1)} \\ \ddot{u}_{dn} \end{Bmatrix}+$$

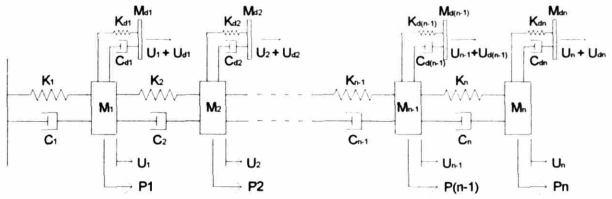

$$\begin{bmatrix} c_1+c_2+c_{d1} & -c_2 & \cdots & 0 & 0 & -c_{d1} & 0 & \cdots & 0 & 0 \\ -c_2 & c_2+c_3+c_{d2} & \cdots & 0 & 0 & 0 & -c_{d2} & \cdots & 0 & 0 \\ \vdots & \vdots & \ddots & \vdots & \vdots & \vdots & \vdots & \ddots & \vdots & \vdots \\ 0 & 0 & \cdots & c_{n-1}+c_n+c_{d(n-1)} & -c_n & 0 & 0 & \cdots & -c_{d(n-1)} & 0 \\ 0 & 0 & \cdots & -c_n & c_n+c_{dn} & 0 & 0 & \cdots & 0 & -c_{dn} \\ -c_{d1} & 0 & \cdots & 0 & 0 & c_{d1} & 0 & \cdots & 0 & 0 \\ 0 & -c_{d2} & \cdots & 0 & 0 & 0 & c_{d2} & \cdots & 0 & 0 \\ \vdots & \vdots & \ddots & \vdots & \vdots & \vdots & \vdots & \ddots & \vdots & \vdots \\ 0 & 0 & \cdots & -c_{d(n-1)} & 0 & 0 & 0 & \cdots & c_{d(n-1)} & 0 \\ 0 & 0 & \cdots & 0 & -c_{dn} & 0 & 0 & \cdots & 0 & c_{dn} \end{bmatrix}\begin{Bmatrix} \dot{u}_1 \\ \dot{u}_2 \\ \vdots \\ \dot{u}_{n-1} \\ \dot{u}_n \\ \dot{u}_{d1} \\ \dot{u}_{d2} \\ \vdots \\ \dot{u}_{d(n-1)} \\ \dot{u}_{dn} \end{Bmatrix}+$$

$$\begin{bmatrix} k_1+k_2+k_{d1} & -k_2 & \cdots & 0 & 0 & -k_{d1} & 0 & \cdots & 0 & 0 \\ -k_2 & k_2+k_3+k_{d2} & \cdots & 0 & 0 & 0 & -k_{d2} & \cdots & 0 & 0 \\ \vdots & \vdots & \ddots & \vdots & \vdots & \vdots & \vdots & \ddots & \vdots & \vdots \\ 0 & 0 & \cdots & k_{n-1}+k_n+k_{d(n-1)} & -k_n & 0 & 0 & \cdots & -k_{d(n-1)} & 0 \\ 0 & 0 & \cdots & -c_n & k_n+c_{dn} & 0 & 0 & \cdots & 0 & -k_{dn} \\ -k_{d1} & 0 & \cdots & 0 & 0 & k_{d1} & 0 & \cdots & 0 & 0 \\ 0 & -k_{d2} & \cdots & 0 & 0 & 0 & k_{d2} & \cdots & 0 & 0 \\ \vdots & \vdots & \ddots & \vdots & \vdots & \vdots & \vdots & \ddots & \vdots & \vdots \\ 0 & 0 & \cdots & -k_{d(n-1)} & 0 & 0 & 0 & \cdots & k_{d(n-1)} & 0 \\ 0 & 0 & \cdots & 0 & -k_{dn} & 0 & 0 & \cdots & 0 & k_{dn} \end{bmatrix}\begin{Bmatrix} u_1 \\ u_2 \\ \vdots \\ u_{n-1} \\ u_n \\ u_{d1} \\ u_{d2} \\ \vdots \\ u_{d(n-1)} \\ u_{dn} \end{Bmatrix}=\begin{Bmatrix} p_1 \\ p_2 \\ \vdots \\ p_{n-1} \\ p_n \\ 0 \\ 0 \\ \vdots \\ 0 \\ 0 \end{Bmatrix} \tag{8.79}$$

When TMDs are not installed to the nodes close to the ground, the matrices shown above are reduced accordingly.

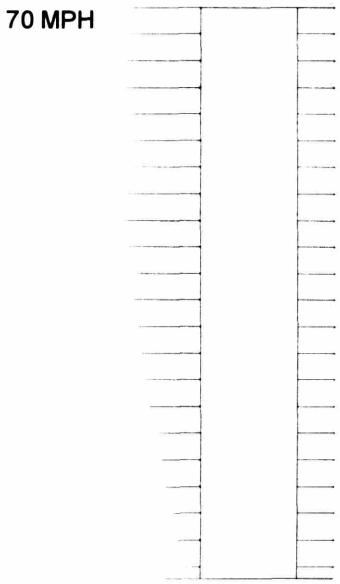

Figure 21

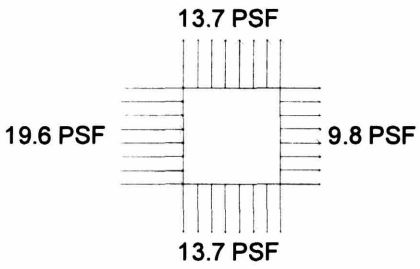

Figure 8.16: Wind Loads for a 60-Story Building in Boston at 70mph Wind Speed

A 240m tall 60-story primary structure in Boston is modeled as a 60DOF system. Its plan dimension is 40m x 40m, story height is 4m typical, and mass density is 190 kg / cubic meter. Thus, its every node has a mass of 1,200,000 kg. The stiffness is configured for the building to have a 6.28 second fundamental period and thus a 1 radian/second circular frequency (0.16Hz). This is achieved using quasi-parabolic stiffness with 2,200,000,000 N/m at the base. With this stiffness calibration, the first mode shape is very close to a linear profile. A 0.5% first mode damping ratio is considered for the structure without any mechanical damping devices.

From Equation 7.19, assuming 0.2 as the Strouhal number for this case, at approximately 70mph wind speed, the first mode lock-in phenomenon occurs regarding vortex shedding. The document SEI/ASCE 7-02 (Minimum Design Loads for Buildings and Other Structures) is used to establish the wind load based on that wind speed. Generally, in tall buildings, a vortex-shedding-induced lock-in phenomenon produces the greatest lateral deflection. Considering the building dimensions and assuming the vortex shedding lift coefficient to be 0.2, harmonic load, whose peak value is 20,000 N, is applied to each node of the 60 degrees of freedom system model. MotionLab is used to analyze the dynamic response of the system. A forcing period of 6.28 seconds is used to simulate the lock-in condition of the original structure.

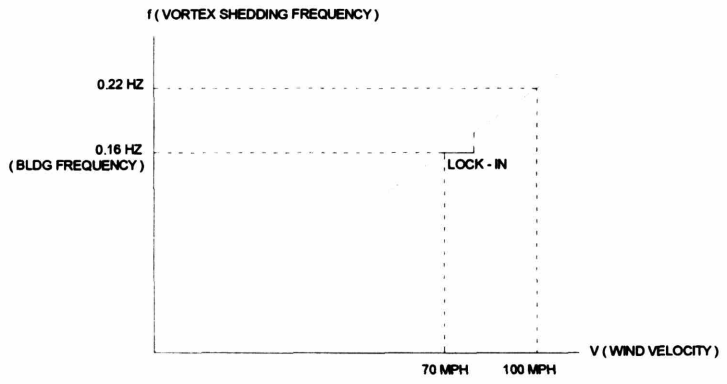

Figure 8.17: Vortex-Shedding-Induced Lock-In Condition for a 60-Story Building

Original Structure Dynamic Response without TMD

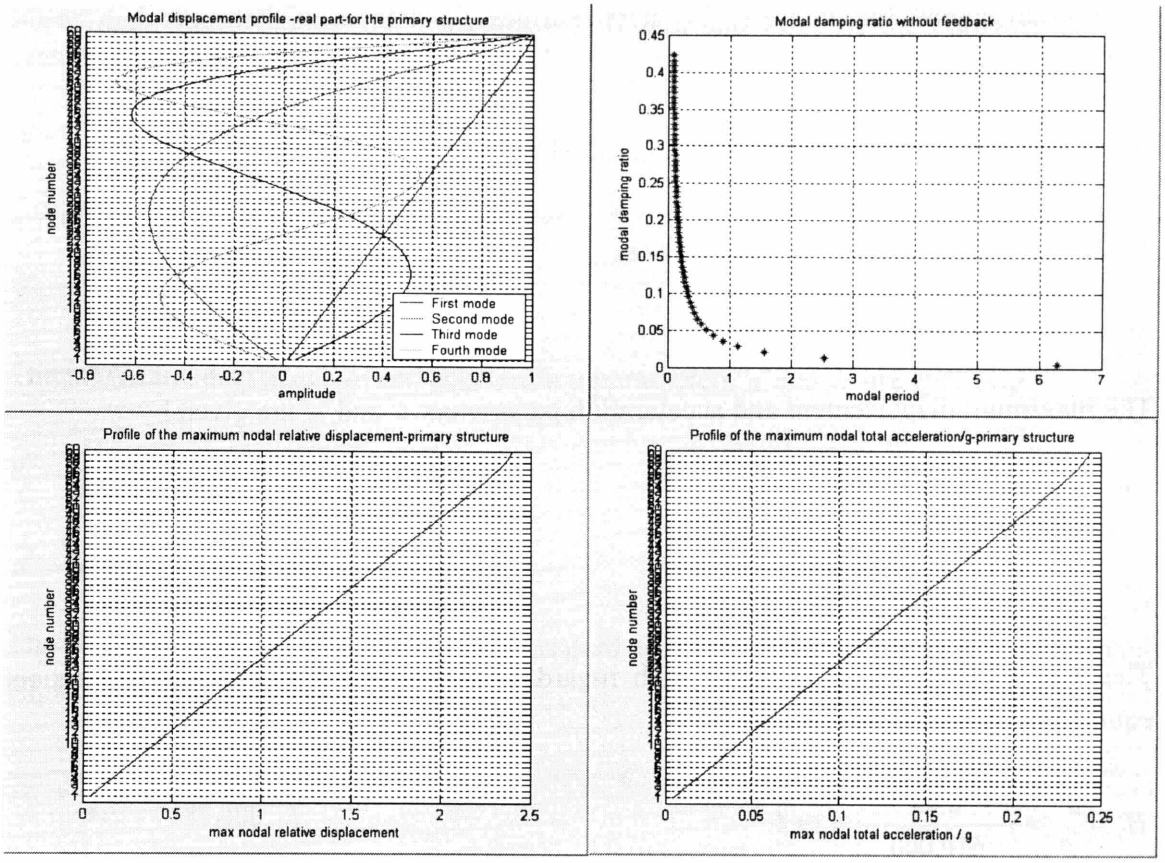

Figure 8.18

Figure 8.18 contains first through fourth mode shapes of the structure, modal damping ratios, maximum nodal relative displacement, and maximum nodal total acceleration. As can be seen from the figure, the original structure, which has a very low inherent first mode damping ratio (0.5%), does not meet the general acceleration requirement, 0.02g. In resonance condition, maximum acceleration at the top is about 0.3g, almost 15 times that of the acceptable value. In addition, maximum displacement at the top is almost 2.4 m (H/100), which is about 5 times the generally employed maximum displacement parameter in practice, H/500. In the following sections, both the conventional and distributed TMD design strategies are investigated to satisfy both the acceleration and displacement design criteria. The study showed that the contribution of the third mode was negligible. Thus, only the first and second mode response controls are presented.

8.4.1. Design Parameters for the First Mode

On the basis of the first mode shape and frequency of the system obtained from the MotionLab eigenvalue analysis, the mass, stiffness, and force of the equivalent SDOF system is estimated as

$$\tilde{m} = \phi^T M \phi = \frac{\Sigma i^2 m_i}{n^2} = \frac{\Sigma i^2 (1{,}200{,}000)}{60^2} = 24{,}603{,}333 Kg$$

$$\tilde{k} = \omega^2 \tilde{m} = 1^2 (24{,}603{,}333) = 24{,}603{,}333 N/m$$

$$\tilde{p} = \phi^T p = 610{,}000 N .$$

The maximum displacement and acceleration parameters u^* and a^* are given by

$$u^* = \frac{H}{500} = 0.48m$$

$$a^* = 0.02g = 0.02(9.87) = 0.197 m/\sec^2 .$$

The dynamic amplification factor with regard to displacement H_1 and the consequent equivalent damping ratio ξ_{e1} are

$$H_1 = \frac{u^*}{\frac{\tilde{p}}{\tilde{k}}} = \frac{0.48}{\left(\frac{610{,}000}{24{,}603{,}333}\right)} = 19.4$$

$$\xi_{e1} \approx \frac{1}{2H_1} = \frac{1}{2(19.4)} = 0.026 .$$

The dynamic amplification factor with regard to displacement H_2 and the consequent equivalent damping ratio ξ_{e2} are

$$H_2 = \frac{a^*}{\left(\frac{\tilde{p}}{\tilde{m}}\right)} = \frac{0.197}{\left(\frac{610{,}000}{24{,}603{,}333}\right)} = 7.9$$

$$\xi_{e2} \approx \frac{1}{2H_2} = \frac{1}{2(7.9)} = 0.063 .$$

Comparison between ξ_{e1} and ξ_{e2} clearly shows that the acceleration controls the design with regard to the first mode response.

8.4.2. Design Parameters for the Second Mode

On the basis of the second mode shape and frequency of the system obtained from the MotionLab eigenvalue analysis, the mass, stiffness, and force of the equivalent SDOF system is estimated as

$$\tilde{m} = \phi^T M \phi = 14{,}866{,}870 Kg$$

$$\tilde{k} = \omega^2 \tilde{m} = 2.5^2 (14{,}866{,}870) = 92{,}918{,}000 N/m$$

$$\tilde{p} = \phi^T p = 185{,}400 N .$$

The maximum displacement and acceleration parameters u^* and a^* are given by

$$u^* = \frac{H}{500} = 0.48m$$

$$a^* = 0.02g = 0.196 m/\sec^2 .$$

The dynamic amplification factor with regard to displacement H_1 and the consequent equivalent damping ratio ξ_{e1} are

$$H_1 = \frac{u^*}{\frac{\tilde{p}}{\tilde{k}}} = \frac{0.48}{\left(\frac{185{,}400}{92{,}918{,}000}\right)} = 241$$

$$\xi_{e1} \approx \frac{1}{2H_1} = \frac{1}{2(241)} = 0.002 .$$

The dynamic amplification factor with regard to displacement H_2 and the consequent equivalent damping ratio ξ_{e2} are

$$H_2 = \frac{a^*}{\left(\frac{\tilde{p}}{\tilde{m}}\right)} = \frac{0.197}{\left(\frac{185{,}400}{14{,}866{,}870}\right)} = 15.8$$

$$\xi_{e2} \approx \frac{1}{2H_2} = \frac{1}{2(15.8)} = 0.032 .$$

Comparison between ξ_{e1} and ξ_{e2} clearly shows that the acceleration controls the design with regard to the second mode response.

8.4.3. TMD Design: Conventional Scheme

In conventional TMD design, a huge single TMD is located near the top of the structure. In order to achieve the 6.3 % first mode equivalent damping ratio estimated in Section 7.4.1, about 2.5% mass ratio is required (m_d = 615,000 kg: 0.85% of total building mass). With this mass ratio the TMD parameters for optimal tuning are: 1) TMD Stiffness: 593,000 N/m (f = 0.98) and 2) TMD Damping: 135,000 Ns/m (11%).

Forcing Period: 6.8 sec (First Mode Period of the Structure)

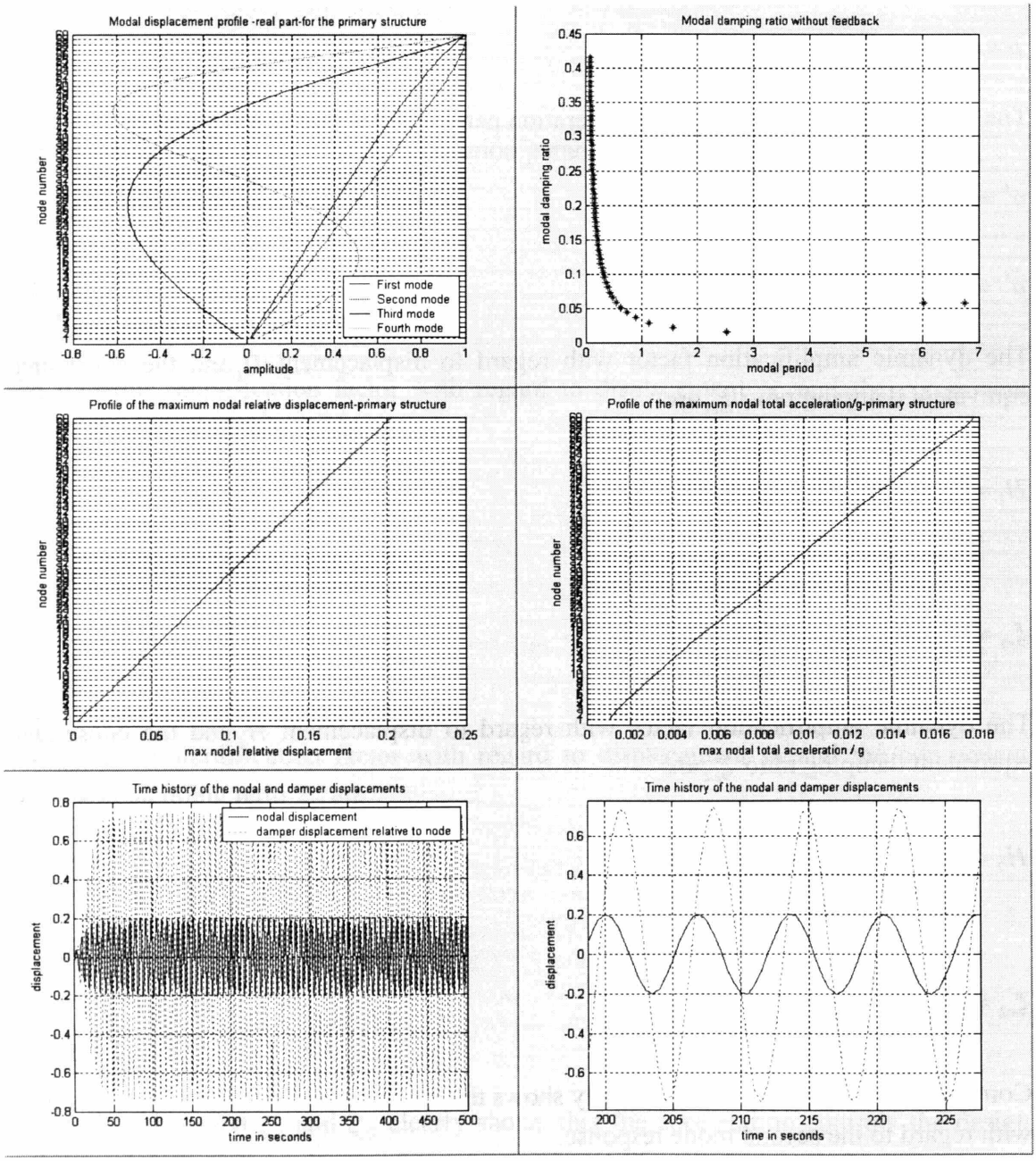

Figure 8.19

Figure 8.19 shows the first through fourth mode shapes of the 60DOF/TMD system, modal damping ratio, maximum nodal relative displacement, maximum nodal total acceleration, and the time history of the nodal and damper displacement. By installing the TMD at the 60th node, the damping ratio increases from an initial 0.5% to around 6%. Both maximum displacement and acceleration are lower than the target maximum values. The nodal and damper displacement plot shows that they are about 90 degrees out of phase, which is close to the theoretical optimum condition.

Forcing Period: 2.5 sec. (Original 2nd Mode Period of the Structure)

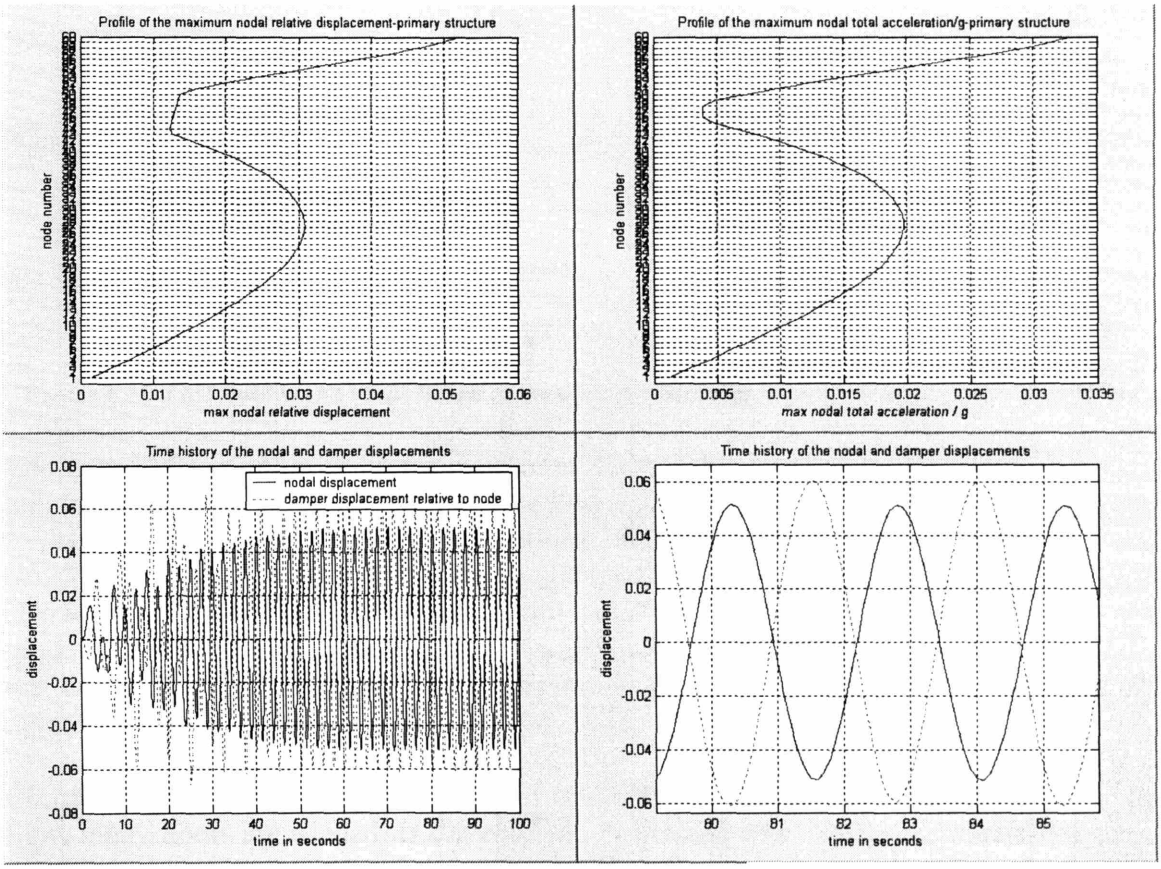

Figure 8.20

As can be seen from Figure 8.20, when the TMD is tuned only for the first mode, if the building's second mode is primarily excited, the structure does not meet the acceleration criteria.[41] In the second mode resonance condition, the acceleration at the top is about 0.033g, which is much larger than the acceptable maximum value, 0.02g. In order to achieve the 3.2 % first mode equivalent damping ratio estimated in Section 5.1.2, about a 0.5 % mass ratio is required (m_d = 74,300 kg: 0.1 % of the total building mass). With this mass ratio the TMD parameters for optimal tuning are 1) TMD Stiffness: 451,500 N/m (f = 0.99) and 2) TMD Damping: 165,000 Ns/m (11%).

[41] This is only true when the inherent damping ratio of the primary structure is very low, such as 0.5% in this study.

TMD at 60th Story (Tuned to the Second Mode)

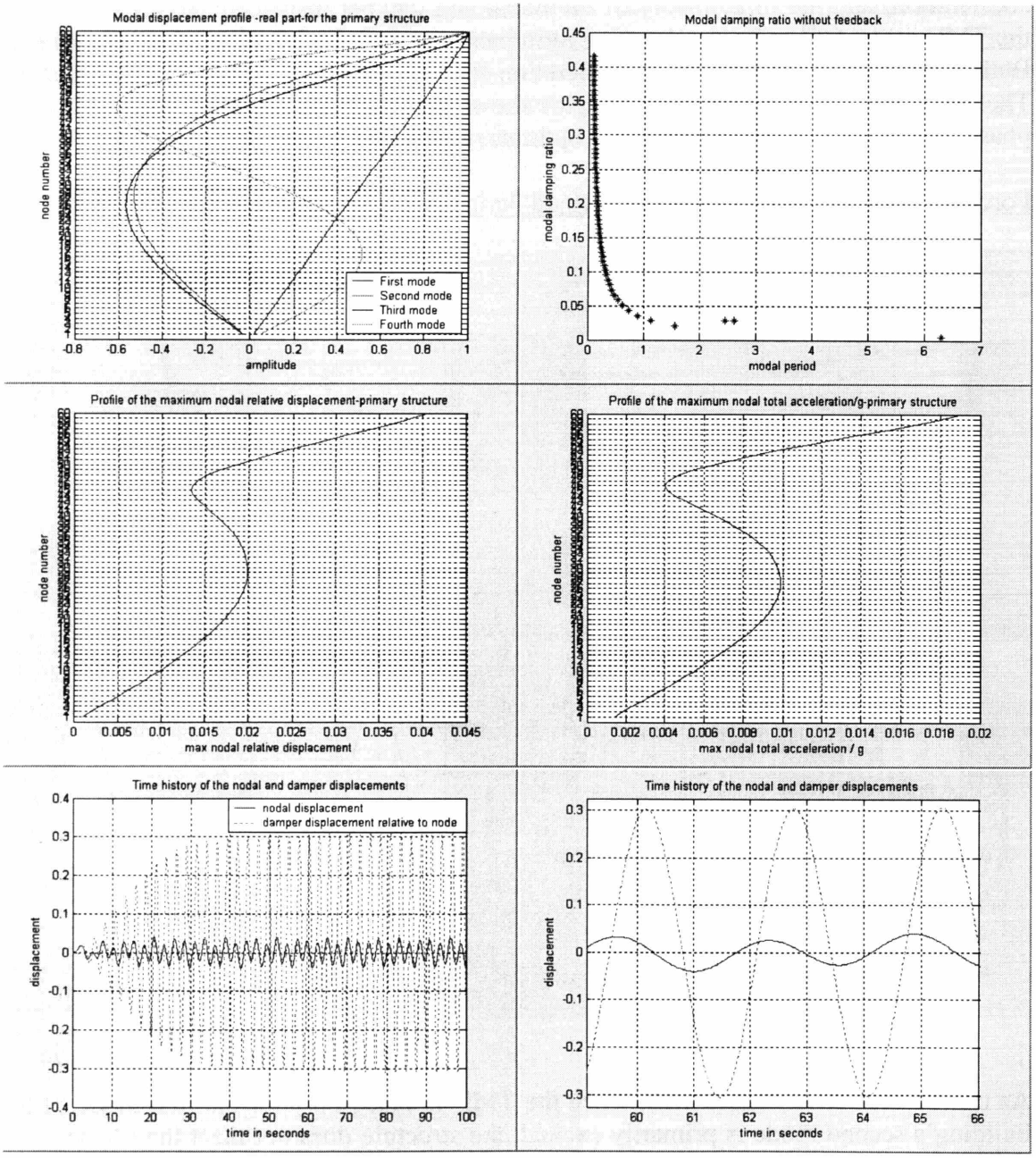

Figure 8.21

As can be seen from Figure 8.21, with a 0.5 % mass ratio, the second mode is controlled, and thus the maximum acceleration is lower than the target maximum values. The nodal and damper displacement plot shows that they are about 90 degrees out of phase, which is close to the theoretical optimum condition.

8.5. Vertically Distributed TMD Design Strategy for Tall Buildings

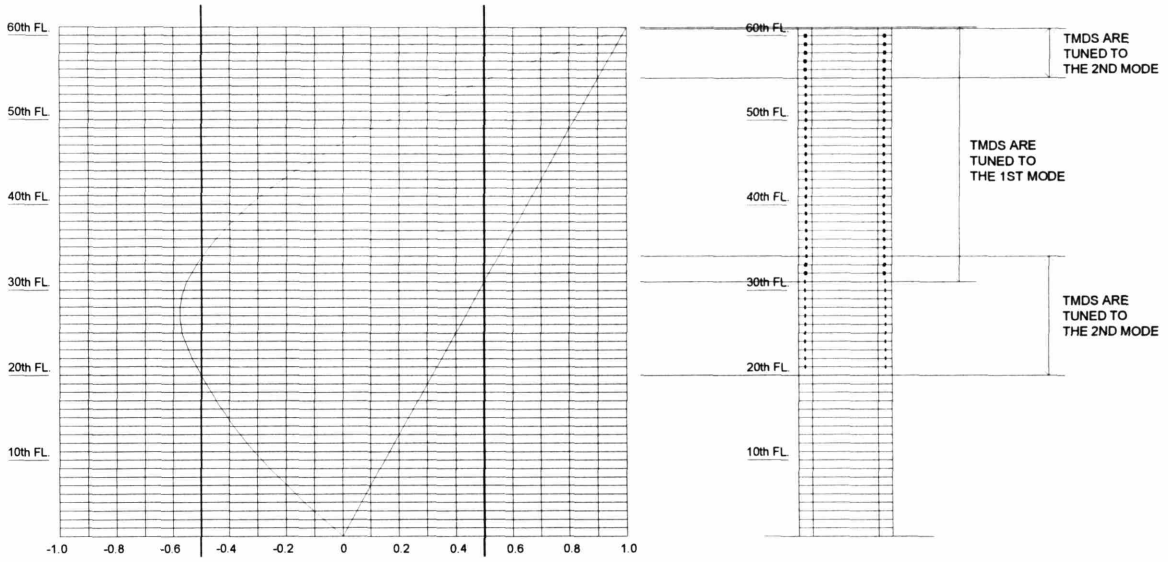

Figure 8.22: First and Second Mode Shape of the 60-Story Building

The best TMD location is where maximum displacement occurs. Thus, for a 60 story building subjected to periodic forcing, the best TMD location is at the top of the building for both the first and second mode excitations. When the vertical distribution of TMDs is considered in order to save the valuable occupiable space at the top of the building and also to maximize torsional vibration control, small TMDs are distributed according to the mode shapes. An example distribution is shown in Figure 8.22. Analysis results show that the contribution of the third mode excitation is negligible. Thus, only the 1^{st} and 2^{nd} modes are presented here.

Considering desirable size and the number of each small TMD, vertical distribution range (how many floors are needed) is determined. Following that, TMDs are distributed from the top down to the determined floors for the 1^{st} mode control. For the 2^{nd} mode control, since the mode shape is non-linear, the vertical distribution might be divided into two zones, near the top and middle of the structure as shown in Figure 8.22.

8.5.1. Vertically Distributed TMD Design - MotionLab Simulation

The vertically distributed TMD design for the same structure studied in the previous section is presented here. The target displacement and acceleration criteria are the same as before. In this design, for the first mode vibration control, we distribute TMDs from node 60 to node 31. As was discussed in Section 8.3.1, this configuration requires a total 67% more mass compared with the conventional system that has a single TMD at the 60^{th} floor.

For the second mode vibration control, we distribute TMDs from node 30 to node 21. This configuration is not as efficient as that shown in Figure 8.22. However, this configuration prevents TMD congestion near the top floors. It is a design decision how to distribute multiple TMDs vertically. Table 8.1 shows TMD tuning properties at each node. Md at each node represents the sum of possibly several dozen small TMDs.

Table 8.1: Vertically Distributed TMDs Tuning Properties

Node	Md (Kg)	Kd (N/m)	f	Cd (N-s/m)	ξd	Tuned to
60	32800	30862	0.9700	7318	0.115	1st Mode
59	32800	30893	0.9705	7306	0.115	1st Mode
58	32800	30925	0.9710	7293	0.115	1st Mode
57	32800	30957	0.9715	7281	0.114	1st Mode
56	32800	30989	0.9720	7269	0.114	1st Mode
55	32800	31021	0.9725	7257	0.114	1st Mode
54	32800	31053	0.9730	7245	0.114	1st Mode
53	32800	31085	0.9735	7232	0.113	1st Mode
52	32800	31117	0.9740	7220	0.113	1st Mode
51	32800	31149	0.9745	7208	0.113	1st Mode
50	32800	31181	0.9750	7196	0.113	1st Mode
49	32800	31212	0.9755	7183	0.112	1st Mode
48	32800	31244	0.9760	7171	0.112	1st Mode
47	32800	31277	0.9765	7159	0.112	1st Mode
46	32800	31309	0.9770	7146	0.112	1st Mode
45	32800	31341	0.9775	7134	0.111	1st Mode
44	32800	31373	0.9780	7121	0.111	1st Mode
43	32800	31405	0.9785	7109	0.111	1st Mode
42	32800	31437	0.9790	7097	0.111	1st Mode
41	32800	31469	0.9795	7084	0.110	1st Mode
40	32800	31501	0.9800	7072	0.110	1st Mode
39	32800	31533	0.9805	7059	0.110	1st Mode
38	32800	31565	0.9810	7047	0.110	1st Mode
37	32800	31598	0.9815	7034	0.109	1st Mode
36	32800	31630	0.9820	7022	0.109	1st Mode
35	32800	31662	0.9825	7009	0.109	1st Mode
34	32800	31694	0.9830	6997	0.109	1st Mode
33	32800	31727	0.9835	6984	0.108	1st Mode
32	32800	31759	0.9840	6971	0.108	1st Mode
31	32800	31791	0.9845	6959	0.108	1st Mode
30	25300	153417	0.9850	6958	0.055	2nd Mode
29	25300	153417	0.9850	6958	0.055	2nd Mode
28	25300	153417	0.9850	6958	0.055	2nd Mode
27	25300	153417	0.9850	6958	0.055	2nd Mode
26	25300	153417	0.9850	6958	0.055	2nd Mode
25	25300	153417	0.9850	6958	0.055	2nd Mode
24	25300	153417	0.9850	6958	0.055	2nd Mode
23	25300	153417	0.9850	6958	0.055	2nd Mode
22	25300	153417	0.9850	6958	0.055	2nd Mode
21	25300	153417	0.9850	6958	0.055	2nd Mode

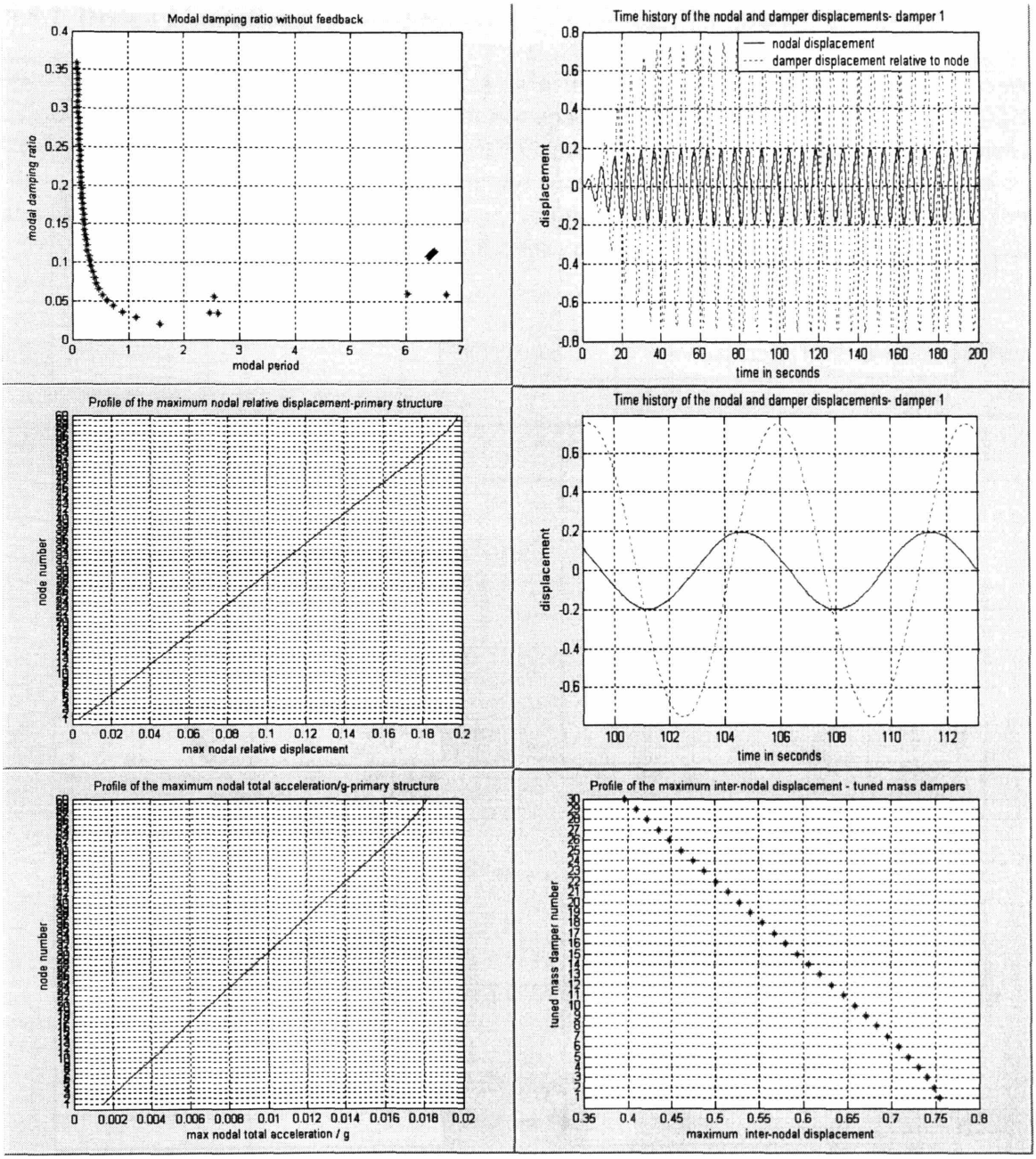

Figure 8.23: Dynamic Response of the 60-Story Structure with Vertically Distributed TMDs tuned to the First and Second Modes when Forcing Period = First Mode Frequency of the Structure

Figure 8.23 shows modal damping ratios, maximum nodal relative displacement, maximum nodal total acceleration, time history of the nodal and damper displacement, and the maximum inter-nodal displacement of TMDs tuned to the first mode in the first mode resonance condition. It can be noticed that the maximum nodal relative displacement and nodal total acceleration are almost the same as in the case with a single TMD at node 60 in Section 8.4.3.

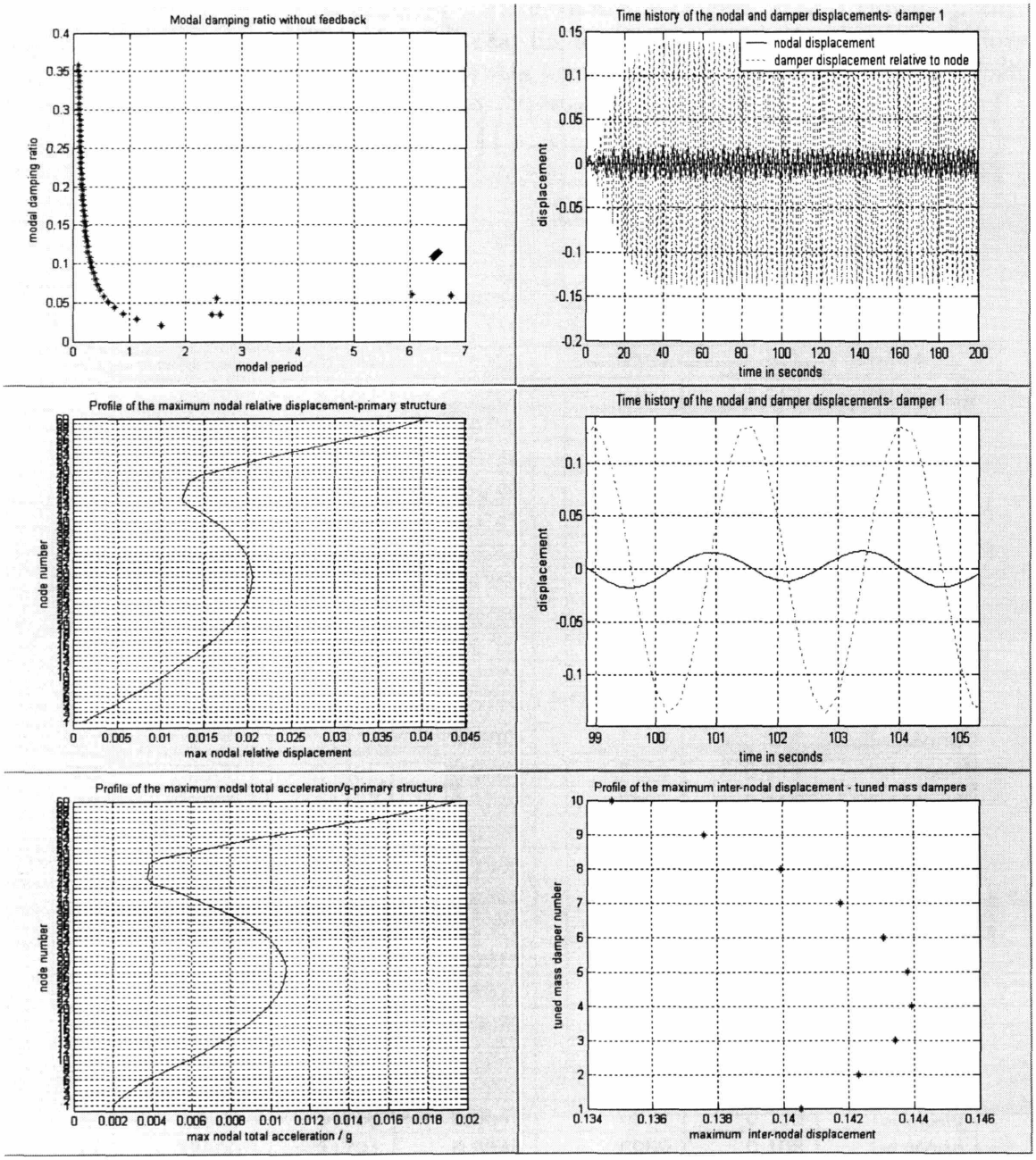

Figure 8.24: Dynamic Response of the 60-Story Structure with Vertically Distributed TMDs tuned to the First and Second Modes when Forcing Period = Second Mode Frequency of the Structure

Figure 7.24 shows modal damping ratios, maximum nodal relative displacement, maximum nodal total acceleration, time history of the nodal and damper displacement, and the maximum inter-nodal displacement of TMDs tuned to the second mode in the 2nd mode resonance condition. It can be noticed that the maximum nodal relative displacement and nodal total acceleration are almost the same as in the case with a single TMD at node 60 in Section 8.4.3.

8.5.2. Design Limitations

The motion of the TMD mass often acts as a limiting factor of TMD design because TMDs are installed within the limited interior space of a building. Figure 8.25 illustrates the ratio of maximum TMD displacement to maximum primary structure displacement. As mass ratio (TMD Mass/ Primary Structure Mass) decreases, for optimal performance, the motion of TMD must become greater, requiring more space to accommodate this motion. This space requirement due to structural requirements may conflict with that due to architectural or other requirements.

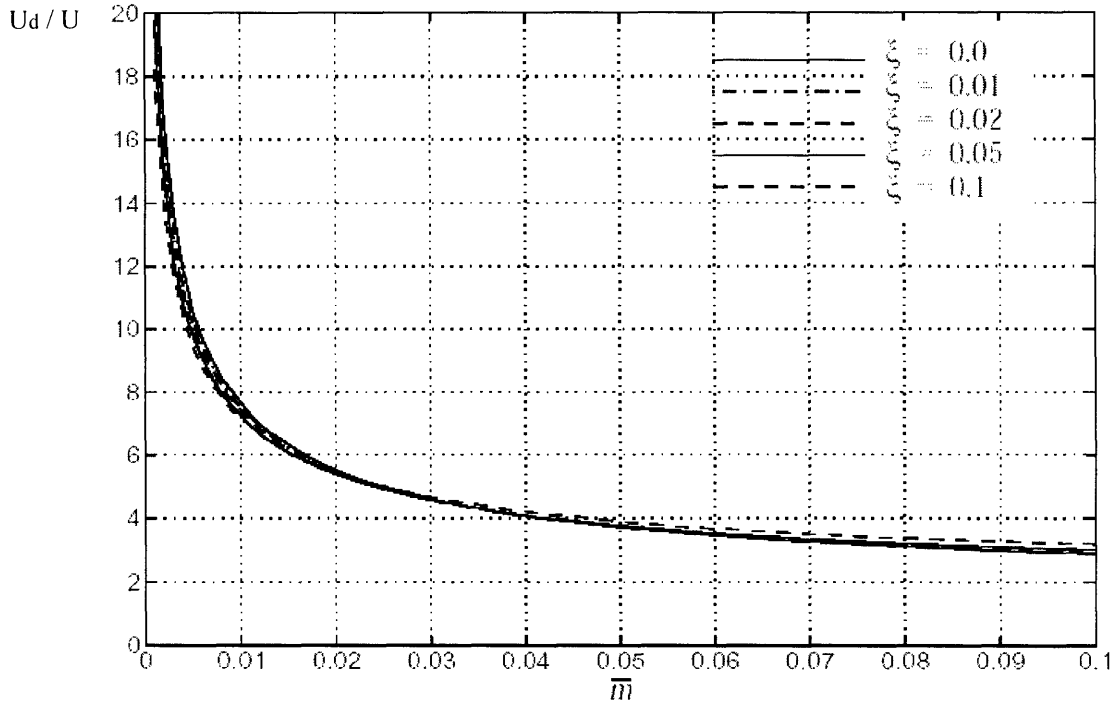

Figure 7.25: Ratio of Maximum TMD Amplitude to Maximum System Amplitude

In the distributed TMD system presented in this chapter, multiple small TMDs are installed within the DSF cavity space, the depth of which typically ranges from 0.3 to 1.5 meters (Arons, 2000). When the TMDs are designed to move in the direction perpendicular to the façade plane, the motion of TMDs should be accommodated within the depth of the DSF cavity, or the depth of the DSF cavity must be wide enough to allow TMD motion for optimal performance. This TMD-motion-induced space requirement can be reduced by decreasing TMD motion. One way to reduce TMD motion is to increase TMD damping ratio over optimal value. This strategy is examined using the distributed TMD model presented in the previous section. The TMDs tuned to the second mode are omitted in this study because they move much less than those tuned to the first mode.

When the first mode of the primary structure is excited, the motions of the TMDs tuned to the 1st mode range from ± 0.4 to ± 0.75 meters, and the TMD damping ratios from 10.8% to 11.5% for optimal performance. Suppose that the motion of the TMDs should be limited to maximum ± 0.5 meters due to the limitation of the DSF cavity space. This limited motion can be achieved by increasing the TMD damping ratios. Table 8.2 contains new properties of the TMDs employed in the previous section to meet this TMD motion constraint. Tuning was performed by iteration. As can be seen from the table, now the TMD damping ratios range from 15.5% to 29.5%, which is much higher than the previous case.

Table 8.2: Vertically Distributed TMDs Tuning Properties

Node	Md (Kg)	Kd (N/m)	f	Cd (N-s/m)	ξd	Tuned to
60	32800	30862	0.9700	18795	0.295	1st Mode
59	32800	30893	0.9705	18655	0.293	1st Mode
58	32800	30925	0.9710	18450	0.290	1st Mode
57	32800	30957	0.9715	18202	0.286	1st Mode
56	32800	30989	0.9720	17932	0.281	1st Mode
55	32800	31021	0.9725	17646	0.277	1st Mode
54	32800	31053	0.9730	17350	0.272	1st Mode
53	32800	31085	0.9735	17044	0.267	1st Mode
52	32800	31117	0.9740	16730	0.262	1st Mode
51	32800	31149	0.9745	16410	0.257	1st Mode
50	32800	31181	0.9750	16088	0.252	1st Mode
49	32800	31212	0.9755	15763	0.246	1st Mode
48	32800	31244	0.9760	15435	0.241	1st Mode
47	32800	31277	0.9765	15106	0.236	1st Mode
46	32800	31309	0.9770	14777	0.231	1st Mode
45	32800	31341	0.9775	14448	0.225	1st Mode
44	32800	31373	0.9780	14120	0.220	1st Mode
43	32800	31405	0.9785	13790	0.215	1st Mode
42	32800	31437	0.9790	13460	0.210	1st Mode
41	32800	31469	0.9795	13130	0.204	1st Mode
40	32800	31501	0.9800	12799	0.199	1st Mode
39	32800	31533	0.9805	12468	0.194	1st Mode
38	32800	31565	0.9810	12138	0.189	1st Mode
37	32800	31598	0.9815	11820	0.184	1st Mode
36	32800	31630	0.9820	11500	0.179	1st Mode
35	32800	31662	0.9825	11200	0.174	1st Mode
34	32800	31694	0.9830	10900	0.169	1st Mode
33	32800	31727	0.9835	10600	0.164	1st Mode
32	32800	31759	0.9840	10300	0.160	1st Mode
31	32800	31791	0.9845	10000	0.155	1st Mode

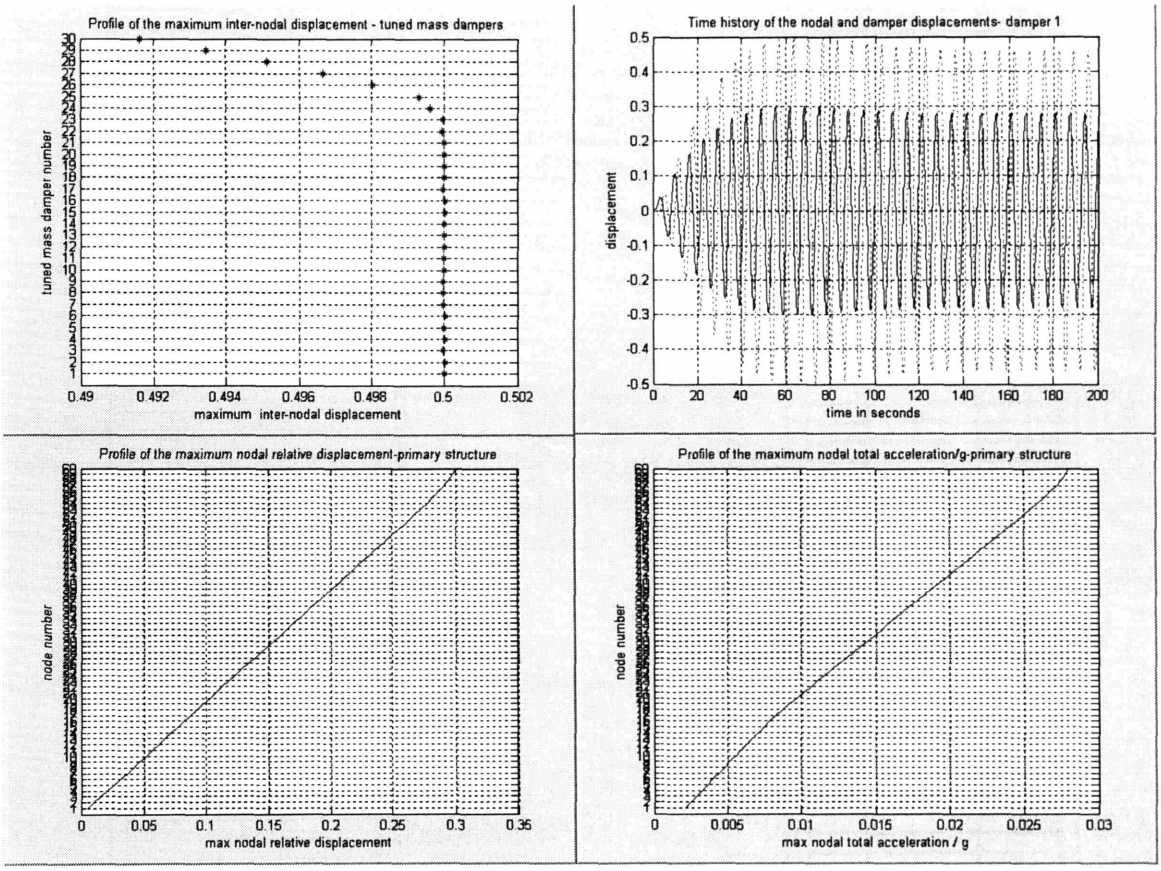

Figure 8.25: Dynamic Response of the 60-Story Structure with Vertically Distributed TMDs with Higher Damping Ratio for Reduced TMD Motion

Figure 8.25 contains the maximum inter-nodal displacement of TMDs, time history of the nodal and damper displacement, maximum nodal relative displacement, and the maximum nodal total acceleration of the system having the properties shown in Table 8.2. As can be seen from the figure, by increasing TMD damping ratios over optimal values, the motions of the TMDs are limited to the target value, ± 0.5 meters. However, the system does not produce optimal performance, even though the TMD motion constraint requirement is met. Now, the maximum acceleration is about 0.028g, which is greater than the generally accepted maximum target value, 0.02g. Thus, in order to resolve this acceleration problem caused by the strategy used to meet the TMD motion constraint, another strategy must be considered. For example, increasing TMD mass will resolve this problem, if it is acceptable. Design decisions should be made in an integrative way considering various complex and sometimes conflicting requirements.

8.5.3. Various TMD Distribution Strategies

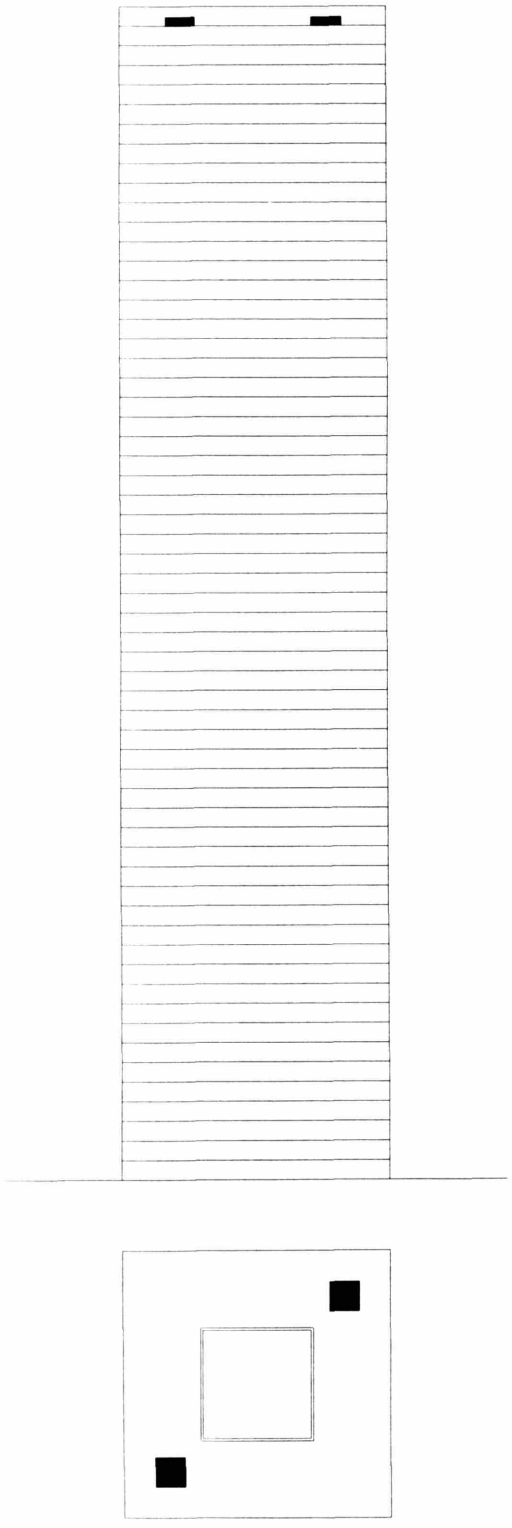

1) Conventional huge TMD at the top

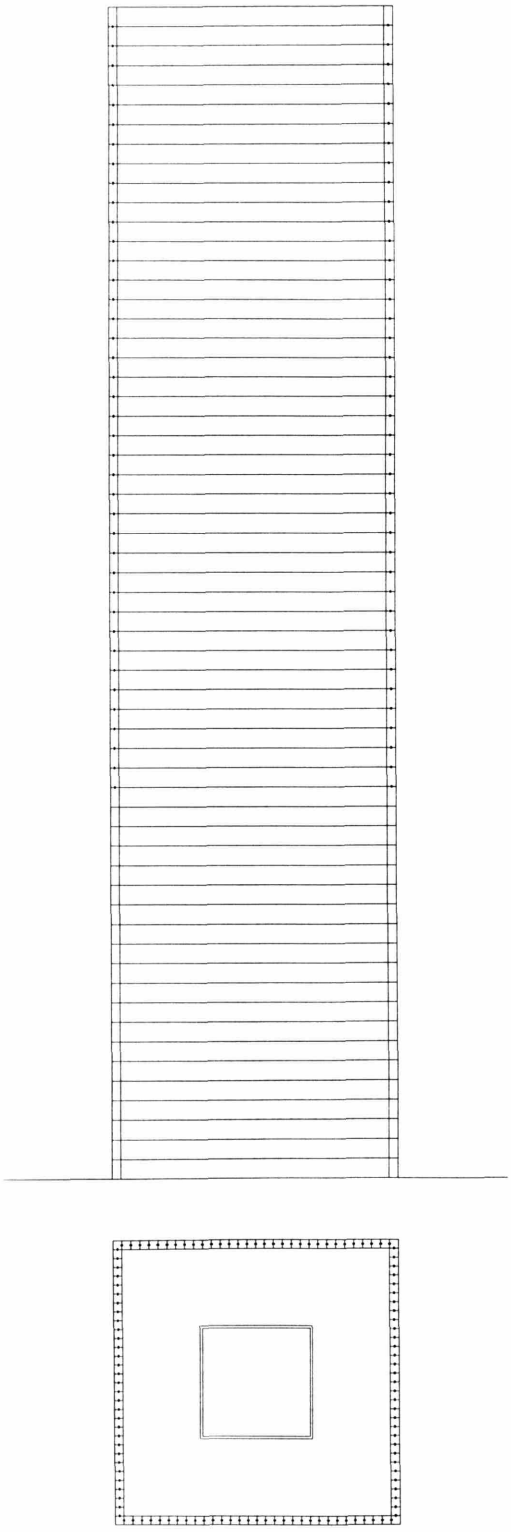

2) Vertically distributed TMD (Alt.1)

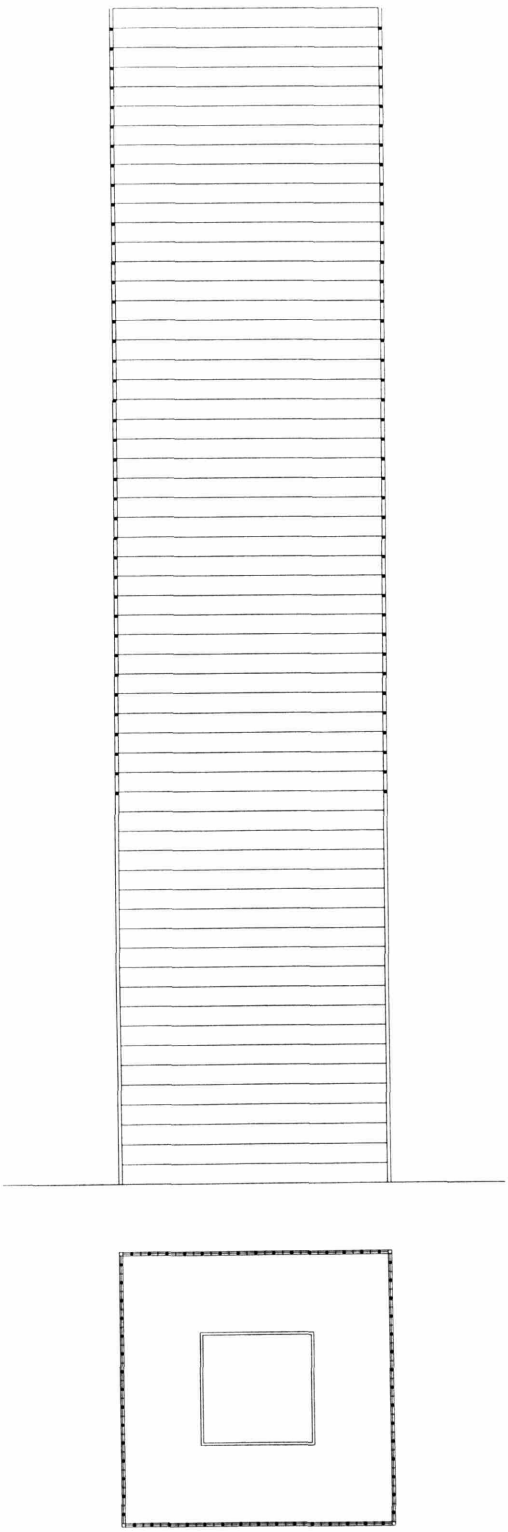

3) Vertically distributed TMD (Alt. 2)

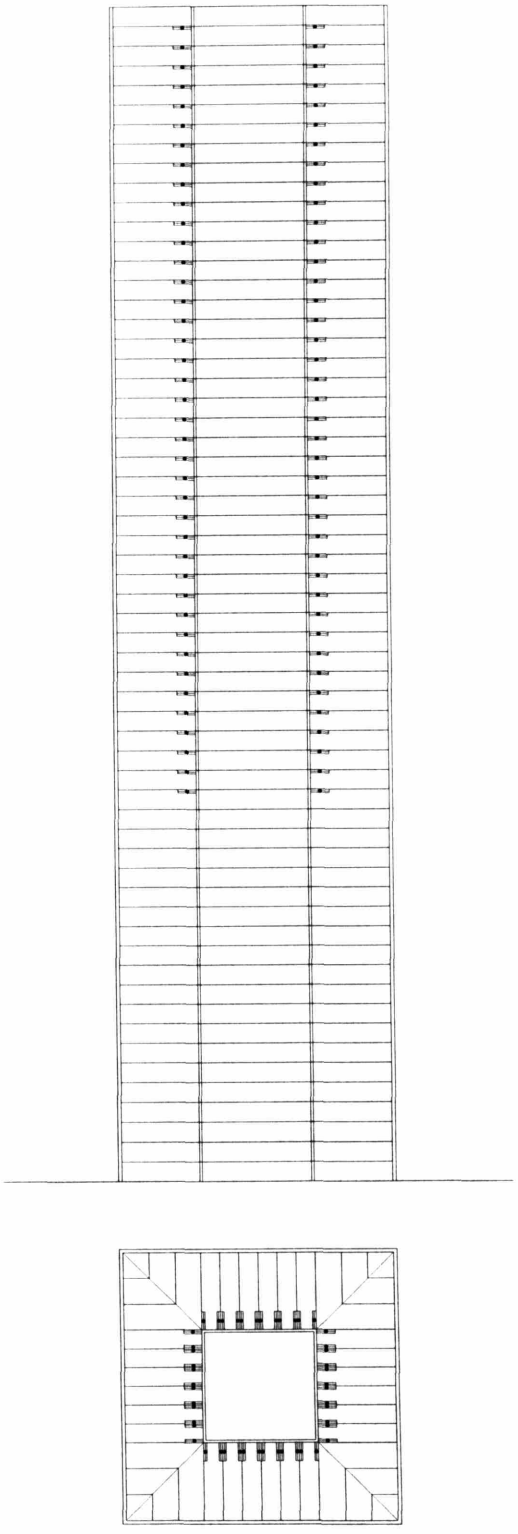

4) Vertically distributed TMD (Alt. 3)

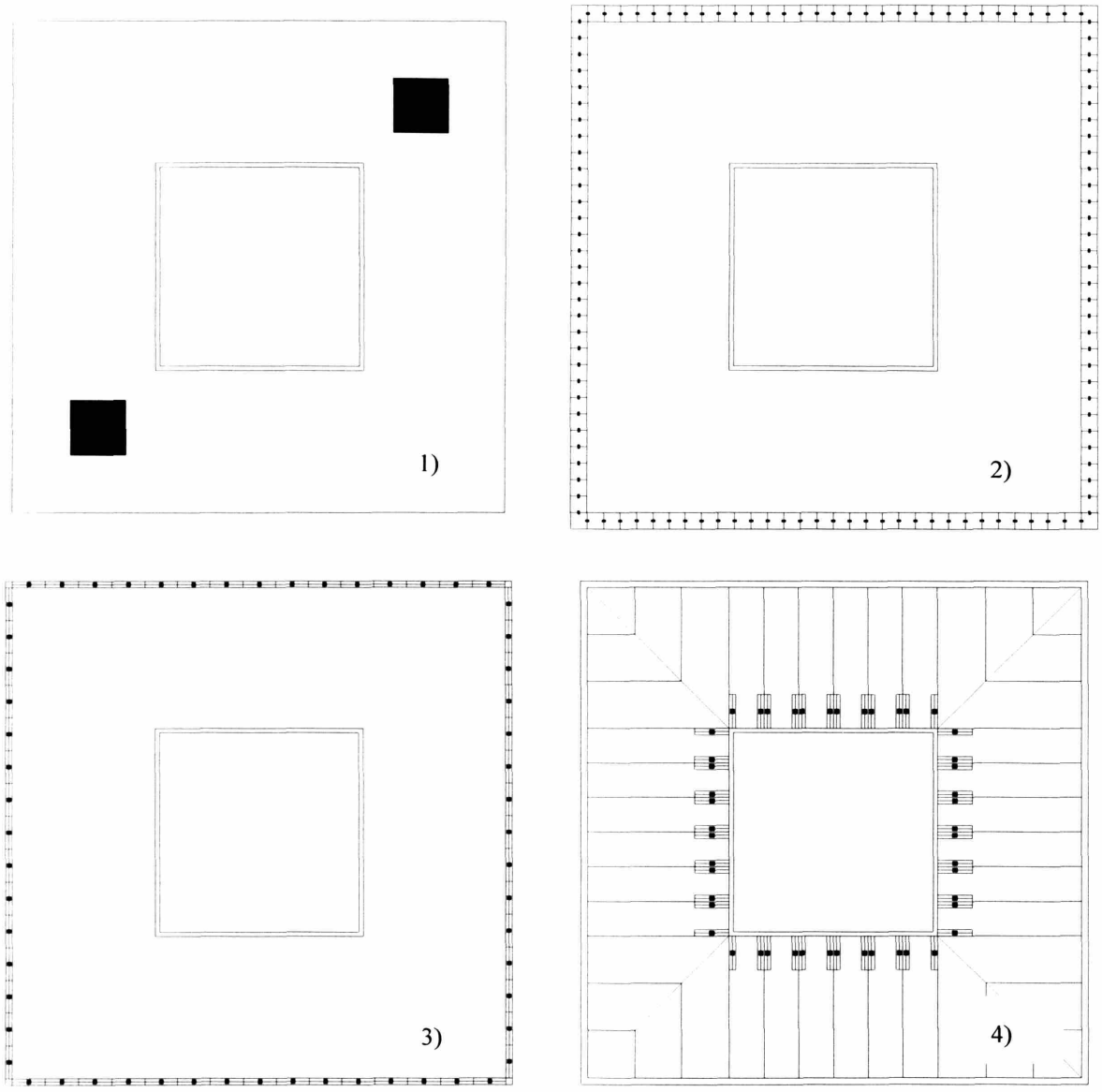

Figure 8.26: Enlarged View of 4 Different TMD Location Schemes

1) Conventional huge TMDs located at the top of the tall building
2) Small TMDs vertically distributed through DSF cavity: Damper masses are moving in the direction perpendicular to the façade plane. Many small TMDs can be installed within the DSF cavity. However, this scheme, in optimized condition, requires deep cavity space (i.e. about 2 - 3 meters).
3) Small TMDs vertically distributed through DSF cavity: Damper masses are moving in the direction parallel to the façade plane. Thus, this scheme does not require deep cavity spacing. However, only a limited amount of small TMDs can be located within the DSF cavity.
4) Small TMDs located underneath the floor slabs: DSF is not necessary for this system.

8.6. Summary

1) By vertically distributing TMDs, no building area is occupied by conventional huge TMDs, which results in valuable space saving near the tops of tall buildings.

2) By distributing TMDs vertically, not only the first mode but also other modes can be effectively controlled if necessary.

3) Since all TMD masses are located at the extreme perimeter of the building, torsional resistance exerted by TMD is maximized.

4) TMD installation becomes easy due to its reduced mass.

5) Vertically distributed small TMDs may be included within the spandrel portions of DSF construction units. In this case, the construction of DSF facades and vertically distributed TMD systems can be performed simultaneously.

Figure 8.27: DSF Construction Unit

6) Vertically distributed small TMDs may be installed in some other locations of a tall building such as underneath floor slabs.

8.7. Future Research

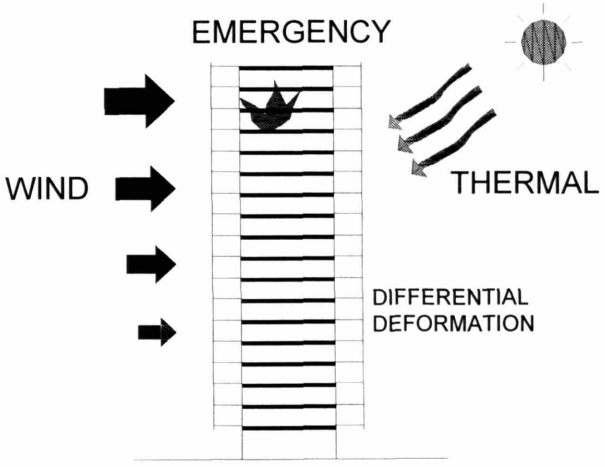

Figure 8.28: Future Research

Tall building dynamic motion control strategies were investigated through design integration between primary structure and double skin façade systems. Originally, the cavity between the inner and outer skin of the DSF system was introduced primarily for the purpose of enhanced environmental control between the interior and exterior. In this research, the potential of the space this cavity provides was further explored with regard to its possible contribution to structural dynamic motion control. Even though the two schemes presented in this thesis were investigated in depth, the research in this area is very new, and, thus, many other projects regarding tall building dynamic motion control using DSF systems can be further initiated and their structural and architectural potential can be explored. In addition, there are future research needs for the following areas.

1) Achieving differential deformation compatibility between building envelope and structural system to prevent premature façade failure and/or to eliminate unwanted air/water infiltration.

2) Designing DSF system to enhance effectiveness of thermal mass storage of the structural components through nighttime cooling strategy in summer: Designing DSF system to maximize nighttime ventilation and daytime insulation.

3) Integrating emergency egress with DSF cavities.

For the accomplishment of these expanded design objectives for tall buildings, integrative design approach among architecture-related disciplines is of critical importance.

Basically, this thesis investigated contemporary technologies and their architectural implications, and further, tried to develop new technologies and study their architectural potentials. The interrelationship between technology and architecture is not determinate, but rather is very dynamic. And this dynamic direction is strongly dependant on the interaction between architects and engineers.

Integrative design approach is desirable for the entire spectrum of architecture from vernacular housing to tall buildings worldwide. Among them, tall buildings were selected as a research focus in this thesis to study the interrelationship between technology and architecture because tall buildings are, in a sense, the accumulation of the most advanced technologies due to their very tallness, and their architectural expressions have significant impact on any urban context in which they soar due to their scale. Thus, it was hypothesized that the interaction between technology and architecture is more dynamic and, at the same time, easier to trace in tall buildings than in any other building types. This research was performed based on this hypothesis, and proved that this hypothesis is valid.

There are future research needs for the further investigations of the dynamic interrelationships between technology and architecture not only for tall buildings but also for other building types. These investigations will lead to higher quality built environments for humans in this technologically advanced and esthetically plural era.

CONCLUSION

Modern architecture was created based on modern technology and grew into a new architectural style that was preferred internationally. Tall buildings, which emerged in Chicago in the late 19th century even before various modern architectural movements in Europe, are clearly forerunners of mainstream modern architecture of the 20th century. This new building type was created through the development of iron/steel braced frames and curtainwall concepts. Today, in this intellectually and culturally pluralistic era, architecture is still deeply rooted in these original technologies, which enabled early tall buildings/modern architecture to prosper as a new style.

Due to the imperfectness of technological originality and the conflicting dual characteristics of any technology – promising reliability and ephemeral nature – original technologies are followed by refining technologies. These refining technologies may be called remedial technologies in the sense that they remedy unforeseen problematic aspects of original technologies and make them perform as intended or even better. Even though remedial technologies are mainly in the domain of function/performance, just as original technologies created new esthetic expressions and in turn a new architectural style, remedial technologies have great architectural potential, and architects and engineers have been exploring this potential. Indeed, through this exploration, the style created by original technologies is entering its culminating phase.

On the basis of the recognition of the symbiotic relationship between building systems, the prevalent strategy to develop remedial technologies to overcome contemporary technological limitations is design integration, which corresponds to the coevolution process in nature. Through integrative design approaches, synergistic effects can be achieved that eventually lead to architecture of higher quality.

In tall buildings, which in a sense are the accumulation of the most advanced architectural technologies, the significance of integrative design approachs is more important than in any other building type to overcome or at least minimize contemporary technological limitations. Design integration requires intimate collaboration between architects and engineers, and this cooperation cannot be achieved without a mutual understanding between the disciplines. From a broader view point, this thesis is devoted to helping enhance this kind of professional environment.

Understanding the technology, science, and mathematics behind the behavior of building systems is the responsibility of contemporary architects who want to create higher quality architecture. Likewise, understanding fundamental architectural design principles is the responsibility of engineers who want to achieve higher quality engineering products that are incorporated into architecture. This mutual understanding can become the potentiality of enhanced design integration.

In Part I of this thesis, the history of tall buildings was re-illuminated through the filter of the interrelationship between the technology and architectural style of tall buildings. Breakthrough technologies allowed the emergence of a new building type, tall buildings,

and eventually led to a new architectural style through the esthetic aspiration of architects who wanted to transform technological products into their esthetic ideology. While this new style at its culminating phase is still a mainstream design direction, many branch-out trends have been prevalent in tall building design. These pluralistic design approaches of architects accompany the technological evolutions enabled by the efforts of engineers.

In Part II of this thesis, current tall building design practices were investigated, again through the filter of the interrelationship between technology and architectural esthetics developed in Part I. Beginning from a broad perspective on these interactions, the research then focused on investigating two specific structural technologies and their architectural implications. Based on the recognition of the motion-induced human discomfort problem as a serious design issue in tall buildings, diagrid structural systems were investigated first for their enhanced lateral stiffness and esthetic potential. With regard to obtaining more damping against the dynamic motion problem, solutions were sought through the integrative design approach between structural systems and façade systems.

Each study, on its own, makes contributions in particular design situations. It is expected that the study of diagrid structures – the optimal angle study, the simple member sizing methodology, and other topics discussed, such as architectural, constructability, and urban contextual issues – will be very useful to both architects and engineers for preliminary design. Based on these studies, structural and architectural decisions in the early stages of design can be made in a more integrative and efficient way.

Through the study of low stiffness double skin facade connectors and vertically distributed tuned mass dampers, a new direction for solving the motion problem of tall buildings was introduced. The studies on the theory, preliminary design guidelines, and architectural implications of the distributed tuned mass dampers will be useful for both architects and engineers. Within today's globally prevalent architectural context, which values energy efficient design approaches more than ever, integrating structural motion control with double skin facade systems has great potential.

From a wider angle, this thesis is intended to contribute to enhancing mutual understanding between architects and engineers. For the author, this work is an initial step toward many potential research projects that will lead to a more desirable professional environment for architecture-related disciplines.

APPENDICES

Appendix 1. Architectural/Structural Perception of Diagrid/Frame Structures

$V = K_T \Delta u$, $M = K_B \Delta \beta$ B: Building Width

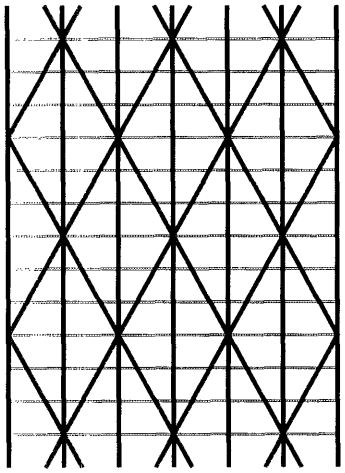

Shear Stiffness of Webs (Square Plan Building)

$$K_T = 12\left(\frac{A_b E_b}{L_b}\cos^2\theta\right) \leftarrow \text{Both Sides}$$

Bending Stiffness of Flanges

$$K_B = 7\left(\frac{B^2 A_c E_c}{2L_c}\right) + 6\left(\frac{B^2 A_d E_d}{2L_c}\right)\sin^3\theta$$

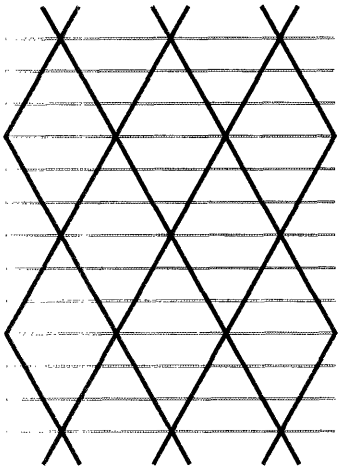

Shear Stiffness of Webs (Square Plan Building)

$$K_T = 12\left(\frac{A_b E_b}{L_b}\cos^2\theta\right), \text{ Same as Above}$$

Bending Stiffness of Flanges

$$K_B = 6\left(\frac{B^2 A_d E_d}{2L_c}\right)\sin^3\theta$$

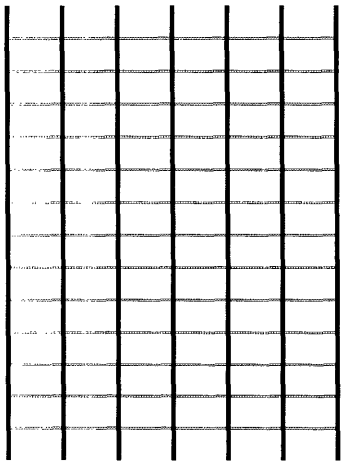

Shear Stiffness of Webs (Square Plan Building)

$$K_T = 10\frac{12EI_c}{h^3(1+r)} + 4\frac{12EI_c}{h^3(1+2r)}, \quad r = \frac{I_c}{h}\frac{L_b}{I_b}$$

Bending Stiffness of Flanges

$$K_B = 7\left(\frac{B^2 A_c E_c}{2L_c}\right)$$

Appendix 2. Velocity Pressure for a 240m-tall 60-story Building in Boston

SEI/ASCE 7-02, Minimum Design Loads for Buildings and Other Structures

60-Story Building (36 m x 36 m Plan, 4m x 60 story = 240m Tall B/H = 1/6.7)
Building Classification: Category III (Buildings and other structures that represent a substantial hazard to human life in the event of failure)
Importance Factor: 1.15 ← Category III
Basic Wind Speed: 110 mph (49 m/sec.) ← Boston
Exposure Category: B ← Urban and Suburban Area
Gust Effect Factor for Flexible or Dynamically Sensitive Structures:

$$G_f = 0.925\left(\frac{1+1.7I_{\bar{z}}\sqrt{g_Q^2Q^2+g_R^2R^2}}{1+1.7g_vI_{\bar{z}}}\right)$$

$I_{\bar{z}}$: Intensity of Turbulence @ Height $\bar{z}$.

$\bar{z}$: Equivalent Height of the Structure, $0.6h \geq \bar{z}_{\min} = 30ft$

$\bar{z} = 480ft$

$I_{\bar{z}} = c(33/\bar{z})^{1/6}$

$c = 0.3$ ← Exposure B

$I_{\bar{z}} = 0.19$

$g_Q = g_v = 3.4$

$$g_R = \sqrt{2\ln(3600n_1)} + \frac{0.577}{\sqrt{2\ln(3600n_1)}}$$

n_1 = Building Natural Frequency (Assume 0.17 Hz, T_1 = 6 sec.)

$g_R = 3.74$

Q: Background Response

$$Q = \sqrt{\frac{1}{1+0.63\left(\frac{B+h}{L_{\bar{z}}}\right)^{0.63}}}$$

$L = B = 120ft.$

$h = 800ft.$

$L_{\bar{z}}$: Internal Length Scale of Turbulence at the Equivalent Height

$L_{\bar{z}} = l(\bar{z}/33)^{\bar{\epsilon}}$

$l = 320ft.$ $\quad \bar{\epsilon} = 1/3$ ← Exposure B

$L_{\bar{z}} = 774$

$Q = 0.77$

R: Resonant Response Factor

$$R = \sqrt{\frac{1}{\beta} R_n R_h R_B (0.53 + 0.47 R_L)}$$

β = Damping Ratio = 1% Assumed

$$R_n = \frac{7.47 N_1}{(1 + 10.3 N_1)^{5/3}}$$

$$N_1 = \frac{n_1 L_{\bar{Z}}}{\bar{V}_{\bar{Z}}}$$

$$V_{\bar{Z}} = \bar{b}\left(\frac{\bar{z}}{33}\right)^{\bar{\alpha}} V\left(\frac{88}{60}\right) \quad \leftarrow \text{Mean Hourly Wind speed}$$

$\bar{b} = 0.45 \quad \bar{\alpha} = 1/4 = 0.25$ ← Exposure B

V = 110 mph (49 m/sec.) ← Boston

$V_{\bar{Z}} = 142$

$N_1 = 1.2$

$R_n = 0.12$

$$R_h = \frac{1}{\eta} - \frac{1}{2\eta^2}\left(1 - e^{-2\eta}\right) \quad \text{for } \eta = 4.6 n_1 h / \bar{V}_{\bar{z}} > 0$$

$R_h = 1 \quad \text{for } \eta = 0$

$R_h = 4.41$

$$R_B = \frac{1}{\eta} - \frac{1}{2\eta^2}\left(1 - e^{-2\eta}\right) \quad \text{for } \eta = 4.6 n_1 / \bar{V}_{\bar{z}} > 0$$

$R_B = 1 \quad \text{for } \eta = 0$

$R_B = 1$

$$R_L = \frac{1}{\eta} - \frac{1}{2\eta^2}\left(1 - e^{-2\eta}\right) \quad \text{for } \eta = 15.4 L / \bar{V}_{\bar{z}} > 0$$

$R_L = 1 \quad \text{for } \eta = 0$

$R_L = 2.21$

$$G_f = 0.925\left(\frac{1 + 1.7 I_{\bar{Z}} \sqrt{g_Q^2 Q^2 + g_R^2 R^2}}{1 + 1.7 g_v I_{\bar{Z}}}\right) = 0.82$$

External Pressure Coefficient: $C_{pww} = 0.8 \quad C_{plw} = 0.5$

Velocity Pressure Exposure Coefficient: K_Z

$$K_Z = 2.01\left(\frac{z}{z_g}\right)^{2/\alpha}$$

$\alpha = 7.0, \qquad z_g = 1200 ft.$ ← Exposure B

$z = 800 ft. > z_{\min} = 30 ft.$ ← Exposure B

$$K_Z = 2.01\left(\frac{z}{z_g}\right)^{2/\alpha} = 1.79$$

Velocity Pressure q_z

$q_z = 0.00256 K_z K_{zt} K_d V^2 I = 63.8 psf$

Design Wind Pressure at the top of the 240m-tall 60-story building is as follows:

$p_z = qG_f C_p - q_i (GC_{pi})$

$p_{zww@top} = 41.9 psf$

$p_{zlw@top} = 26.2 psf$

$p_{ztoatl@top} = 68.1 psf$.

Following the same procedure, Design Wind Pressure at the mid-height of the 240m-tall 60-story building is as follows:

$p_{zww@mid-height} = 33.5 psf$

$p_{zlw@mid-height} = 21.0 psf$

$p_{ztoatl@mid-height} = 54.5 psf$.

Design Wind Pressure at the base of the 240m-tall 60-story building is as follows:

$p_{zww@base} = 12.6 psf$

$p_{zlw@base} = 8.0 psf$

$p_{ztoatl@base} = 20.6 psf$.

Leeward Velocity Pressure

Windward Velocity Pressure

$p_{zlw@top} = 26.2 psf$

$p_{zww@top} = 41.9 psf$

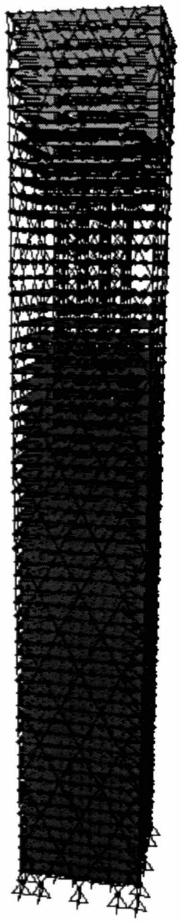

$p_{zlw@mid-height} = 21.0 psf$

$p_{zww@mid-height} = 33.5 psf$

$p_{zlw@base} = 8.0 psf$

$p_{zww@base} = 12.6 psf$

Appendix 3. LRFD Member Stress Check for Structures in Section 5.2

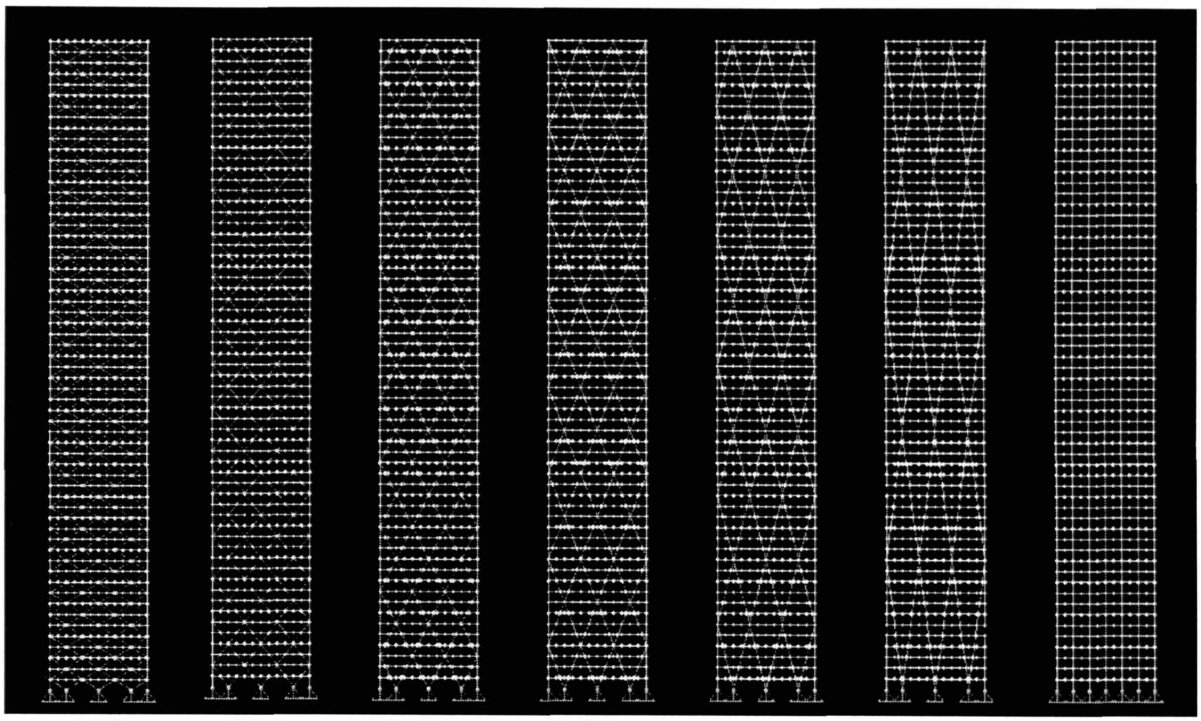

1.39 0.85 0.61 0.55 0.53 2.16 0.31

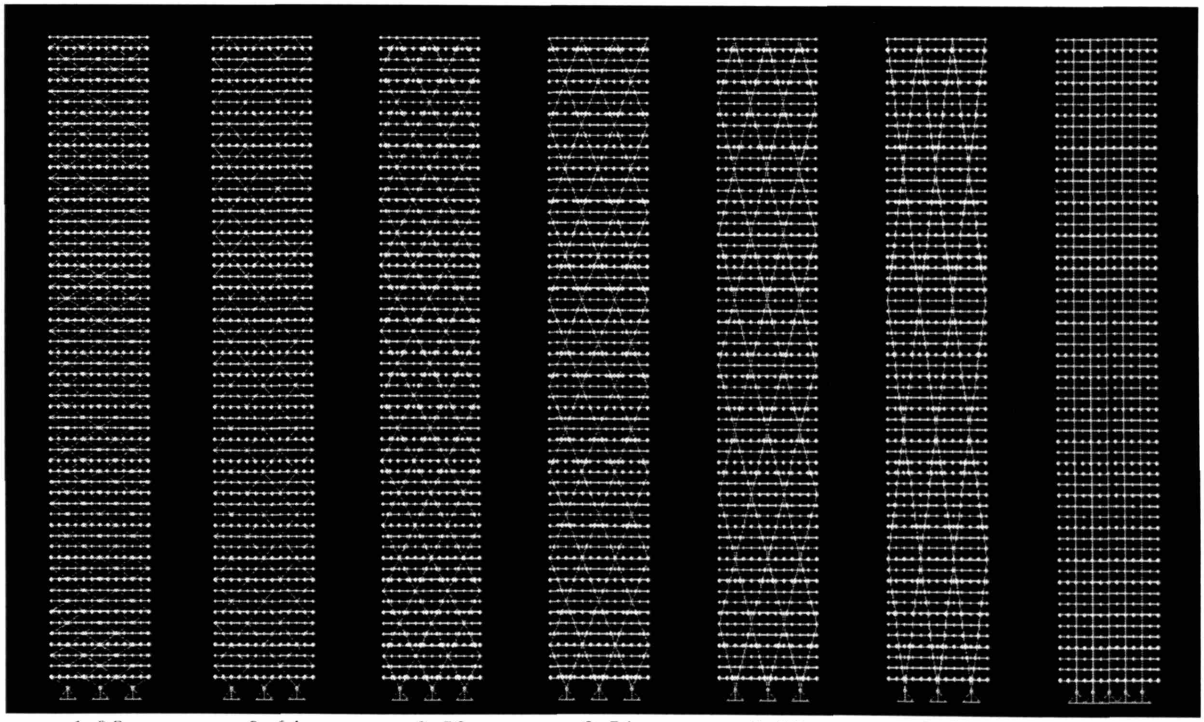

1.08 0.64 0.53 0.51 0.50 0.52 0.41

Appendix 4. Equivalent Plate Model of Diagrid Structures

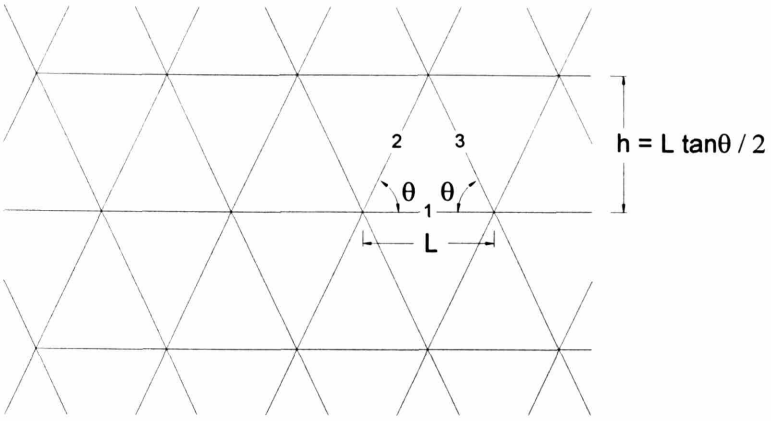

Strain energy for a bar (A, L) is $\frac{1}{2}F\delta = \frac{EA}{2L}\delta^2 = \frac{EAL}{2}\varepsilon^2$.

Strain energy for a triangle is

$$V = \frac{EAL}{2}\varepsilon_1^{\ 2} + \frac{EAL}{4\cos\theta}(\varepsilon_2^{\ 2} + \varepsilon_3^{\ 2}) = \frac{EAL}{4\cos\theta}\{(\sqrt{2\cos\theta}\varepsilon_1)^2 + \varepsilon_2^{\ 2} + \varepsilon_3^{\ 2}\} = \frac{EAL}{4\cos\theta}\varepsilon^{*,T}\varepsilon^*$$

where $\varepsilon^* = \{\varepsilon_1^{\ \circ}, \varepsilon_2, \varepsilon_3\}$, $\varepsilon_1^{\ \circ} = \sqrt{2\cos\theta}\varepsilon_1$. Then,

$$\overline{V} = \frac{V}{EffectiveArea} = \frac{\frac{EAL}{4\cos\theta}}{\frac{L^2\tan\theta}{2}}\varepsilon^{*,T}\varepsilon^* = \frac{EA}{2L\sin\theta}\varepsilon^{*,T}\varepsilon^*. \qquad \text{(a)}$$

The bar extensions are expressed in terms of the cartesian strains using $\varepsilon^* = T^*\varepsilon$:

$$\begin{Bmatrix}\varepsilon_1^{\ \circ}\\ \varepsilon_2\\ \varepsilon_3\end{Bmatrix} = \begin{bmatrix}\sqrt{2\cos\theta} & 0 & 0\\ \cos^2\theta & \sin^2\theta & -\cos\theta\sin\theta\\ \cos^2\theta & \sin^2\theta & \cos\theta\sin\theta\end{bmatrix} = \begin{Bmatrix}\varepsilon_x\\ \varepsilon_y\\ \gamma_{xy}\end{Bmatrix}. \qquad \text{(b)}$$

Substituting (b) in (a) leads to

$$\overline{V} = \frac{EA}{2L\sin\theta}\varepsilon^T(T^{*,T}T^*)\varepsilon \equiv \frac{1}{2}\varepsilon^T D_{s,eq}\varepsilon$$

$$D_{s,eq} = \frac{EA}{L\sin\theta}(T^{*,T}T^*) = \frac{EA}{L\sin\theta}\begin{bmatrix}2\cos\theta + 2\cos^4\theta & 2\cos^2\theta\sin^2\theta & 0\\ 2\cos^2\theta\sin^2\theta & 2\sin^4\theta & 0\\ 0 & 0 & 2\cos^2\theta\sin^2\theta\end{bmatrix}.$$

Thus, the thickness of the equivalent plate $t_{eq} = \frac{A}{L\sin\theta}(2\cos\theta + 2\cos^4\theta)$.

When the grid consists of equilateral triangles,

$$D_{s,eq} = \frac{3\sqrt{3}}{4}\frac{EA}{L}\begin{bmatrix} 1 & 1/3 & 0 \\ 1/3 & 1 & 0 \\ 0 & 0 & 1/3 \end{bmatrix}.$$

Thus, the thickness of the equivalent plate $t_{eq} = \frac{3\sqrt{3}}{4}\frac{A}{L}$.

Suppose L = 12 meters and A = 0.09 square meters, then $t_{eq} \approx 1cm$.

60-Story Model Comparisons

Diagrid Model

L (m)	A (sq. m)	T_{eq} (cm)	1st Mode Period (sec.)
4	0.03	1	2.23
12	0.09	1	1.89
24	0.18	1	1.64

Equivalent Plate Model

T_{eq} (cm)	1st Mode Period (sec.)
1	1.91

Appendix 5. Preliminary Design of Diagrid Structures & Verification of Empirical Equation 4.24: $s = \left(\frac{H}{B} - 3\right), \quad \frac{H}{B} \geq 5$

5.1. 69-Story Diagrid Structure $(H / B \approx 8)$

5.1.1. 69-Story Diagrid Structure with s = 1

Story	V(KN)	M(KN-M)	Ad(bndg)	Ad(Shear)
67th - 69th	1,325	1,988	0.0004	**0.0030**
61st - 66th	3,975	31,800	0.0060	**0.0089**
55th - 60th	6,625	127,200	**0.0241**	0.0148
49th - 54th	9,275	286,200	**0.0542**	0.0207
43rd - 48th	11,925	508,800	**0.0964**	0.0266
37th - 42nd	14,417	794,526	**0.1506**	0.0322
31st - 36th	16,820	1,140,267	**0.2161**	0.0375
25th - 30th	19,223	1,543,947	**0.2926**	0.0429
19th - 24th	21,359	2,004,498	**0.3799**	0.0477
13th - 18th	22,961	2,515,512	**0.4768**	0.0513
7th - 12th	24,563	3,066,576	**0.5813**	0.0548
1st - 6th	26,165	3,656,088	**0.6930**	0.0584

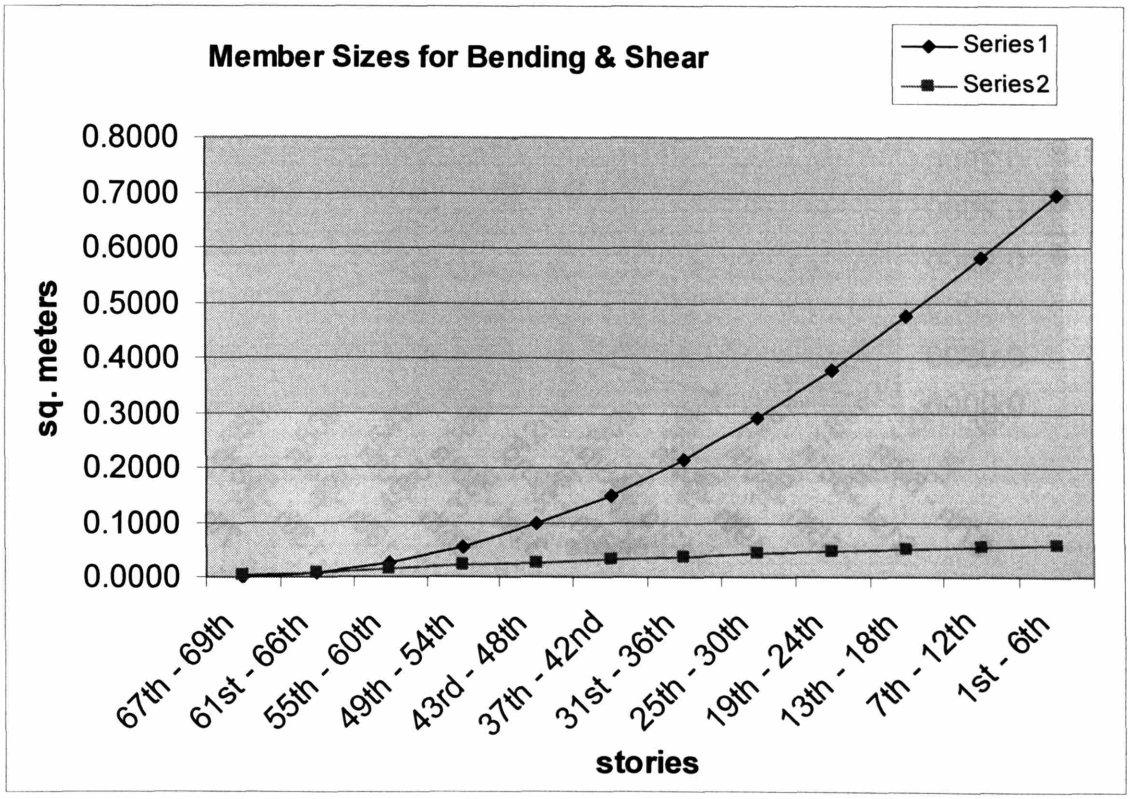

5.1.2. 69-Story Diagrid Structure with s = 5

Story	V(KN)	M(KN-M)	Ad(bndg)	Ad(Shear)
67th - 69th	1,325	1,988	0.0002	**0.0089**
61st - 66th	3,975	31,800	0.0036	**0.0266**
55th - 60th	6,625	127,200	0.0145	**0.0444**
49th - 54th	9,275	286,200	0.0325	**0.0621**
43rd - 48th	11,925	508,800	0.0579	**0.0799**
37th - 42nd	14,417	794,526	0.0904	**0.0965**
31st - 36th	16,820	1,140,267	**0.1297**	0.1126
25th - 30th	19,223	1,543,947	**0.1756**	0.1287
19th - 24th	21,359	2,004,498	**0.2280**	0.1430
13th - 18th	22,961	2,515,512	**0.2861**	0.1538
7th - 12th	24,563	3,066,576	**0.3488**	0.1645
1st - 6th	26,165	3,656,088	**0.4158**	0.1752

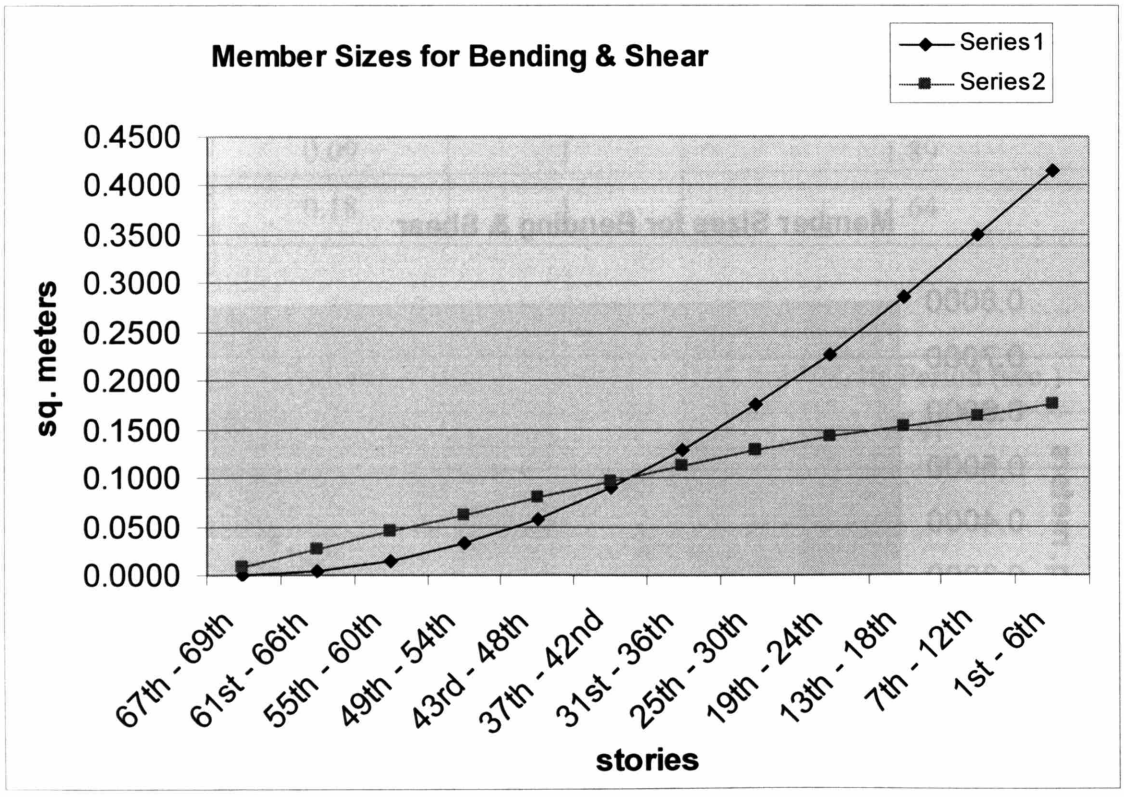

5.1.3. 69-Story Diagrid Structure with s = 12

Story	V(KN)	M(KN-M)	Ad(bndg)	Ad(Shear)
67th - 69th	1,325	1,988	0.0002	**0.0192**
61st - 66th	3,975	31,800	0.0033	**0.0577**
55th - 60th	6,625	127,200	0.0131	**0.0961**
49th - 54th	9,275	286,200	0.0294	**0.1346**
43rd - 48th	11,925	508,800	0.0522	**0.1730**
37th - 42nd	14,417	794,526	0.0816	**0.2092**
31st - 36th	16,820	1,140,267	0.1171	**0.2440**
25th - 30th	19,223	1,543,947	0.1585	**0.2789**
19th - 24th	21,359	2,004,498	0.2058	**0.3099**
13th - 18th	22,961	2,515,512	0.2583	**0.3331**
7th - 12th	24,563	3,066,576	0.3148	**0.3564**
1st - 6th	26,165	3,656,088	0.3754	**0.3796**

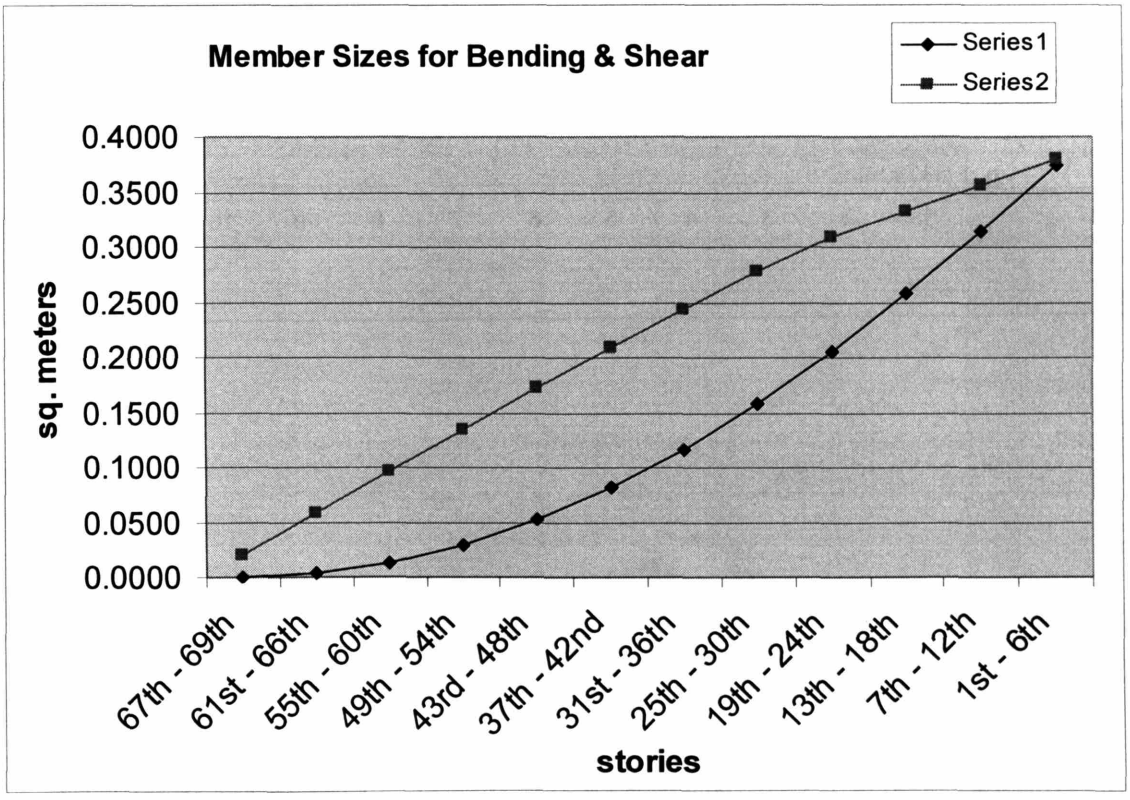

5.1.4. 69-Story Structure Diagrid Steel Mass

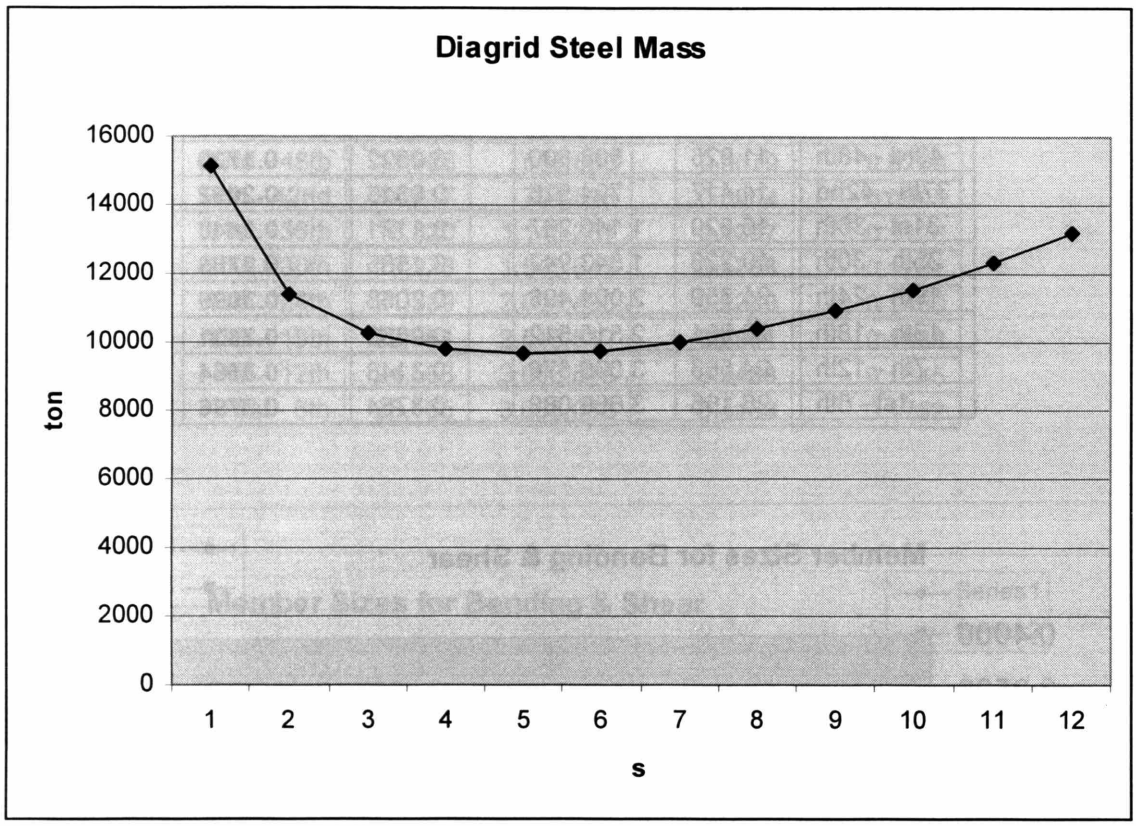

5.2. 60-Story Diagrid Structure ($H / B \approx 7$)

5.2.1. 60-Story Diagrid Structure with s = 1

Story	V(KN)	M(KN-M)	Ad(bndg)	Ad(Shear)
55th - 60th	2,650	7,950	0.0013	**0.0059**
49th - 54th	5,300	71,550	**0.0118**	**0.0118**
43rd - 48th	7,950	198,750	**0.0328**	0.0177
37th - 42nd	10,442	389,076	**0.0641**	0.0233
31st - 36th	12,845	639,417	**0.1054**	0.0287
25th - 30th	15,248	947,697	**0.1562**	0.0340
19th - 24th	17,384	1,312,848	**0.2164**	0.0388
13th - 18th	18,986	1,728,462	**0.2849**	0.0424
7th - 12th	20,588	2,184,126	**0.3600**	0.0460
1st - 6th	22,190	2,788,776	**0.4596**	0.0495

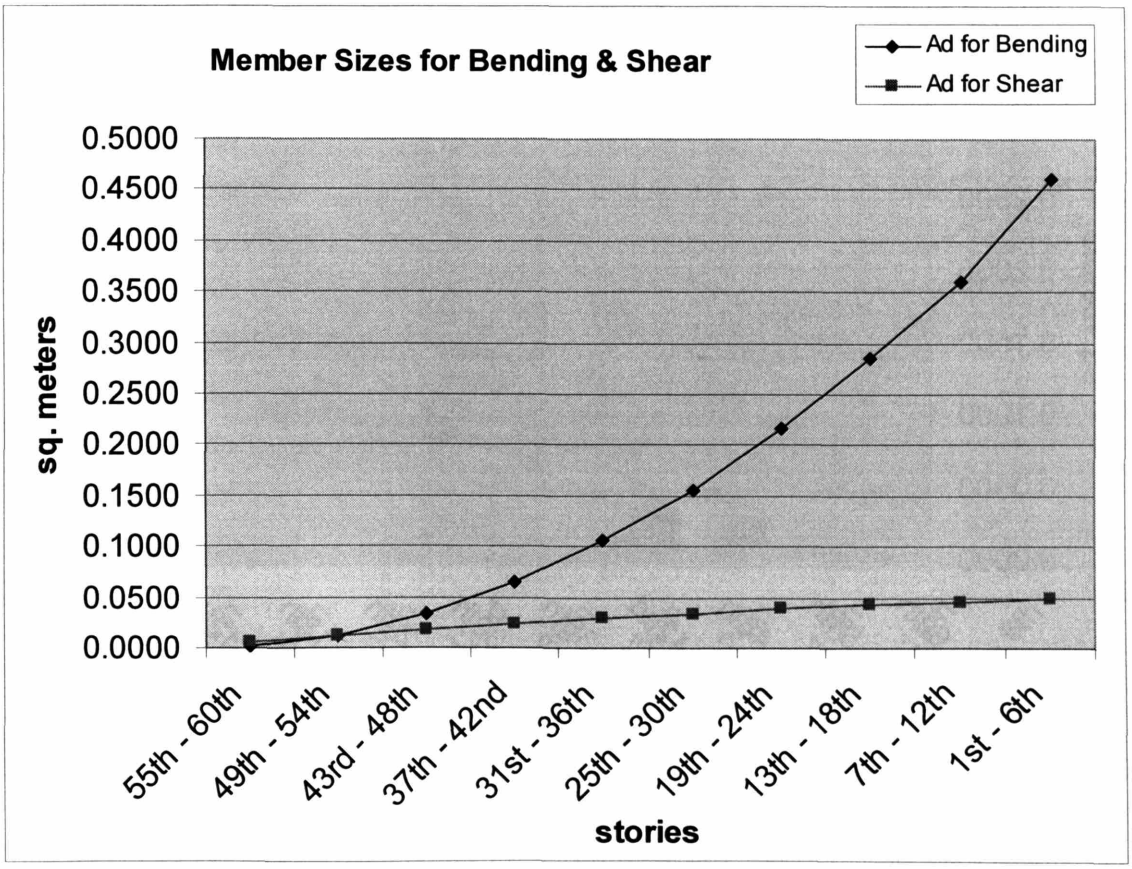

5.2.2. 60-Story Diagrid Structure with s = 4

Story	V(KN)	M(KN-M)	Ad(bndg)	Ad(Shear)
55th - 60th	2,650	7,950	0.0008	**0.0148**
49th - 54th	5,300	71,550	0.0074	**0.0296**
43rd - 48th	7,950	198,750	0.0205	**0.0444**
37th - 42nd	10,442	389,076	0.0401	**0.0583**
31st - 36th	12,845	639,417	0.0659	**0.0717**
25th - 30th	15,248	947,697	**0.0976**	0.0851
19th - 24th	17,384	1,312,848	**0.1352**	0.0970
13th - 18th	18,986	1,728,462	**0.1781**	0.1059
7th - 12th	20,588	2,184,126	**0.2250**	0.1149
1st - 6th	22,190	2,788,776	**0.2873**	0.1238

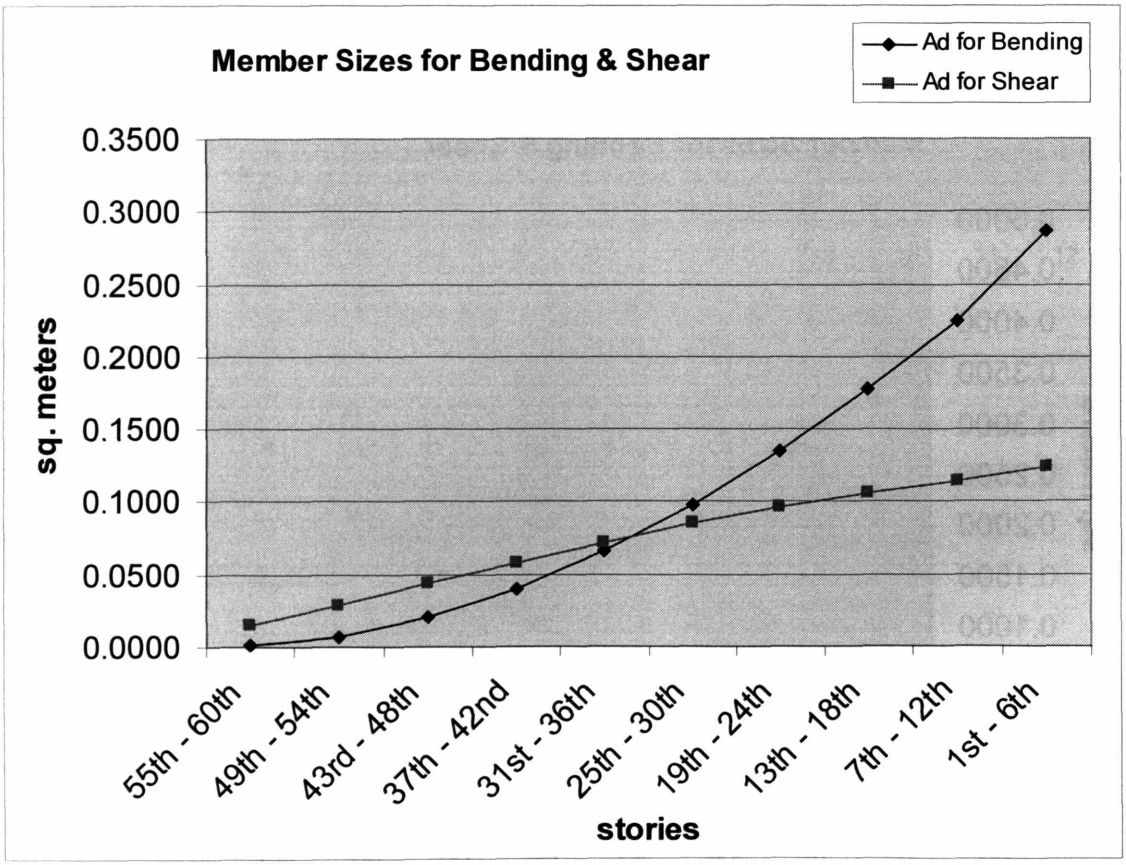

5.2.3. 60-Story Diagrid Structure with s = 9

Story	V(KN)	M(KN-M)	Ad(bndg)	Ad(Shear)
55th - 60th	2,650	7,950	0.0007	**0.0296**
49th - 54th	5,300	71,550	0.0066	**0.0592**
43rd - 48th	7,950	198,750	0.0182	**0.0887**
37th - 42nd	10,442	389,076	0.0356	**0.1165**
31st - 36th	12,845	639,417	0.0585	**0.1434**
25th - 30th	15,248	947,697	0.0868	**0.1702**
19th - 24th	17,384	1,312,848	0.1202	**0.1940**
13th - 18th	18,986	1,728,462	0.1583	**0.2119**
7th - 12th	20,588	2,184,126	0.2000	**0.2298**
1st - 6th	22,190	2,788,776	**0.2554**	0.2477

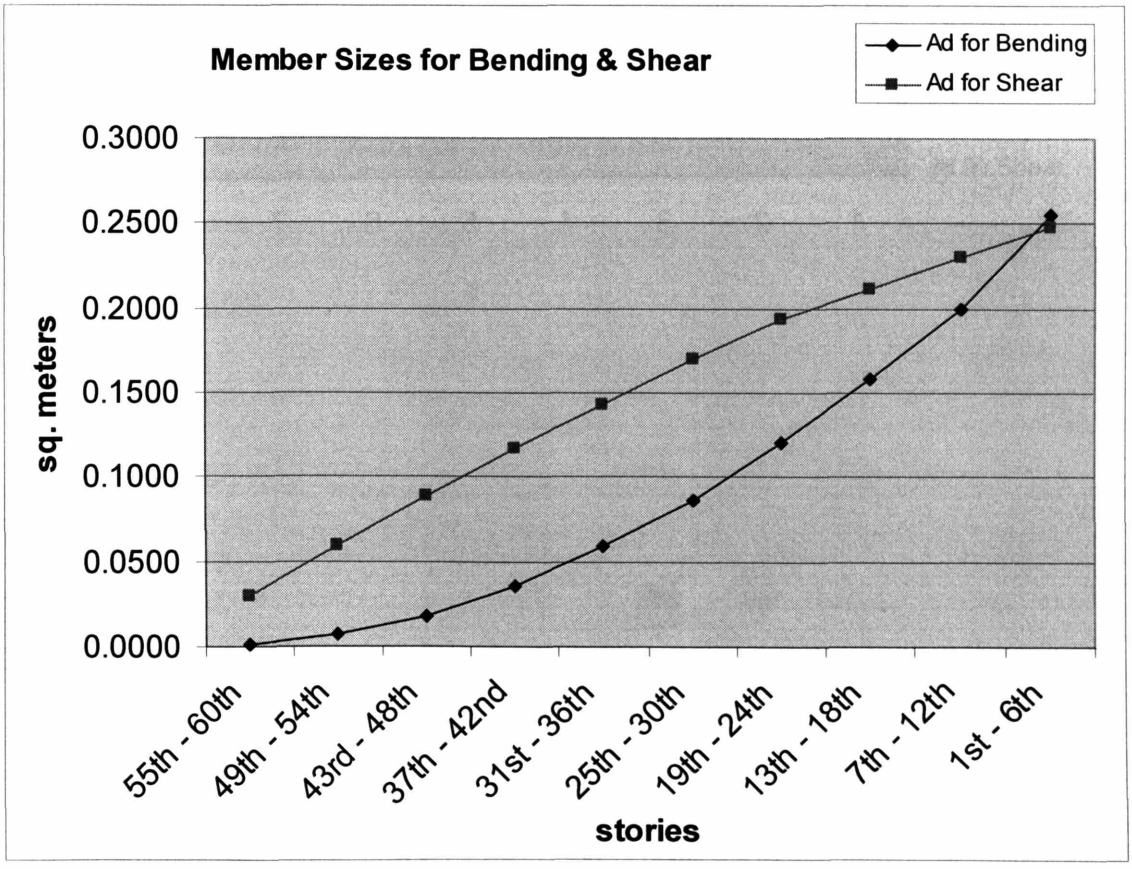

5.2.4. 60-Story Structure Diagrid Steel Mass

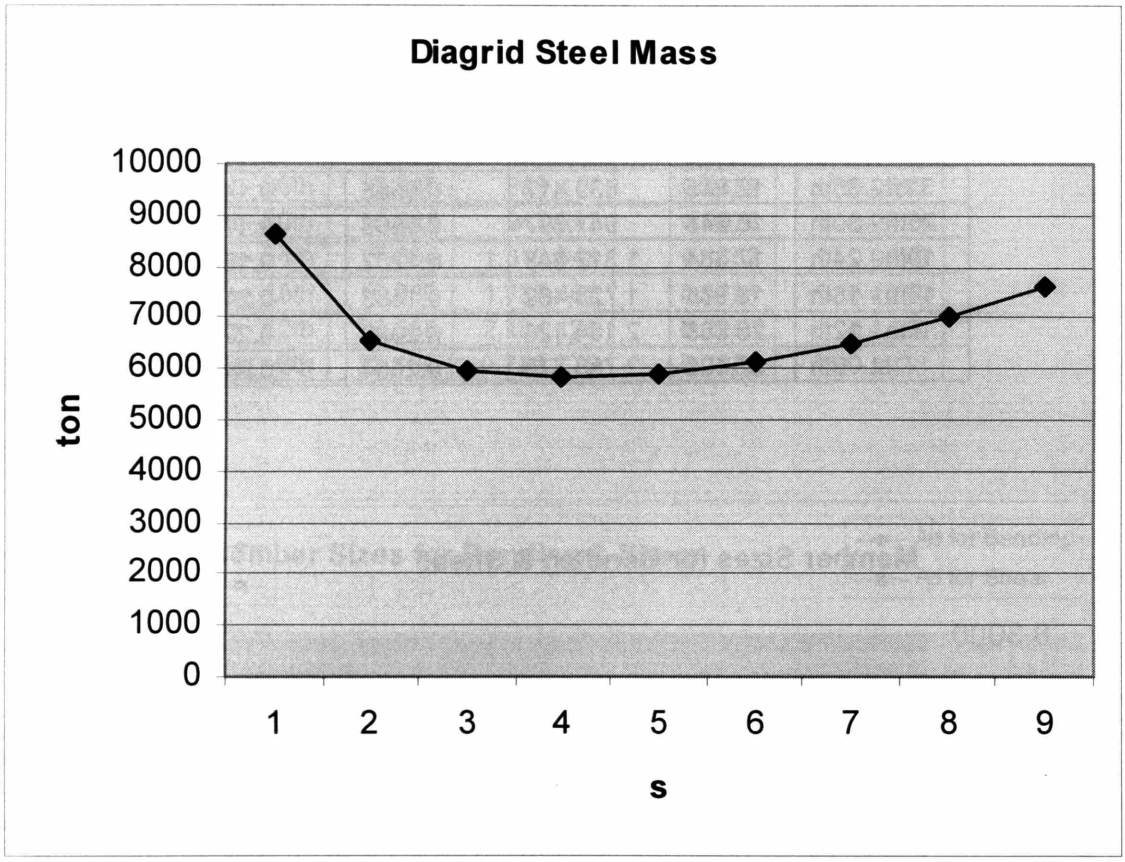

5.3. 51-Story Diagrid Structure ($H / B \approx 6$)

5.3.1. 51-Story Diagrid Structure with s = 1

Story	V(KN)	M(KN-M)	Ad(bndg)	Ad(Shear)
49th - 51th	1,325	1,988	0.0003	**0.0030**
43rd - 48th	3,975	31,800	0.0045	**0.0089**
37th - 42nd	6,467	126,726	**0.0178**	0.0144
31st - 36th	8,870	281,667	**0.0395**	0.0198
25th - 30th	11,273	494,547	**0.0693**	0.0252
19th - 24th	13,409	764,298	**0.1071**	0.0299
13th - 18th	15,011	1,084,512	**0.1519**	0.0335
7th - 12th	16,613	1,444,776	**0.2024**	0.0371
1st - 6th	18,215	1,954,026	**0.2738**	0.0407

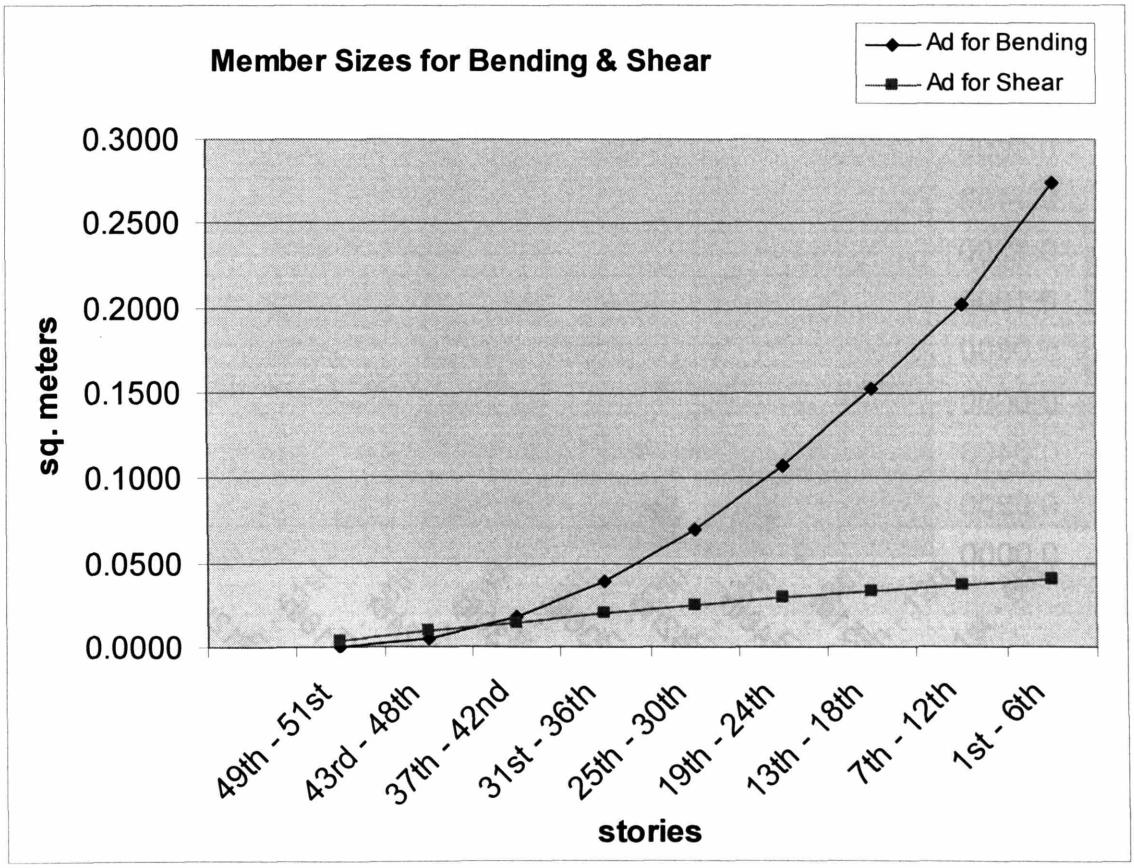

5.3.2 51-Story Diagrid Structure with s = 3

Story	V(KN)	M(KN-M)	Ad(bndg)	Ad(Shear)
49th - 51th	1,325	1,988	0.0002	**0.0059**
43rd - 48th	3,975	31,800	0.0030	**0.0177**
37th - 42nd	6,467	126,726	0.0118	**0.0289**
31st - 36th	8,870	281,667	0.0263	**0.0396**
25th - 30th	11,273	494,547	0.0462	**0.0503**
19th - 24th	13,409	764,298	**0.0714**	0.0599
13th - 18th	15,011	1,084,512	**0.1013**	0.0670
7th - 12th	16,613	1,444,776	**0.1349**	0.0742
1st - 6th	18,215	1,954,026	**0.1825**	0.0813

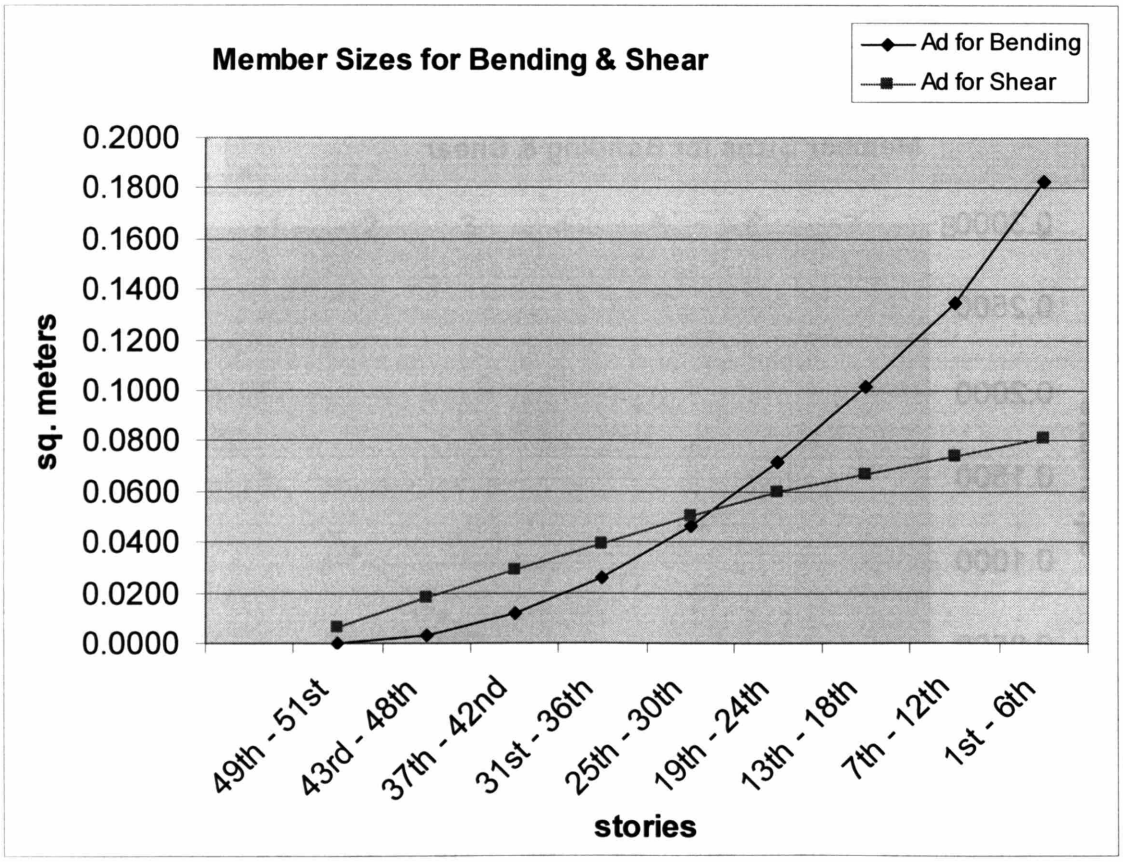

5.3.3. 51-Story Diagrid Structure with s = 7

Story	V(KN)	M(KN-M)	Ad(bndg)	Ad(Shear)
49th - 51th	1,325	1,988	0.0002	**0.0118**
43rd - 48th	3,975	31,800	0.0025	**0.0355**
37th - 42nd	6,467	126,726	0.0101	**0.0577**
31st - 36th	8,870	281,667	0.0225	**0.0792**
25th - 30th	11,273	494,547	0.0396	**0.1007**
19th - 24th	13,409	764,298	0.0612	**0.1197**
13th - 18th	15,011	1,084,512	0.0868	**0.1340**
7th - 12th	16,613	1,444,776	0.1157	**0.1483**
1st - 6th	18,215	1,954,026	0.1564	**0.1626**

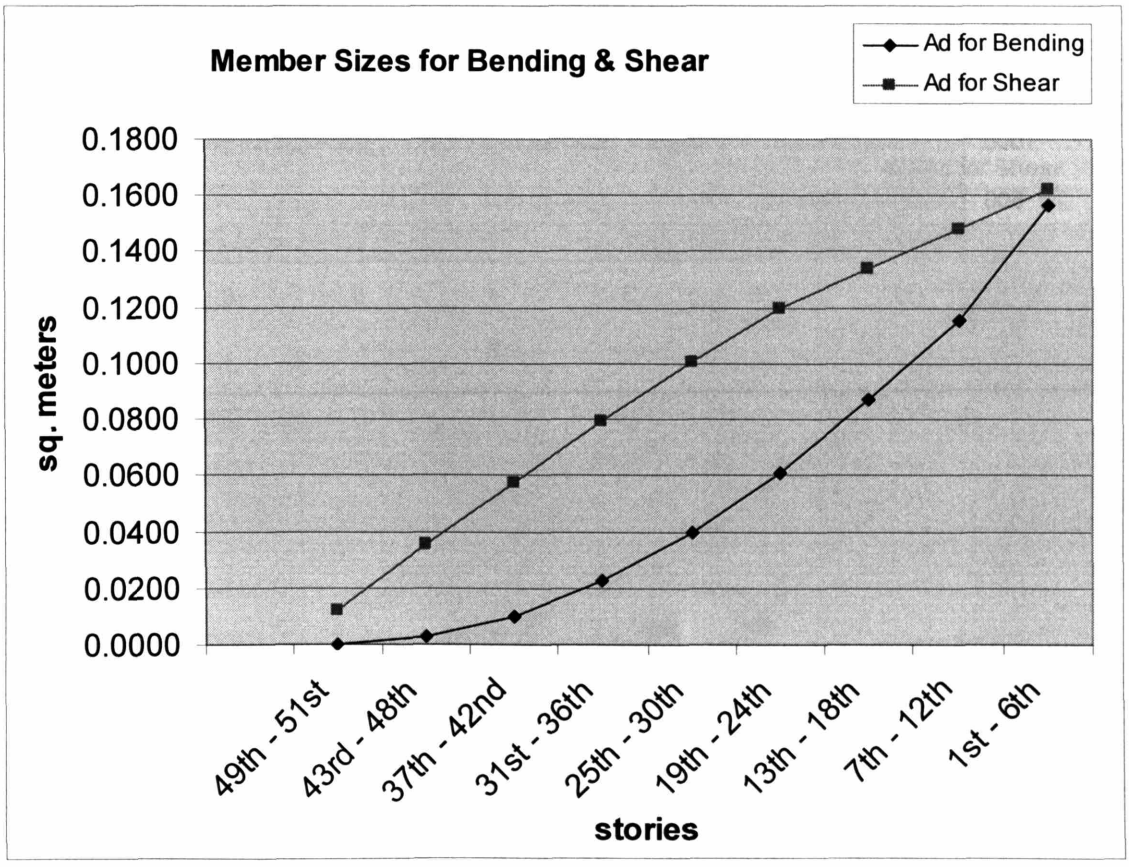

5.3.4. 51-Story Structure Diagrid Steel Mass

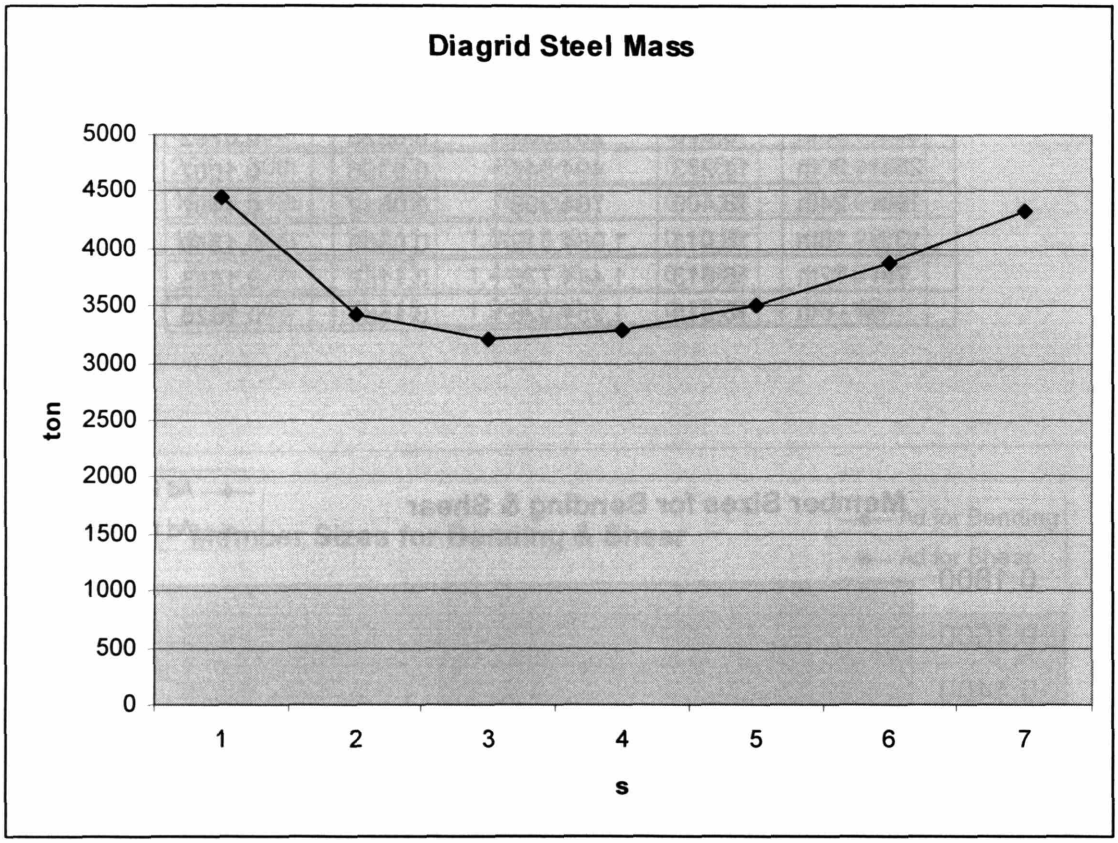

5.4. 42-Story Diagrid Structure ($H / B \approx 5$)

5.4.1. 42-Story Diagrid Structure with s = 1

Story	V(KN)	M(KN-M)	Ad(bndg)	Ad(Shear)
37th - 42nd	2,492	7,476	0.0009	**0.0056**
31st - 36th	4,895	67,017	0.0077	**0.0109**
25th - 30th	7,298	184,497	**0.0213**	0.0163
19th - 24th	9,434	358,848	**0.0414**	0.0211
13th - 18th	11,036	583,662	**0.0673**	0.0246
7th - 12th	12,638	848,526	**0.0979**	0.0282
1st - 6th	14,240	1,262,376	**0.1456**	0.0318

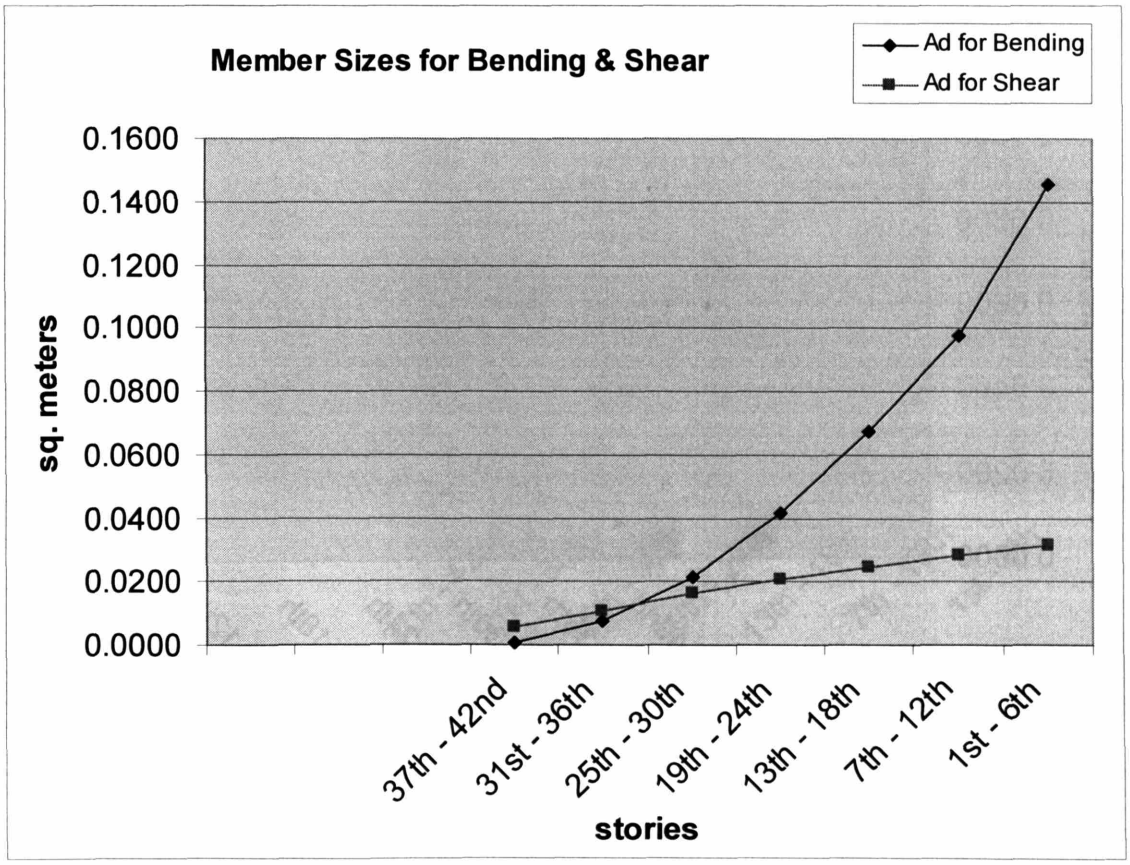

5.4.2 42-Story Diagrid Structure with s = 2

Story	V(KN)	M(KN-M)	Ad(bndg)	Ad(Shear)
37th - 42nd	2,492	7,476	0.0006	0.0083
31st - 36th	4,895	67,017	0.0058	0.0164
25th - 30th	7,298	184,497	0.0160	0.0244
19th - 24th	9,434	358,848	0.0311	0.0316
13th - 18th	11,036	583,662	0.0505	0.0370
7th - 12th	12,638	848,526	0.0734	0.0423
1st - 6th	14,240	1,262,376	0.1092	0.0477

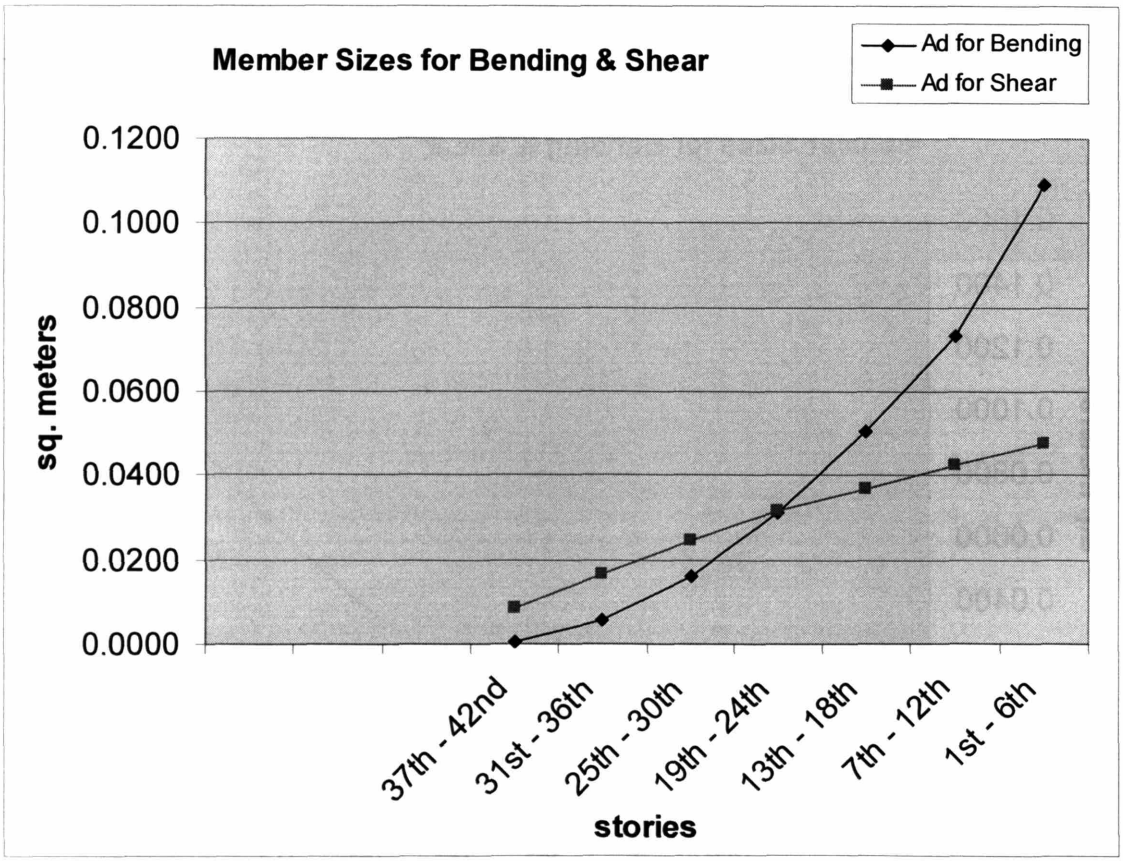

5.4.3. 42 Story Diagrid Structure with s = 4

Story	V(KN)	M(KN-M)	Ad(bndg)	Ad(Shear)
37th - 42nd	2,492	7,476	0.0005	0.0139
31st - 36th	4,895	67,017	0.0048	0.0273
25th - 30th	7,298	184,497	0.0133	0.0407
19th - 24th	9,434	358,848	0.0259	0.0526
13th - 18th	11,036	583,662	0.0421	0.0616
7th - 12th	12,638	848,526	0.0612	0.0705
1st - 6th	14,240	1,262,376	0.0910	0.0795

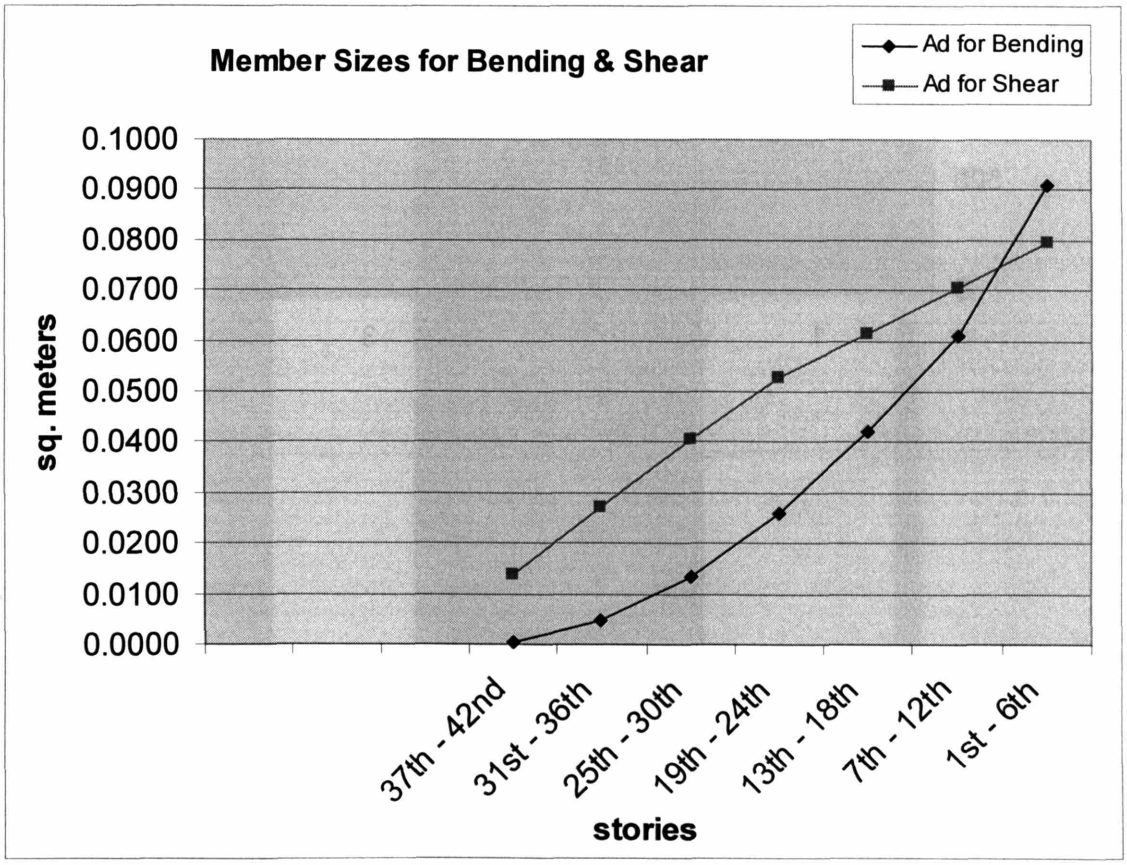

5.3.4. 42-Story Structure Diagrid Steel Mass

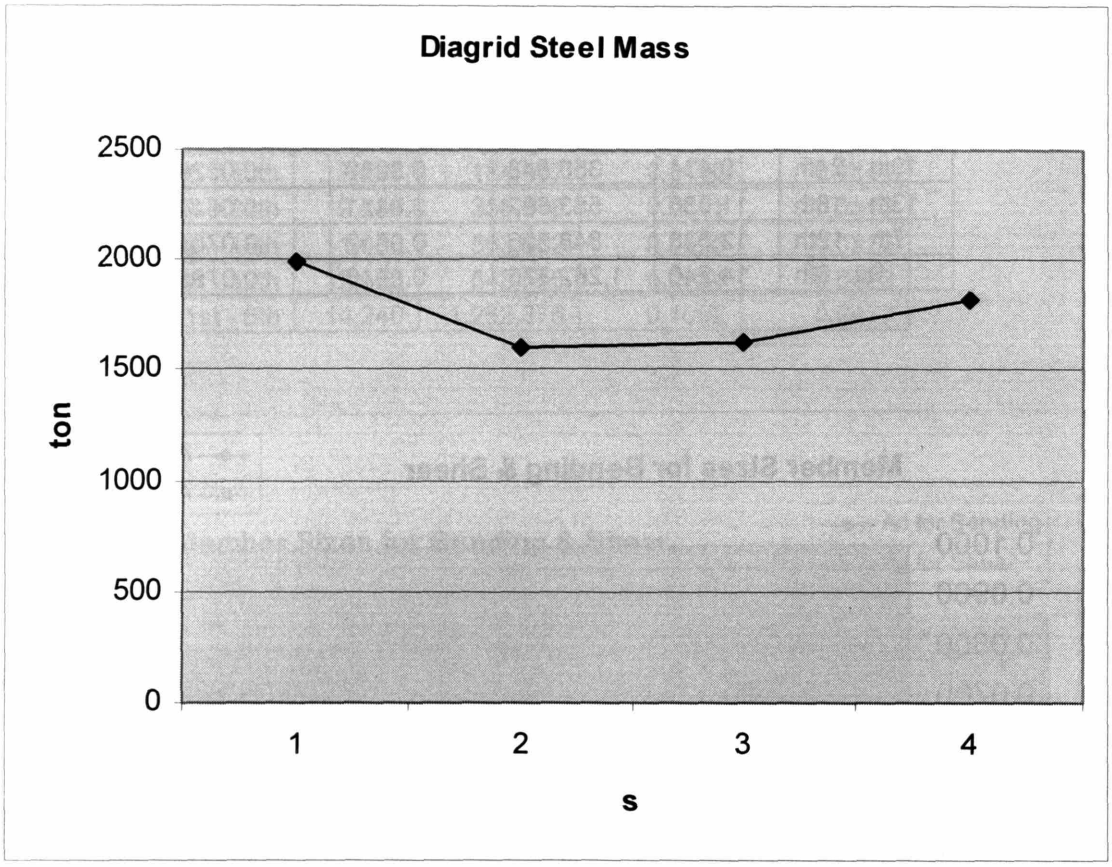

Appendix 6. LRFD Code Check for Diagrid Structures with Varying Displacement Constraints

6.1. 60-Story Diagrid Structures

Leeward surface diagrids began to fail the strength code requirement from u/H=1/250.

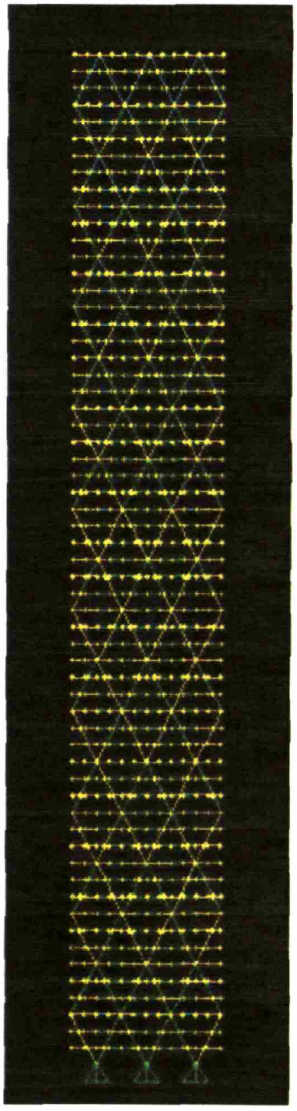

u/H = 1/300

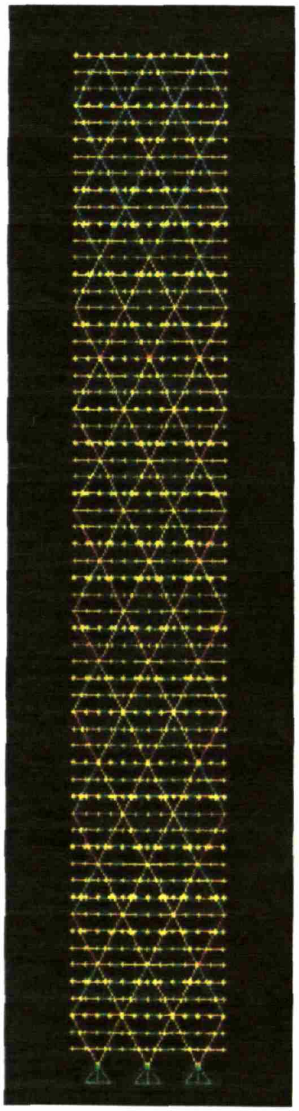

u/H = 1/250

6.2. 42-Story Diagrid Structures

Leeward surface diagrids began to fail the strength code requirement from u/H=1/400.

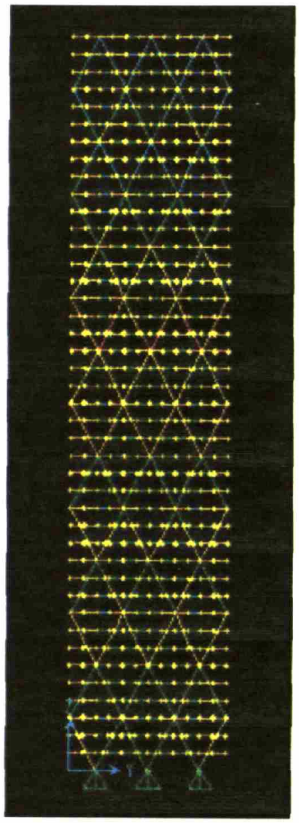

u/H = 1/450

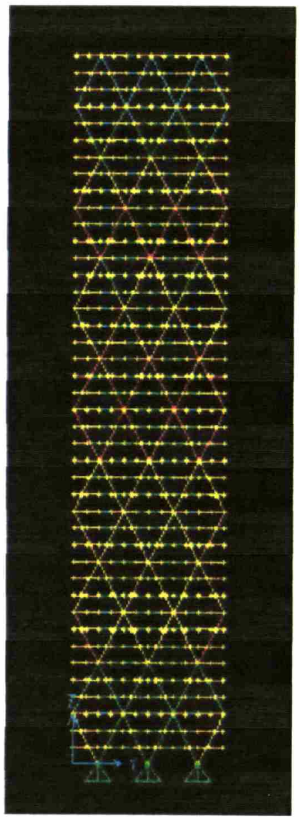

u/H = 1/400

Appendix 7. Structural Behavior of the 2DOF (Primary Structure + DSF Outer Skin) System: Optimization for all ρ (Forcing Frequency/Natural Building Frequency) Values

For this study, the primary mass damping coefficient C is considered to be 0 in order to investigate if damping applied only to the DSF can control the primary structure motion.

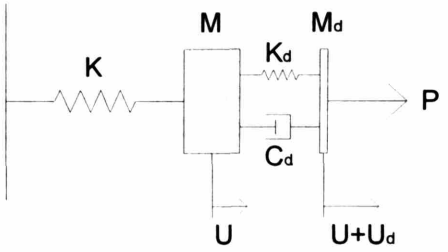

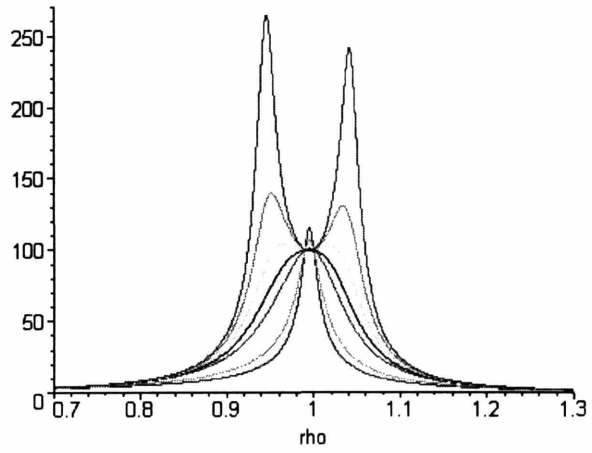

H plot, U = (P/K) H
Mass Ratio (Md/M) = 0.01
Façade Damping Ratio = 0.02, 0.04, 0.06, 0.08, 0.1, 0.2, 0.3

$$H := \frac{\sqrt{f^4 + 4 f^2 \xi^2 \rho^2}}{\sqrt{\left(\rho^2 f^2 + \rho^2 - f^2 + m \rho^2 f^2 - \rho^4\right)^2 + \left(2 \rho^3 \xi f - 2 f \xi \rho + 2 m \rho^3 \xi f\right)^2}}$$

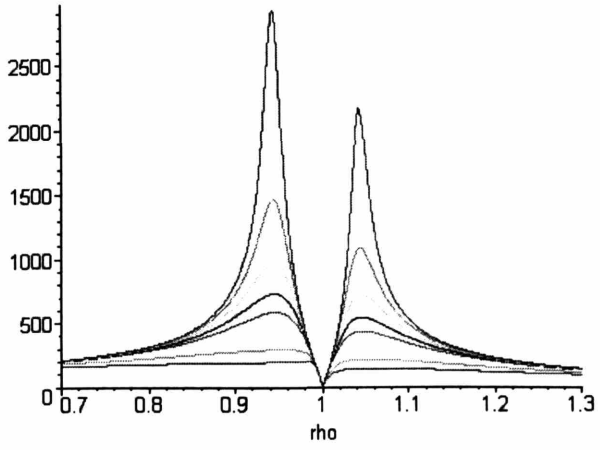

Hd Plot, Ud = (P/K) Hd
Mass Ratio (Md/M) = 0.01
Façade Damping Ratio = 0.02, 0.04, 0.06, 0.08, 0.1, 0.2, 0.3

$$Hd := \frac{\sqrt{\frac{\left(\rho^2 - 1\right)^2}{m^2}}}{\sqrt{\left(\rho^2 f^2 + \rho^2 - f^2 + m \rho^2 f^2 - \rho^4\right)^2 + \left(2 \rho^3 \xi f - 2 f \xi \rho + 2 m \rho^3 \xi f\right)^2}}$$

7.1. Primary Structure Behavior

Regardless of damping ratio, dynamic response amplification factors of the primary structure (H) always pass through two common points at two frequency ratios, $\rho 1 = [(1-m) / (1+m)] \wedge (1/2)$ and $\rho 2 = 1$. There is an optimum damping ratio at which H (max) becomes minimum. Before passing this optimum damping ratio, as the damping ratio increases, H (max) becomes lower. After passing this optimum damping ratio, as the damping ratio increases, H (max) becomes higher. However, this H (max) increase is not significant.

7.2. Secondary Structure (DSF Outer Skin) Behavior

Regardless of the damping ratio, dynamic response amplification factors (Hd) of the secondary structure are always 0 at $\rho = 1$. As the damping ratio becomes higher, Hd (max) of the secondary structure becomes lower. There is no optimum damping ratio after which Hd (max) becomes higher.

7.3. Entire System Behavior

There is no single optimum damping ratio that minimizes both H (max) and Hd (max), which is different from the situation in Tuned Mass Damper Systems.

At the optimum damping ratio for the primary structure, Hd (max) is much higher than H (max), which is not desirable because Hd represents the displacement of the DSF outer skin. As the damping ratio keeps increasing (passing through the optimum damping ratio for the primary structure), Hd (max) becomes lower and closer to H (max). Even though H (max) becomes higher after passing the optimum damping ratio for the primary structure, this H (max) increase is not significant. Thus, the final damping ratio can be determined by considering both H (max) and Hd (max). This process satisfies the displacement requirements of both the primary structure and the DSF outer skin.

7.4. Limitations

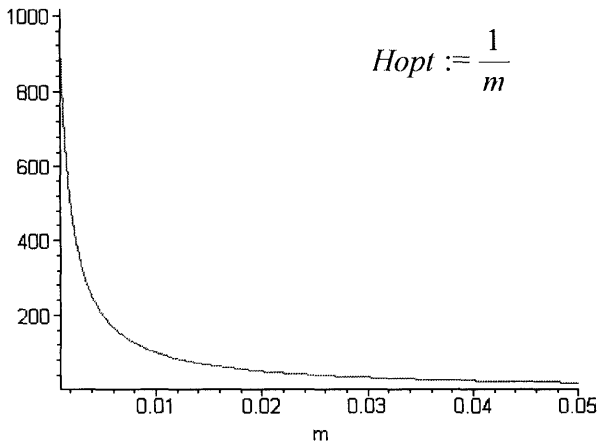

$$Hopt := \frac{1}{m}$$

As can be seen in the Hopt (optimized dynamic amplification factor of the primary mass) vs. m (mass ratio) plot, the movement of the primary mass is highly dependent upon the mass of the secondary mass: The heavier, the better. For example, if the mass ratio changes from 1/100 to 1/50, the displacement of the primary mass is reduced by 50%. However, there is a practical limitation to making the DSF outer skin heavier than what is required for other purposes.

More importantly, when primary structure damping is considered, it turns out that the secondary mass acts as a force amplifier instead of an energy dissipater in the region where ρ is close to 1. This phenomenon occurs because the optimized f (ω_d/ω, where ω_d is the natural frequency of Md, and ω is the natural frequency of M) value is very close to 1 as can be seen in the optimized f vs. m plot. In this case, if the forcing frequency is close to the primary mass frequency, it is also close to the secondary mass frequency. Thus, the transmissibility between the force and the primary structure – through the secondary structure – becomes bigger than 1, which is undesirable for the concept of this system. (Transmissibility can be seen from the H_3 plot blow.)

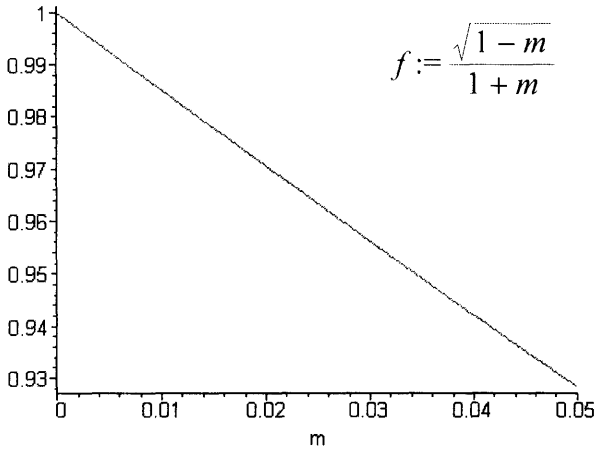

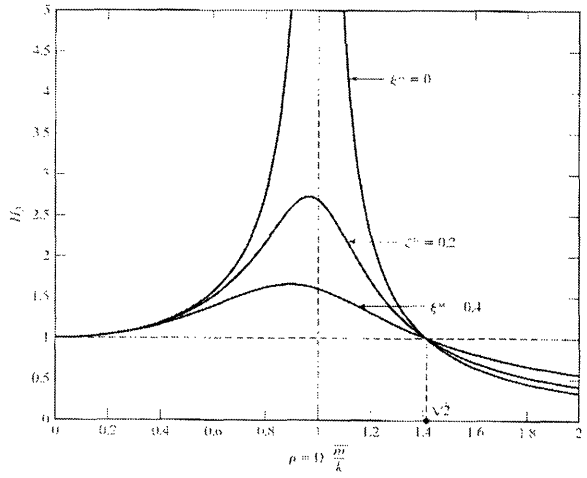

Transmissibility H_3 Plot
R = H_3P
R: Reaction
P: Applied Force

Appendix 8. Phase Angle between the Primary Structure and TMD

8.1. SDOF/TMD Analysis

An SDOF/TMD system is analyzed here in order to investigate phase shifts between the primary structure and TMD in various forcing frequency conditions.

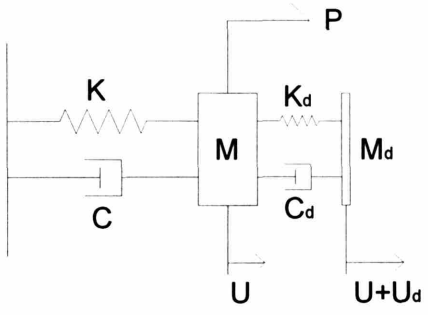

English/Greek Symbols

M: Mass
K: Stiffness
C: Viscous Damping Parameter
P: Applied Loading
U: Displacement
ϖ: Natural Frequency of Structure
Ω: Forcing Frequency
ρ: Forcing Frequency to Natural Frequency Ratio (Ω/ϖ)
f: TMD Frequency to Primary Structure Frequency Ratio (ϖd / ϖ)
ξ: Damping Ratio
ϕ: Mode Shape Vector

The governing equations for the system shown are

$$m\,\ddot{u} + c\,\dot{u} + k\,u - c_d\dot{u}_d - k_d u_d = p \qquad \text{(eq.1-1)}$$

$$m_d\ddot{u}_d + c_d\dot{u}_d + k_d u_d = -m_d\ddot{u}\ . \qquad \text{(eq.2-1)}$$

It is convenient to work with the solution expressed in terms of complex quantities. The force is expressed as

$$p = \hat{p}e^{i\Omega t}, \qquad \text{(eq.3)}$$

where $\hat{p}$ is real quantity. The response is taken as

$$u = \bar{u}e^{i\Omega t} \qquad \text{(eq.4)}$$

$$u_d = \bar{u}_d e^{i\Omega t}, \qquad \text{(eq.5)}$$

where the response amplitudes, $\bar{u}$ and $\bar{u}_d$, are considered to be complex quantities. Then the corresponding solution is given by either the real or imaginary part of u and u_d.

Considering the following notation

$$\omega^2 = k/m \qquad \text{(eq.8)}$$

$$c = 2\xi\omega m \qquad \text{(eq.9)}$$

$$\omega_d{}^2 = k_d / m_d \qquad \text{(eq.10)}$$

$$c_d = 2\xi_d \omega_d m_d \qquad \text{(eq.11)}$$

and defining $\overline{m}$ as the mass ratio,

$$\overline{m} = m_d / m, \qquad \text{(eq.12)}$$

the governing equations 1-1 and 2-1 become

$$(-m\Omega^2 + ic\Omega + k)\overline{u} - (i\Omega c_d + k_d)\overline{u}_d = \hat{p} \qquad \text{(eq.1-2)}$$

$$(-m\rho^2\omega^2 + i2\xi\omega^2 m\rho + \omega^2 m)\overline{u} - (i\omega\rho 2\xi_d\omega_d m_d + \omega_d{}^2 m_d)\overline{u}_d = \hat{p} \qquad \text{(eq.1-3)}$$

$$(-\rho^2 + i2\xi\rho + 1)\overline{u} - (i\rho 2\xi_d f\overline{m} + f^2\overline{m})\overline{u}_d = \hat{p}/k \qquad \text{(eq.1-4)}$$

$$(-m_d\Omega^2 + ic_d\Omega + k_d)\overline{u}_d - m_d\Omega^2\overline{u} = 0 \qquad \text{(eq.2-2)}$$

$$(-m_d\rho^2\omega^2 + i2\xi_d\varpi_d m_d\rho\omega + \omega_d{}^2 m_d)\overline{u}_d - m_d\rho^2\omega^2\overline{u} = 0 \qquad \text{(eq.2-3)}$$

$$(-\overline{m}\rho^2 + i2\xi_d f\overline{m}\rho + f^2\overline{m})\overline{u}_d - \overline{m}\rho^2\overline{u} = 0. \qquad \text{(eq.2-4)}$$

The solution due to periodic excitation is expressed as

$$\overline{u} = \frac{\hat{p}}{k} H \qquad \text{(eq.13)}$$

$$\overline{u}_d = \frac{\hat{p}}{k} H_d \qquad \text{(eq.14)}$$

$$H = \frac{\sqrt{[f^2 - \rho^2]^2 + [2\xi_d\rho f]^2}}{|D|} \qquad \text{(eq.15)}$$

$$H_d = \frac{\rho^2}{|D|} \qquad \text{(eq.16)}$$

$$|D| = \sqrt{[-f^2\rho^2\overline{m} + (1-\rho^2)(f^2-\rho^2) - 4\xi\xi_d f\rho^2]^2 + 4[\xi\rho(f^2-\rho^2) + \xi_d f\rho(1-\rho^2(1+\overline{m}))]^2} \ .$$

(eq.17)

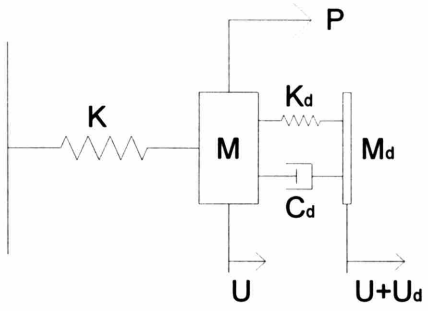

If structural damping for the primary structure is not considered, the equations reduce to

$$\overline{u} = \frac{\hat{p}}{k} H_1 \qquad \text{(eq.18)}$$

$$\overline{u}_d = \frac{\hat{p}}{k} H_{d1} \qquad \text{(eq.19)}$$

$$H_1 = \frac{\sqrt{[f^2-\rho^2]^2 + [2\xi_d\rho f]^2}}{|D_1|} \qquad \text{(eq.20)}$$

$$H_{d1} = \frac{\rho^2}{|D_1|} \qquad \text{(eq.21)}$$

$$|D_1| = \sqrt{[-f^2\rho^2\overline{m} + (1-\rho^2)(f^2-\rho^2)]^2 + 4[\xi_d f\rho(1-\rho^2(1+\overline{m}))]^2} \ . \qquad \text{(eq.22)}$$

For the condition when primary structure damping is not considered, the phase angle α between the primary structure and the TMD is expressed as

$$\tan\alpha = \frac{2\xi_d\rho f}{f^2-\rho^2} \ . \qquad \text{(eq.23)}$$

α can be rewritten as in degrees

$$\alpha = \frac{\arctan\left(\frac{2\xi_d \rho f}{f^2 - \rho^2}\right)}{\pi}(180) = 57.29582790 \arctan\left(\frac{2\xi_d \rho f}{f^2 - \rho^2}\right).$$

Considering

$$\xi_d|_{opt} = \sqrt{\frac{\overline{m}(3 - \sqrt{0.5\overline{m}})}{8(1+\overline{m})(1-0.5\overline{m})}} \qquad \text{(eq.24)}$$

$$f_{opt} = \frac{\sqrt{1 - 0.5\overline{m}}}{1+\overline{m}} \qquad \text{(eq.25)}$$

α can be plotted for $\overline{m} = 0.005$.

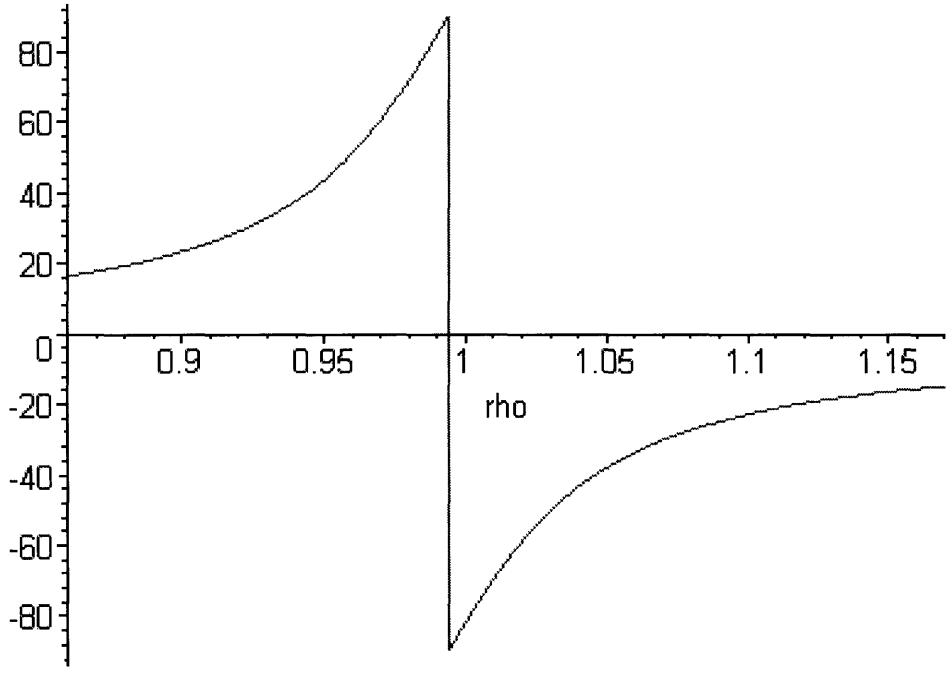

(Graph. 1)

ρ: Forcing Frequency to Natural Frequency Ratio (Ω/ϖ)

8.2. Phase Angle between Primary Structure and TMD (MotionLab Simulation)

The phase angle between the primary structure and TMD is investigated using MotionLab simulations. For the condition when primary structure damping is not considered and $\overline{m} = 0.005$, the system is studied 40 times using 0.05 second intervals between forcing frequencies around the resonance zone. The results are tabulated below.

No	Tn(sec.)	Tf(sec.)	rho	alpha(degree)	Notes
1	6.28	7.33	0.857	10	
2	6.28	7.28	0.863	10	
3	6.28	7.23	0.869	10	
4	6.28	7.18	0.875	10	
5	6.28	7.13	0.881	11	
6	6.28	7.08	0.887	13	
7	6.28	7.03	0.893	15	
8	6.28	6.98	0.900	17	
9	6.28	6.93	0.906	19	
10	6.28	6.88	0.913	21	
11	6.28	6.83	0.919	24	
12	6.28	6.78	0.926	27	
13	6.28	6.73	0.933	30	
14	6.28	6.68	0.940	34	
15	6.28	6.63	0.947	39	
16	6.28	6.58	0.954	45	
17	6.28	6.53	0.962	52	
18	6.28	6.48	0.969	60	
19	6.28	6.43	0.977	70	Forcing: First Mode Frequency
20	6.28	6.38	0.984	80	
21	6.28	6.33	0.992	90	
22	6.28	6.28	1.000	100	
23	6.28	6.23	1.008	110	
24	6.28	6.18	1.016	120	
25	6.28	6.13	1.024	128	Forcing: Second Mode Frequency
26	6.28	6.08	1.033	135	
27	6.28	6.03	1.041	141	
28	6.28	5.98	1.050	146	
29	6.28	5.93	1.059	150	
30	6.28	5.88	1.068	153	
31	6.28	5.83	1.077	156	
32	6.28	5.78	1.087	158	
33	6.28	5.73	1.096	160	
34	6.28	5.68	1.106	162	
35	6.28	5.63	1.115	164	
36	6.28	5.58	1.125	166	
37	6.28	5.53	1.136	168	
38	6.28	5.48	1.146	170	
39	6.28	5.43	1.157	170	
40	6.28	5.38	1.167	170	

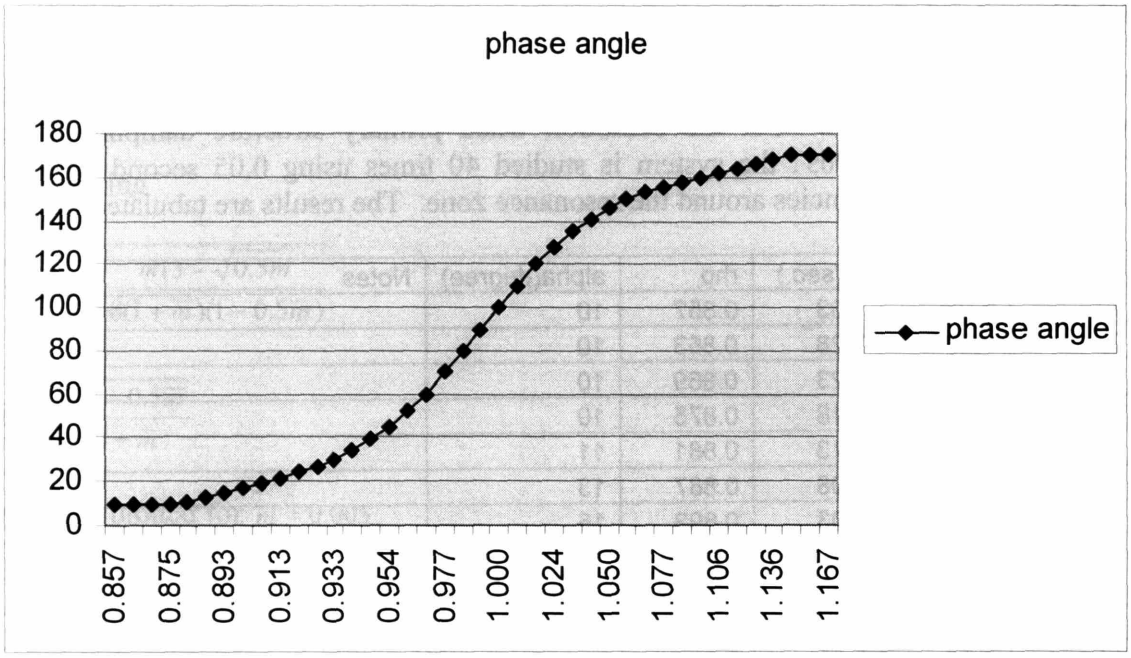

(Graph. 2)

Graph 2 plots 40 MotionLab simulation results regarding the phase angle between the primary structure and TMD. Actual MotionLab simulation results are shown in the Appendix 8.2.1.

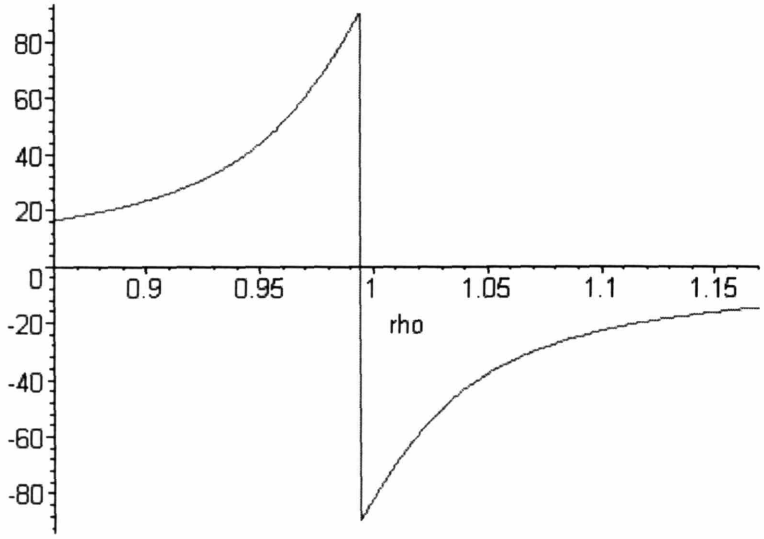

In order to make a clear comparison between the theoretical results and the MotionLab results, Graph 1 is shown here again. Should the theoretical results be true, Graphs 1 and 2 should be identical. At a glance, the two graphs do not look identical. However, considering the fact that Graph 1 is generated using the tangent function, Graphs 1 and 2 agree with each other.

8.2.1. SDOF/TMD Simulation Results

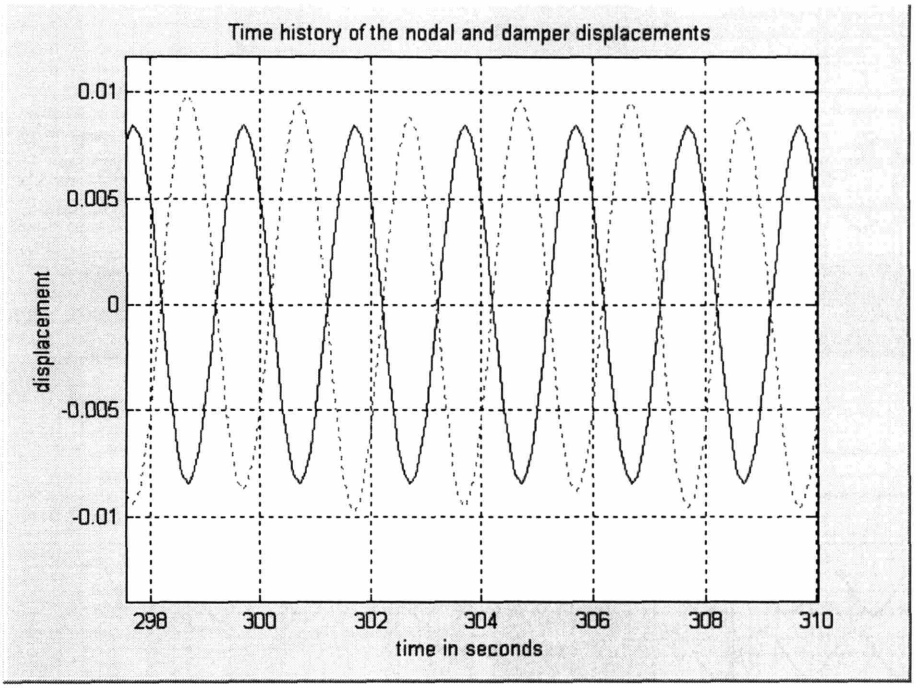

Tf = 2 (almost 180 degree out of phase)

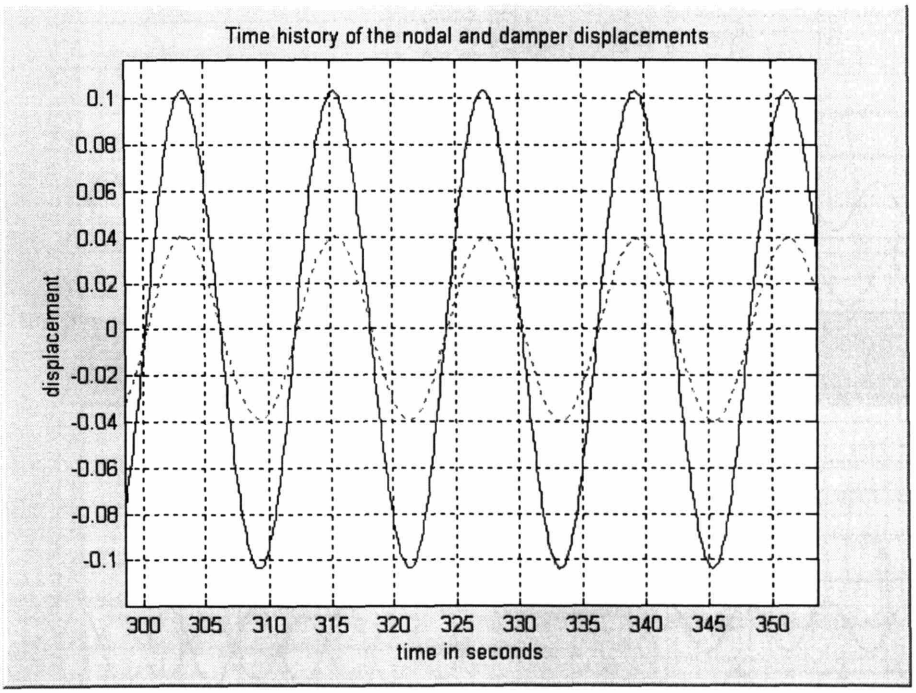

Tf = 12 (almost in phase)

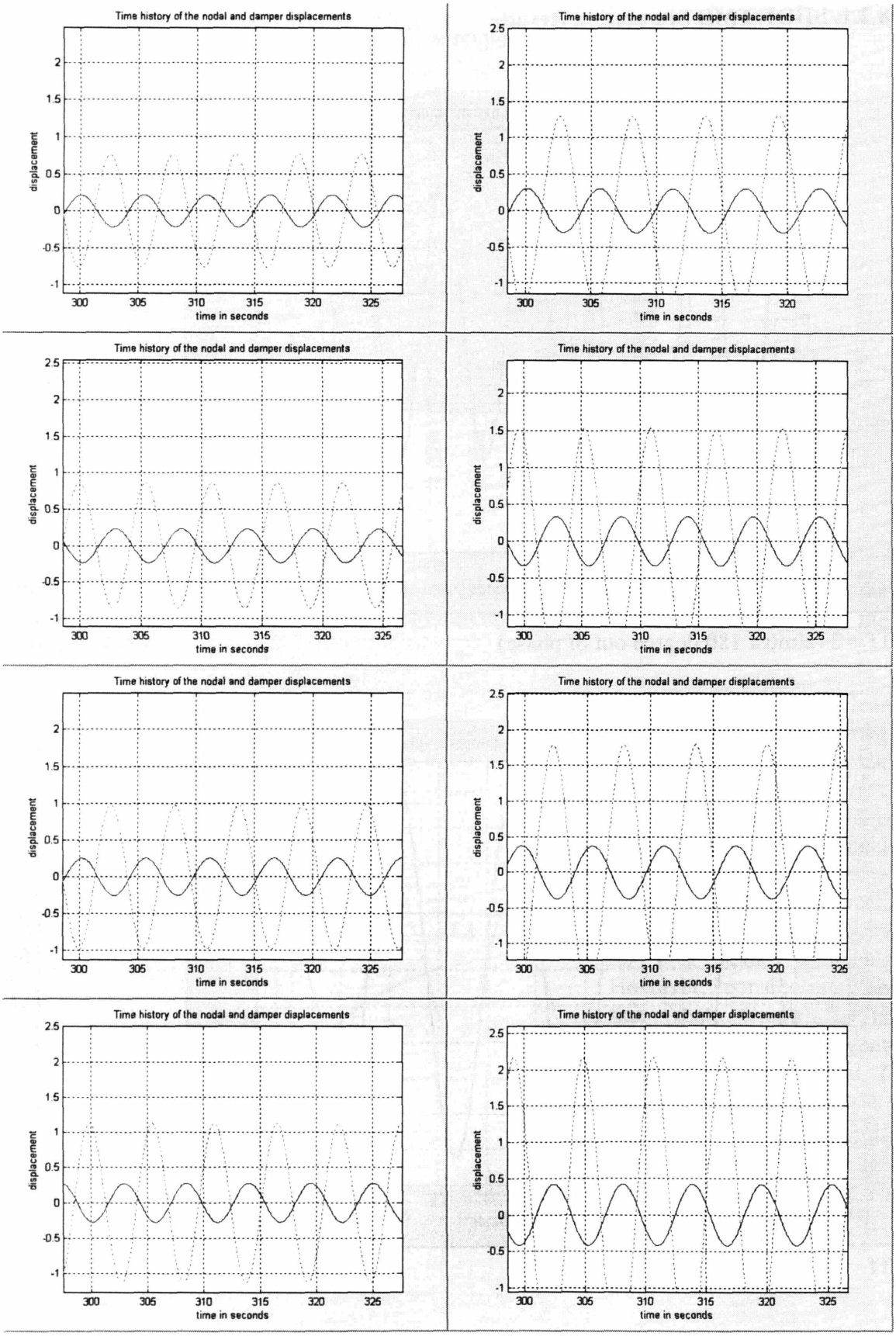

Tf = 5.38 / 5.43 / 5.48 / 5.53

Tf = 5.58 / 5.63 / 5.68 / 5.73

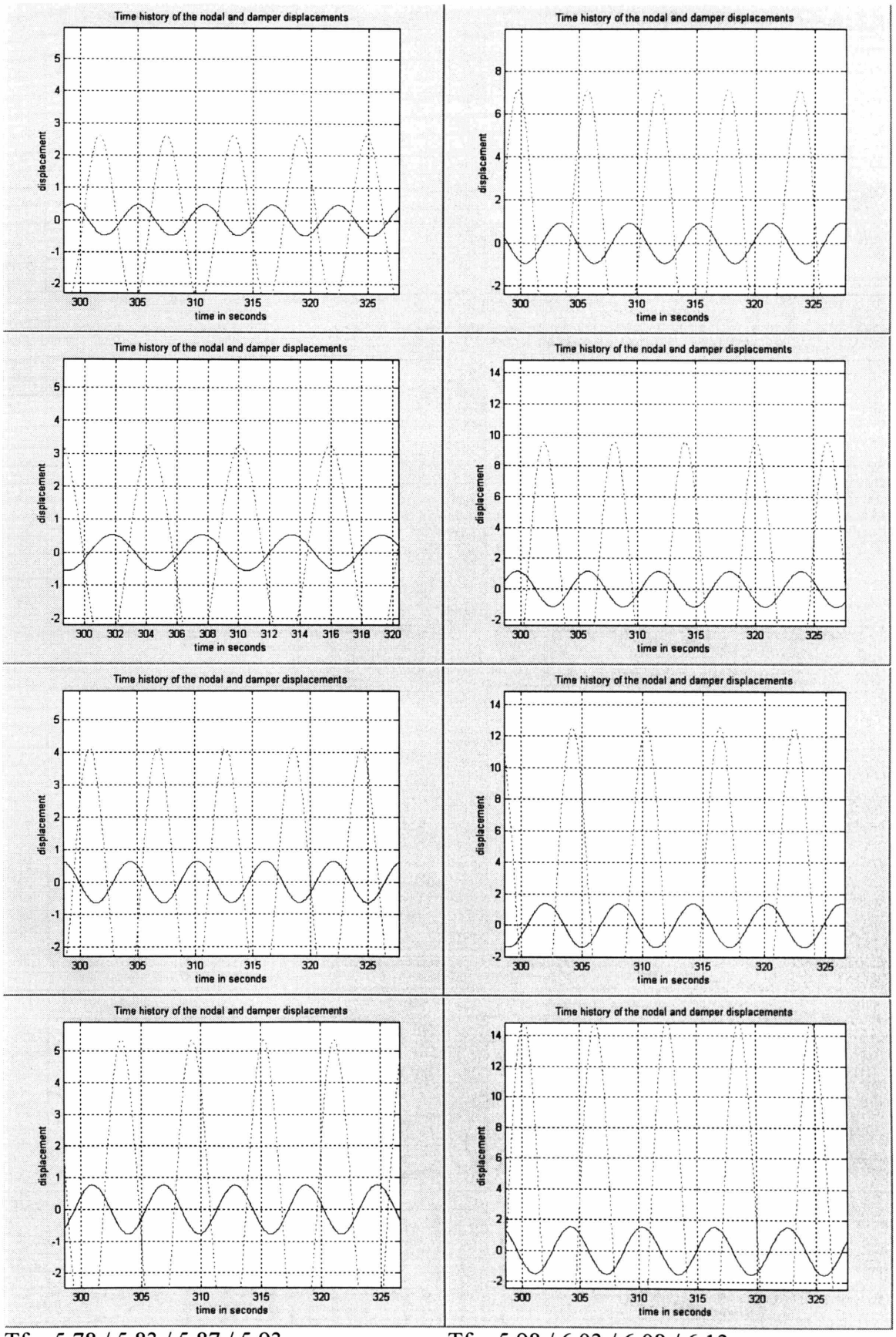

Tf = 5.78 / 5.83 / 5.87 / 5.93

Tf = 5.98 / 6.03 / 6.08 / 6.13

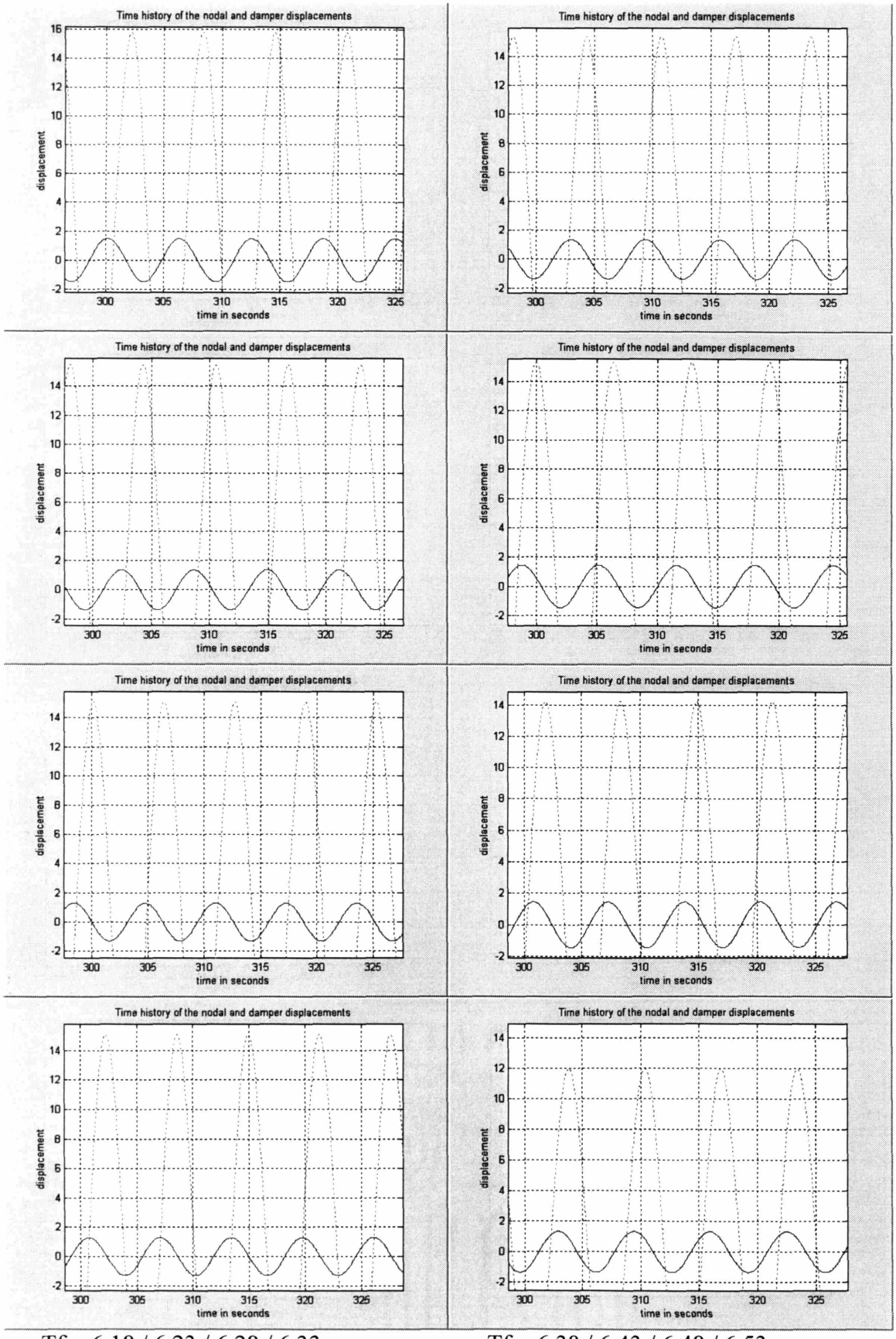

Tf = 6.18 / 6.23 / 6.28 / 6.33

Tf = 6.38 / 6.43 / 6.48 / 6.53

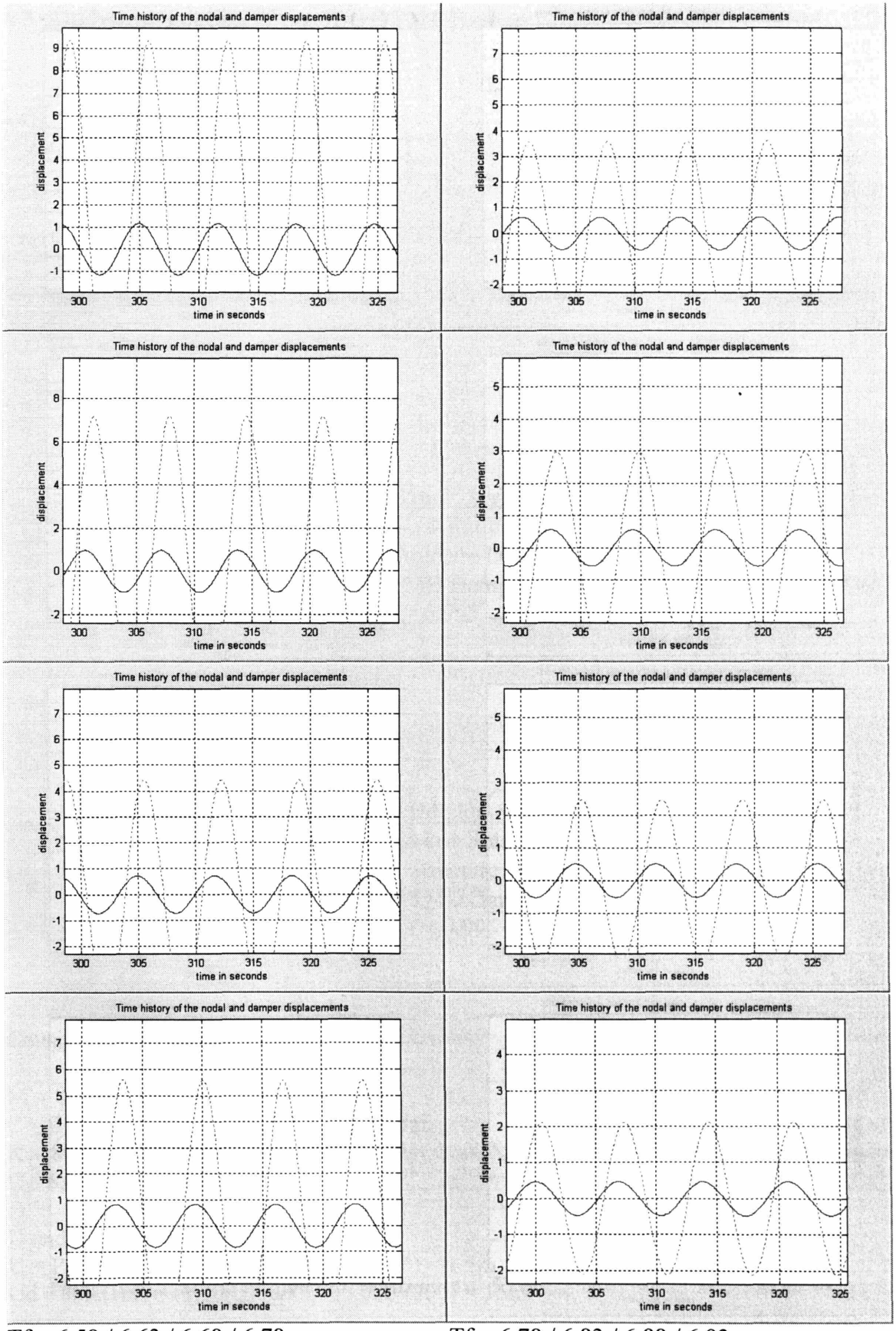

Tf = 6.58 / 6.63 / 6.68 / 6.78

Tf = 6.78 / 6.83 / 6.88 / 6.93

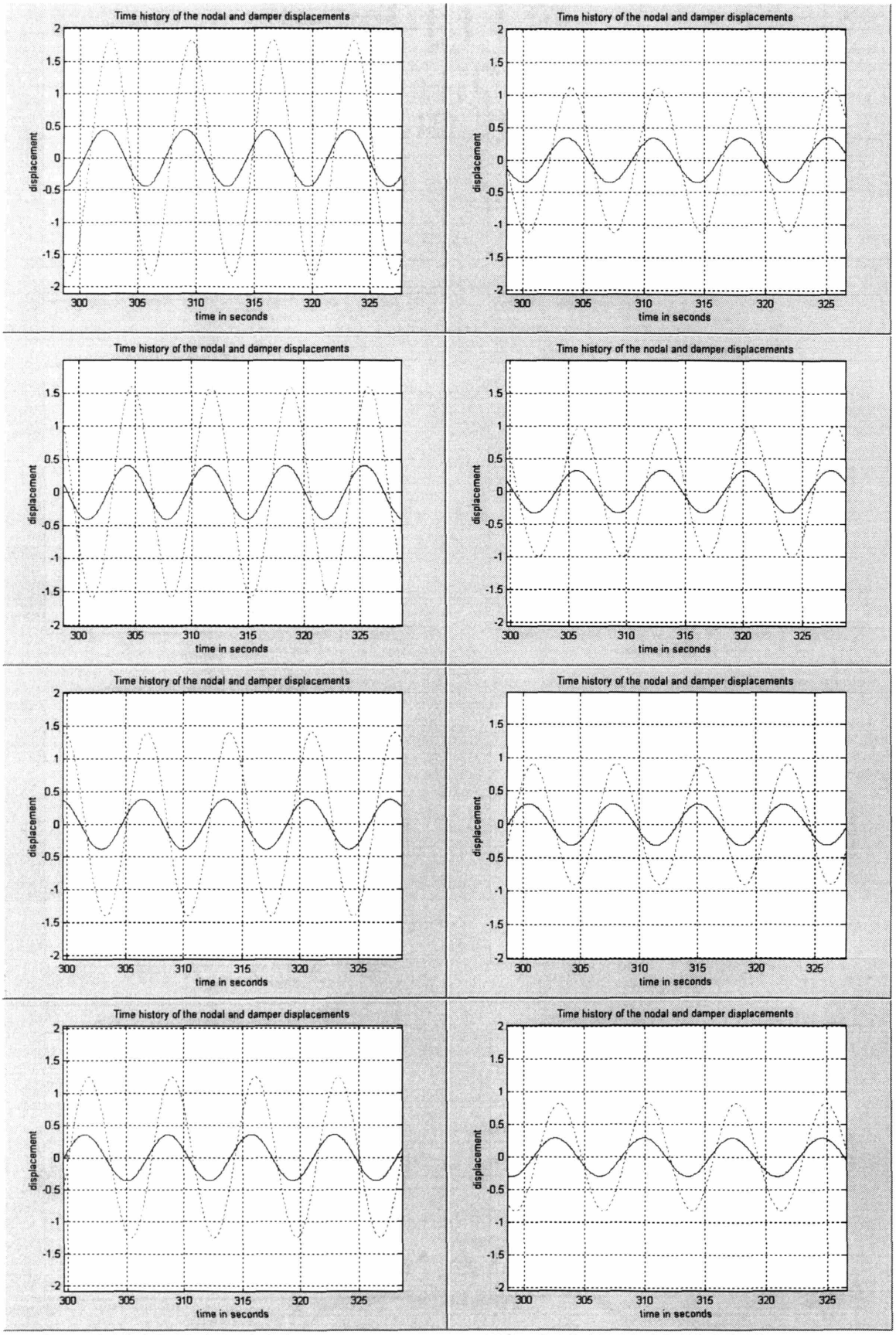

Tf = 6.98 / 7.03 / 7.08 / 7.13

Tf = 7.18 / 7.23 / 7.28 / 7.33

8.3. Analytical Solution of the SDOF/TMD System

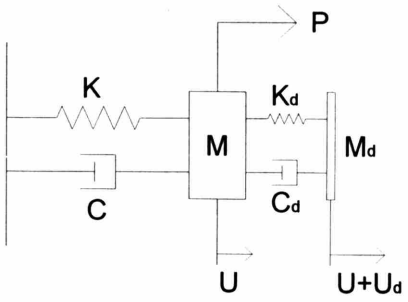

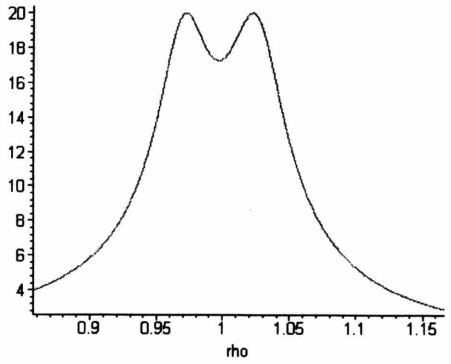

H plot , U= (P/K) H
Mass Ratio (M_d/M) = 0.005
Structure Damping Ratio ξ = 0
TMD Damping Ratio ξ_d = 0.043
f = 0.995

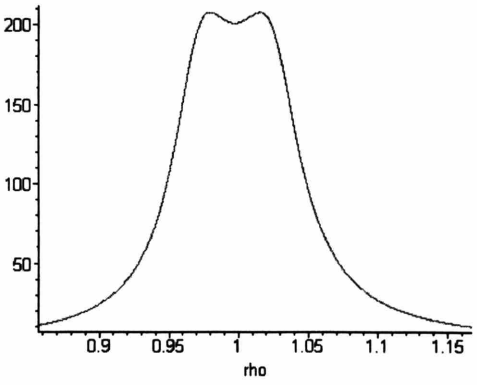

Hd plot , Ud = (P/K) Hd
Mass Ratio (M_d/M) = 0.005
Structure Damping Ratio ξ = 0
TMD Damping Ratio ξ_d = 0.043
f = 0.995

Considering the values below,

M = 80,000,000 kg Md= 400,000 k
C = 0 N-s/m Cd = 34,095 N-s/m
K = 80,000,000 N/m Kd = 395,040 N/m
P = 6,000,000 sin(wt) N,

U and Ud follow:
U = P/K(H) = (6,000,000/80,000,000)(20) = 1.5m
Ud = P/K(Hd) = (6,000,000/80,000,000)(200) = 15m.

8.4. Phase Angle vs. Mode Shapes

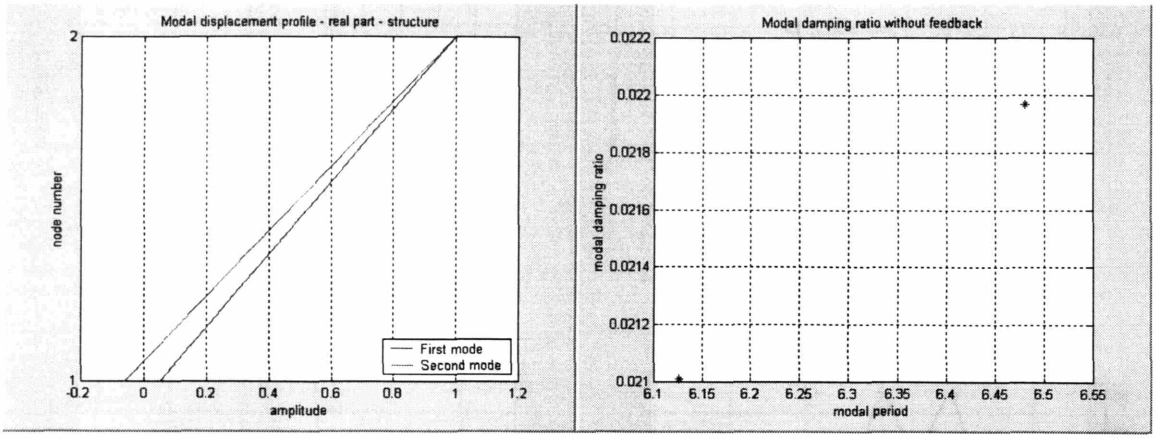

The two MotionLab result graphs above show two mode shapes, first and second modal period and the modal damping ratio of the SDOF/TMD system. In the mode shape graph, node number 1 represents the primary structure and node number 2 represents TMD. As can be seen from the graph, the primary structure and TMD are in phase in the first mode, while they are out of phase in the second mode.

Considering sinusoidal periodic loading applied to the first node of the system, when forcing frequency is 6.48 seconds (first mode period of the structure), the first mode response governs the overall response of the system. On the contrary, when forcing frequency is 6.13 seconds (second mode period of the structure), the second mode response governs the overall response of the system.

Considering the first mode shape, it can be speculated that the primary structure and TMD motions become in phase when the first mode response governs. Likewise, it can also be speculated that the primary structure and TMD motions become out of phase by around 180 degrees when the second mode response governs. However, as was observed from Graphs 1 and 2, phase angles are close to 90 degrees in both cases.

As can be seen from the Appendix 8.2.1, zero degrees in phase and 180 degrees out of phase occur in extreme forcing periods. A zero degree phase angle occurs when the ρ (Forcing Frequency to Natural Frequency Ratio (Ω/ϖ)) value is close to zero, while the 180 degree phase angle occurs when the ρ value is close to around 2 (infinity more exactly speaking).

8.5. Phase Angles for Vertically Distributed TMD Systems

2DOF System with Multiple Distributed TMDs at both the first and the second Nodes – Tuned by Iteration

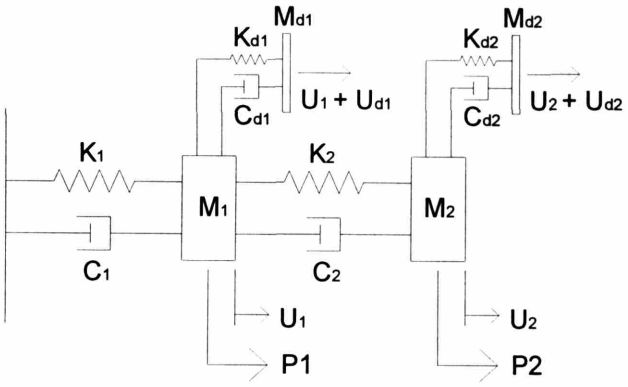

M1 = M2 = 40,000,000 kg
Md1 = Md2 = 250,000 kg
C1 = C2 = 2,000,000 N-s/m (ξ = 0.01)
Cd1 = 35,000 (ξ_d = 0.070)
Cd2 = 35,000 (ξ_d = 0.071)
K1 = 120,000,000 N/m
K2 = 80,000,000 N/m
Kd1 = 249,000 N/m (f_1 = 0.998)
Kd2 = 245,000 N/m (f_2 = 0.990)
P1 = 0
P2= 4,500,000 sin(wt) N

Since optimal parameters for vertically distributed TMDs cannot be analytically obtained, the parameters used above are based on trial and error. Three different forcing frequencies were used for the simulation: forcing frequency = first mode frequency; forcing frequency = second mode frequency; and forcing frequency = third mode frequency. The system was tuned until peak displacements of the primary structure became the same in all three forcing frequency conditions. Because tuning was done only by trial and error, it is hard to say that what is shown here is the absolutely optimized condition for the system. Better tuning parameters, which reduce even more the dynamic response of the primary structure, may exist.

As can be seen from the plots of the time history of the nodal and damper displacements, phase angles between the primary structure nodes and TMDs are around 90 degrees in all three forcing conditions.

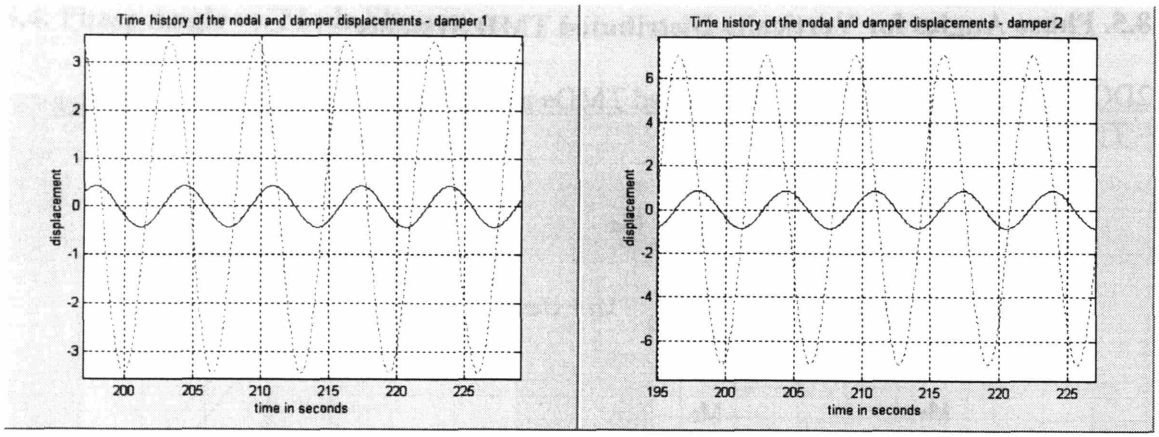

Forcing Frequency = First Mode Frequency

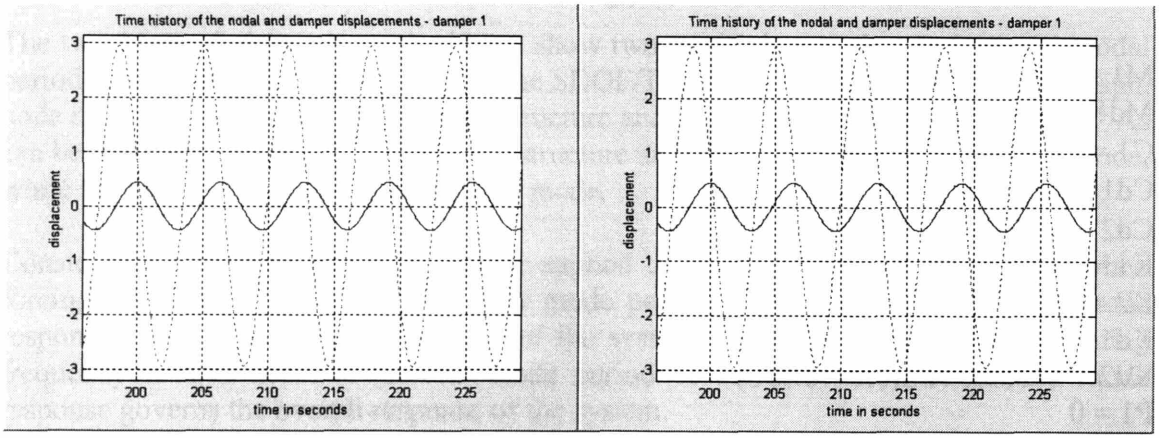

Forcing Frequency = Second Mode Frequency

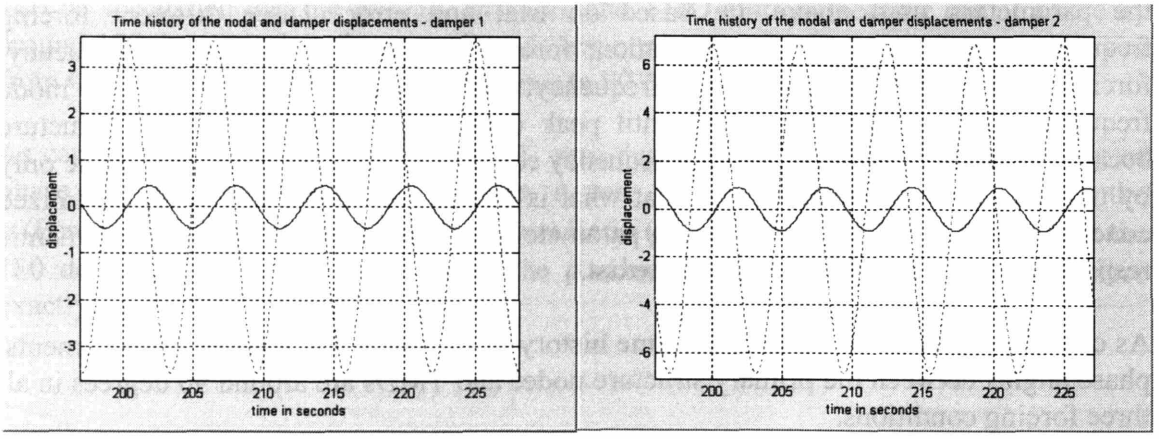

Forcing frequency = Third Mode Frequency

8.6. Phase Angle Study Conclusion

In an optimized SDOF/TMD system, the phase angle between the primary structure and the TMD changes as the forcing period changes. When the ρ (Forcing Frequency to Natural Frequency Ratio (Ω/ϖ)) value is close to zero the phase angle becomes close to zero, while when the ρ value is close to 2 (infinity, more exactly speaking), 180 degrees out of phase occurs. Around resonance condition (ρ value is close to 1, around peak points region in both H and Hd plots), which is the primary concern of the TMD design, the phase angle between the primary structure and TMD is around 90 degrees.

In a 2DOF/2TMD system, phase angles between the primary structure nodes and TMDs around resonance condition are still around 90 degrees. However, since optimal parameters for vertically distributed TMDs cannot be analytically obtained, they are based on trial and error. For this reason, what is shown here might not be the optimized condition for the system. Better tuning parameters, which reduce even more the dynamic response of the primary structure, may exist.

Appendix 9. 2 DOF + 2 TMD H, H_{d1} & H_{d2} for the Approximate Solution

$$eq1 := (-m2\,\rho^2 + 2\,i\,\xi2\,f2\,m2\,\rho + f2^2\,m2)\,Ud2 - m2\,\rho^2\,U = 0$$

$$eq2 := (-m1\,\rho^2 + 2\,i\,\xi1\,f1\,m1\,\rho + f1^2\,m1)\,Ud1 - \alpha\,m1\,\rho^2\,U = 0$$

$$eq3 := -\alpha\,(2\,i\,\xi1\,f1\,m1\,\rho + f1^2\,m1)\,Ud1 - (2\,i\,\xi2\,f2\,m2\,\rho + f2^2\,m2)\,Ud2 + (-\rho^2 + 2\,i\,C\,\rho + 1)\,U = \frac{P}{K}$$

English/Greek Symbols

m: Mass Ratio
K: Primary Structure Stiffness
C: Primary Structure Damping Ratio
P: Applied Loading
U: Primary Structure Displacement
Ud: TMD Displacement
ρ: Forcing Frequency to Natural Frequency Ratio (Ω/ϖ)
f: TMD Frequency to Primary Structure Frequency Ratio (ϖd / ϖ)
ξ: TMD Damping Ratio

$$\begin{aligned} H := {} & ((\rho^4 - \rho^2 f1^2 - 4\,\xi1\,\xi2\,f1\,f2\,\rho^2 - f2^2\,\rho^2 + f1^2 f2^2)^2 \\ & + (-2\,\xi1\,f1\,\rho^3 - 2\,\xi2\,f2\,\rho^3 + 2\,\xi2\,f1^2 f2\,\rho + 2\,\xi1\,f1\,f2^2\,\rho)^2)^{(1/2)} \Big/ ((-\rho^2 f1^2 \\ & + f1^2\,\rho^4 - f1^2\,\rho^2 f2^2 + \rho^4 f2^2\,m2 - \rho^6 + f1^2 f2^2 + \rho^4 f2^2 - f2^2\,\rho^2 \\ & + 4\,\rho^4\,\alpha^2 f1\,m1\,\xi1\,\xi2\,f2 + \rho^4\,\alpha^2 f1^2\,m1 - \rho^2\,\alpha\,f1^2\,m1\,f2^2 + 4\,\xi1\,f1\,\rho^4\,C \\ & - 4\,\xi1\,f1\,\rho^2\,C\,f2^2 - 4\,\xi1\,\xi2\,f1\,f2\,\rho^2 - f1^2\,\rho^2 f2^2\,m2 - 4\,f1^2\,C\,\rho^2\,\xi2\,f2 \\ & + 4\,\rho^4\,C\,\xi2\,f2 + 4\,\xi1\,f1\,\rho^4 f2\,m2\,\xi2 + 4\,\xi1\,f1\,\rho^4\,\xi2\,f2 + \rho^4)^2 + (2\,\rho^5\,C + 2\,\rho^5 f1\,\xi1 \\ & - 2\,\xi1\,f1\,\rho^3 + 2\,\rho^5\,\alpha^2 f1\,m1\,\xi1 - 2\,\rho^3\,\alpha^2 f1\,m1\,\xi1\,f2^2 - 2\,\rho^3\,\alpha^2 f1^2\,m1\,\xi2\,f2 \\ & + 2\,\rho^5\,\xi2\,f2 - 2\,\xi1\,f1\,\rho^3 f2^2 - 8\,\xi1\,f1\,\rho^3\,C\,\xi2\,f2 - 2\,f1^2\,\rho^3 f2\,m2\,\xi2 + 2\,f1^2\,C\,\rho\,f2^2 \\ & + 2\,\xi2\,f1^2 f2\,\rho - 2\,f1^2\,\rho^3\,\xi2\,f2 - 2\,f1^2\,C\,\rho^3 + 2\,\rho^5 f2\,m2\,\xi2 - 2\,\rho^3\,C\,f2^2 \\ & - 2\,\xi1\,f1\,\rho^3 f2^2\,m2 + 2\,\xi1\,f1\,f2^2\,\rho - 2\,\xi2\,f2\,\rho^3)^2)^{(1/2)} \end{aligned}$$

$$Hd1 := \sqrt{(\alpha\,\rho^4 - \alpha\,f2^2\,\rho^2)^2 + 4\,\alpha^2\,\xi2^2\,f2^2\,\rho^6} \;/\; ((-f1^2\,\rho^2 + f1^2\,\rho^4 - f1^2\,\rho^2\,f2^2$$
$$+ \rho^4\,f2^2\,m2 - \rho^6 + f1^2\,f2^2 + \rho^4\,f2^2 - \rho^2\,f2^2 + 4\,\rho^4\,\alpha^2\,f1\,m1\,\xi1\,\xi2\,f2 + \rho^4\,\alpha^2\,f1^2\,m1$$
$$- \rho^2\,\alpha\,f1^2\,m1\,f2^2 + 4\,\xi1\,f1\,\rho^4\,C - 4\,\xi1\,f1\,\rho^2\,C\,f2^2 - 4\,\xi1\,f1\,\rho^2\,\xi2\,f2$$
$$- f1^2\,\rho^2\,f2^2\,m2 - 4\,f1^2\,C\,\rho^2\,\xi2\,f2 + 4\,\rho^4\,C\,\xi2\,f2 + 4\,\xi1\,f1\,\rho^4\,f2\,m2\,\xi2$$
$$+ 4\,\xi1\,f1\,\rho^4\,\xi2\,f2 + \rho^4)^2 + (2\,\rho^5\,C + 2\,\rho^5\,f1\,\xi1 - 2\,\xi1\,f1\,\rho^3 + 2\,\rho^5\,\alpha^2\,f1\,m1\,\xi1$$
$$- 2\,\rho^3\,\alpha^2\,f1\,m1\,\xi1\,f2^2 - 2\,\rho^3\,\alpha^2\,f1^2\,m1\,\xi2\,f2 + 2\,\rho^5\,\xi2\,f2 - 2\,\xi1\,f1\,\rho^3\,f2^2$$
$$- 8\,\xi1\,f1\,\rho^3\,C\,\xi2\,f2 - 2\,f1^2\,\rho^3\,f2\,m2\,\xi2 + 2\,f1^2\,C\,\rho\,f2^2 + 2\,f1^2\,\xi2\,f2\,\rho$$
$$- 2\,f1^2\,\rho^3\,\xi2\,f2 - 2\,f1^2\,C\,\rho^3 + 2\,\rho^5\,f2\,m2\,\xi2 - 2\,\rho^3\,C\,f2^2 - 2\,\xi1\,f1\,\rho^3\,f2^2\,m2$$
$$+ 2\,\xi1\,f1\,\rho\,f2^2 - 2\,\rho^3\,\xi2\,f2)^2)^{(1/2)}$$

$$Hd2 := \sqrt{(\rho^4 - f1^2\,\rho^2)^2 + 4\,\xi1^2\,f1^2\,\rho^6} \;/\; ((-f1^2\,\rho^2 + f1^2\,\rho^4 - f1^2\,\rho^2\,f2^2 + \rho^4\,f2^2\,m2$$
$$- \rho^6 + f1^2\,f2^2 + \rho^4\,f2^2 - \rho^2\,f2^2 + 4\,\rho^4\,\alpha^2\,f1\,m1\,\xi1\,\xi2\,f2 + \rho^4\,\alpha^2\,f1^2\,m1$$
$$- \rho^2\,\alpha\,f1^2\,m1\,f2^2 + 4\,\xi1\,f1\,\rho^4\,C - 4\,\xi1\,f1\,\rho^2\,C\,f2^2 - 4\,\xi1\,f1\,\rho^2\,\xi2\,f2$$
$$- f1^2\,\rho^2\,f2^2\,m2 - 4\,f1^2\,C\,\rho^2\,\xi2\,f2 + 4\,\rho^4\,C\,\xi2\,f2 + 4\,\xi1\,f1\,\rho^4\,f2\,m2\,\xi2$$
$$+ 4\,\xi1\,f1\,\rho^4\,\xi2\,f2 + \rho^4)^2 + (2\,\rho^5\,C + 2\,\rho^5\,f1\,\xi1 - 2\,\xi1\,f1\,\rho^3 + 2\,\rho^5\,\alpha^2\,f1\,m1\,\xi1$$
$$- 2\,\rho^3\,\alpha^2\,f1\,m1\,\xi1\,f2^2 - 2\,\rho^3\,\alpha^2\,f1^2\,m1\,\xi2\,f2 + 2\,\rho^5\,\xi2\,f2 - 2\,\xi1\,f1\,\rho^3\,f2^2$$
$$- 8\,\xi1\,f1\,\rho^3\,C\,\xi2\,f2 - 2\,f1^2\,\rho^3\,f2\,m2\,\xi2 + 2\,f1^2\,C\,\rho\,f2^2 + 2\,f1^2\,\xi2\,f2\,\rho$$
$$- 2\,f1^2\,\rho^3\,\xi2\,f2 - 2\,f1^2\,C\,\rho^3 + 2\,\rho^5\,f2\,m2\,\xi2 - 2\,\rho^3\,C\,f2^2 - 2\,\xi1\,f1\,\rho^3\,f2^2\,m2$$
$$+ 2\,\xi1\,f1\,\rho\,f2^2 - 2\,\rho^3\,\xi2\,f2)^2)^{(1/2)}$$

Appendix 10. Tuning TMDs regarding Acceleration for Structures in Section7.2.2

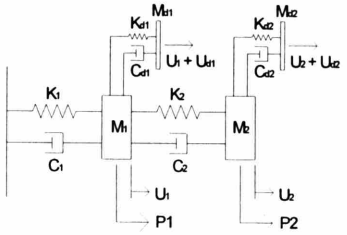

First & Second Mode Resonance Zone
Dynamic Amplification Factor
- TMD's are Tuned to the First Mode
- Optimized for Entire 2DOF/2TMD System by Trial & Error for Acceleration

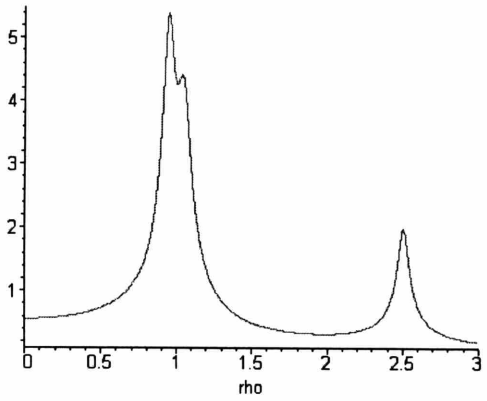

H_1 plot , $U_1 = (P/K)\, H_1$
$\phi 11 = 0.5$, $\phi 12 = 1.0$
$\phi 21 = 1.0$, $\phi 22 = -0.5$
$\omega 1 = 1$
$\omega 2 = 2.5$
Mass Ratio M1 = 0.015
Mass Ratio M2 = 0.015
Struc. Damping Ratio $\xi_1 = 0.005$, $\xi_2 = 0.0132$
f1 = 0.995, f2 = 990
TMD Damping Ratio $\xi_{d1} = 0.065$, $\xi_{d2} = 0.095$

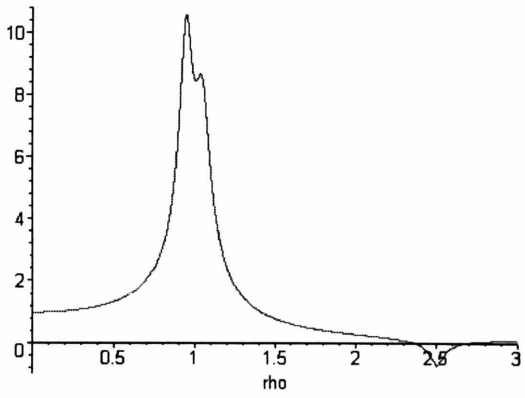

H_2 plot , $U_2 = (P/K)\, H_2$
$\phi 11 = 0.5$, $\phi 12 = 1.0$
$\phi 21 = 1.0$, $\phi 22 = -0.5$
$\omega 1 = 1$
$\omega 2 = 2.5$
Mass Ratio M1 = 0.015
Mass Ratio M2 = 0.015
Struc. Damping Ratio $\xi_1 = 0.005$, $\xi_2 = 0.0132$
f1 = 0.995, f2 = 990
TMD Damping Ratio $\xi_{d1} = 0.065$, $\xi_{d2} = 0.095$

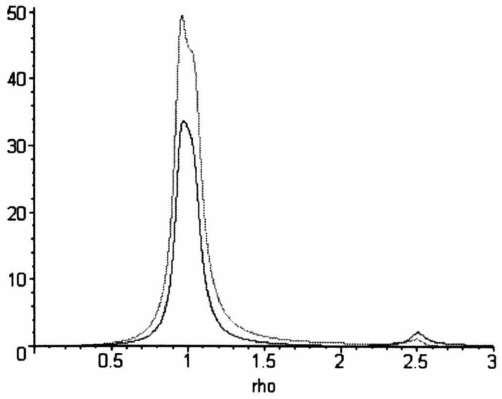

H_{d1}, H_{d2} plot , $U_{d1} = (P/K)\, H_{d1}$, $U_{d2} = (P/K)\, H_{d2}$
$\phi 11 = 0.5$, $\phi 12 = 1.0$
$\phi 21 = 1.0$, $\phi 22 = -0.5$
$\omega 1 = 1$
$\omega 2 = 2.5$
Mass Ratio M1 = 0.015
Mass Ratio M2 = 0.015
Struc. Damping Ratio $\xi_1 = 0.005$, $\xi_2 = 0.0132$
f1 = 0.995, f2 = 990
TMD Damping Ratio $\xi_{d1} = 0.065$, $\xi_{d2} = 0.095$

Optimal parameters for minimum H_A are slightly different from those for minimum H. However, this difference is not significant.

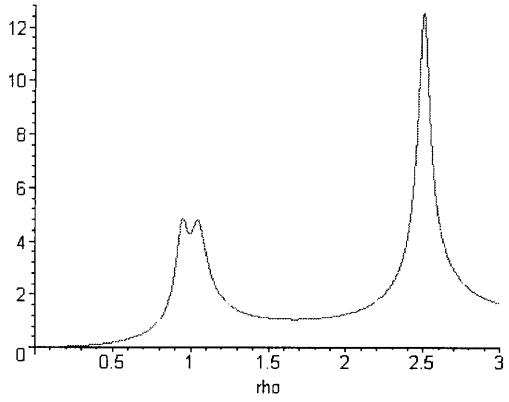

H_{A1} plot , A_1= (P/M) H_{A1}
$\phi 11 = 0.5$, $\phi 12 = 1.0$
$\phi 21 = 1.0$, $\phi 22 = -0.5$
$\omega 1 = 1$
$\omega 2 = 2.5$
Mass Ratio M1 = 0.015
Mass Ratio M2 = 0.015
Struc. Damping Ratio $\xi_1 = 0.005$, $\xi_2 = 0.0132$
f1 = 0.985, f2 = 980
TMD Damping Ratio $\xi_{d1} = 0.065$, $\xi_{d2} = 0.095$

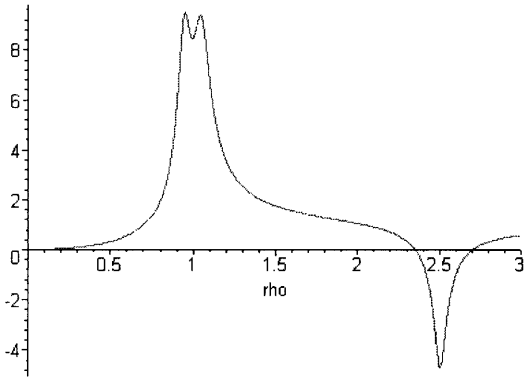

H_{A2} plot , A_1= (P/M) H_{A2}
$\phi 11 = 0.5$, $\phi 12 = 1.0$
$\phi 21 = 1.0$, $\phi 22 = -0.5$
$\omega 1 = 1$
$\omega 2 = 2.5$
Mass Ratio M1 = 0.015
Mass Ratio M2 = 0.015
Struc. Damping Ratio $\xi_1 = 0.005$, $\xi_2 = 0.0132$
f1 = 0.985, f2 = 980
TMD Damping Ratio $\xi_{d1} = 0.065$, $\xi_{d2} = 0.095$

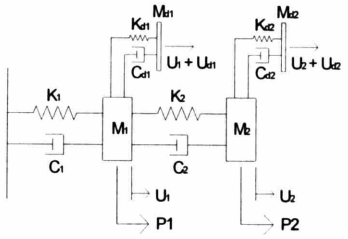

First & Second Mode Resonance Zone
Dynamic Amplification Factor
- TMD's are Tuned to the First Mode
- Optimized for Entire 2DOF/2TMD System by Trial & Error for Acceleration

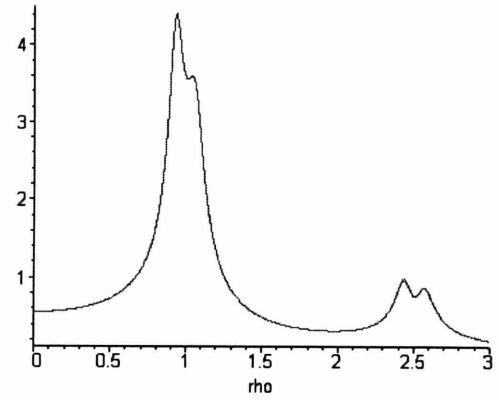

H_1 plot , $U_1 = (P/K)\, H_1$
$\phi 11 = 0.5$, $\phi 12 = 1.0$
$\phi 21 = 1.0$, $\phi 22 = -0.5$
$\omega 1 = 1$
$\omega 2 = 2.5$
Mass Ratio M1 = 0.003
Mass Ratio M2 = 0.030
Struc. Damping Ratio $\xi_1 = 0.005$, $\xi_2 = 0.0132$
f1 = 2.51, f2 = 0.985
TMD Damping Ratio $\xi_{d1} = 0.03$, $\xi_{d2} = 0.11$

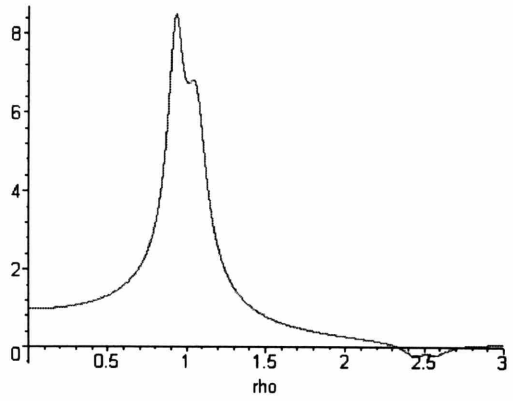

H_2 plot , $U_2 = (P/K)\, H_2$
$\phi 11 = 0.5$, $\phi 12 = 1.0$
$\phi 21 = 1.0$, $\phi 22 = -0.5$
$\omega 1 = 1$
$\omega 2 = 2.5$
Mass Ratio M1 = 0.003
Mass Ratio M2 = 0.030
Struc. Damping Ratio $\xi_1 = 0.005$, $\xi_2 = 0.0132$
f1 = 2.51, f2 = 0.985
TMD Damping Ratio $\xi_{d1} = 0.03$, $\xi_{d2} = 0.11$

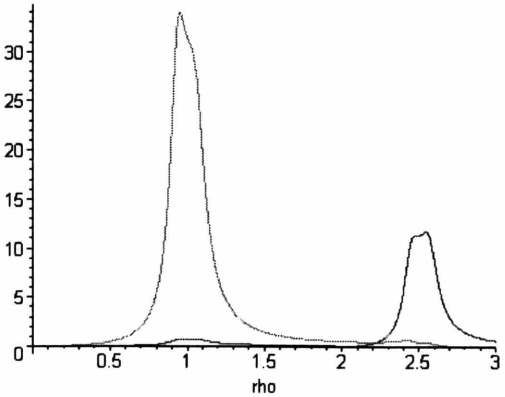

H_{d1}, H_{d2} plot , $U_{d1} = (P/K)\, H_{d1}$, $U_{d2} = (P/K)\, H_{d2}$
$\phi 11 = 0.5$, $\phi 12 = 1.0$
$\phi 21 = 1.0$, $\phi 22 = -0.5$
$\omega 1 = 1$
$\omega 2 = 2.5$
Mass Ratio M1 = 0.003
Mass Ratio M2 = 0.030
Struc. Damping Ratio $\xi_1 = 0.005$, $\xi_2 = 0.0132$
f1 = 2.51, f2 = 0.985
TMD Damping Ratio $\xi_{d1} = 0.03$, $\xi_{d2} = 0.11$

Optimal parameters for minimum H_A are slightly different from those for minimum H. However, this difference is not significant.

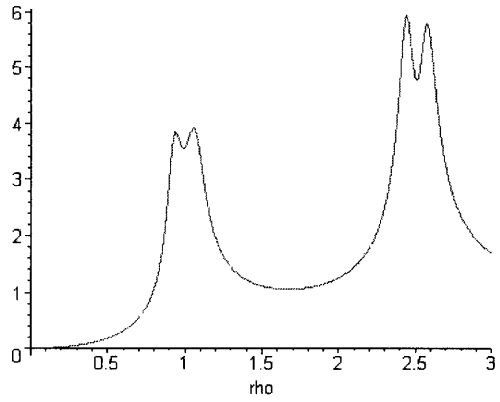

H_{A1} plot , A_1= (P/M) H_{A1}
$\phi 11 = 0.5$, $\phi 12 = 1.0$
$\phi 21 = 1.0$, $\phi 22 = -0.5$
$\omega 1 = 1$
$\omega 2 = 2.5$
Mass Ratio M1 = 0.003
Mass Ratio M2 = 0.030
Struc. Damping Ratio $\xi_1 = 0.005$, $\xi_2 = 0.0132$
f1 = 2.51, f2 = 0.985
TMD Damping Ratio $\xi_{d1} = 0.03$, $\xi_{d2} = 0.11$

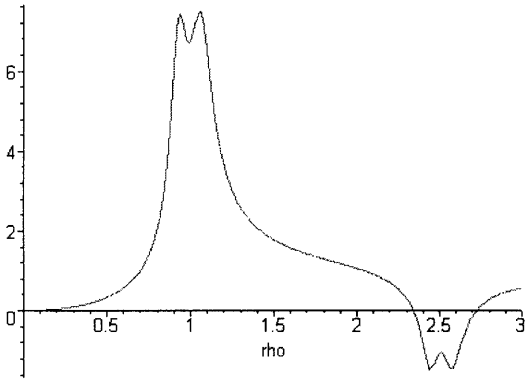

H_{A2} plot , A_1= (P/M) H_{A2}
$\phi 11 = 0.5$, $\phi 12 = 1.0$
$\phi 21 = 1.0$, $\phi 22 = -0.5$
$\omega 1 = 1$
$\omega 2 = 2.5$
Mass Ratio M1 = 0.003
Mass Ratio M2 = 0.030
Struc. Damping Ratio $\xi_1 = 0.005$, $\xi_2 = 0.0132$
f1 = 2.51, f2 = 0.985
TMD Damping Ratio $\xi_{d1} = 0.03$, $\xi_{d2} = 0.11$

Appendix 11. 3DOF + 3TMD Eigenvalue Check

11.1. Eigenvalue Check

$\alpha 1 = 1/3$, $\alpha 2 = 2/3$
$\xi 1 = 0$, $\xi 2 = 0$, $\xi 3 = 0$, $\xi = 0$
f1 = 0.996, f2 = 0.994, f3 = 0.992
m1 = 0.00333, m2 = 0.00333, m3 = 0.00333

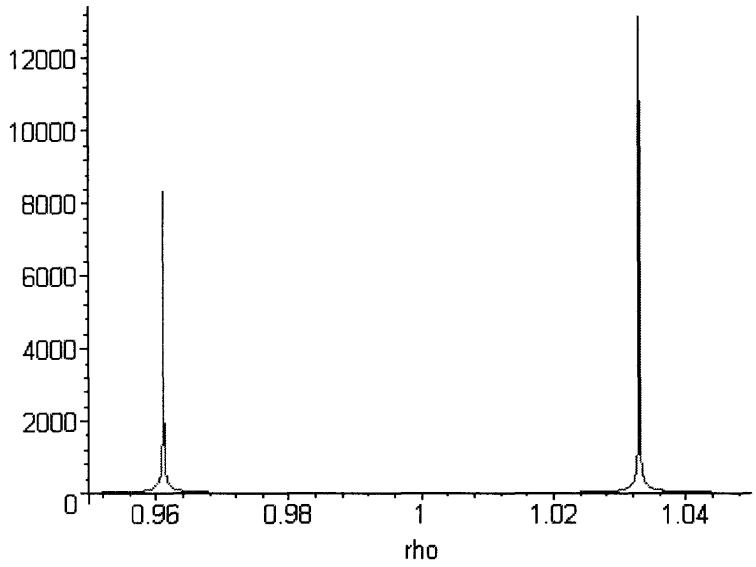

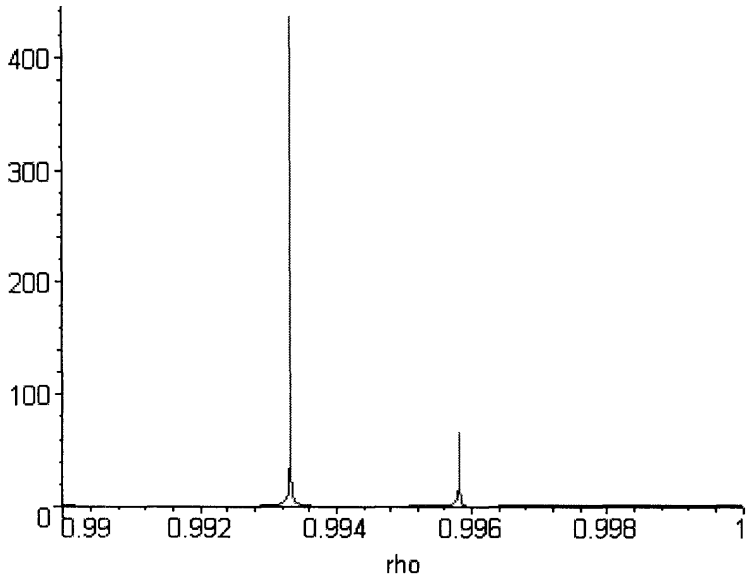

$H = \infty$, $\rho = \Omega / \omega = T_n / T_f = 0.961, 0.9934, 0.9958, 1.034$

Zero Damping Condition

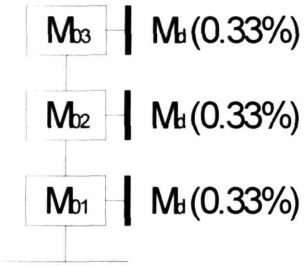

$\xi 1 = 0, \xi 2 = 0, \xi 3 = 0, \xi = 0$

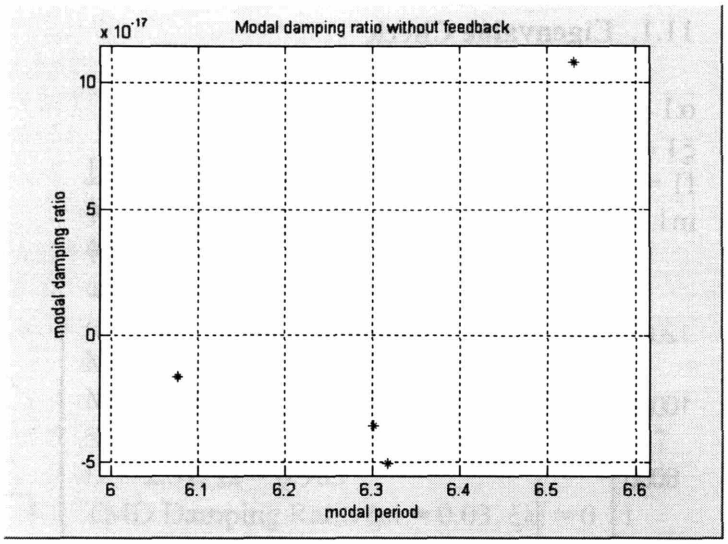

MotionLab Tn

ρ	0.961	0.9934	0.9958	1.034
Tn	6.09	6.3	6.31	6.56

Calculated Tn from Analytical Solution H plot

Optimized Condition

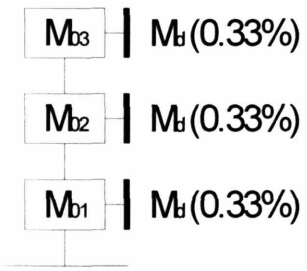

Cd3 = 13,593N-s/m ($\xi_{d3} = 0.055$)
Cd2 = 11,144N-s/m ($\xi_{d2} = 0.045$)
Cd1 = 8,685N-s/m ($\xi_{d1} = 0.035$)
$\xi = 0.005$

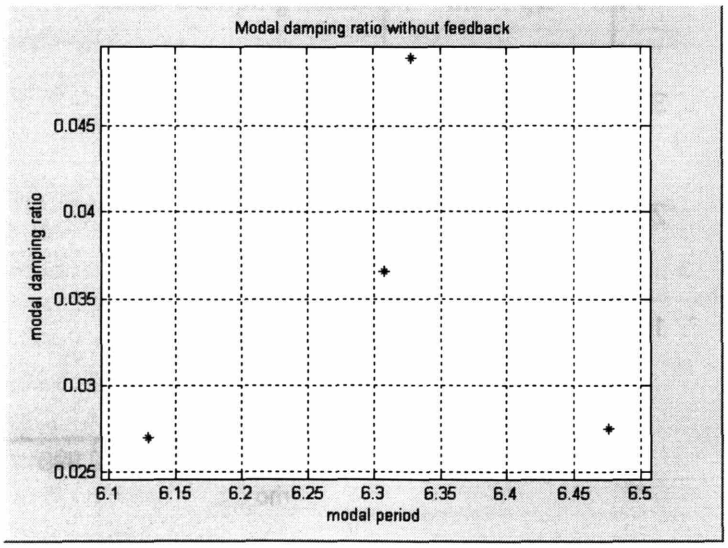

11.2. Sensitivity of the System to the Change of the Primary Structure Damping

$\alpha 1 = 1/3$, $\alpha 2 = 2/3$
$\xi 1 = 0$, $\xi 2 = 0$, $\xi 3 = 0$, $\xi = 0.01$
f1 = 0.996, f2 = 0.994, f3 = 0.992
m1 = 0.00333, m2 = 0.00333, m3 = 0.00333

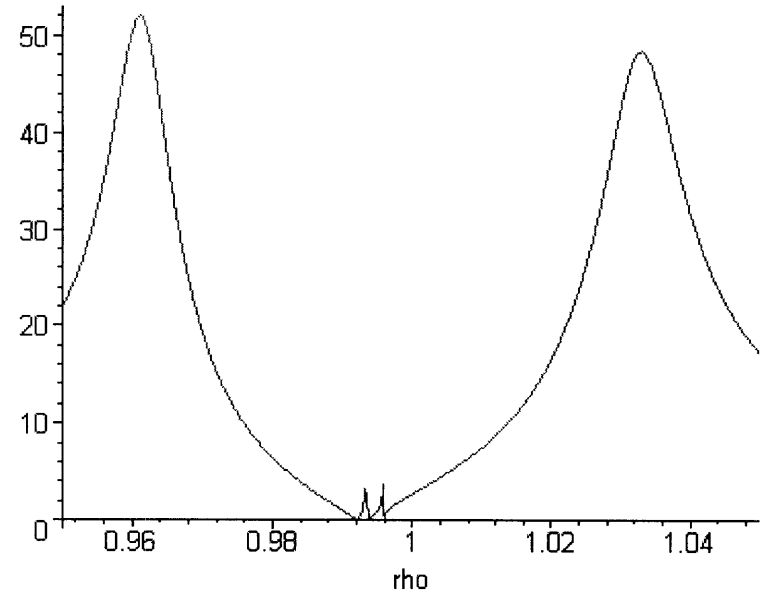

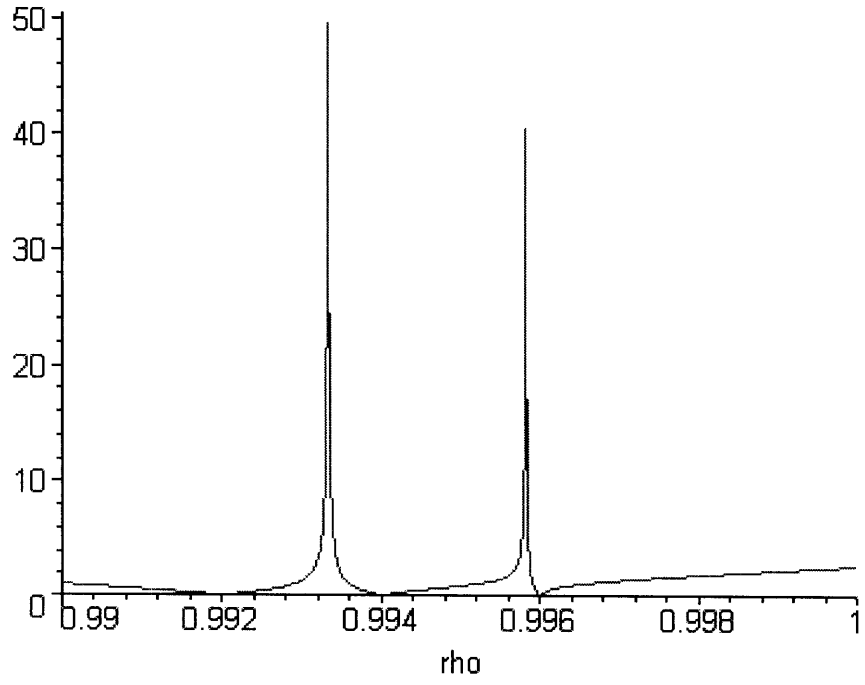

11.3. Sensitivity of the System to the Change of TMD Damping

$\alpha 1 = 1/3$, $\alpha 2 = 2/3$
$\xi 1 = 0.001$, $\xi 2 = 0.001$, $\xi 3 = 0.001$, $\xi = 0.01$
$f1 = 0.996$, $f2 = 0.994$, $f3 = 0.992$
$m1 = 0.00333$, $m2 = 0.00333$, $m3 = 0.00333$

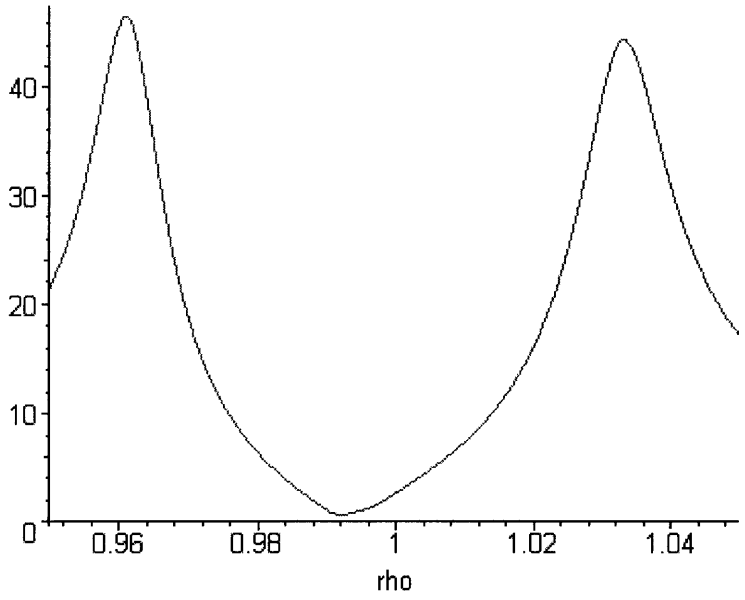

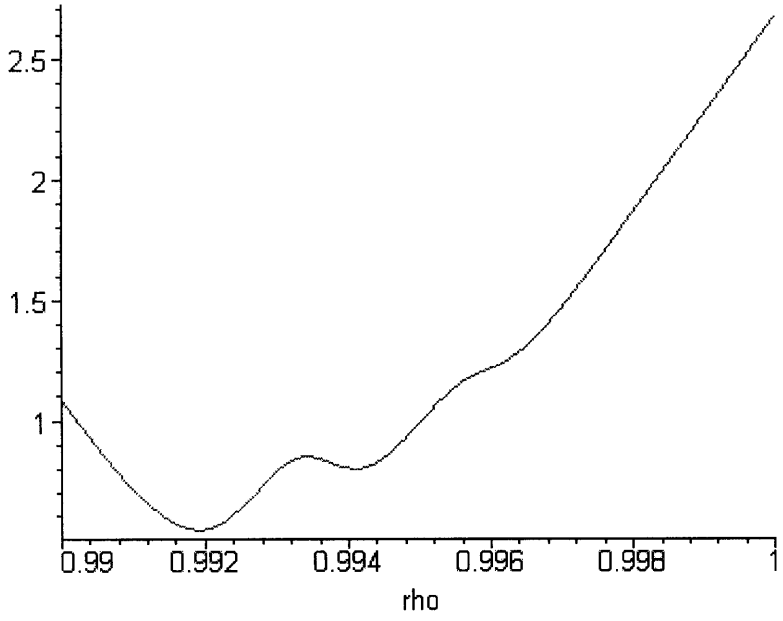

Appendix 12. Horizontal Distribution of TMDs

In the vertically distributed TMD scheme in this thesis, each TMD at each node represents multiple small dampers. In order to make the discussion regarding the distributed multiple TMDs complete, horizontal distribution equations are presented here. The governing equations for the system shown in Figure (a) are

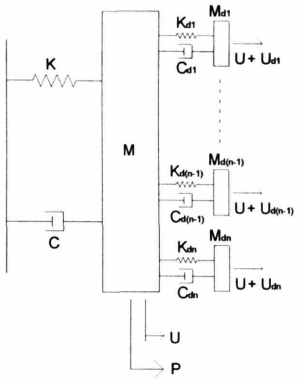

Figure (a)

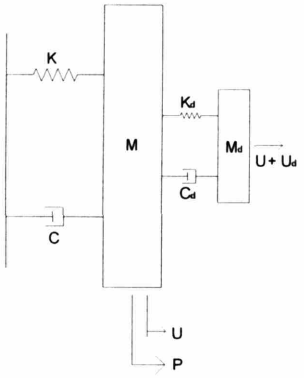

Figure (b)

$$m\ddot{u} + c\dot{u} + ku = P + (k_{d1}u_{d1} + c_{d1}\dot{u}_{d1}) + ... + (k_{d(n-1)}u_{d(n-1)} + c_{d(n-1)}\dot{u}_{d(n-1)}) + (k_{dn}u_{dn} + c_{dn}\dot{u}_{dn})$$

$$m_{d1}\ddot{u}_{d1} + c_{d1}\dot{u}_{d1} + k_{d1}u_{d1} = -m_{d1}\ddot{u}$$

.....

.....

$$m_{d(n-1)}\ddot{u}_{d(n-1)} + c_{d(n-1)}\dot{u}_{d(n-1)} + k_{d(n-1)}u_{d(n-1)} = -m_{d(n-1)}\ddot{u}$$

$$m_{dn}\ddot{u}_{dn} + c_{dn}\dot{u}_{dn} + k_{dn}u_{dn} = -m_{dn}\ddot{u}$$

Suppose all damper properties are the same. Then,

$$m\ddot{u} + c\dot{u} + ku = P + n(k_{d1}u_{d1} + c_{d1}\dot{u}_{d1}).$$

Let $nm_{d1} = m_d$, $nk_{d1} = k_d$, $nc_{d1} = c_d$, and $u_{d1} = u_d$. Then,

$$m\ddot{u} + c\dot{u} + ku = P + k_d u_d + c_d \dot{u}_d$$

$$m_d\ddot{u}_d + c_d\dot{u}_d + k_d u_d = -m_d\ddot{u}$$

Thus, the model in Figure (a) composed of multiple TMDs can be simplified into the model in Figure (b) composed of a single TMD, and the following simple relationships exist between the two models.

$$m_{d1} = ... = m_{d(n-1)} = m_{dn} = m_d / n$$

$$k_{d1} = ... = k_{d(n-1)} = k_{dn} = k_d / n$$

$$c_{d1} = ... = c_{d(n-1)} = c_{dn} = c_d / n$$

$$u_{d1} = ... = u_{d(n-1)} = u_{dn} = u_d$$

Appendix 13. H & Hd Plots with and without Structural Damping

13.1. SDOF+TMD with Structure Damping Ratio $\xi = 0$

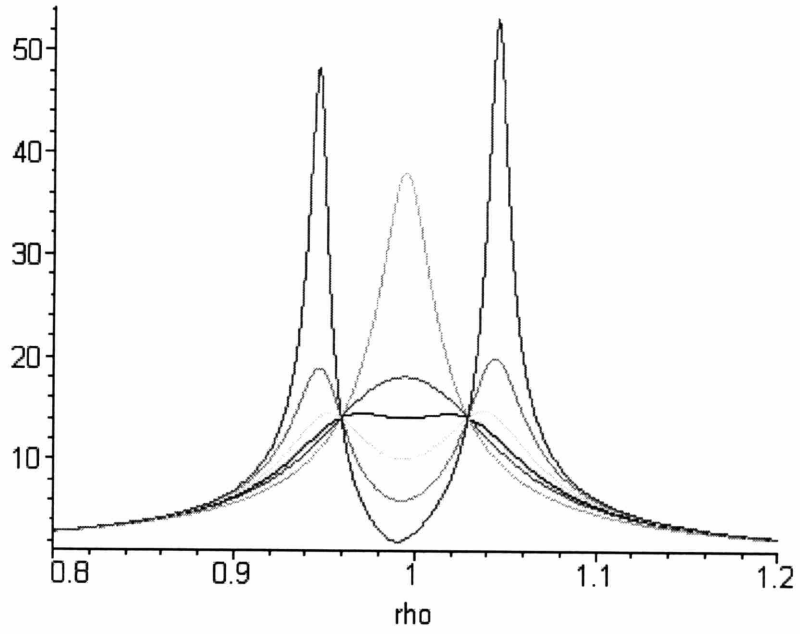

H plot , U= (P/K) H

Mass Ratio = 0.01
Structure Damping Ratio
$\xi = 0$
TMD Damping Ratio
ξ_d = 0.01, 0.03, 0.05, 0.07, 0.09, 0.2
f = 0.99

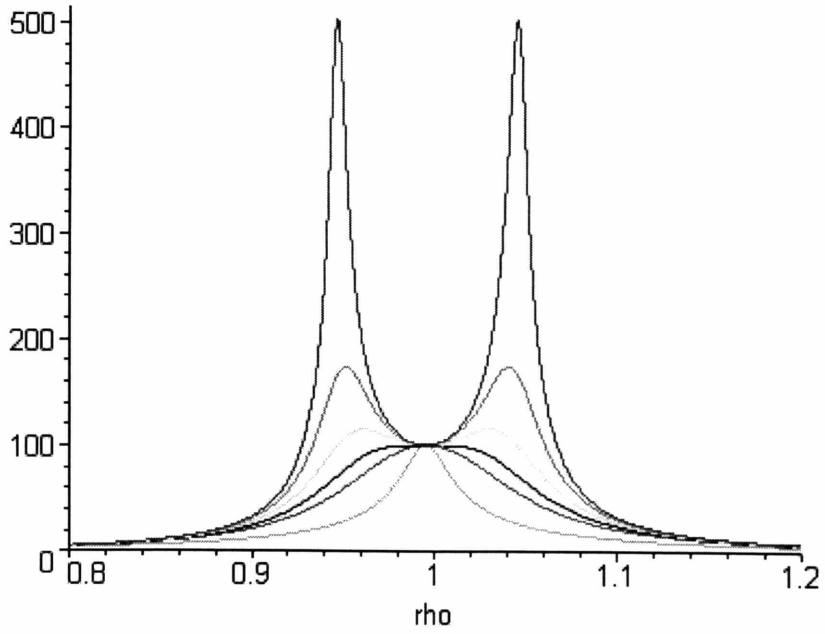

Hd plot , Ud = (P/K) Hd

Mass Ratio = 0.01
Structure Damping Ratio
$\xi = 0$
TMD Damping Ratio
ξ_d = 0.01, 0.03, 0.05, 0.07, 0.09, 0.2
f = 0.99

13.2. SDOF+TMD with Structure Damping Ratio ξ = 1%

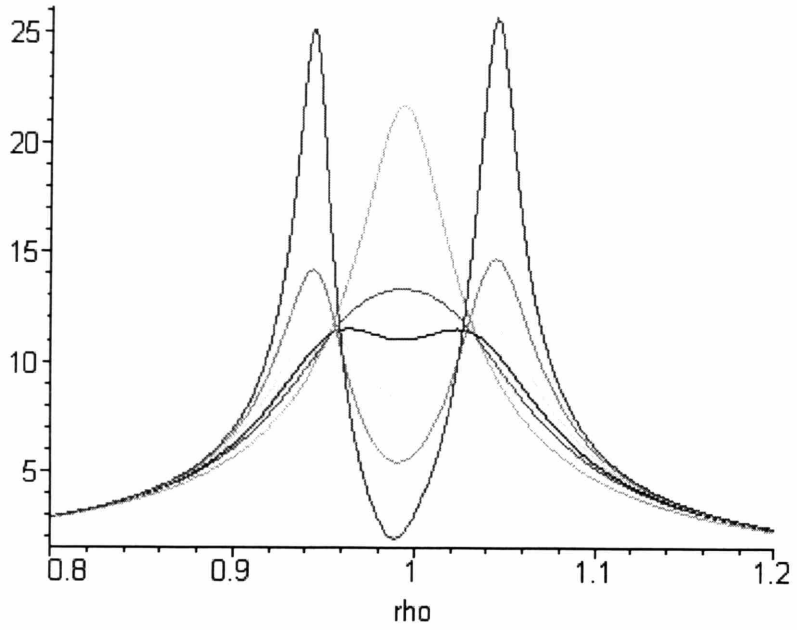

H plot , U= (P/K) H

Mass Ratio = 0.01
Structure Damping Ratio
ξ = 0.01
TMD Damping Ratio
ξ_d = 0.01, 0.03, 0.05, 0.07, 0.09, 0.2
f = 0.9885

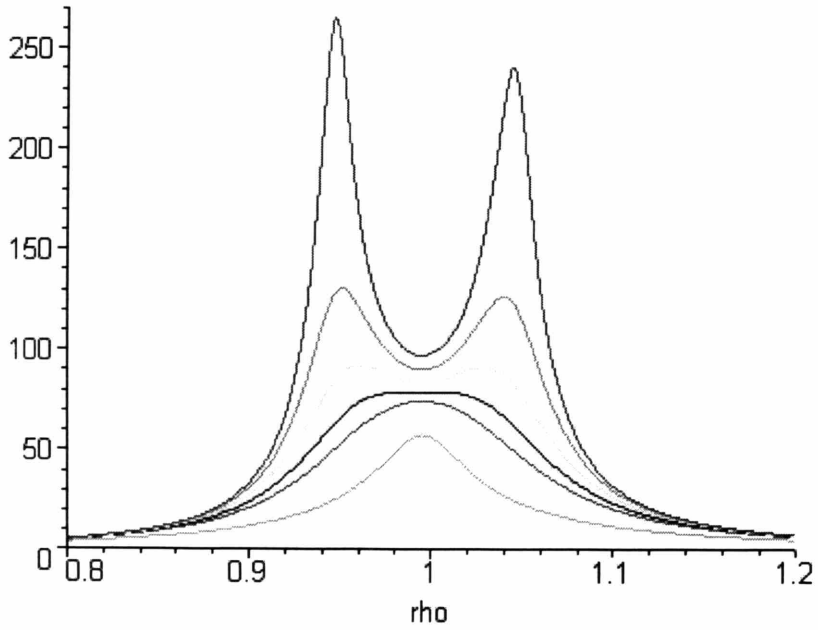

Hd plot , Ud = (P/K) Hd

Mass Ratio = 0.01
Structure Damping Ratio
ξ = 0.01
TMD Damping Ratio
ξ_d = 0.01, 0.03, 0.05, 0.07, 0.09, 0.2
f = 0.9885

13.3. SDOF+TMD with Structure Damping Ratio $\xi = 2\%$

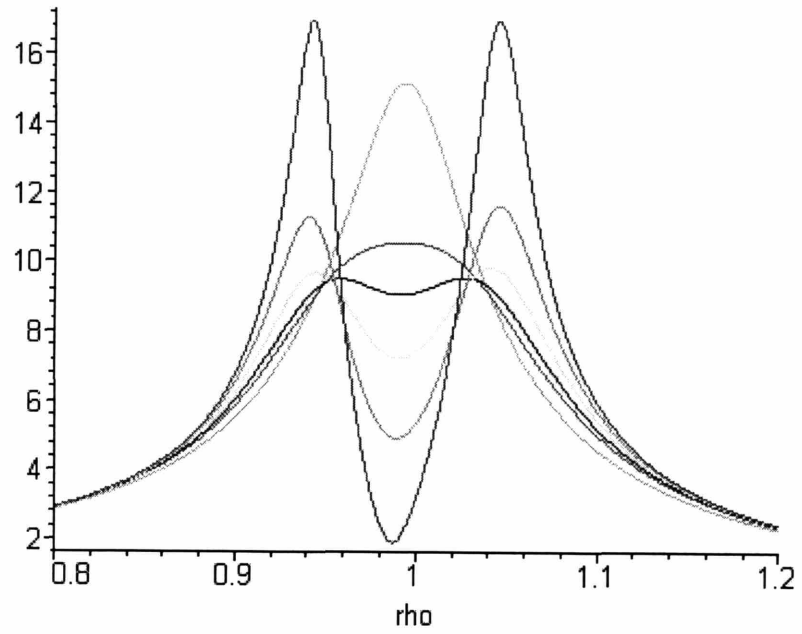

H plot , U= (P/K) H

Mass Ratio = 0.01
Structure Damping Ratio
$\xi = 0.02$
TMD Damping Ratio
$\xi_d = 0.01, 0.03, 0.05, 0.07, 0.09, 0.2$
f = 0.9865

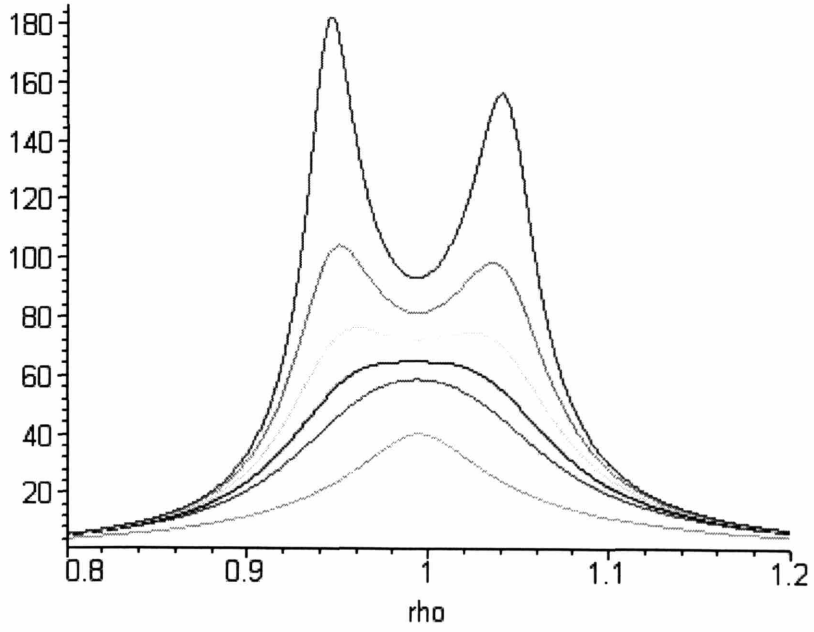

Hd plot , Ud = (P/K) Hd

Mass Ratio = 0.01
Structure Damping Ratio
$\xi = 0.02$
TMD Damping Ratio
$\xi_d = 0.01, 0.03, 0.05, 0.07, 0.09, 0.2$
f = 0.9865

13.4. SDOF+TMD with Structure Damping Ratio $\xi = 5\%$

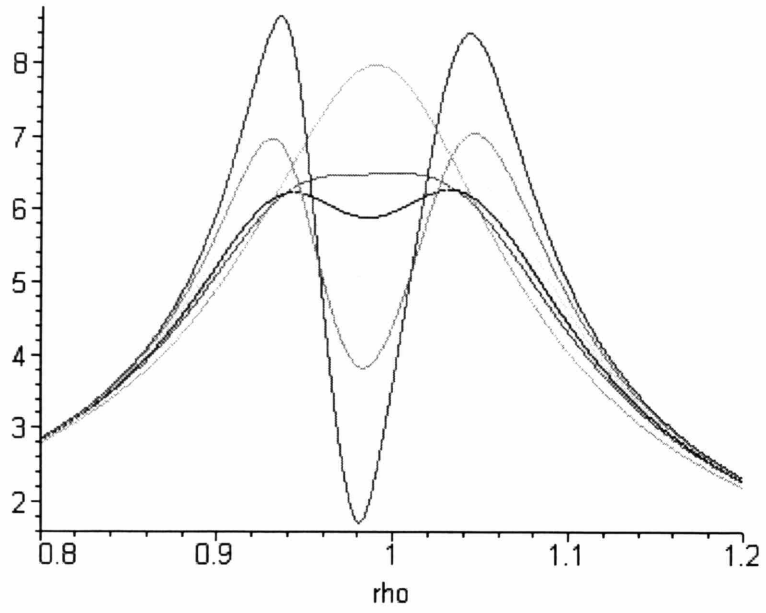

H plot , U= (P/K) H

Mass Ratio = 0.01
Structure Damping Ratio
$\xi = 0.05$
TMD Damping Ratio
$\xi_d = 0.01, 0.03, 0.05, 0.07, 0.09, 0.2$
f = 0.98

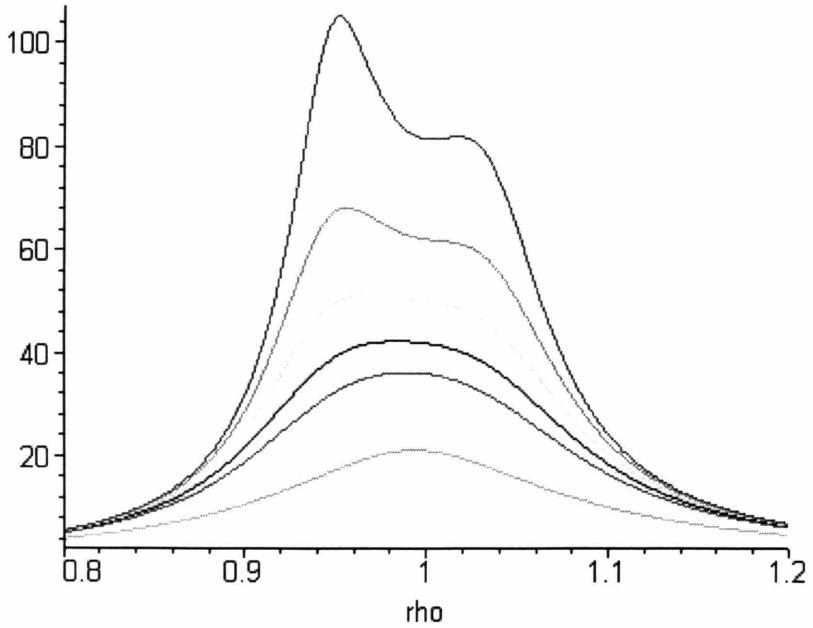

Hd plot , Ud = (P/K) Hd

Mass Ratio = 0.01
Structure Damping Ratio
$\xi = 0.05$
TMD Damping Ratio
$\xi_d = 0.01, 0.03, 0.05, 0.07, 0.09, 0.2$
f = 0.98

Part I References

Abalos, Inaki and Juan Herreros. *Tower and Office: From Modernist Theory to Contemporary Practice.* Cambridge: MIT Press, 2003.

Basalla, George. *The Evolution of Technology.* New York: Cambridge University Press, 1988.

Banham, Reyner. *Theory and Design in the First Machine Age.* London: Architectural Press, 1960.

Bruno, Leonard. *The Tradition of Technology: Landmarks of Western Technology in the Collections of the Library of Congress.* Washington: Library of Congress, 1995.

Campi, Mario. *Skyscrapers: An Architectural Type of Modern Urbanism.* Basel: Birkhauser, 2000.

Clark, W. and J Kingston. *The skyscraper; a study in the economic height of modern office buildings.* New York: American Institute of Steel Construction, 1930.

Condit, Carl. *American Building Art: The 19th Century.* New York: Oxford University Press, 1961.

Condit, Carl. *American Building Art: The 20th Century.* New York: Oxford University Press, 1961.

Condit, Carl. *American Building: Materials and Techniques from the First Colonial Settlements to the Present.* Chicago: University of Chicago Press, 1968.

Connor, Jerome. *Introduction to Structural Motion Control.* New York: Prentice Hall, 2003.

Fernandez, John. *MIT 4.463: Advanced Structures and Building Envelopes, Lecture Note.* MIT, 2004.

Gidion, Sigfried. *Space, Time and Architecture: The Growth of a New Tradition.* 5th Edition. Cambridge: Harvard University Press, 1967.

Goldberger, Paul. *The Skyscraper.* New York: Random House, 1981.

Grodecki, Louis. *Gothic Architecture.* New York: Electra/Rizzoli, 1985.

Hitchcock, Henri-Russell and Philip Johnson. *The International Style.* New York: Norton & Company, 1932.

Jencks, Charles. *The New Paradigm in Architecture: The Language of Post-Modernism.* New Haven: Yale University Press, 2002.

Landau, Sarah and Carl Condit. *Rise of the New York Skyscraper, 1865-1913.* New Haven: Yale University Press, 1996.

Letherbarrow, David. *Uncommon Ground.* Cambridge: MIT Press, 2000.

Letherbarrow, David and Mohsen Mostafavi. *Surface Architecture.* Cambridge: MIT Press, 2002.

Mark, Robert. *Experiments in Gothic Architecture.* Cambridge: MIT Press, 1982.

Messler, Norbert. *The Art Deco Skyscraper in New York.* New York: P. Lang, 1986.

Loughran, Patrick. *Falling Glass: Problems and Solutions in Contemporary Architecture.* Basel: Birkhauser, 2003.

Pevsner, Nikolaus. *The Source of Modern Architecture and Design.* New York: F. A. Praeger, 1968.

Robinson, Cervin. *Skyscraper Style*. New York: Oxford University Press, 1975.

Rowe, Colin and Robert Slutzky. *Transparency.* Basel: Birkhauser Verlag, 1997.

Russell, James. *Architectural Style and Management Ideals.* AV Monographs 103, 2003.

Schueller, Wolfgang. *The Vertical Building Structure.* New York: Van Nostrand Reinhold, 1990.

Solomonson, Katherine. *The Chicago Tribune Tower Competition: Skyscraper Design and Cultural Change in the 1920s.* New York: Cambridge University Press, 2001.

Soong, T. T. and G. F. Dargush. *Passive Energy Dissipation System in Structural Engineering.* New York: Wiley, 1997.

Steele, James. *Architecture Today.* London: Phaidon, 1997.

Smith, Bryan and Alex Coull. *Tall Building Structures: Analysis and Design.* New York: Wiley, 1991.

Turner, Gregory. *Construction Economics and Building Design: A Historical Approach.* New York: Van Nostrand Reinhold, 1986.

Wigginton, Michael. *Glass in Architecture*, London: Phaidon, 1996.

Willis, Carol. *Form Follows Finance: Skyscrapers and Skylines in New York and Chicago.* New York: Princeton Architectural Press, 1995.

Part II References

AISC. *Manual of Steel construction: Load & Resistance Factor Design.* American Institute of Steel Construction Inc., 1998.

ASCE. *Minimum Design Loads for Buildings and Other Structures.* American Society of Civil Engineers, 1996.

Abe, M. & T. Igusa. "Tuned Mass Dampers for Structures with Closely Spaced Natural Frequencies." *Earthquake Engineering and Structural Dynamics.* vol.24, no.2. Feb. 1995. 247-61.

Abe, M. & Y. Fugino. "Dynamic Characterization of Multiple Tuned Mass Dampers and Some Design Formulas." *Earthquake Engineering and Structural Dynamics.* vol.23, no.8. Aug. 1994. 813-35.

Ankireddi, S. & H. Yang. "Simple ATMD Control Methodology for Tall Buildings subject to Wind Loads." *Journal of Structural Engineering.* vol.122, no.1. Jan. 1996. 83-91.

Arons, Daniel M. *Properties and Applications of Double-Skin Building Facades.* MIT, Dissertation, 2000.

Bergman, L.A. et al. "Optimal Distribution of Tuned Mass Dampers in Wind Sensitive Structures." *Proc., 5th Int. Conf. on Structural Safety and Reliability (ICOSSAR).* ASCE, 1989.

The Chicago Committee on High Rise Buildings. *Exterior Claddings on High Rise Buildings: Past Experience, Present Directions, and Future Trends.* The Chicago Committee on High Rise Buildings, 1990.

Clough, R. & J. Penzien. *Dynamics of Structures.* New York: McGraw-Hill, 1975.

Compagno, Andrea. *Intelligent Glass Facades.* Basel: Birkhauser, 1999.

Council on Tall Buildings and Urban Habitat. *Architecture of Tall Buildings.* New York: McGraw-Hill, 1995.

Council on Tall Buildings and Urban Habitat. *Tall Building Criteria and Loading.* Council on Tall Buildings and Urban Habitat, 1978.

Council on Tall Buildings and Urban Habitat. *Advances in Tall Buildings.* Council on Tall Buildings and Urban Habitat, 1980.
Council on Tall Buildings and Urban Habitat. *Habitat and The High-Rise: Tradition and Innovation.* Dutch Council on Tall Buildings, 1995.

Council on Tall Buildings and Urban Habitat. *Cladding.* New York: McGraw-Hill, 1992.

Council on Tall Buildings and Urban Habitat. *Structural Systems for Tall Buildings.* New York: McGraw-Hill, 1995.

Council on Tall Buildings and Urban Habitat. *Tall Buildings: 2000 and Beyond.* Council on Tall Buildings and Urban Habitat, 1990.

Council on Tall Buildings and Urban Habitat. *Tall Building Systems and Concepts.* American Society of Civil Engineers, 1980.

Den Hartog, J. *Mechanical Vibrations.* 4th Edition. New York: McGraw-Hill, 1956.

Kareem, A. et al. "Performance of Multiple Mass Dampers Under Random Loading." *Journal of Structural Engineering.* vol.121, no.2. Feb. 1995. 348-61.

Kareem, A. "Lateral-Torsional Motion of Tall Buildings to Wind Loads." *Journal of Structural Engineering.* vol.111, no.11. Nov. 1985. 2479-96.

Kim, Michael. *Arch. 444: Building Systems and Design Integration, Class Note.* University of Illinois at Urbana-Champaign. 1998

Kim, Michael. *Arch. 445: Design and Constructability, Class Note.* University of Illinois at Urbana-Champaign. 1997

Peetathawatchai, Chatmongkol. *Preliminary Design Strategies for Tall Buildings.* MIT, Dissertation, 1992.

Samali, B. et al. "Control of Lateral-Torsional Motion of Wind-Excited Buildings." *Journal of Structural Engineering.* vol.111, no.6. Jun. 1985. 777-96.

Schueller, Wolfgang. *High-Rise Building Structures.* 2nd Edition. Robert E. Krieger Publishing Company, 1986.

Schueller, Wolfgang. *The Vertical Building Structure.* Van Nostrand Reinhold, 1990.

Taranath, B. *Steel, Concrete, & Composite Design of Tall Buildings.* New York: McGraw-Hill, 1998.

Xu, K. and T. Igusa. "Dynamic Characteristics of Multiple Substructures with Closely Spaced Frequencies." *Earthquake Engineering and Structural Dynamics.* vol.21. 1992. 1059-70.

Xu, K. and T. Igusa. "Vibration Control using Multiple Tuned Mass Dampers." *Journal of Sound and Vibration.* vol.175. 1994. 491-503.

Yamaguchi, H. and N. Harnpornchai. "Fundamental Characteristics of Multiple Tuned Mass Dampers for Suppressing Harmonically Forced Oscillation." *Earthquake Engineering and Structural Dynamics.* vol.22. 1993. 51-62.